DEPARTMENT OF CIVIL ENGINEERING

UNIVERSITY OF CANTERBURY

SEISMIC BEHAVIOUR OF BEAM-COLUMN JOINT SUBASSEMBLIES REINFORCED WITH STEEL FIBRES

By Liu, Cong

January, 2006

SEISMIC BEHAVIOUR OF BEAM-COLUMN JOINT SUBASSEMBLIES REINFORCED WITH STEEL FIBRES

A thesis submitted in partial fulfilment
of the requirements for the Degree
of Master of Engineering at the University of Canterbury,
Christchurch, New Zealand

By

Liu, Cong

Supervised by

Dr. Stefano Pampanin

Co-Supervisor

Dr. Rajesh Dhakal

Department of Civil Engineering
University of Canterbury
Christchurch, New Zealand

January, 2006

ABSTRACT

High performance cementitious composites have been increasingly used for a range of structural applications in many countries. More recently, a notable interest has been focused on structural performance under seismic loading. However, a critical lack of coherent information and experimental/numerical data available in the literature has to be recognized along with the absence of specific and well-accepted code-guidelines for use of FRC in seismic applications.

More specifically, when dealing with seismic resistant frame systems, few researchers have investigated in the past the seismic response of beam-column joints reinforced with steel fibres. These preliminary experimental tests have shown that adding steel fibres in joints is an effective method for improving joint behaviour and energy absorption capacity as well as enhancing the damage tolerance of joints and reducing the number of stirrups in seismic joints. However, due to the limited number of experimental tests as well as of the wide dispersion in the type and mechanical properties of the fibres adopted in these independent researches, the actual contributions of concrete, steel fibres and stirrups to the overall joint shear capacity has not yet been clearly identified and understood.

This research aims to investigate the seismic behaviour and failure modes of beam-column joint subassemblies reinforced with steel fibres with the intent to provide preliminary suggestions for a simple but rational analytical procedure to evaluate the joint shear strength when either fibres and/or stirrups are adopted.

As part of a more comprehensive on-going research campaign on the seismic behaviour of FRC members and systems, six 2-D exterior beam-column joint subassemblies were tested under simulated seismic loading (quasi-static cyclic loading regime) at the Civil Engineering Laboratory of the University of Canterbury. In order to assess the contribution of steel fibres to the joint (panel zone) shear strength, both under-designed systems (with no transverse reinforcement in the joint, following older practice before the pre-1970s) and well designed systems (following the NZ concrete design standard NZS 3101:1995) were adopted as benchmark specimens.

The performance of steel fibre reinforced beam-column joints were compared with that of conventional joints. Results showed that using steel fibre reinforced concrete (SFRC) within

beam-column joints can significantly enhance the shear resistance capacity of joints. However, using steel fibre reinforcement alone can not prevent buckling of the reinforcing bars when joints are under high intensity seismic loading. Furthermore, the test results also showed that using steel fibre reinforcement is an effective method to reduce the lateral reinforcement in the beam plastic hinge region.

As part of the analytical investigation, a simplified procedure to evaluate the joint shear contribution provided by different amounts of fibres with or without the presence of stirrups has been also introduced. Influence of the axial load on the joint nominal shear capacity has been accounted for by adopting principle stresses. Tentative strength degradation curves (principle tensile stress vs. shear deformation) have also been calibrated on the experimental data which confirmed that a tentative relationship between the joint shear contributions provided by concrete, stirrups and steel fibres was a viable tool for designing SFRC joint. Furthermore, joint shear resistance coefficient K_f contributed by steel fibres has been compared with previous experimental test available in literature to obtain an appropriate value for SFRC joint design guidelines. M_N performance based domain visualization has also been used to evaluate the hierarchy of strength and sequence of events of beam-column joint subassemblies.

ACKNOWLEDGEMENTS

This research was carried out in the Department of Civil Engineering, University of Canterbury, New Zealand. The researcher would like to thank the following people. Without their advice, encouragement and support, this thesis would not be completed.

I wish to express my heartfelt emotion to my supervisors, Dr. Stefano Pampanin and Dr. Rajesh Dhakal of the University of Canterbury for their inspiration, guidance and enthusiasm.

I am thankful to Dr. James Mackechnie for his interest and advice.

Thanks are extended to Gary Harvey for his help with the experimental program.

Thanks are also given to my friends Eric Hertanto and Te-Hsiu Chen for their friendship and discussions.

The material support provided by Firth Industries Ltd., Christchurch is also gratefully acknowledged, without which the experimental work could not have been undertaken.

Last but foremost, to my parents and grandparents, for their unwavering support in spirit and livelihood.

TABLE OF CONTENTS

LIST OF FIGURES

LIST OF TABLES

NOTATION

f'_c	=	concrete compressive cylinder strength	MPa
f_y	=	yield strength of longitudinal reinforcement	MPa
f_{yt}	=	yield strength of transverse reinforcement	MPa
N^*	=	compressive axial column load	N
A_g	=	gross area of column section	mm^2
b	=	width of beam	mm
d	=	distance from extreme compression fiber of beam to centroid of beam tension reinforcement	mm
p	=	ratio pf area of the top beam longitudinal bars to b_d of beam	
p'	=	ratio of area of the bottom beam longitudinal bars to b_d of beam	
p_c	=	the nominal principal compression stress	MPa
p_t	=	the nominal principal tension stress	MPa
f_v	=	the average axial stress in vertical direction	MPa
f_h	=	the average axial stress in horizontal direction	MPa
ε_y	=	steel yield strain	
d_b	=	diameter of longitudinal steel	mm
s	=	spacing of transverse reinforcement	
ϕ	=	the strength reduction factor, being unity here	
h_b	=	beam depth	mm
h_c	=	column depth	mm
ϕ_u	=	ultimate curvature	mm^{-1}
ϕ_y	=	yield curvature	mm^{-1}
v_{jh}	=	the nominal horizontal joint shear stress	MPa
V_{jh}	=	the imposed horizontal joint shear force	N
A_j	=	effective joint area	mm^2
V_c	=	the equivalent storey shear	N
γ	=	the joint shear distortion	
Δ	=	estimated storey displacement	mm
δ_n	=	measurement of the left side of the joint panel	mm

δ_s	=	measurement of the right side of the joint panel	mm
δ_t	=	measurement of the top joint panel	mm
δ_b	=	measurement of the bottom joint panel	mm
Δ_s	=	measurement of shear deformation of the bottom joint panel	mm
A_{total}	=	summation of area of every cycle of load	
ξ	=	the equivalent viscous damping coefficient	
l_f	=	the length of steel fibres	mm
d_f	=	the diameter of steel fibres	mm
V_F	=	the volume content of steel fibres	N
v_{jf}	=	the joint shear stress carried by steel fibres	MPa
v_{jc}	=	the joint shear stress carried by concrete	MPa
v_{js}	=	the joint shear stress carried by stirrups	MPa

CHAPTER ONE

1. INTRODUCTION AND SCOPE OF THE RESEARCH

1.1. Introduction

The intrinsic problem of normal concrete is its brittle nature which may cause collapse in non-seismically detailed structural members after the first crack during a large earthquake. The use of steel fibres may convert the brittle characteristics to ductile ones. The principal role of fibres is to bridge cracks and resist their formation. Therefore a considerable improvement in tensile strength and higher ultimate strain can be obtained.

Many researches have been conducted to investigate the flexural behaviour of steel fibre reinforced beam-column joints, such as using steel fibre to replace the lateral reinforcement in the plastic hinges of beam-column joints. However, only a few studies are available on the shear behaviour of steel fibre reinforced concrete joints, and there are no studies which have established a feasible method of designing a beam-column joint reinforced with steel fibre. The purpose of this study is to explore the mechanical behaviour of steel fibre reinforced concrete in shear resistance in the application of beam-column joints.

The experimental tests were carried out on joints reinforced with steel fibres only and the combination of stirrups and steel fibres to determine the effect of steel fibre and the combination of stirrups and steel fibres on the shear behaviour of joints. Furthermore, the potential use for steel fibres to be used to replace the stirrups is also obtained. Based on the experimental test results and earlier published studies, a formula for predicting the ultimate shear strength for joints reinforced with steel fibres and both stirrups and steel fibres is proposed. Moreover, an effective procedure for designing steel fibre reinforced joints is also introduced.

1.2. The joint vulnerability problem

Since the 1960s, many experimental and theoretical studies have been conducted to investigate and form the seismic resistance of beam-column joints. The performance of tested

structural frames indicated that the joints have frequently been found to be the critical component of beam-column subassemblies after seismic cycle load.

The deficiencies of joints are mainly caused by inadequate transverse reinforcement and insufficient anchorage capacity in the joint. These problems have been highlighted by the damage observed in recent devastating earthquakes in different countries. Evidence from recent earthquakes, such as the 1995 Hyogo-ken Nanbu (Japan), the 1999 Kocaeli (Turkey) and Chi-Chi (Taiwan) earthquakes, shows the total collapse of many structures caused by brittle shear failure in the joint. A damaged structure after the Kocaeli earthquake is shown in **Figure 1-1** demonstrating a good example of this failure mode. Most of these joint brittle shear failures were due to non-ductile performance, either poor anchorage of the main reinforcing bars or simply inadequate transverse reinforcement in the joints, of reinforced concrete moment-resisting frames. In the 1995 Hyogo-ken Nanbu earthquake, a phenomenon was found that reinforced concrete buildings built in the pre-1970s suffered more severely than those built after the development of current seismic codes.

Figure 1 - 1: Damaged beam-column joint during earthquake (1999 Kocaeli, Turkey)

1.2.1. Capacity design philosophy for beam-column joints

After the current seismic design code was developed in the 1980s, it has been possible to avoid the potential structural brittle failure by using controllable inelastic deformations to dissipate the large seismic energy. To achieve this, the philosophy of capacity design leads to a weak beam-strong column mechanism and ensures that the energy is dissipated by beam plastic hinges. On the basis of capacity design approach, the strength of the joint should not

be less than the maximum strength of the weakest member. Moreover, the capacity of the column should not be jeopardised by strength degradation within the joint. Otherwise, column failure or joint shear failure may occur and cause column side-sway mechanisms in multi-story frames. If the joint is designed according to capacity design, the energy dissipation occurs mainly in the beam plastic hinges, which prevents the joint suffering from excessive strength and stiffness degradation when subjected to seismic load in the inelastic range.

1.3. High-performance, high strength, and fibre reinforced concrete

In civil engineering, research into new composite materials is an important topic [1] [2] [3] [4] [5] [6]. Since the strong points of high-performance concrete (HPC), high strength concrete (HSC) and fibre reinforced concrete (FRC) were significantly developed, those cementitious composites have been widely used in civil engineering structures. High–performance concretes (HPC) are more expensive than normal concretes in the initial cost of a structure, but this disadvantage can be overcome by their better behaviour and lower concrete weight. As HSC are often more brittle than conventional concretes, in some critical area of structures the strength does not increase in proportion to concrete strength. Since 1989, many structural members with HSC (over 60 MPa) have been tested in Japan [7]. Those test results showed that HSC members failed in a very brittle mode in the anchorage zone and showed significant bond deterioration of beam reinforcement in the joint region. However this drawback can be overcome by introducing fibres into the mix. The increased toughness of the material improves the structural ductility, which is instrumental in preserving the overall performances of a structure, especially in improving the energy dissipation capacity of the overall structure.

1.4. Steel fibre reinforced concrete

Steel fibre reinforced concrete (SFRC) is a concrete mix that contains discontinuous, discrete steel fibres dispersed randomly and uniformly distributed. Previous research ([8] [9] [10]) has shown that steel fibre concrete has higher tensile strength, higher shear resistance, greater toughness and better seismic resistance than plain concrete. It is also shown that SFRC combined with the steel reinforcement in structural elements provides a complex effect between the two forms of reinforcement and an efficient performance. Because of these advantages, SFRC has emerged as an alternative construction material for floors, pavements, and precast products. Used in seismic beam-column joints especially SFRC can reduce the congested shear reinforcement in joint regions and reduce joint construction, and the result of

use showed significant increased behaviours such as joint integrity, structural ductility, and energy dissipation capacity.

1.4.1. Potential use of steel fibre in joint regions

In modern building codes, there is a considerable amount of reinforcement required to ensure sufficient ductility in the joint regions, therefore the spacing of the joint hoops is decreased. However a problem has arisen in that the pouring and consolidation of concrete in the joint becomes very difficult due to closely spaced hoops in the joint regions. Moreover, with a decreased spacing of the joint hoops the congestion of reinforcement may cause a problem of concrete flow ability during construction, leading to unbonded areas between the steel and concrete and space voids within the joint core.

Steel Fibre Reinforced Concrete (SFRC) represents a potential application for more cost-effective ductile beam-column joints in structure frames owing to its high seismic energy dissipation capability and relatively simple construction technique. Therefore, it is considered that using SFRC in beam-column joint regions may achieve the necessary ductility with increased spacing of stirrups in the joint region without compromising the shear strength of the joint.

Several earlier research reports show that using SFRC is an effective alternative method to increase the joint strength and integrity, ductility, and the energy-dissipation capacities with increased spacing of hoops in the joint region. However previous work on fibre reinforced concrete introduced the solution of experimental results only and was devoid of an effective design method for the prediction of the SFRC joint behaviour. Hence, a design method must be developed and rationally characterize not only steel fibre reinforced concrete itself, but also the complex interaction between steel fibre reinforced concrete and steel reinforcement to finally achieve an appropriate design code for construction application. Otherwise this material (SFRC) only remains as a phase of research.

In this research, strength degradation curve for joints [11], based on principal tensile stress, is used to analyse the behaviour and failure mode of SFRC joints. A previous formula to estimate joint shear strength [12], taking into account steel fibre properties such as the aspect ratio and the dosage of fibres, is modified for modern steel fibres. Through this analysis philosophy the relationship of the shear resistance capacity of concrete, steel fibres and

stirrups in the joint core is clearly shown, therefore the number of stirrups which may be replaced by a controlled dosage of steel fibre and the properties of steel fibre can be estimated.

1.5. Objectives of the Research

The objectives of this thesis are:

1. To experimentally investigate the behaviour of 2-D exterior beam-column joints reinforced with Dramix steel fibre under a simulated seismic load.

2. To investigate the shear resistance capacity of exterior joints reinforced with or without steel fibre and the behaviour of steel fibre reinforced concrete in the plastic hinge zone.

3. To develop a simplified analytical method and design procedure based on principle tensile/compression stresses in the joint region to account for the contribution of steel fibre in seismically-designed beam-column joints.

1.6. Organization of the Thesis

This thesis includes seven chapters and is organised as follows.

Chapter one introduces the background of this research project and the research significance. The objectives and scope of the research are also outlined.

Chapter two briefly outlines the material properties of high-performance fibre concretes and reviews previous work on steel fibre reinforced structural members. It mainly reviews previous work in the field of shear resistance capacity of SFRC beam-column joints.

In Chapter three, the analytical procedure to evaluate the fibre contribution to the joint shear of exterior beam-column joints, based on principle stresses shear strength degradation models, is introduced and discussed.

Chapter four describes the specimen details, along with test setup and loading regime characteristics. Theoretical procedures used during the data reduction process will also be explained.

Chapter five discusses and compares the experimental results with the findings of analytical work and provide a feasible analytical procedure and simplified equation for the use of steel fibre reinforced concrete in seismic joints design.

In chapter six, comparison of seismic performance of tested units between analytical and experimental results are carried out. In addition, models proposed for analysis of the behaviour of SFRC and non-liner dynamic analysis modelling of beam-column joints are briefly reviewed.

Based on the results of this research investigation, Chapter seven provide conclusive remarks and recommendations for further research.

CHAPTER TWO

2. LITERATURE REVIEW

2.1. Basics properties of fibre reinforced concrete

Conventional concrete made with portland cement is relatively strong in compression but weak in tension. It is the reason why reinforcing bars are used in concrete to overcome its weakness in tension. However, with the fibre technology developed, the weakness in tension can be partly surmounted by the inclusion of a sufficient volume of fibres. The concrete incorporated with sufficient fibres can improve the post-cracking behaviour of the fibre-matrix composites, thereby improving its toughness (**Figure 2-1**). Fibres are used in not only structural areas but also in other special applications such as reducing cracking, drying cracking, chemical resistance, abrasion resistance, and fire resistance. **Table 2-1** shows the different purposes for which fibres may be used.

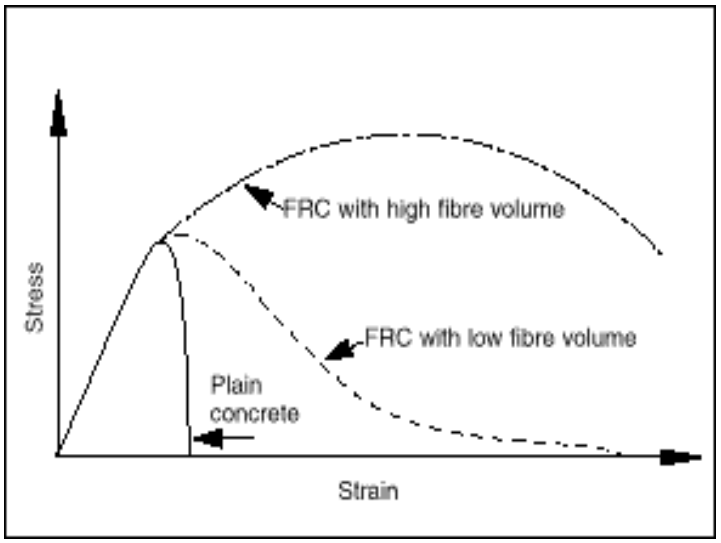

Figure 2 - 1: Typical load-deflection curves for fibre-reinforced concrete from [8]

Table 2 - 1: Uses for different types of fibre in concrete

Fibre Type	Application
Steel	Seismic-resistant structures, bridge decks, cellular concrete roofing units, pavement overlays, concrete pipe, airport runways, pressure vessels, tunnel linings, ship-hull construction.
Glass	Precast panels, small containers, sewer pipe, thin concrete shell roofs, wall plaster for concrete block. Agriculture, architectural cladding and components.
Carbon	Single and double curvature membrane structures, boat hulls, scaffold boards.
Polypropylene, nylon	Foundation piles, prestressed piles, facing panels, floatation units for walkways and moorings in marinas, road-patching material, heavyweight coatings for underwater pipes.
Asbestos	Sheet, pipe, boards, fireproofing and insulating materials, sewer pipes, corrugated and flat roofing sheets, wall lining.
Mica Flakes	Partially replace asbestos in cement boards, concrete pipe, repair materials.
Natural fibres	Roof tiles, corrugated sheets, pipes, silos and tanks.

2.1.1. Types of fibres

In this section, the most commonly used commercial fibres are introduced. The manufacture of these fibres, their properties and applications are briefly discussed. Steel fibres used in this research are mainly discussed in detail.

Glass fibres

Since the late 1960s, alkali-resistant glass fibres have been used for reinforcing cement because of their excellent engineering properties. Generally glass fibres have from 25 to 35 mm length. These fibres have high tensile strength (2 – 4 GPa) and elastic modulus (70 – 80 GPa) but have brittle stress-strain characteristics (breaking at 2.5 – 4.8% elongation). Claims have been made that up to 5% glass fibre by volume has been used successfully in sand-cement mortar without balling. However, the limitation of glass-fibre products is their durability because of loss of strength when exposed to outdoor environments. Therefore GRC has not been used in structural applications.

Carbon fibres

The use of carbon fibres is limited in commercial areas because of their expensive price compared with other types of fibres. Carbon fibres are generally manufactured from fibres

materials such as carbonizing suitable organic. Carbon fibres are normally classified to two types as either high modulus or high strength for their physical properties. Carbon fibres are continuous strands which are generally pre-placed with optimum orientation in concrete. Carbon fibre has high tensile strength and modulus of elasticity but has a brittle stress-strain characteristic.

Steel fibres

Steel fibres have been used in concrete since the early 1900s. The early fibres were round, straight, and smooth with cut or chopped lengths. These fibres have not been used in recent years and replaced by modern fibres because of their intrinsic shortages of property. Modern commercial steel fibres are manufactured from drawn steel wire with either rough surface, hooked (or paddled) ends or crimped through their length. The physical dimensions of modern steel fibres vary from 0.15 to 2 mm for equivalent diameters and from 10 to 75 mm for length. The fibres aspect ratio, defined as fibre length divided by its diameter (l_f / d_f), range from 20 to 100. Steel fibres have generally ductile stress-strain characteristics with the relatively higher tensile strength (0.5-2 GPa) and the high modulus of elasticity (200 GPa).

Synthetic fibres: nylon, acrylic, polyester, polyolefin and etc.

Synthetic fibres, accounted for half of all fibre usage, are manufactured from the petrochemical and textile industries. Although many classes of fibre based on synthetic polymers are available, four of those, being nylon, acrylic, polyester, and polyolefin, dominate the main market. The range of physical properties of some synthetic fibres is summarised in **Table 2 - 2**. Two kinds of physical fibre forms, monofilament fibres and fibres produced from fibrillated tape fibre, are used in a wide range of applications. The synthetic fibre volumes used in current applications are classified as low-volume percentage (0.1 to 0.3% by volume) and high-volume percentage (0.4 to 0.8% by volume). Most synthetic fibre applications use 0.1% fibres by volume, as this dosage does not reduce the strength of the concrete and yet enhances the crack control ability.

Natural fibres

Natural fibres are used because of its lower cost and low levels of energy using local manpower and technology. Natural fibre reinforced concrete is mainly used where conventional construction materials are too expensive or not available. Typically there are two kinds of natural fibres being used, processed natural fibres and unprocessed natural fibres.

Table 2 - 2: Selected synthetic fibre types and properties from [8]

Fibre type	Equivalent diameter µm	Relative density	Tensile strength MPa	Elastic modulus GPa	Ultimate elongation %	Ignition temperature °C	Melt, oxidation, or decomposition temperature °C	Water absorption per ASTM D 570, % by mass
Acrylic	13 - 104	1,16 - 1,18	270 - 1 000	14 - 19	7,5 - 50,0	-	220 - 235	1,0 - 2,5
Aramid I	12	1,44	2 900	60	4,4	high	480	4,3
Aramid II†	10	1,44	2 350	115	2,5	high	480	1,2
Carbon, PAN HM‡	8	1,6 - 1,7	2 500 - 3 000	380	0,5 - 0,7	high	400	nil
Carbon, PAN HT§	9	1,6 - 1,7	3 450 - 4 000	230	1,0 - 1,5	high	400	nil
Carbon, pitch GP**	10 - 13	1,6 - 1,7	480 - 790	27 - 35	2,0 - 2,4	high	400	3 - 7
Carbon, pitch HP††	9 - 18	1,8 - 2,15	1 500 - 3 100	150 - 480	0,5 - 1,1	high	500	nil
Nylon‡‡	23	1,14	970	5	20	-	200 - 220	2,8 - 5,0
Polyester	20	1,34 - 1,39	230 - 1 100	17	12 - 150	600	260	0,4
Polyethylene‡‡	25 - 1 000	0,92 - 0,96	75 - 590	5	3 - 80	-	130	nil
Polypropylene‡‡	-	0,90 - 0,91	140 - 700	3,5 - 4,8	15	600	165	nil

Notes

* Not all fibre types are currently used for commercial production of FRC

† High modulus

‡ Polyacrylonitrile based, high modulus

§ Polyacrylonitrile based, high tensile strength

** Isotropic pitch based, general purpose

†† Mesophase pitch based, high performance

‡‡ Data listed is only for fibres commercially available for FRC

Table 2 - 3: Typical properties of some of natural fibres from [8]

Fibre type	Coconut	Sisal	Sugar cane bagasse	Bamboo	Jute	Flax	Elephant grass	Water reed	Plantain	Musamba	Wood fibre (Kraft pulp)
Fibre length, mm	50 - 100	N/A	N/A	N/A	175 - 300	500	N/A	N/A	N/A	N/A	2,5 - 5,0
Fibre diameter, mm	0,1 - 0,4	N/A	0,2 - 0,4	0,05 - 0,4	0,1 - 0,2	N/A	N/A	N/A	N/A	N/A	0,025 - 0,075
Relative density	1,12 - 1,15	N/A	1,2 - 1,3	1,5	1,02 - 1,04	N/A	N/A	N/A	N/A	N/A	1,5
Modulus of elasticity, GPa	19 - 26	13 - 26	15 - 19	33 - 40	26 - 32	100	5	5	1,5	1,0	N/A
Ultimate tensile strength, MPa	120 - 200	275 - 570	180 - 290	350 - 500	250 - 350	1 000	180	70	90	80	700
Elongation at break, %	10 - 25	3 - 5	N/A	N/A	1,5 - 1,9	1,8 - 2,2	3,6	1,2	5,9	9,7	N/A
Water absorption, %	130 - 180	60 - 70	70 - 75	40 - 45	N/A	N/A	N/A	N/A	N/A	N/A	50 - 75

Notes

N/A Properties not readily available or not applicable.

Processed natural fibres are commonly obtained from natural material, mainly made from wood cellulose. Natural fibres have better mechanical properties compared with many synthetic fibres such as polyethylene and polyester. For example, cellulose fibres from selected grades of wood can be produced with tensile strengths up to approximately 2.0 GPa. However the properties of these fibres vary and depend mainly on the original material

properties and the chemical pulping process used to manufacture the fibres. Products made with unprocessed natural fibres such as coconut coir, sisal, and bamboo have been investigated by researchers. The properties of concrete incorporated with unprocessed natural fibres depend on many factors such as the fibre type and the volume fraction. However the long-term durability is the intrinsic problem of some of these products. The properties some of natural fibres are summarised in **Table 2 - 3**.

2.1.2. Steel fibre reinforced concrete

During the last three decades, steel fibres have been applied in pavement and shotcrete linings. However the use of steel fibre reinforced concrete (SFRC) in real seismic design is restricted because of the lack of validated design formulae and appropriate codes. Recently, a range of steel fibres and SFRC products are commercially available, and the use of steel fibre reinforced concretes (SFRC) in structures in seismic regions has developed progressively.

Steel fibre reinforced concrete is a concrete mix that contains discontinuous, discrete steel fibres that are randomly dispersed and uniformly distributed. The quality and quantity of steel fibres influence the mechanical properties of concrete. It is generally accepted that addition of steel fibres significantly increases tensile toughness and ductility, also slightly enhances the compressive strength (**Figure 2-2 and 2-3**). The benefits of using steel fibres become apparent after concrete cracking because the tensile stress is then redistributed to fibres (**Figure 2-4**). For structural design purpose less than 1% fibre dosage rates are not helpful to withstand stresses after significant cracking.

Workability

One of the problems of using SFRC is its workability. The workability of SFRC is affected by the workability of plain concrete, content of fibres used, and the fibre aspect ratio (l_f / d_f). Normally the workability of SFRC is improved by adding these admixtures, limiting the aggregate size and reducing the water to cement (w/c) ratio. Many researchers strongly recommend that the volume fraction of SFRC (V_f) be limited to 2.0% and the maximum aspect ratio (l_f / d_f) to 100.

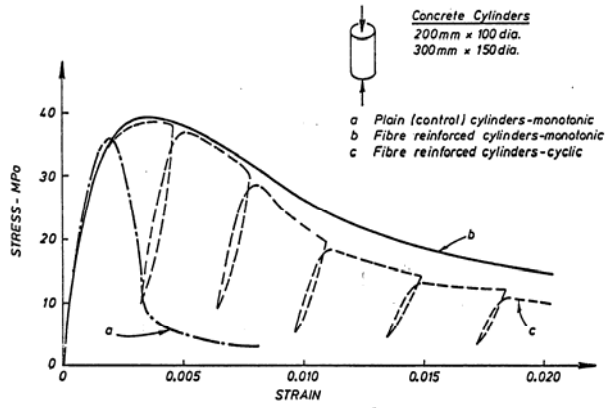

Figure 2 - 2: Compressive Stress-Strain Relationship from [13]

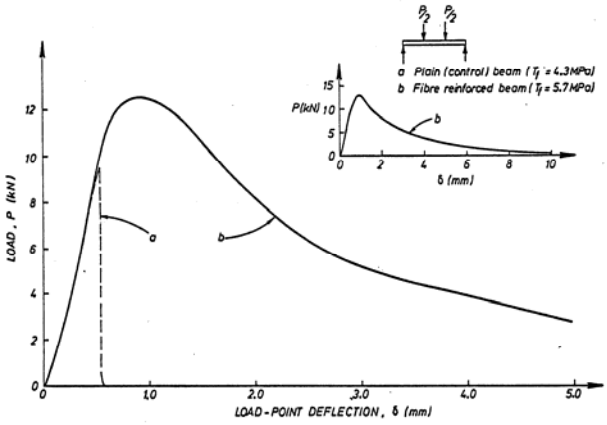

Figure 2 - 3: Flexural load-deflection relationship from [13]

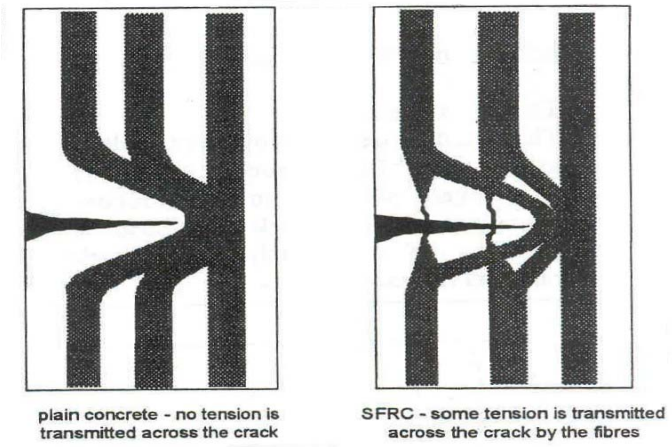

Figure 2 - 4: Stress Carrying Mechanism in SFRC

Fibre shapes

The shape and size of steel fibres vary widely in the world. Steel fibres used in structural areas are commonly restricted from 1.5 to 75mm in length and from 30 to 100 in aspect ratio. The cross section of steel fibres may be rectangular, circular, or round with different shapes/styles such as hooked, paddled, and crimped (illustrated in **Figure2-5**)

The concept of toughness

Toughness, the ability of the material to withstand large amounts of post-elastic strains and deformations before failure and resist the propagation of cracks, is an important characteristic to distinguish fibre reinforced concrete from plain concrete. It is normally defined as the area under a load-deflection or stress-strain curve in flexure. The comparison between SFRC and plain concrete specimens for typical load–deflection curves is shown in **Figure 2-6** [14]. From this Figure, it can be seen that the toughness of concrete can be significantly improved by adding fibres to concrete. The reason is that SFRC is able to sustain significant load after the fibre matrix is cracked and the load-deformation energy is dissipated through fibres pulling-out from matrix, thereby improving the toughness.

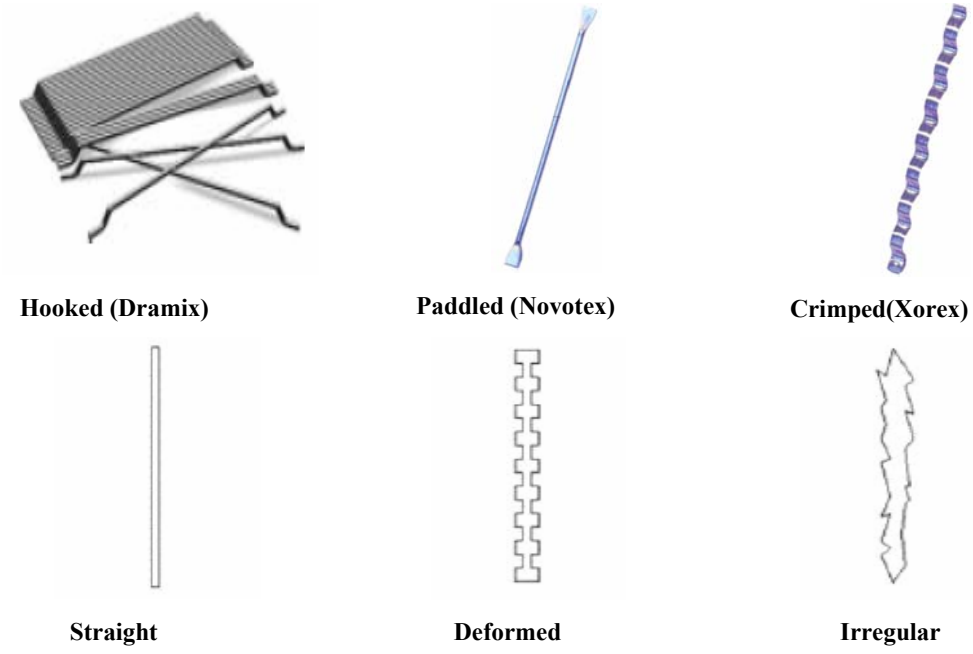

Figure 2 - 5: Shapes of steel fibres

Toughness index, a measure for evaluating the toughness of fibre reinforced composites, is defined in ASTM C 1018 [15]: *The toughness index is calculated as the area under the load–*

deflection curve up to the prescribed service deflection divided by the area under the load–deflection curve up to the first cracking deflection. Three indexes are described in ASTM C 1018: I_5, I_{10} and I_{30} corresponding respectively to deflections of 3, 5.5 and 15.5 times the deflection at first cracking [14].

An example of index values computed using a fixed deflection of 1.9 mm to define the test end point for a 100×100×350 mm beam are shown in **Figure 2-7** [9]. Examples of index values I_5, I_{10} and I_{30}, which can be computted for any size or shape of specimen, are shown in **Figure 2-8** [9]. It should be pointed out that factors such as the type of fibre, volume fraction of fibre, the aspect ratio, the fibre's surface deformation, and bond characteristics, which affect the ultimate flexural stength of SFRC, also influence the flexural toughness.

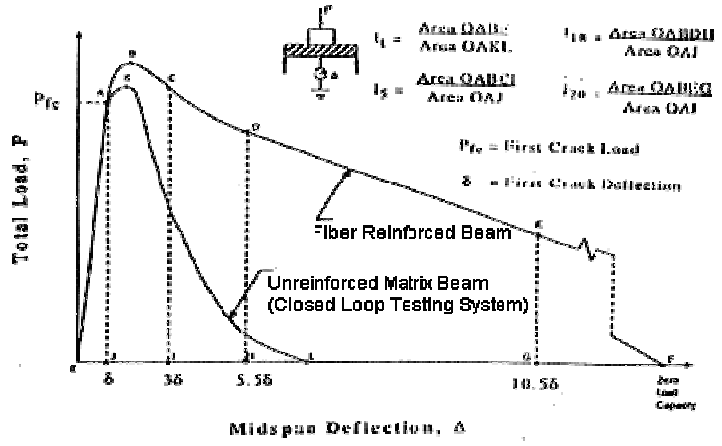

Figure 2 - 6: Toughness indexes from flexure load-deflection diagram from [14]

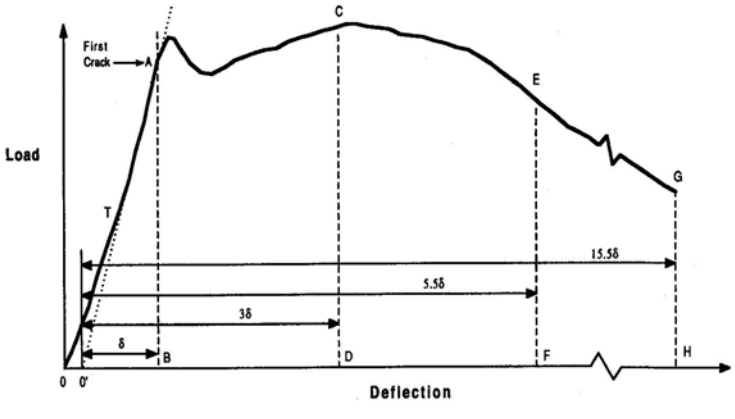

Figure 2 - 7: important characteristics of the load-deflection curve (ASTM C 1018) from [9]

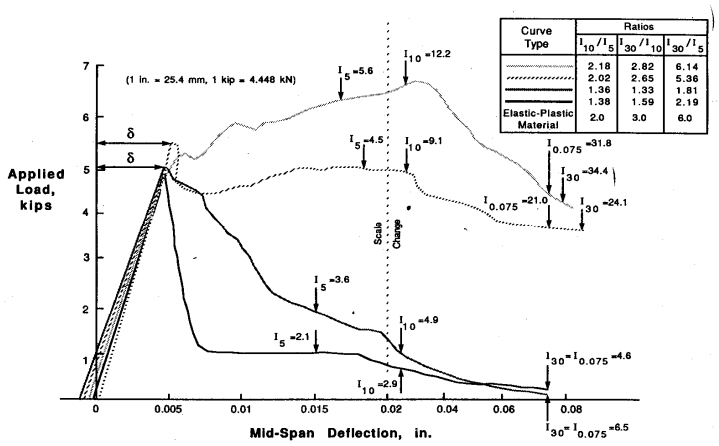

Figure 2 - 8: Load-deflection curves with different amounts and types of fibres from [9]

Compressive strength and failure

The effect of steel fibres on the compressive strength of concrete is variable (**Figure 2-9**). The range of increase is from negligible in most cases to 23% for concrete containing 2% by volume of fibre [9]. The compression stress-strain curves for steel fibre reinforced concrete showed that using steel fibres does not necessarily increase the peak stress dramatically, but the post-peak descending slope of SFRC is significantly less steep than that of plain concrete. These two curves also indicate the increase in toughness or ductility of SFRC, which also reflects the energy dissipation capacity.

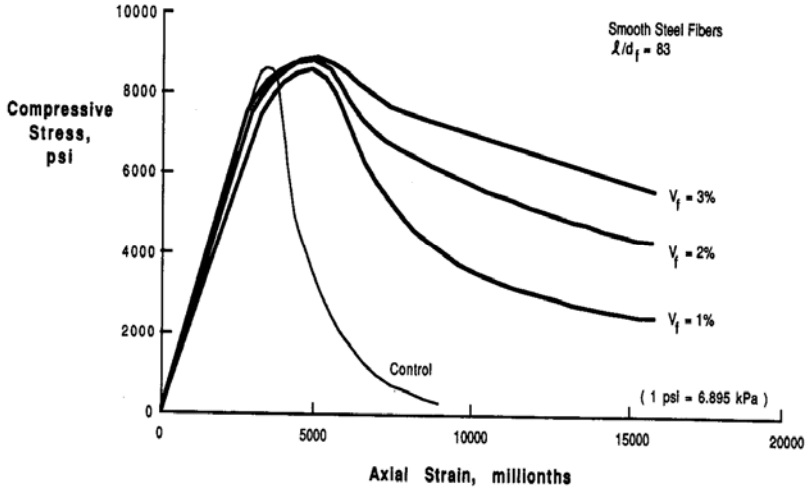

(a)

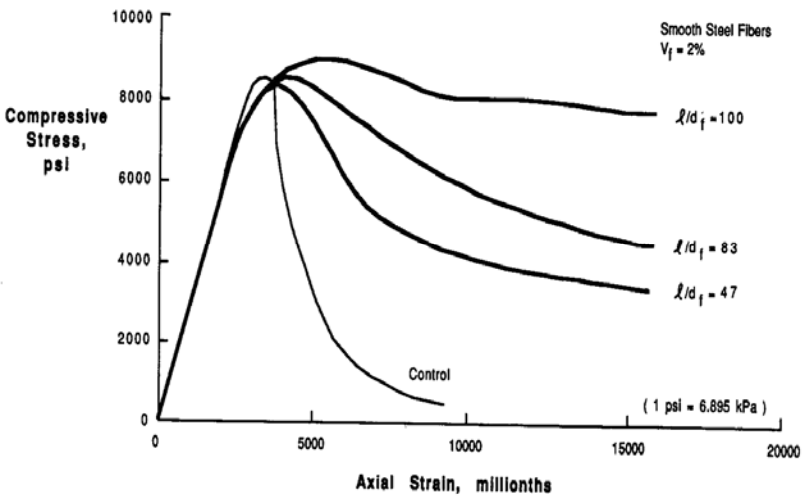

(b)

Figure 2 - 9: Influence of the steel fibre with different volume fraction and aspect ratio from [9]

Tensile strength

The stress-strain curve of fibre reinforced concrete in direct tension can not be exactly determined because of difficulty in conducting the standard tension test. Available observed curves vary, as the values depend on the size of specimen and method of testing. It is generally accepted that the strength of steel fibre reinforced concrete in direct tension is of the same order as that of normal concrete, i.e., 2 to 4 MPa. The toughness of FFRC is one to two orders of magnitude greater than that of unreinforced concrete, primarily because of the frictional and strain energy developed during fibre pull-out and the formation of multiple cracks when failure occurs [9].

Flexural strength

Compared with tensile and compressive strength, flexural strength is a more representative factor to indicate the influence of steel fibres on concrete. Previous studies have shown that *"ultimate flexural strength generally increases in relation to the product of fibre volume concentration* V_F *and aspect ratio* l_f / d_f. *Concentrations less than 0.5 volume percent of low aspect fibres have negligible effect on static strength properties. Prismatic fibres, or hooked or enlarged end (better anchorage) fibres, have produced flexural strength increasing over unreinforced matrices of as much as 100 percent"* [9].

Self-Compacting Fibre Reinforced Concrete (SCFRC)

Self compacting concrete (SCC) is made by using special admixtures to make a material which flows under its own weight, without compaction, into forms and around obstacles such as steel reinforcing. Since the special properties of Self compacting concrete were realized in the early 1988 in Japan, SCC has undergone research and development throughout South-East Asia, Europe, and North America throughout the 1990's [16] [17] [18].

The fibres affected the workability of the concrete, seen in the fact that slump doubled when fibres were removed from the mix. Many researches have proposed that the use of fibres in self compacting concrete was successful, with the self compacting mixes performing better overall than the normal concrete mix. This was due to alignment of the fibres and greater bond due to the different concrete microstructure [19] [20] [21].

2.2. Fibre reinforced concrete applied in structural members

As advantages of fibre reinforced concrete (FRC), FRC has been applied in flexural members to investigate the improving structural performance in many studies. Compared with conventional reinforced flexural members, FRC is characterized with relatively stable inelastic load-deformation behaviour and large deflection capacity [22]. The ductile deformation behaviour of FRC has significant effect on the structure integrity and helps structures to maintain stable inelastic deformations and assists stable steel yielding in order to utilize its energy dissipation (see **Figure 2-10**). Hence such advantages make comprehensive application for using FRC in some special applications of structure, such as retrofits, dampers, infill panels and plastic hinge region of structures.

Research by Fukuyama et al.

Since stiffness of steel structures is relatively lower that those of RC structures, stiffer dampers are normally used for reducing the seismic response. The topic of using high performance fibre reinforced cementitious composite (HPFRCC) dampers for structural control was investigated by Fukuyama et al. [22] in the year 2002. Three types of damper materials were used to combine with different bar arrangement (see **Figure 2-11**). They are normal mortar, PE-HPFRCC (mortar mixed with 1% polyethylene fibre cords by volumetric ratio) and PS-FPFRCC (mortar mixed with 1% polyethylene fibres and 1% steel cords by volumetric ratio). The test results showed that HPFRCC dampers presented increased

elemental ductility with decreasing damage and cracks. The HPFRCC dampers also exhibited steady hysteresis properties after suffering a larger deformation.

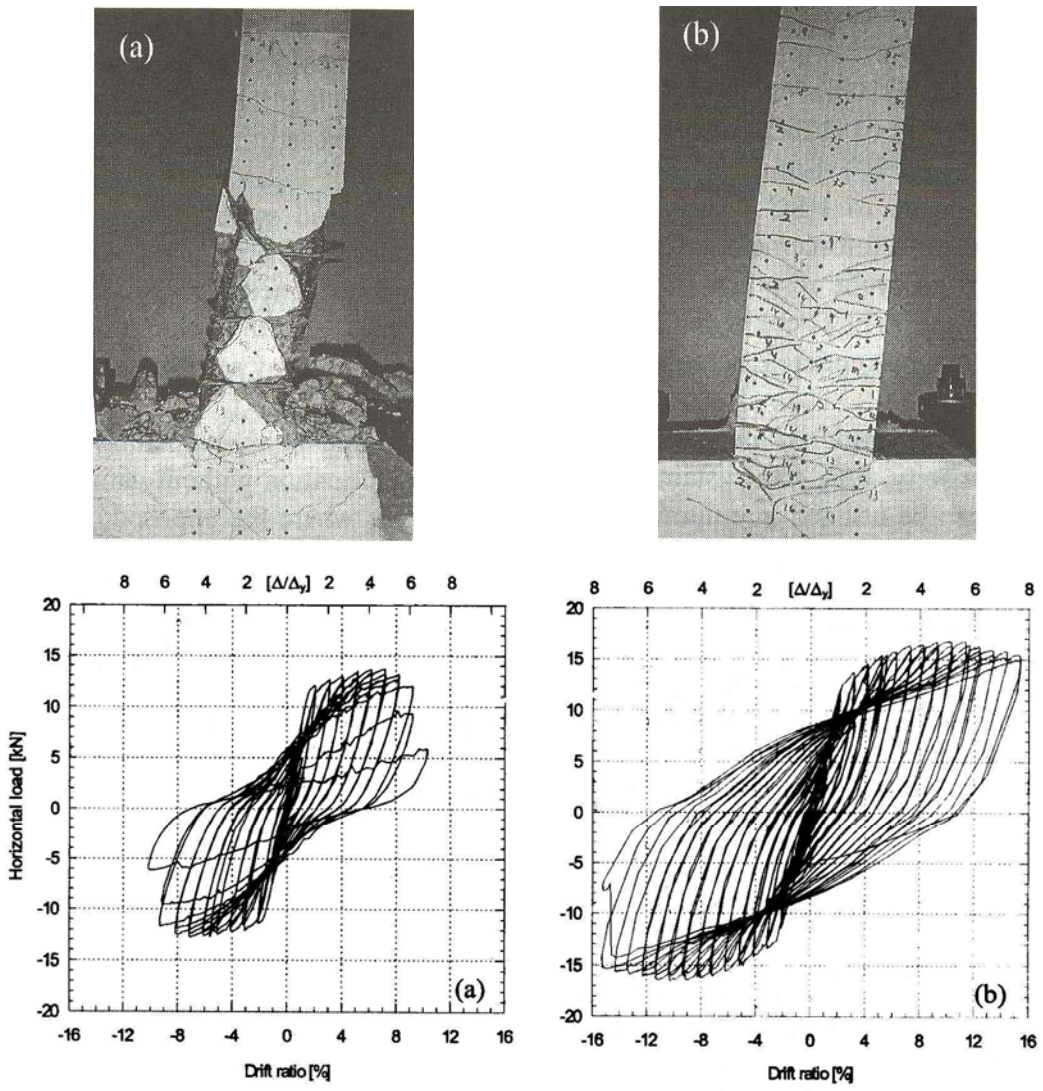

Figure 2 - 10: Damage behaviour and hysteresis loop (a) R/C, (b) R/FRC without stirrups from [22]

(Note: Even at high drift level, no spalling of the R/FRC was observed)

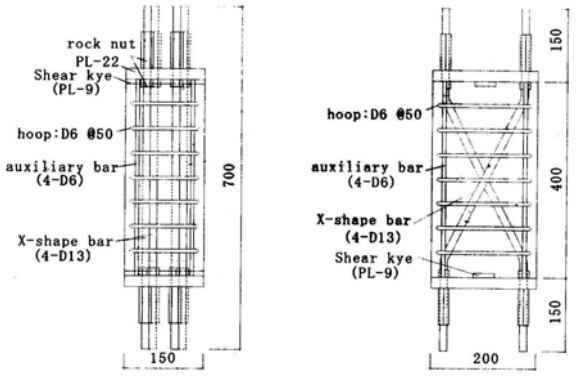

Figure 2 - 11: Configuration and bar arrangement of specimens from [22]

Research by Kesner and Billington

A new type of infill system, which was intended for use as a retrofit strategy in steel framed hospital structures, was investigated by Kesner and Billington [22] to evaluate the load-displacement response and energy dissipation of full-scale precast ductile fibre reinforced cementitious composite (DFRCC) panels under seismic loading. The infill system was precast DFRCC (2% fibre by volume) infill panels connecting with an existing structure through bolted and pre-tensioned connections. The behaviour of a single panel was tested with the setup shown in **Figure 2-12**. The test result demonstrated that as a consequence of pseudo-strain hardening response in tension of the reinforced DFRCC material, all of the DFRCC panels showed better response in the aspects of strength, drift capacity, and energy dissipation compared to the conventional reinforced concrete panel.

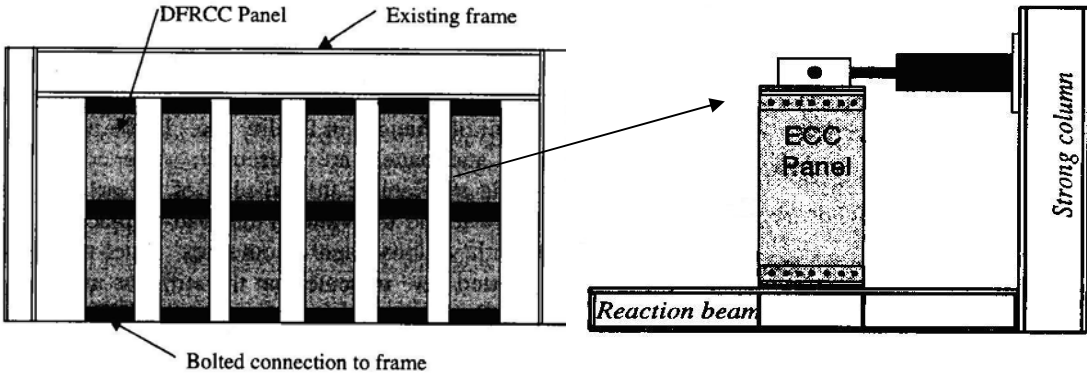

Figure 2 - 12: Schematic representation of DFRCC infill system from [22]

Research by Fischer et al.

Fischer et al. [22] published their results of research on flexural behaviour of ECC (Engineered Cementitious Composite) cantilever tests. The use of ECC, a class of ultra ductile fibre reinforced compendious composites, was investigated in this paper. The ECC matrix used in this study was 2%-vol. Polyvinyl alcohol (PVA) fibres and cementitious materials such as cements, limestone power, fly ash was employed to enhance the fresh properties of the mix. Four column specimens with 1400 mm height and square cross-sectional dimensions of 240 mm (**Figure 2-13**) were tested to determine the behaviour of different composite system columns under reversed cyclic loading. The specified axial loadings were also applied on the top of the columns to investigate the proper flexural load-deformation behaviour. Comparisons amongst results in four specimens were presented. The four different composite system columns were a steel reinforced concrete column (S-1), an FRP reinforced concrete column (S-2), a steel reinforced ECC column (S-3), and an FRP reinforced ECC column (S-4). The results showed that the performance of ECC specimens combined with either steel or FRP reinforcement were assessed with better load-deformation behaviour, higher energy dissipation capacity and more damage resisting evaluation. Furthermore, important findings in this study were that in the process of experiencing relatively large deformation reversals the steel reinforced ECC members with reduced transverse reinforcement showed an extraordinary ductile response reduction as well as reduced structural damage (**Figure 2-14**). Moreover, it was also found that the composite members (S-4) presented behaviour of elastic load-deformation response and small residual displacement.

Research by Billington and Yoon

The use of ECC in a precast segmental concrete bridge pier system (see **Figure 2-15**) at potential plastic hinge regions was investigated by Billington and Yoon in 2002. Small-scale cantilever columns with unbonded post-tensioning connecting with precast segments were conducted. ECC was used to replace conventional concrete in the plastic hinge of the columns to compare with conventional reinforced concrete columns. Four short and three tall specimens (380 mm and 685 mm tall respectively) with a similar cross-section (200 mm×200 mm) were tested under cyclic load (see **Figure 2-16**). For each high group, one convention reinforced concrete column was tested to compare the behaviour between the RC columns and ECC reinforced columns. Connecting joints between segments were either match-cast and

epoxy-filled or cast “loose-fit” and filled with an epoxy grout. The results showed that ECC reinforced columns reached higher peak loads at each drift cycle and exhibited higher energy dissipation up to drifts between 3 to 6% than conventional column specimens.

It was also found that the specimens, either short or tall, with deeply embedded ECC segments (76mm) exhibited better behaviour in all aspects compared to the specimens with less embedment of the ECC segments (38mm). Furthermore, the most important finding in this study was that when high compressive loads were applied to the top of specimens, ECC reinforced columns without any transverse confinement maintained their integrity better than the conventional RC columns and exceeded what was required for shear strength. Moreover the point must to be noted that the ECC material did not spall up to the end of testing (between 13.5 and 30% drift).

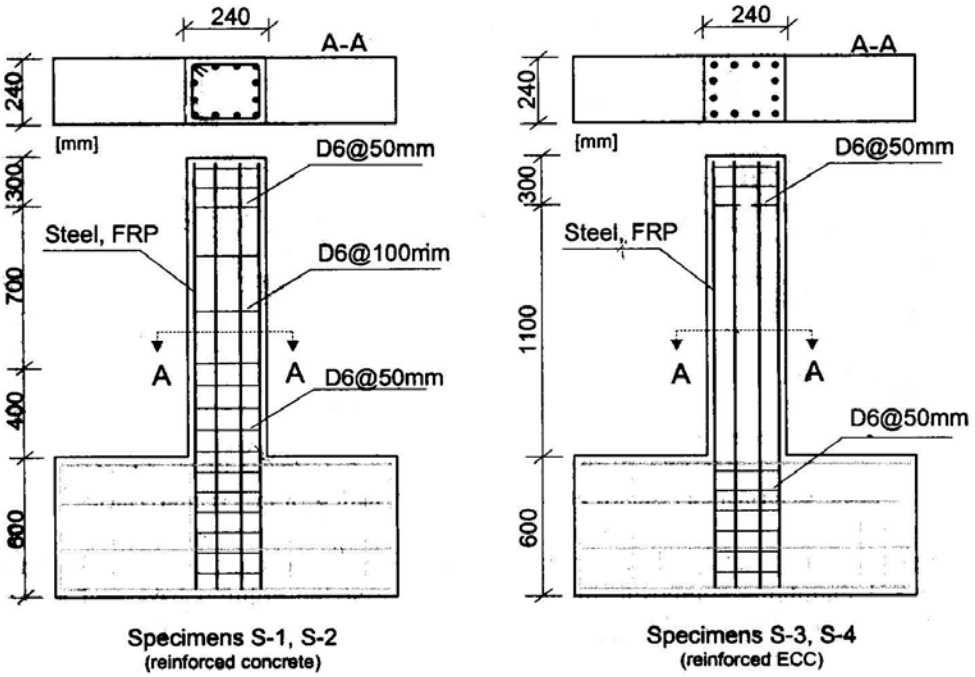

Figure 2 - 13: Specimen configurations [22]

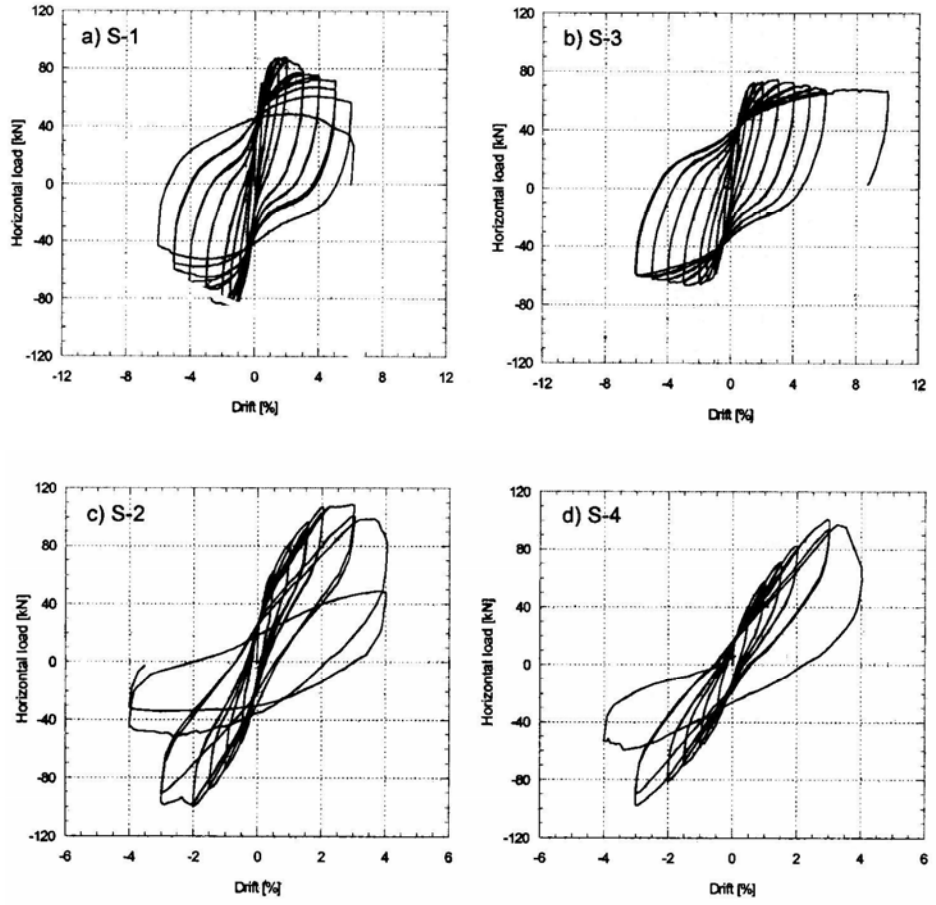

Figure 2 - 14: Load-deformation response from [22]

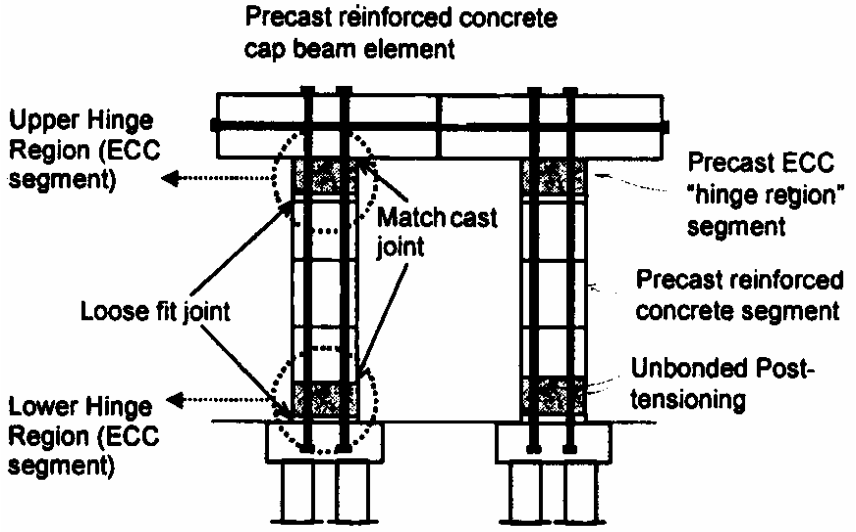

Figure 2 - 15: Precast segmental bridge pier system from [22]

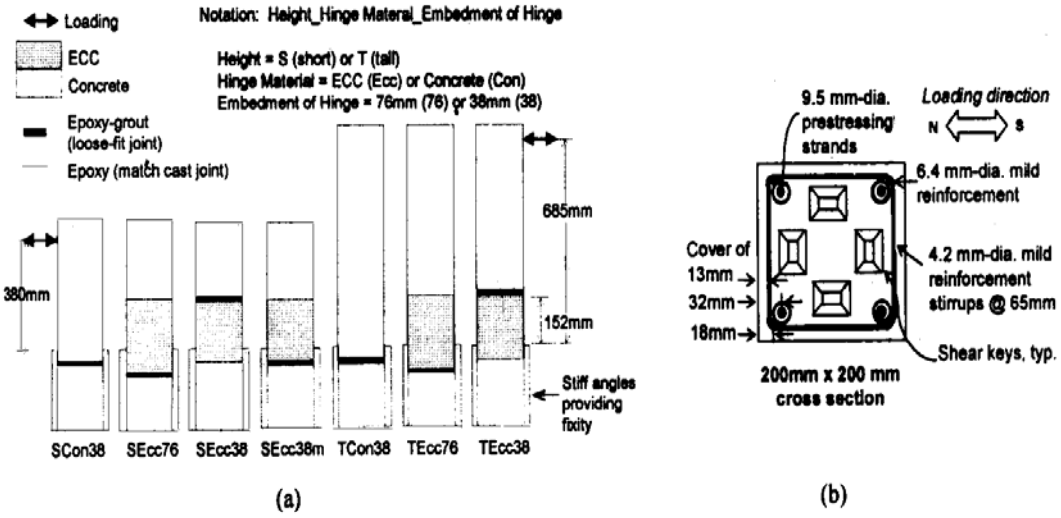

Figure 2 - 16: Schematic diagram of test specimens (a) elevation; (b) cross section from [22]

Research by Parra-Montesino

Recently several high-performance fiber-reinforced cement composites (HPFRCC) materials have been evaluated for use in earthquake-resistant structures including beam-column connections, low-rise walls, and coupling beams by Parra-Montesinos at the University of Michigan. These researches discussed the potential of HPFRCC for use in earthquake resistant structures.

In 2000, to investigate the seismic behaviour of beams after increasing hoops spacing and evaluate the potential of HPFRCC materials as a replacement of joint transverse reinforcement, Parra-Montesinos and Wight tested a 3/4-scale exterior beam-column subassembly under large displacement reversals. **Figure 2-17** shows the shear force versus shear deformation response of the connection and the joint condition at the end of the test, respectively. The result indicated that *'the specimen with ECC material exhibited a large number of hairline diagonal cracks with little damage at the end of the test (5.0% drift). In terms of shear distortion response (Fig. 7(b)), it is clear that the ECC connection exhibited excellent performance during the test, even though no transverse steel reinforcement was used in the connection region.'* [23]

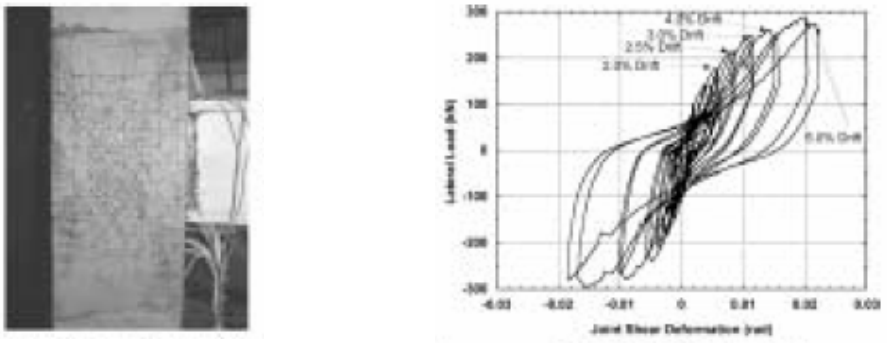

Figure 2 - 17: Behavior of hybrid RCS connection constructed with engineered cementitious composite ECC material from [23]

In 2003, Kim and Parra- Montesinos proposed their experimental results of HPFRCC low-rise walls under the large displacement reversals loading. Two low-rise walls with a shear span-to-depth ratio of 1.5 were constructed. One wall contained 1.5% PE fibers (by volume), while the HPFRCC in the other wall contained a 2.0% volume fraction of hooked steel fibers. To evaluate wall shear distortion capacity and contribution of fibers to shear strength, both of tested walls were designed to fail by a shear diagonal tension mechanism with limited flexural yielding. **Figure 2-18** shows the observed damage during testing and seismic behaviour of HPRCC low-rise walls. The results showed that '*It is worth mentioning that even though the hysteretic behavior of both wall specimens was nearly identical, the HPFRCC wall with PE fibers exhibited a larger number of cracks of smaller width and larger damage tolerance compared to the wall with hooked steel fibers.'* [24]

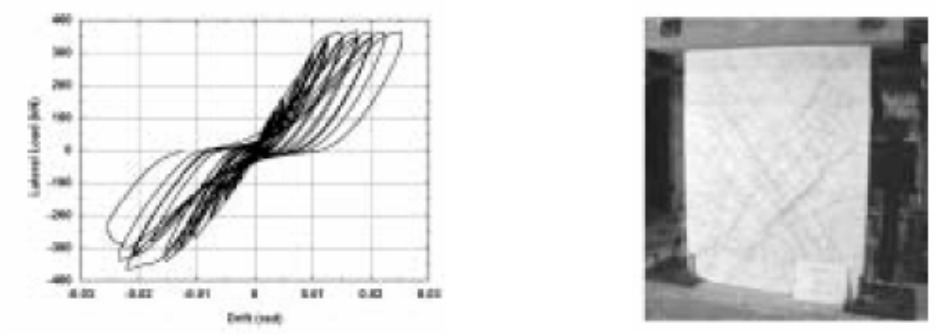

Figure 2 - 18: Seismic behaviour of HPFRCC low-rise walls from [24]

In 2005, to eliminate the need for transverse reinforcement around the main diagonal bars, two specimens were constructed and tested by Canbolat, Parra-Montesinos, and Wight. One specimen was reinforced with 2.0% PE fibers by volume, and the other was reinforced with 1.5% twisted steel fibers by volume. **Figure 2-19** shows the reinforcement detail and seismic behaviour of tested HPFRCC coupling beams. The results showed *'It should be mentioned that the HPFRCC material was effective in preventing buckling of the diagonal bars, even after damage localization occurred.'* [25]

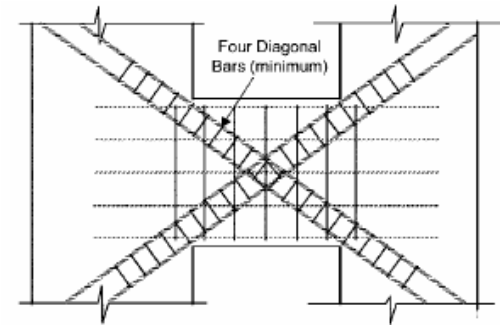

(a) Reinforcement detail in RC coupling beams

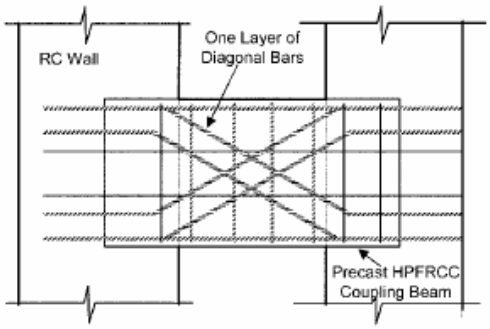

(b) Reinforcement detail in HPFRCC coupling beams

a) Cracking Pattern at 2.0% Drift

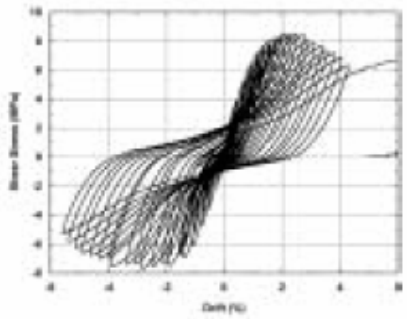

b) Average Shear Stress versus Drift Response

(c) seismic behaviour of HPFRCC coupling beams

Figure 2 - 19: Reinforcement detail beams and seismic behaviour of tested coupling beams from [25]

2.3. Steel fibre reinforced concrete applied in structural members

Recently an increasing number of projects with structural elements reinforced with steel fibre have been reported. The structural members made of ordinary concrete show a good compression behaviour but poor tension behaviour because of their brittle material property. The addition of steel fibres to plain concrete can change its mechanical properties. Taking into account the advantages of steel fibre reinforced concrete demonstrated above, steel fibres are supposed to be an alternative material to ordinary steel reinforcement. In both side, under service and ultimate loading conditions, fibre reinforcement are expected to carry tensile loads.

Depending on the type and amount of fibres, an increase in ductility and better cracking behaviour can be achieved. Especially by the use of steel wire fibres, remarkable stresses can be transferred across cracks. The fibre itself can be seen as a kind of reinforcement. A verification concept for SFRC structural members can be derived from this principle.

2.3.1. Steel fibre reinforced concrete applied in beams

Flexure in beams

SFRC can sustain higher ultimate load than plain concrete can and SFRC also shows improved ductility. The reasons for the improvement in flexural strength can be illustrated by the stress block (see **Figure 2-20**), in which it is shown that SFRC has extra tensile strength which does not exist in the plain concrete. This method of static flexural analysis of beams reinforced by steel bars and fibres has been developed by Henager and Doherty [9]. In this method, the contribution of steel bars and steel fibre for tensile strength are both considered for predicting the ultimate moment. The basic assumptions that have been made are shown in **Figure 2-20**. The equation for the nominal moment M_n of a singly reinforced steel fibrous concrete beam is:

$$M_n = A_s f_y \left(d - \frac{a}{2}\right) + \sigma_t b (h - e)\left(\frac{h}{2} + \frac{e}{2} - \frac{a}{2}\right) \qquad (2.1)$$

where:

$$e = [\varepsilon_s(fibers) + 0.003] \cdot \frac{c}{0.003} \qquad (2.2)$$

$$\sigma_t = 0{,}00772\, l/d_f\, \rho_f\, F_{bu} \qquad \text{[MPa]}$$

It has to be noted that the value of ultimate compressive strain in the extreme concrete fibre may exceed 0.003. It is mentioned in some reports that "*0.0033 may be more realistic for steel fibre concrete. Swamy and Al-Ta'an recommend 0.0035. Based on a study of plastic hinges, Hassoun and Sahebjam recommend a failure strain of 0.0035 for concrete with 1.0 percent steel fibres, and 0.004 for 1 to 3 percent fibres"* [9].

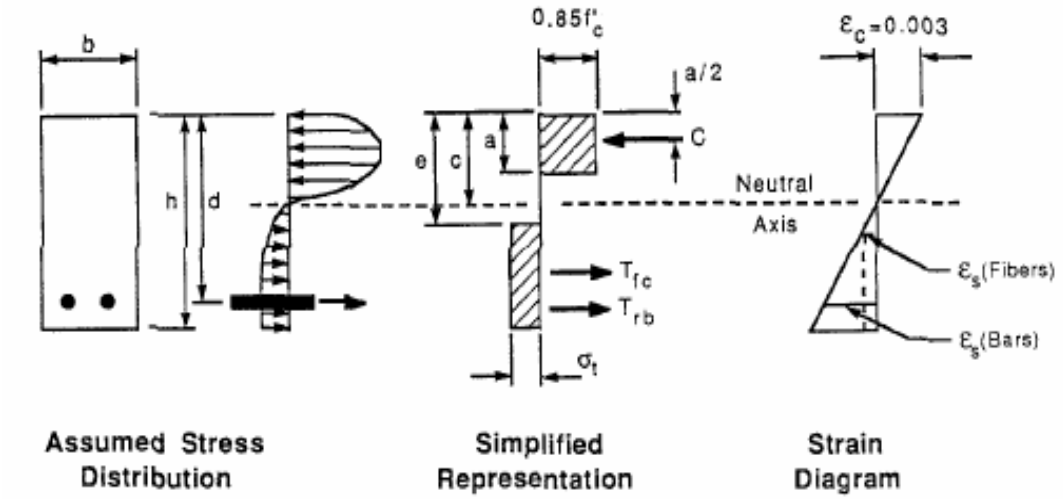

Figure 2 - 20: Design assumptions of singly reinforced concrete beams containing steel fibres from [9]

Shear behaviour in beams

Numerous investigations have been reported about the shear behaviour of SFRC beams. Some of these include Swamy and Bahia [26], Sharma [27], Mansur et al. [28], Ashour et al. [29], Tan et al. [30], Narayanan [31]. In these papers, factors affecting the shear behaviour of steel fibre reinforced concrete beams were studied. In brief, the results of these investigations showed that fibre reinforcement can reduce the needed amount of shear stirrups and that the combination of fibres and stirrups may accomplish the strength requirement as well as the ductility requirement. The ultimate shear strength of beams with stirrups and fibres showed significant improvement compared with the companion beams without fibres. It was found that the combination of 75% of full conventional stirrups with 1% steel fibre volume contents gives the same ultimate shear strength as the conventional beam, and that the combination of 50% of full conventional stirrups with 2% fibre contents also gives almost similar shear resistance to the beam with full stirrups without fibres [32]. The increase of shear strength due to fibres became lager for the beams with less shear stirrups. It was also concluded that short steel fibres in the concrete mix provides effective shear reinforcement and tends to change the

mode of failure from shear to flexure [28]. Moreover, for the cracking control capacity, the use of steel fibre in beams was seen to be reduced to a fifth of that in the companion beams with or without stirrups because of the uniform redistribution of stresses [31], especially for the first shear cracking. Furthermore fibre reinforced concrete beams also showed a better ductility and a significant energy absorption capacity [27].

The SFRC beams also showed an enhanced flexural strength, about 55% when the fibre content increased to two percent [32]. For the bending behaviour of SFRC beams, it was also concluded that curvature decreased with an increase in fibre content, thus indicating the stiffening of the beams with the inclusion of fibres [31].

2.3.2. Steel fibre reinforced concrete applied in slab

Research by Falkner and Gossla

Falkner and Gossla reported the result of three different SFRC flat slabs with different reinforcing conceptions, SFRC, SFRC incorporated rebar, and prestressed SFRC, under the large scale loading experiments (see **Figure 2-21**). The steel fibres used were (0.5% by volume) Dramix steel fibres with a length of 60 mm and a diameter of 0.75 mm.

The slabs were supported on 9 rigid columns, which could simulate uneven settlements, and loaded by four centre point. The result showed that all slab tests failed in bending. Although the SFRC slab failed with lower strength after developing a yield line mechanism, ductile behaviour was observed in the slab with reinforcement and those with unbonded prestressing. Though the increase of total reinforcement ratio by the rebars was only 20% compared to the SFRC slab, the cracks in the critical zones were controlled. For the slab with unbonded prestressing, the crack control could be achieved due to an increase in the toughness ratio of SFRC. Nevertheless, the load was mainly carried by SFRC in the yield lines, which were almost the same as in the SFRC slab [33].

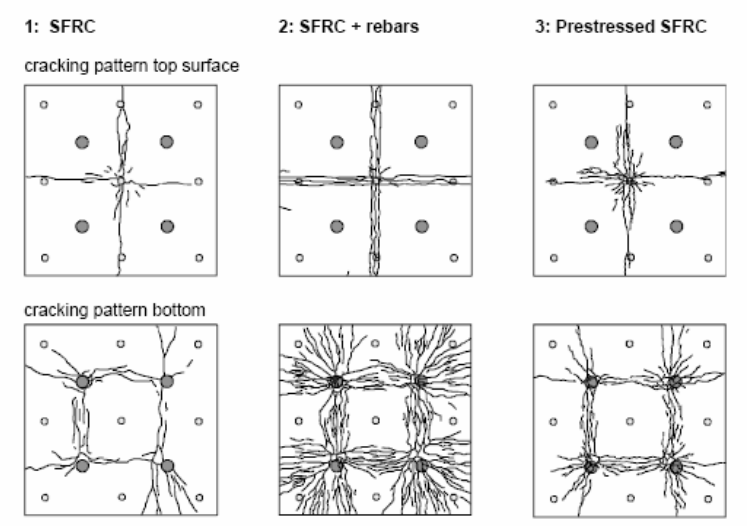

Figure 2 - 21: Cracking pattern and load deflection curve of the three different slab systems from [33]

2.3.3. Steel fibre reinforced concrete applied in seismic beam-column joints

2.3.3.1 Shear resistance capacity

The beam-column joint region is a very important area in seismic-resistant frame; especially for the exterior T joints as they carry larger shear forces compared with interior joints. During an earthquake, large lateral forces apply on the side of the building and the shear forces caused by longitudinal beam steel bar penetrate into joint core. The shear force may cause a corner to corner diagonal tension failure. Joints not designed to resist high shear, such as pre-70's beam column joints, are likely to undergo shear failure in joints. Well confined joints show a better behaviour, but the stirrups and hoops in joint area may cause steel congestion.

Considering the advantages of steel fibre reinforced concrete described earlier, such as high energy absorption capacity, improved tensile strength and damage tolerance of concrete, using steel fibres in beam column joints may be an effective method for relaxing the stirrup congestion and improving the shear capacity of joints in seismic resistance frames.

Research by Stevenson

In 1980, two interior beam-column joint assemblies and two beam assemblies cast with column-stubs at midspan were tested under quasi-static cyclic load to investigate the shear force resistance of steel fibre reinforced joints and flexure behaviour of steel fibre reinforced concrete in the beam plastic hinge region. [13] One of the interior beam-column joints was a conventional joint designed by seismic design code (draft SANZ concrete design DZ3101).

The other one had the same dimension as the conventional one, but with steel fibre reinforced concrete and no shear reinforcement in the joint region. For the two beam assemblies of 2667 mm and 1143 mm length respectively, the reinforcement was the same as the beam of the beam-column joint, but steel fibres were used in the beam plastic hinge area to replace all lateral reinforcement (**Figure 2-22**). All units were designed to form the plastic hinge adjacent to the connections. The steel fibre used was 18 mm long with a cross-section of 0.6×0.3 mm. The amount of fibres was adapted to 2.3% by volume. It should be noticed that the reinforcement reduction ratio in both joint and beam plastic hinge region was 100%.

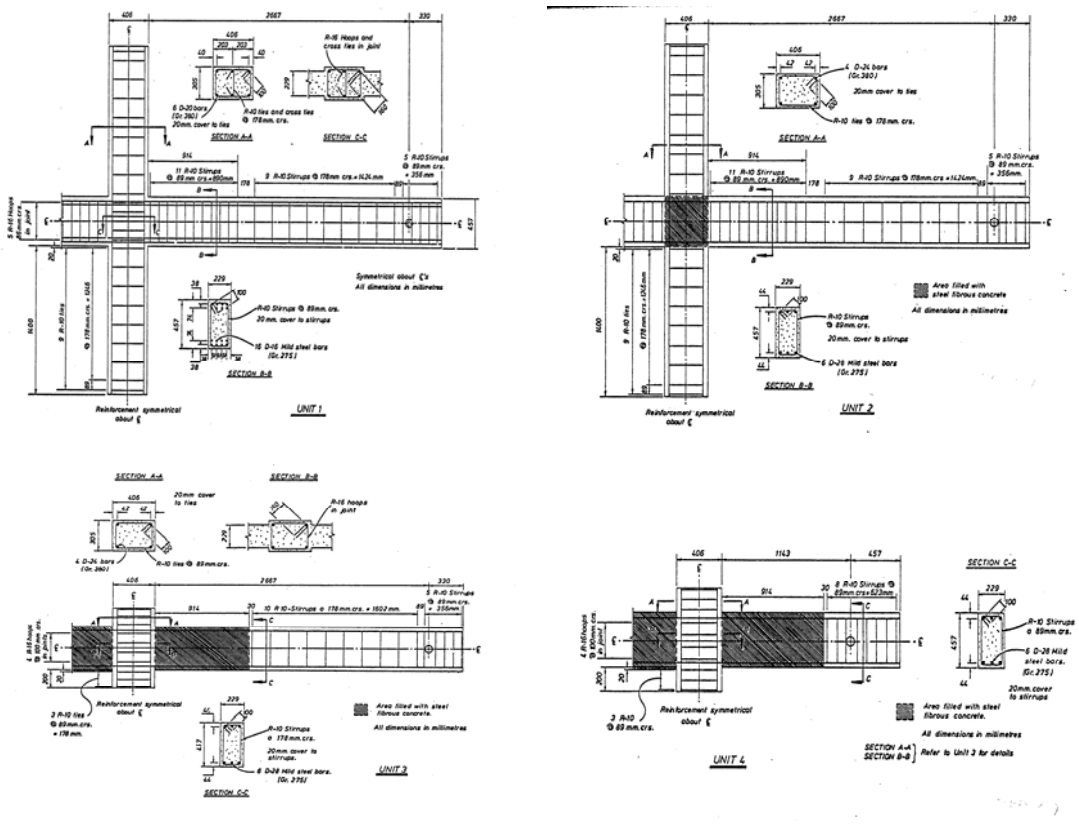

Figure 2 - 22: The details of the research from [13]

It was found that using steel fibre alone without any shear reinforcement was not able to prevent the joint shear failure and was inadequate to prevent buckling of the reinforcing bars. It was also found that in compression, even after significant flexural yielding, the steel fibre confinement was deteriorated rapidly. The conventional unit designed by seismic design code (draft SANZ concrete design DZ3101) showed that adequate horizontal shear reinforcement was necessary to provide high level shear resistance under intense seismic loading.

Research by Tang et al.

In 1992, Tang et al. published results of SFRC Joint tests [12]. In their laboratory five exterior joints and 7 interior joints were constructed and tested under reverse cyclic loading (**Figure 2-23**)**.** Two types of steel fibres were used in their test. The first was of rectangular cross-section with dimensions of 0.4×0.4 - 0.5×0.5 mm by shearing a thin low-carbon steel plate. The length of these fibres was 25-30 mm and aspect ratio was 54-62. Another was cut wire fibre manufactured by cutting round high strength steel wire which had the diameter of 0.7-0.8 mm with 50-55 mm length and aspect ratio of 66-75. A formula for determining the contribution of the shear resistance of steel fibres in the joint was given in this research.

$$V_f = 2\frac{l_f}{d_f}\rho_f A_j \qquad (2.3)$$

The results showed that using steel fibres can significantly increase the joint shear strength and also the shear stress corresponding to the first crack. It was also found that in exterior joint tests the problem of bar slip in the SFRC joint was significantly less than that in the RC joint; the slip reduced from 0.8 mm (RC) to 0.46 mm (SFRC). In interior joints tested, the steel fibres provided a better bond capacity and improved the bar anchorage capacity.

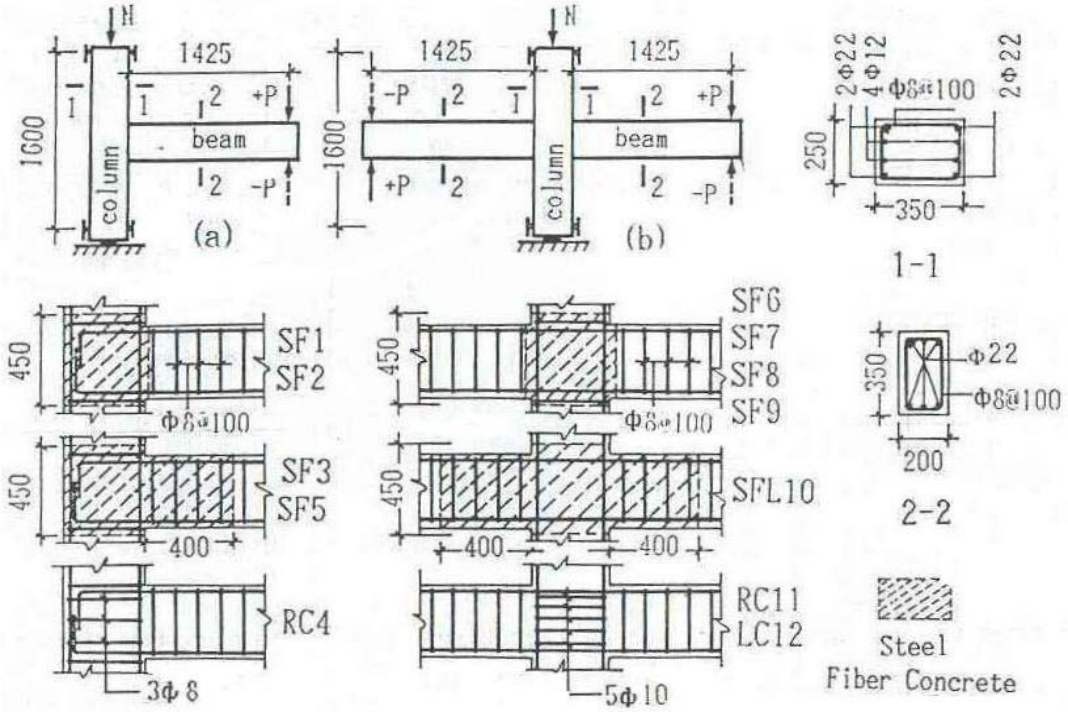

Figure 2 - 23: Details and types of test specimens from [12]

Research by Gefken and Ramey

Similar results were found by Gefken and Ramey in 1989. They also conclude that using steel fibres in reinforced concrete not only increased joint hoop spacing but also exhibited the same or better ductility compared with conventional concrete specimens [34]. Steel fibres with two different tensile strengths (2069 MPa and 2758 MPa) were used in the specimens. Both types of fibre were straight steel brass-coated fibres with 25 mm length and 0.41 mm diameter. Ten specimens were constructed (**Figure 2-24**) with the same steel fibre content (2% by volume) in the joint region. The specimens were divided into two groups for two different intensities of seismic loading. The ductility, ultimate strength, first cracking width, first crushing width and joint stiffness of conventional concrete specimens were compared with those of specimens with steel fibres and larger joint hoop spacing specimens. The result showed that compared with conventional concrete specimens the fibre reinforced concrete specimens with increased joint hoop spacing demonstrated the same or better ductility and higher ultimate and final strength. However the width of first cracking was 50 percent wider than that in conventional concrete joints.

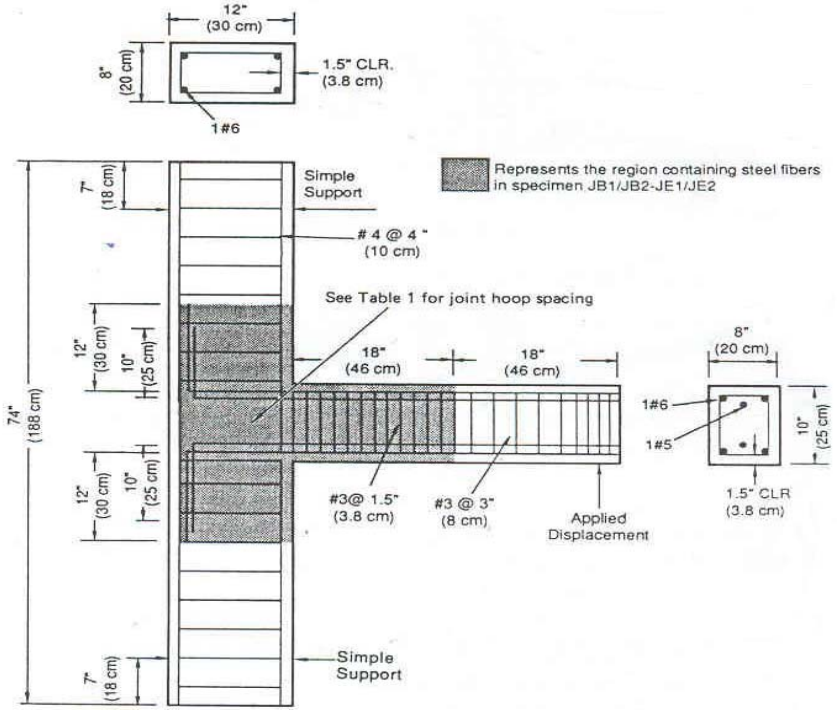

Figure 2 - 24: Test beam-column specimen detail from [34]

Research by Filiatrault et al.

The research result published by Filiatrault et al. [35] showed that performance of a SFRC joint can be influenced by the physical properties of the fibres, such as the volume content and aspect ratio of the steel fibres. Four full scale exterior beam-column joints were tested under cyclic reverse loading (**Figure 2-25**). The first two were normal concrete specimens. One of which ignored the seismic recommendations and the other followed the full seismic design recommended by National Building Code of Canada. Another two were similar to the first non-seismic detail specimen but using hooked-end steel fibres in the joint region with different percentage of steel fibres by volume (1% and 1.6%) and different aspect ratio (l_f / d_f) of steel fibres (60 and 100 respectively). Results showed that compared with the joint reinforced by the steel fibre with less amount (1%) and lower aspect ratio (60), the joint reinforced by a higher volume ratio of fibres (1.6%) with a larger aspect ratio (100) exhibited significant improvement in joint shear strength resistance capacity and changed the failure mode form joint shear failure to beam plastic hinge failure. It was also observed that adding a reasonable amount of steel fibres in a beam-column joint not only reduced the lateral reinforcement and provided adequate ductility but also provided virtually identical energy dissipation capacity to the ones reinforced by full seismic reinforcement.

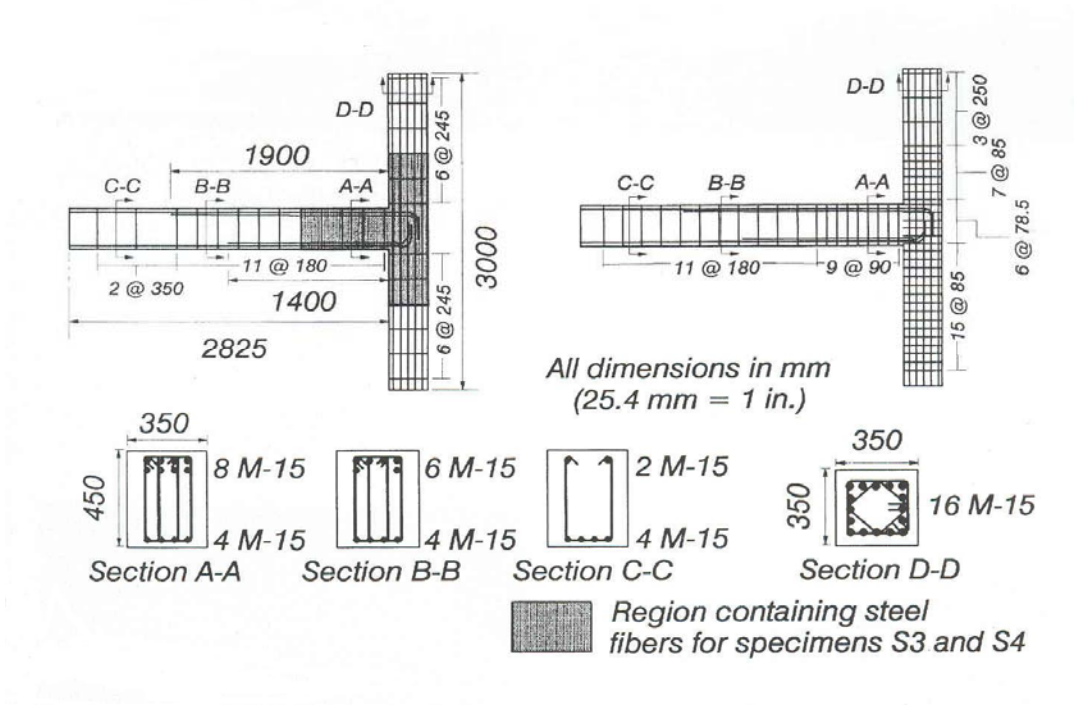

Figure 2 - 25: Detail of test specimens from [35]

Research by Filiatrault et al.

Interior SFRC joints were tested by Filiatrault et al. in 1995 [36] to investigate the performance of internal joints reinforced by steel fibres. Three full-scale internal joints were made: The first one was the normal concrete internal joint without seismic reinforcement in the beams, column and joint (**Figure 2-26**). The second one was the normal concrete joint with well designed seismic reinforcement. The last one was similar to the first one, but had hook-end steel fibre (50mm length and 0.5 mm in diameter) to replace the seismic reinforcement to achieve similar seismic behaviour to the second one. Displacement controlled reversed cyclic loading was applied to the specimens. It was found that the steel fibre reinforced specimen had the highest shear strength amongst the three specimens and provided adequate ductility and energy dissipation capacity.

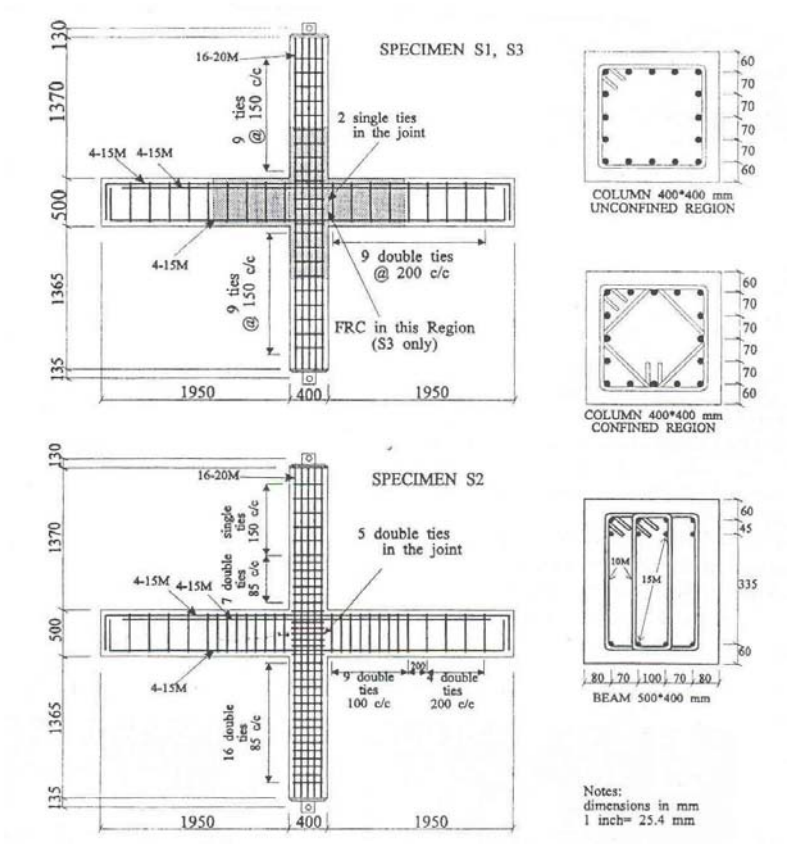

Figure 2 - 26: Test specimens from [36]

Research by Shannag

In 2005, Shannag published his experimental result [37]. Six 1/3-scale beam–column joint specimens were constructed to represent the case of existing old Jordanian buildings which were designed for gravity loads according to ACI code (**Figure 2-27**). One specimen

simulated the non-seismic reinforcement as the part of existing practice. The other specimen was constructed with seismic reinforcement detail. The last four specimens used high performance steel fibre reinforced concrete which contained brass-coated or hooked steel fibres with 2% or 4% by volume in the joint regions. All six specimens were tested under cyclic load and several comparisons were done amongst the tested results to determine the effect of using high performance steel fibre in the seismic joints. From the comparisons, it was found that: (1) using steel fibre in the non-seismically designed beam-column joint was useful to improve the seismic behaviour of the joint, such as higher joint strength, higher displacement and ductility, better energy dissipation, and slower stiffness degradation; (2) the specimens with hooked-end steel fibre reinforced concrete showed better behaviour compared with those reinforced with brass-coated fibre because of the better bond strength of hooked steel fibres.

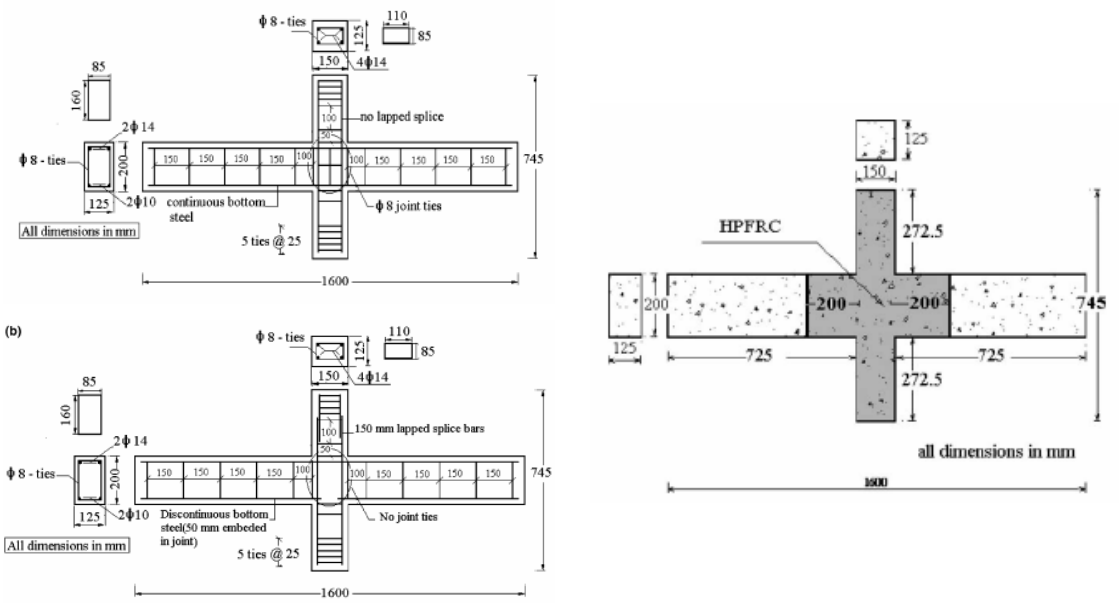

Figure 2 - 27: Details of the test specimens from [37]

2.3.3.2 Reduction of lateral reinforcement

Research by Bayasi and Gebman

The effective application of steel fibres in the joint region under seismic loading has been researched in the last three decades. The main purpose of the researches are to use the advantages of steel fibres to improve the seismic resistance capacity of the joint or/and to

reduce the number of hoops in the joint region. A summary of using steel fibres to reduce lateral reinforcement in seismic beam-column joint was published by Bayasi and Gebman in 2002 [38]. The summary showed a comprehensive comparison amongst results of research on using steel fibres in seismic joints to increase hoop spacing. The range of the amount of steel fibres used between 0 and 2.0% (by volume) for steel fibres aspect ratios (l_f / d_f) ranging between 1.0 and 1.6. Hoops spacing and lateral reinforcement of joints reduced from 50% to more than 200%. The comparison of the available test data is shown in **Table 2-4** and in the column graph (**Figure 2-28**). From the available data on using steel fibres to reduce the lateral reinforcement while keeping joint behaviour as good as the conventional joint with seismic reinforcement, it was summarized that the reduction of lateral reinforcement are between 40% and 100% and the fibre reinforcement index, $V_f \cdot (l_f / d_f)$, is in the range between 0.74 to 2. The adequate amount of steel fibres to be added in joints was suggested to be not less than 1% (by volume) and at least 1.5% (by volume) was strongly recommended for a significant reduction of lateral reinforcement in seismic joints.

Table 2 - 4: Summary of available data using steel fibres in place of hoops in seismic beam-column joints from [38]

Series No.	Lateral Reinforcement Ratio (LRR), Av/bws,%	Lateral Reinforcement Reduction Ratio (LRRR), %	Reduction (R) ,%	Fibre Volume , %	Fibre Length (l), mm	Fibre Reinforcement Index, V_f(l/d)
1	3.1	3.1	100	1.7	38	1.28
2	0.2	0.12	60	2	25	2
3	0.36	0.2988	83	1	32	1
4	0.47	0.282	60	1	28	0.74
5	1.38	0.552	40	2	25	1.2
6	0.63	0.63	100	1.5	41	1.13
7	0.87	0.87	100	1.5	45	1.77
8	1.14	1.14	100	1.6	50	1.6
9	0.12	0.0876	73	1.6	50	1.6
10	0.55	0.275	50	2	30	1.2

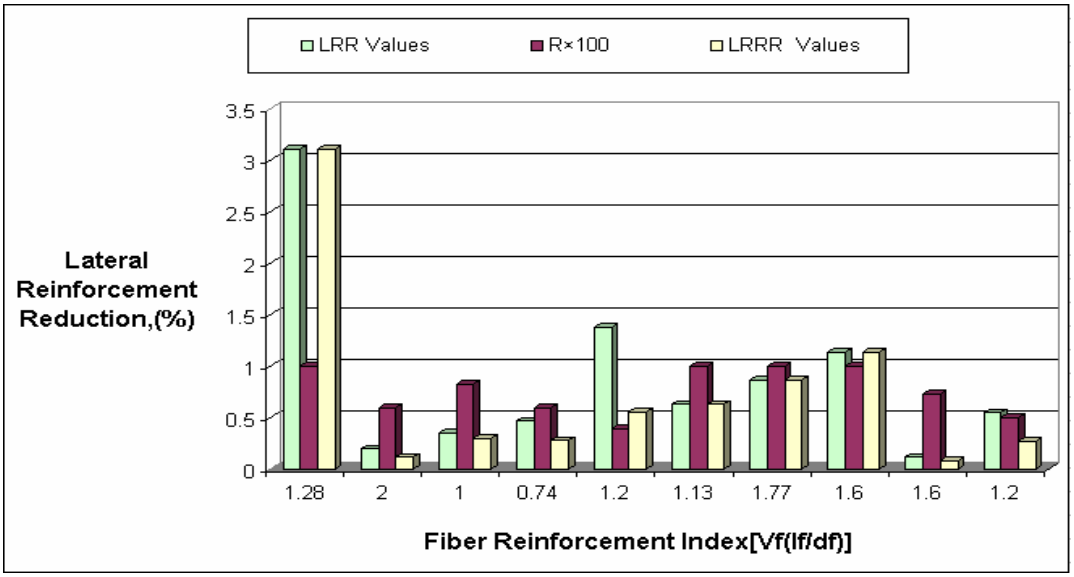

Figure 2 - 28: Summary of test data regarding steel fibre effect in lateral reinforcement reduction from [38]

Research by Gebman

In 2001, Gebman made six 1/2-scale beam-column joints, two of those were conventional joint specimens and four steel fibres reinforced joints [39]. The steel fibres used were of 30mm length and an aspect ratio of 60. For reducing the amount of lateral hoops in the joint, 2% steel fibres (by volume) was added in the joint region to increase the joint hoop spacing from 10.2 cm (for two conventional joints) to 15.2cm (for two fibre joints) and 20.3cm (for the other two fibre joints) (**Figure 2 - 29**). Residual load-bearing capacity, damage tolerance, and energy dissipation capacity were considered in this research for comparing the joint behaviour. The test results showed that the performance of specimens with steel fibres was better than other specimens. Steel fibre specimens had a significant improvement on load bearing capacity as well as the damage tolerance because of the smaller width of cracking. However, it was observed that the steel fibre joints had more cracks than the conventional joints had. The energy dissipation capacity of the steel fibre specimens dramatically increased, and the increase was approximately 100% (for hoop spacing of 20.3cm) and 300% (for hoop spacing at 15.2cm) compared with the conventional joints.

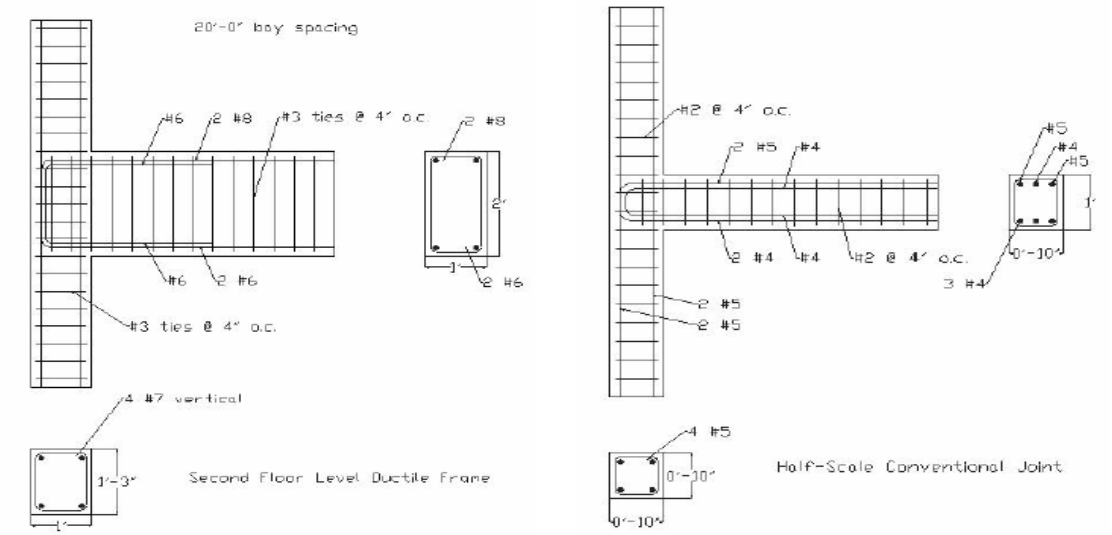

Figure 2 - 29: Typical test specimen from [39]

2.3.3.3 Energy dissipation

During seismic loading, to maintain structural integrity and to prevent the building from collapsing, the structural elements must be able to dissipate enormous amount of energy. Like the most critical area, the beam-column joints is designed to be very ductile and confined with large amount of stirrups for forming a plastic hinge in the beam adjacent the column face. The use of steel fibre reinforced concrete in beam-column joints is to increase the joint hoop spacing is valuable because it would alleviate the congestion of reinforcing steel, making the joint easier to construct and reduce the cost.

Research by Katzensteiner and Mindess

To investigate the effectiveness of steel fibre concrete in seismic frame structures, two plane frames with two-bay and two-storey were tested by Katzensteiner, B and Mindess, S. [40]. One frame was designed to be a seismic resistant frame (**Figure 2-30** designed by CAN3-A23.3-M84 Canada concrete code), the other one was constructed with 0.76% by volume of hooked-end Dramix steel fibres to reduce the lateral confining hoops in the joint region (**Figure 2-31**). The fibres were Dramix steel fibres with 30mm length×0.5mm in diameter. Both the frames were set on an aluminium table which simulated several earthquake acceleration records. The energy absorption capacity was the main criteria for comparison between the conventional frame and fibres reinforced frame. Through the analysis of

hysteretic loops (base shear vs. the lateral displacement of the joint), it was found that the hysteretic loops of SFRC structure were approximately 40% fatter than that of conventional concrete structures. The SFRC structure also showed better behaviour in terms of ductility and the integrity of the structure compared with the one with the seismically-detailed structure.

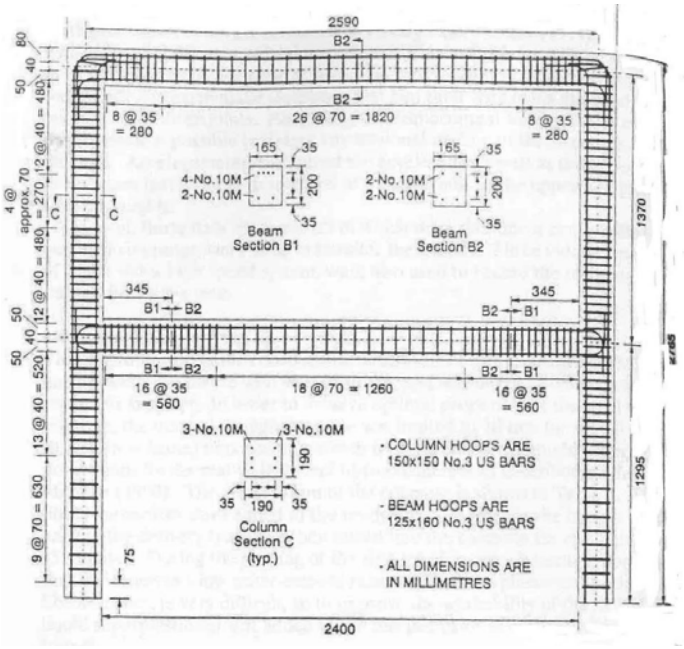

Figure 2 - 30: Reinforced steel layout of structure #1 frames from [40]

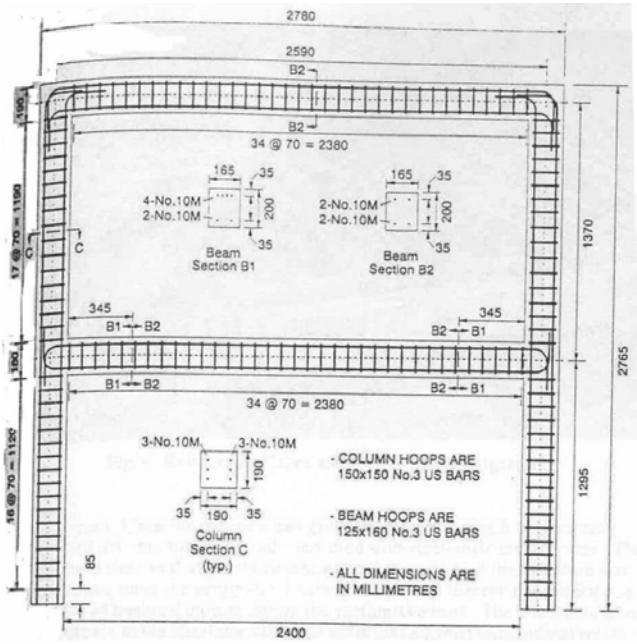

Figure 2 - 31: Reinforced steel layout of structure #2 frames from [40]

Research by Henager

Two full-scale beam-column joints were constructed by Henager in 1977 [41]. One specimen was designed as a conventional ductile reinforced concrete joint using hoops in accordance with the seismic design method and the other specimen was a modified joint with 1.67% by volume of steel fibre incorporated with fewer hoops in the joint region (**Figure 2-32**). The steel fibres were smooth, round, cold-drawn, brass-plated steel fibres with 38mm length and 0.51 mm in diameter resulting in an aspect ratio of 75. Both specimens were tested under reverse cycle loading. It was found that steel fibres reinforced joint had significantly improved the capacity of damage tolerance, slower strength deterioration and higher energy dispassion after the 10^{th} cycle of loading compared with the conventional ductile joint.

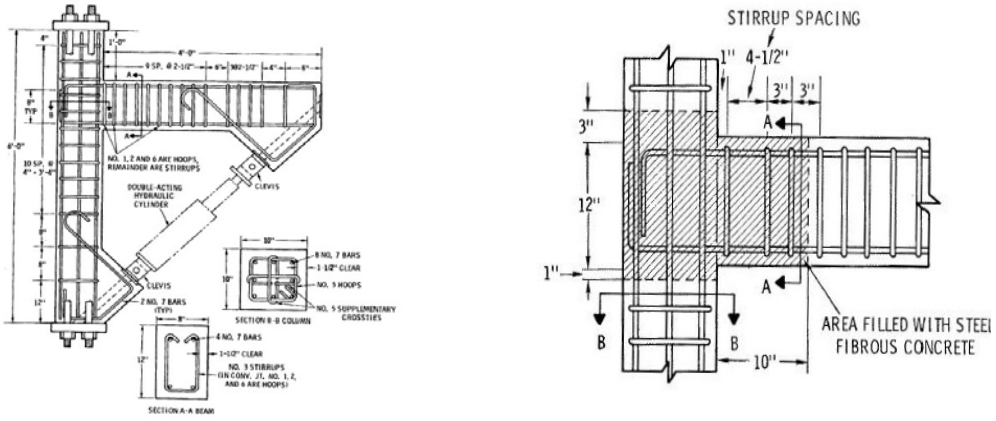

Figure 2 - 32: Details of the test specimens from [41]

Research by Gencoglu and Eren

Gencoglu and Eren, in 2002, tested four full scale exterior beam-column joint specimens under displacement controlled reverse cyclic loading to investigate the effect of steel fibres in seismic beam-column joints [42]. The first two specimens were prepared with closely spaced stirrups in the joints. The other two specimens were to use steel fibre to increase the spacing of stirrups in the joint region (**Figure 2-33**). The steel fibre used was 60mm length and 0.8mm in diameter with yield strength of 1100 MPa. The amount of steel fibre added into the concrete mix was restricted to 1% by volume because of the issues of concrete workability. The results indicated that using steel fibres in the joint allowed reducing the hoops in the joints and the lateral confinement in the plastic hinge zone without deteriorating the joint behaviour. Moreover, the use of SFRC also increased ductility and strength capacity. It was also found that the steel fibre reinforced joint with less lateral reinforcement showed improved energy dissipation capacity. However it was also recommended to use both steel

fibre and transverse reinforcement in the critical regions because compared with SFRC joint the first two normal concrete joints showed better ductility.

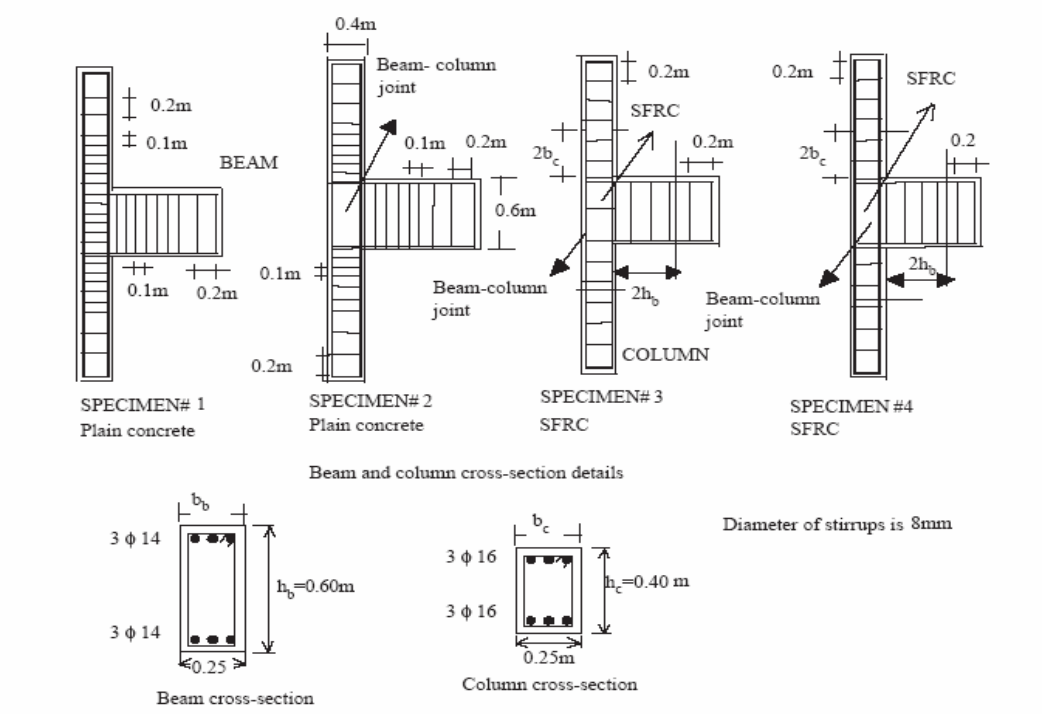

Figure 2 - 33: Details of the test specimens from [42]

2.3.3.4 Bonding of confined steel fibre reinforced concrete to deformed bars

Research by Soroushian

During an earthquake, beam-column joints respond with large deformation, and plastic hinges are expected to form in beams adjacent to the column surfaces. The slippage of the beam's flexural steel though the joint is the main factor to influence the degradation of strength and stiffness. As it is known, the beam's flexure steels surrounding by concrete is general well confined by lateral stirrups in beam plastic hinge region, such confinement tend to protect anchored bars from slipping at beam-column connections.

Many researches have been done using steel fibre reinforced concrete to replace the lateral reinforcement in the beam-column joint region. It was well confirmed that using steel fibres in joint connections can significantly improve the ductility and the bond strength.

The effects of local bond behaviour of deformed bars in steel fibre reinforced concrete was investigated by Soroushian [10]. This study was a comprehensive research for bond stress of deformed bar in different steel fibre reinforced concrete in beam-column joint regions. Several tests were done to explore general aspects of SFRC, such as the influence of the aspect ratio (l_f / d_f=60, 80, and 100), the volume fraction (V_f=0, 0.5%, 1.0%, and 1.5%), and the type of steel fibres (hooked, crimped, and straight). Based on a large number of tests, it was concluded that adding 0.5% volume of steel fibre to concrete could increase the local bond strength by more than 30%. Compared with the effect of volume of fibres, aspect ratio and fibre type did not significantly influence the bond strength, however the value of slips at peak bond stress increased with increasing aspect ratio.

2.3.3.5 Precast fibre joint

Research by Soubra

The research on using fibres in connection between precast concrete elements under the seismic load has also been done. Soubra published his report in 1992 (**Figure 2-34**) [43].

Polypropylene plastic fibres and hooked steel fibres with fibre volume fraction of 0, 1 and 2% were used in the tests. The fibre aspect ratio was 60, 100 and 200. Series different fibre reinforced composites, classified in polypropylene plastic fibre reinforced composites and steel fibre reinforced composites, was tested to select a suitable FRC composite that could provide the required properties for a cast-in-place joint. Six beams and four beam-column joint subassemblies with selected fibres then were tested under seismic load. It was found that the fibre reinforced concrete in cast-in-place connections for beam and the bean-column joint subassemblies showed a significantly improved strength and energy dissipation capacity. Using hooked steel fibre in cast-in-place connection could provide higher load carrying capacity and increased energy dissipation capacity compared with those of polypropylene plastic fibres reinforced connections.

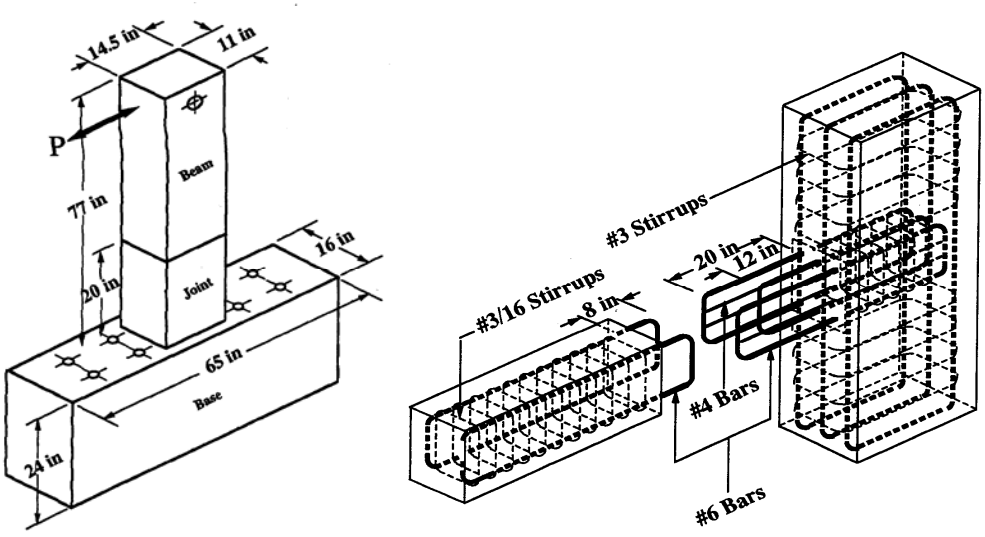

Figure 2 - 34: Typical beam-column specimen and reinforcing arrangement from [43]

Research by Tuleasca et al.

A similar test was done by Tuleasca et al. to evaluate the response of a monolithic precast joint, with cast-in-place steel fibre reinforced concrete (SFRC), subjected to high magnitudes of static and dynamic actions (**Figure 2-35**).

The specimen was constructed to use longitudinal beams with double-tee cross section and a flange height equal to the height of concrete floor, with the two web cores of the longitudinal beams "wrapping" the column and being supported by the transverse beams. The longitudinal double-tee beams were manufactured with projecting hairpin reinforcement. The necessity of satisfactory interaction between the precast double-tee beams and the column, permitting transmission of important bending moments, led to the use of a SFRC circumferential joint about the column perimeter, ensuring rigid response of the connection between the structural elements. The column was made in one piece (450×500 mm), with corbels for transverse beams seating, and projecting reinforcement for connection to the precast transverse beams [44].

It was found that this joint reinforced with steel fibre provided greater strength and deformation capacity than the ordinary concrete joint, despite incorporating a smaller quantity of conventional reinforcement. Only superficial damage was found in the SFRC joint and full beam plastic hinging was then developed.

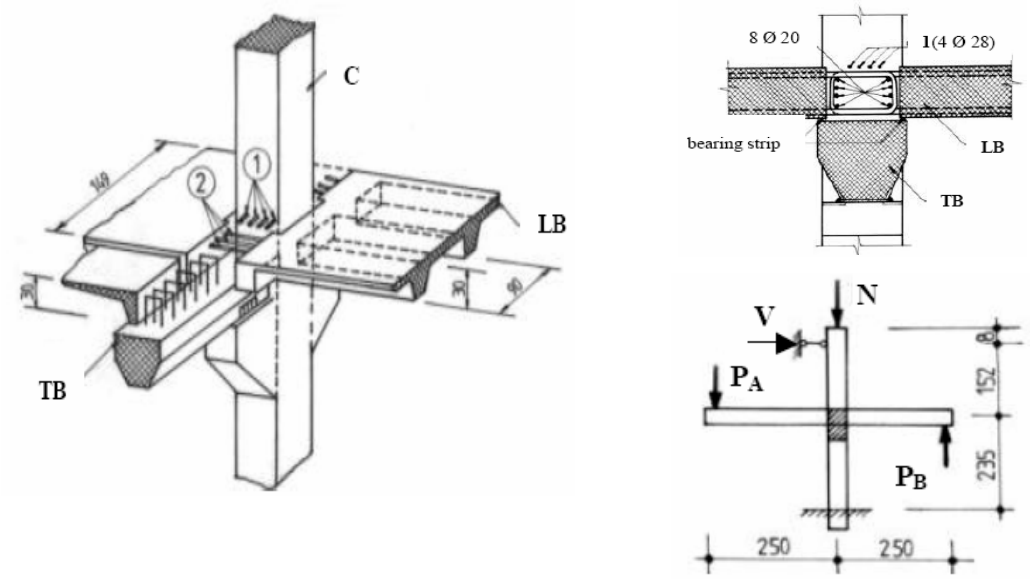

Figure 2 - 35: Detail of the assemblage from [44]

CHAPTER THREE

3. SEISMIC BEHAVIOUR OF BEAM-COLUMN JOINT SUBASSEMBLIES

3.1. Introduction

It is well known that beam-column joints can be critical regions compared with other parts of reinforced concrete frames designed for resisting seismic attack. As a consequence of the seismic moment of the beam across the joint and the moments in columns existing above and below the joint, the joint is suffered by large horizontal and vertical shear forces (**Figure 3-1**). If the joints are not well designed, such as the joints designed in the pre-1970s, joint shear failure may result in the collapse of frame buildings during a seismic load (**Figure 3-2**). The objective of this chapter is to analyze the effectiveness of beam-column joints reinforced with high performance steel fibre concrete. An appropriate analysis method, the hierarchy of strength diagram, is used to handle the failure mode of joints. This analysis result will be compared with those experimental results constructed in the laboratory of the University of Canterbury (specimens' details shown in **Chapter four**). The joints are designed to simulate nonductile detailing characteristics of pre-seismic code construction and ductile detailing capacity code designed construction (NZS 3101:1995) [45]. The analyses concentrate on the shear strength of joints with steel fibres and the combination of fibres and stirrups when subjected to cyclic loading at the column top. A brief theory review for exterior beam-column joints is also presented in this chapter. The comparisons between the analytical results and experimental results are shown in **Chapter five**.

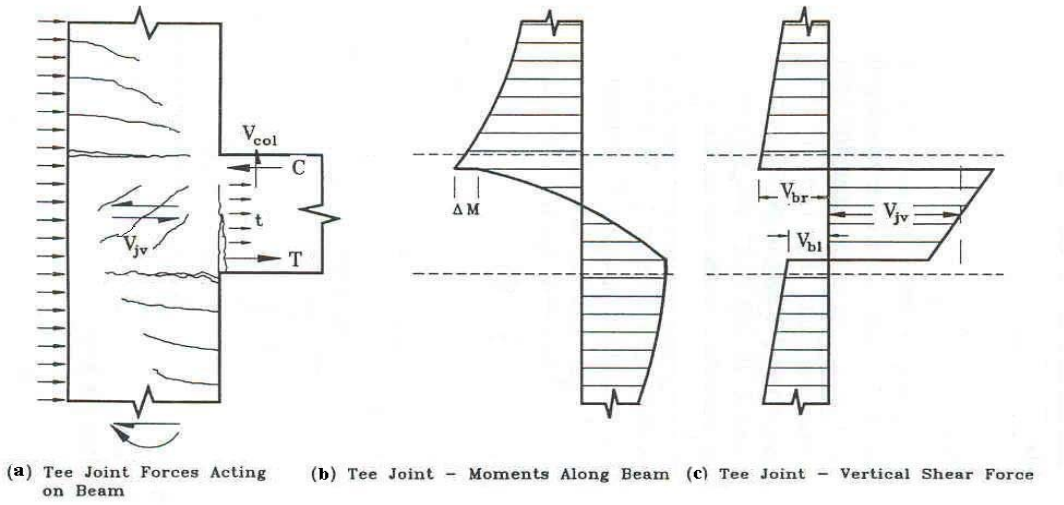

Figure 3 - 1: Shear force in tee-joints.

Figure 3 - 2: Joint failure during the Kocaeli (Turkey) earthquake

3.2. Actions of exterior frame joints

The deflected shape of a framed structure responding to lateral seismic loading is shown in **Figure 3-3**. Based on inelastic analysis, all points of contraflexure are assumed at the midpoint of the members of beams and columns. For an exterior joint, the encircled part in **Figure 3-3**, only one beam frame is connected into a column. Hence the moments and shears acting at a typical exterior beam-column joint core region under seismic loading can be presented as those in **Figure 3-4** and **Figure 3-5**. It can be concluded by considering the equilibrium of moment about the centre of the joint core and assuming $V_{col} = V_{col}'$, that

$$M_b + 0.5 h_c V_b = 0.5 l_c V_{col} + 0.5 l_c' V_{col}' \tag{3. 1}$$

The horizontal shear force acting on an exterior beam-column joint core can be expressed as:

$$V_{jh} = T - V_{col} = A_s \cdot f_s - V_{col} \tag{3. 2}$$

Where f_s is the stress in the beam top reinforcement, depending on the yield strength of the beam bars. When designing horizontal joint shear force, an overstrength factor of α should be taken into account. Thus the evaluation of f_s can be expressed as [46]:

$$f_s = \alpha f_y \qquad where \quad \alpha \geq 1.0 \tag{3. 3}$$

From Equation 3.1, the main horizontal shear force across the column, which is sufficiently accurate for design purpose, can be evaluated as

$$V_{col} = \frac{M_b + 0.5 h_c V_b}{0.5 (l_c + l_c')} \tag{3. 4}$$

From Equations 3.2 and 3.4, the vertical joint shear force can therefore be calculated as:

$$V_{jv} = T''+C_c'+C_s' = T'+C_c''+C_s''-V_b \quad (3.5)$$

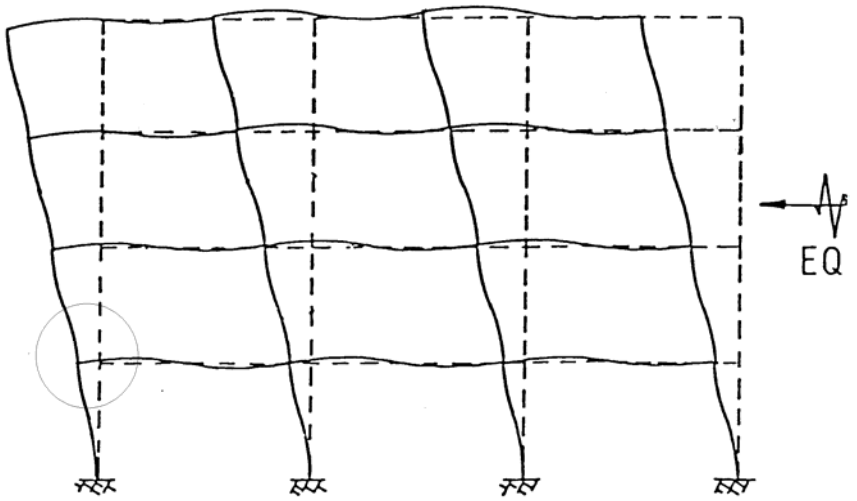

Figure 3 - 3: Response of a framed structure to a later load from [47]

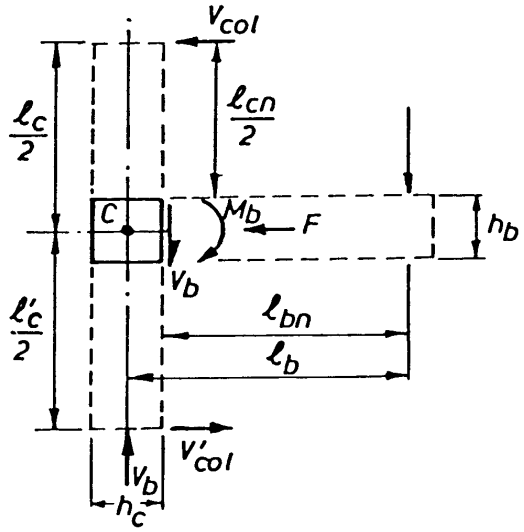

Figure 3 - 4: Action on an exterior beam-column joint from [48]

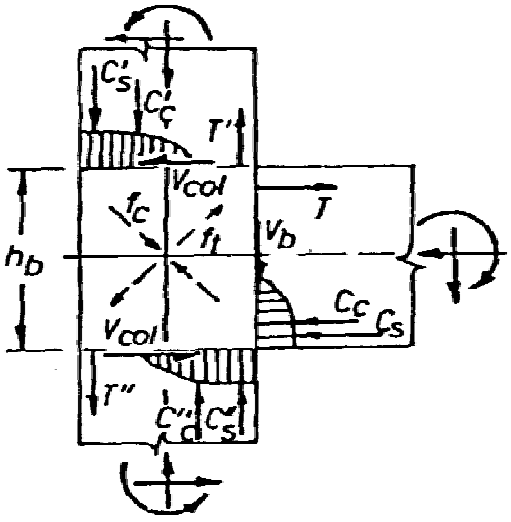

Figure 3 - 5: Forces acting on the joint core from [48]

3.3. Mechanisms of shear resistance for exterior beam-column joints

3.3.1. Shear forces acting on the joint core

In an exterior beam-column joint, the horizontal shear force applied to the top of the joint must be transmitted through the joint and equilibrated by the bottom horizontal shear force. Similarly, both sides of the vertical joint shear force, the outer face of the column and the face adjacent to the beam, also must remain in equilibrium.

The previous research [46], for conventional joints, classifies three modes of transmission of component forces within the joint. "*They are*:

1. *Forces from the column flexural reinforcement.*
2. *Forces from the beam flexural reinforcement*
3. *Concrete compressive forces"*

The bond stresses transfer mechanism is shown in **Figure 3-6**. It can be seen that the bond stresses from the column bars in the outer layer are transferred into the joint core and distributed uniformly through the beam depth along the outer column bars. The bond stress transfer into the joint core can be considered as $C_s'+T''$, and the bond force introduced by the intermediate column bars, T_1' and T_1'', can be assumed to be small and can be neglected.

After several reversal cyclic loads, the anchorage forces from beam flexural reinforcement will apply to the joint core along the straight beam bars, as shown in **Figure 3-6**. If the beam bar anchorage lengths and the lateral confinement in the joint core are inadequate, the bar force may cause a loss of concrete cover and reduce the flexural strength. It may also increase the risk of forming a plastic hinge in the column. **Figure 3-6** also shows the concrete compressive forces being introduced into the joint core as a shear force.

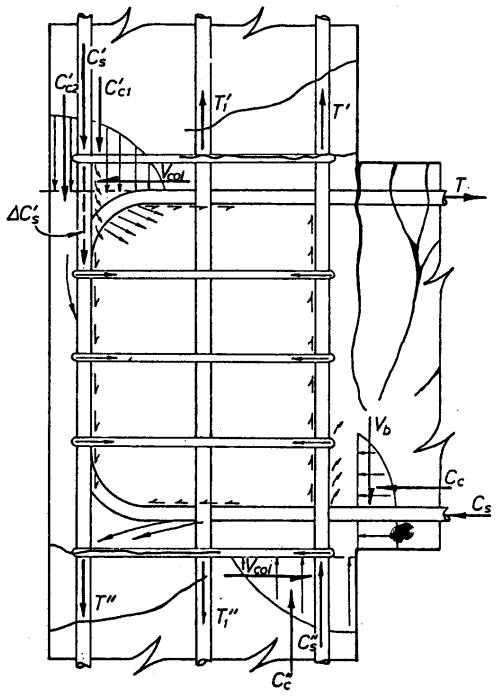

Figure 3 - 6: Bond stresses transfer mechanism for exterior beam-column joint from [46]

3.3.2. Contribution of joint shear mechanisms within the joint core

A previous researcher, Cook, mentioned in his research [46] *that within the joint core there exist three components which can carry the joint shear forces, these being:*

1. *The core concrete*
2. *Horizontal joint ties*
3. *Intermediate column bars*

Figure 3-7 shows a shear transfer mechanism within an exterior beam-column joint. It can be seen that a "concrete strut" resulted as the bend of the hooked top beam bars and the lower right-hand corner of the joint sustain a diagonal compression field. As concrete is strong in compression and weak in tension, the mechanism of shear resistance of concrete mainly depends on a diagonal compression field. However, the neglected tension strength capacity of concrete, the weakness of cementitious material, will lead to intersecting diagonal cracking after cyclic loadings. Therefore an adequate horizontal confinement should be required.

The possible compression stress paths are shown in **Figure 3-8**. These stresses can be determined to two diagonal struts D_i and D_1, the diagonal strut resulting from equilibrium conditions at the beam hook and the diagonal strut containing the vertical force V_{sv}.

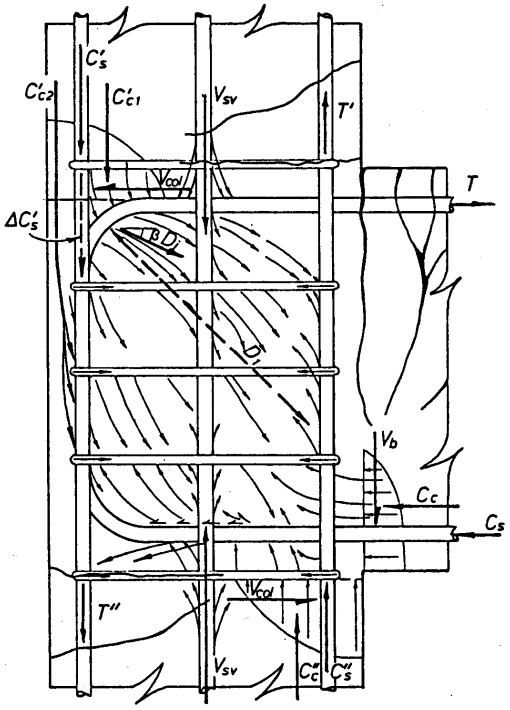

Figure 3 - 7: Compressive stresses strut of concrete in a joint core from [46]

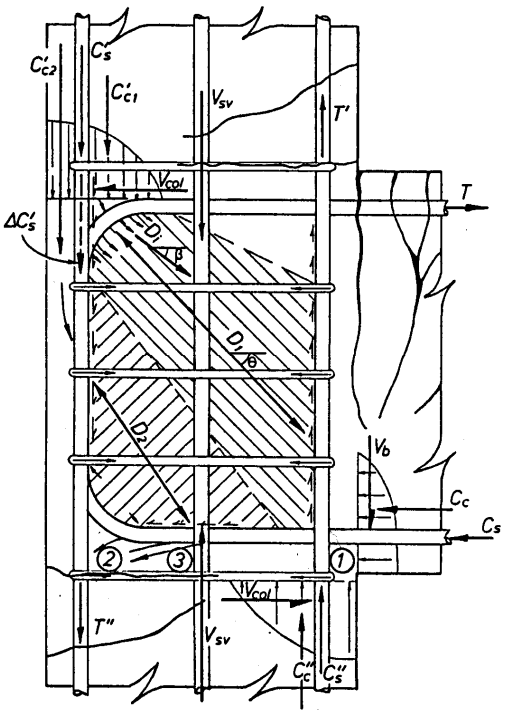

Figure 3 - 8: Idealised compressive stress strut mode from [46]

3.3.3. Important factors and parameters influencing the performance of a joint

3.3.3.1 Joints with lack of seismic detailing

Pampanin et al (2002) [11] mentioned in his report that absence of capacity design principles and poor reinforcement detailing can cause weak-column/strong-beam system results and tend to develop soft-storey mechanisms. As a result, beam-column connections of reinforced concrete frames with lack of capacity design and inadequate detailing of reinforcement suffer intrinsic structural weaknesses such as a brittle failure mechanism. Moreover, during an earthquake, such joints suffer a large interaction of shear cracking and then formation of the

shear hinges, which are caused by the interaction of shear cracking and stress concentration in the joint region (**Figure 3-9 and 3-10**).

The following deficiencies of typical structure are mentioned by Pampanin et al (2002) [11]:

1. *Insufficient amount, if any, of transverse reinforcement in the joint regions*
2. *Insufficient amount of column longitudinal reinforcement, when considering seismic lateral forces*
3. *Inadequate anchorage detailing, for both longitudinal and transverse reinforcement*
4. *Lower quality of materials (concrete and steel) when compared to current practice, in particular : (a) use of smooth (plain) bars for both longitudinal and transverse reinforcement; (b) low-strength concrete* [11]

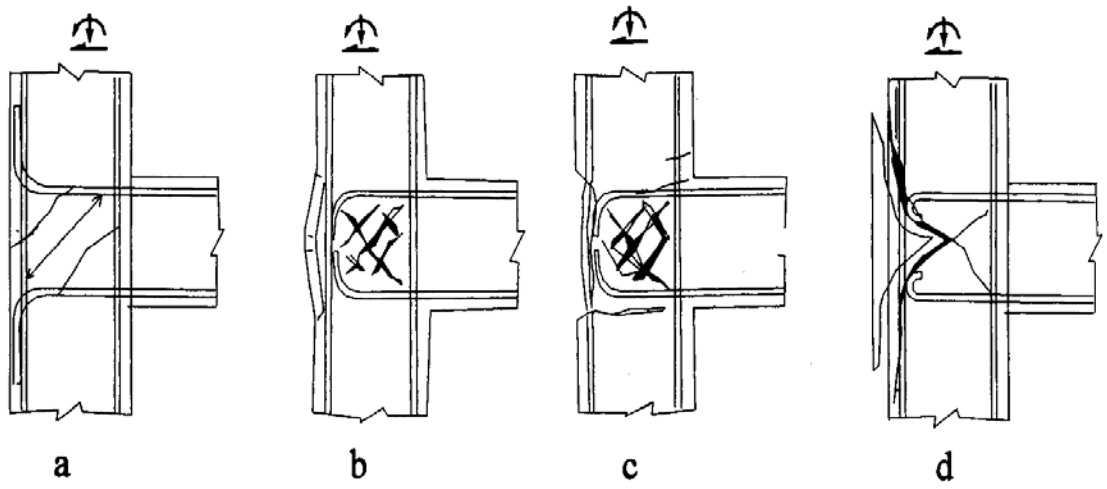

Figure 3 - 9: Alternative damage mechanisms for exterior Tee-joints: (a) beam bars bent away from joint region; (b), (c) beam bars bent in joint region; (d) end-hook anchorage: "concrete wedge" mechanism from [11]

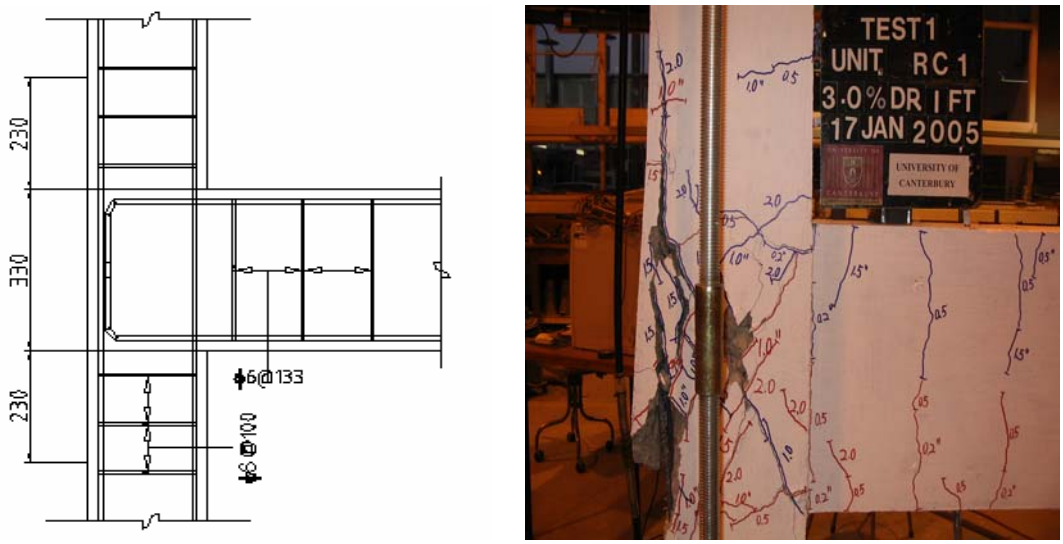

(a) **(b)**

Figure 3 - 10: (a) Details of Unit RC-1; (b) shear hinge occurring during testing

3.3.3.2 Important parameters in the behaviour of conventional exterior joints

Many parameters can affect the amount of joint reinforcement required to achieve satisfactory joint performance. Cook mentioned the following parameters which were identified by their effect on the amount of horizontal joint reinforcement required [46].

1. *Joint aspect ratio* (**Figure 3-11**)
2. *Level of column axial load*
3. *Area ratio of top bottom beam flexural reinforcement*
4. *State of the beam adjacent to the joint face*
5. *Anchorage of beam flexural reinforcement*
6. *Interacting unloaded later beams at the joint*

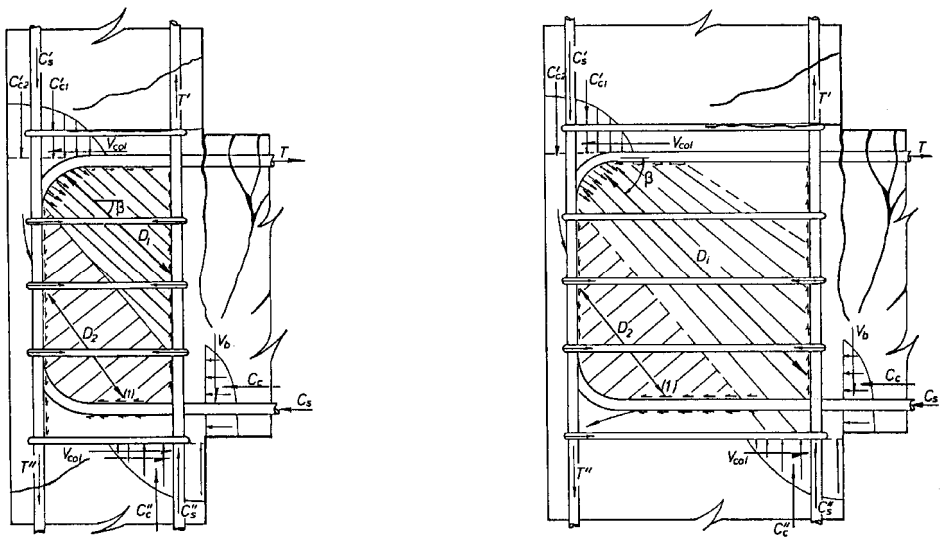

Figure 3 - 11: Shear resistance in (a) a high aspect ratio joint; (b) a low aspect ratio joint from [46]

3.3.4. Principal stress in joints

In the design of beam-column joints, it has been the practice to set joint shear stress limitations in terms of either nominal shear stress (v_{jh}) or principal compression/tension stress (P_c, P_t). Thus, for typical tee joint conditions, the current seismic code tends to limit shear stress v_{jh} expressed as a function of concrete tensile strength $K_1\sqrt{f'_c}$ (i.e. ACI 318-95 and similarly EC8) or concrete compressive strength $K_2\, f'_c$ (NZS3101:1995). In this function, K_1 and K_2 are constant values obtained from experimental tests.

Many researchers have reported that SFRC can enhance the joints' nominal shear stress (see **Chapter two**). However there is inadequate information which can provide a feasible procedure to analyze the performance of SFRC beam-column joints under a seismic load. In this research the performance of such joints is estimated by using principal tension stress of joints. It may be argued that this philosophy, which is based on the performance of joints designed without specific consideration of shear reinforcement, is somewhat arbitrary to use in joints confined with stirrups or steel fibres. However, such nominal principal tension stress in the SFRC joint can be obtained from several comparisons between experimental results and analytical results. During the testing of a joint, if the average principal tension stress is less than the cracking strength of the concrete in the joint, the joint will exhibit distress. In such a way, the performance of joints reinforced with either SFRC or the combination of steel fibres

and stirrups can be estimated. Although the performance of joints can also be influenced by the nominal principal compression stress when it exceeds the crushing strength of the concrete, compared with principal tension stress it is a minor factor and can be ignored when analysing the behaviour of joints.

A simple analysis for stress in the literature [49] shows that the nominal principal stress in a conventional joint region is given by:

$$P_c, P_t = \frac{f_v + f_h}{2} \pm \sqrt{(\frac{f_v - f_h}{2})^2 + v_j{}^2} \qquad (3.6)$$

Where P_c and P_t are nominal principal compression and tension stresses, respectively; v_j is the joint stress; and f_v and f_h are average axial stresses in the vertical and horizontal direction.

3.3.5. Strength degradation curve for exterior joints

Figure 3-12 shows the typical strength degradation models for poorly designed exterior Tee joints published by Pampanin [11]. This philosophy underlines that the first crack failure for exterior joints without transverse reinforcement occurs at the principal tension stress $P_t = 0.29\sqrt{f'_c}$ (MPa). Extensive damage failure is only up to $P_t = 0.42\sqrt{f'_c}$, because of a progressively severe diagonal cracking developing in the joint region and no transfer mechanism sources being allowed. Generally the value of P_t cannot be enhanced through the steel hardening behaviour.

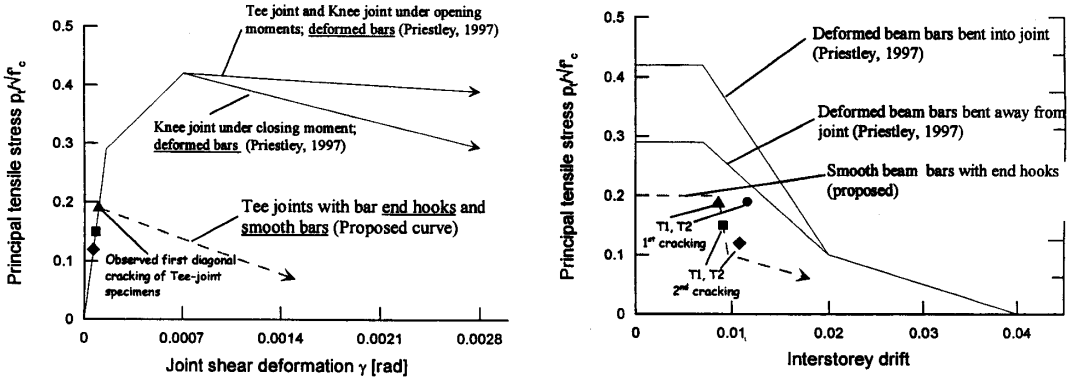

Figure 3 - 12: Typical strength degradation models from [11]

CHAPTER FOUR

4. TEST PROGRAM

4.1. Introduction

This chapter introduces the units tested in the current research project. The experimental work conducted in this project investigated the seismic behaviour of exterior beam-column joint subassemblies under simulated cyclic loading patterns. Comparisons of conventional concrete joints, the SFRC joints and the SFRC joint with reduced transverse reinforcement in the joint and potential plastic hinge region were performed based on the experimental results of seven beam-column joint units.

The parameters studied in these tests were the joint critical principal strength, ductility, joint behaviour, and energy dissipation. The first three non-seismic beam-column joints reinforced with or without steel fibre in the joint region were analysed to find the contribution of steel fibres to the joint shear resistance capacity. A further three joints with seismic detail designed by the Concrete Design Code NZS3101:1995 [45] were tested to estimate the proportion of the joint shear resistant capacity provided by steel fibre and stirrups. These tests also give information on the flexure behaviour of steel fibre reinforced concrete in the plastic hinge region.

4.2. Details of test specimens

4.2.1. Overall dimensions and loading

The current research involved seven exterior beam-column joint units. Each unit represents a part of multi-storey plane frame as shown in **Figure 3-3**. The test units were loaded by hydraulic load to the top of the column to simulate the building gravity load, but no 'P-Δ effect' was taken into account. By reversing the direction of the lateral loads applied to the column, the effects of earthquake loading were simulated and the applied lateral column loads induced reactive shear at the ends of the beam.

4.2.2. Group I (Unit RC-1, Unit FS-2 and Unit FS-3)

The dimensions and reinforcement details of the three units in Group I are shown in the following figures (from **Figure 4-1** to **Figure 4-3**). In all units, the beam had rectangular cross section of 330 mm×200 mm dimension whereas the column was of square cross section with 230 mm×230 mm dimension. The longitudinal reinforcement of each beam included 12 number of 10 mm diameter deformed bars of Grade 300 steel, with four corner bars and eight intermediate bars. The longitudinal reinforcement of each column consisted of 6-10 mm diameter deformed bars of Grade 300 steel, with four corner bars and two intermediate bars at the mid-depth of each column in the plane of loading. Over the length of beams and columns in all units, transverse reinforcement was 10 mm diameter plain round bars of Grade 300 steel at 133 mm spacing for the beams and 100 mm spacing for the columns. No shear reinforcement was placed in the joint core.

Steel fibre reinforced concrete was used in the joint region in two units of the Group I; 1% SFRC by volume in Unit SF-2 and 2% SFRC by volume in Unit SF-3.

4.2.3. Groups II and III (Unit SF-4, Unit SF-5, Unit RC-6 and Unit NZ-7)

The units of Group II and Group III were designed by the NZ concrete code NZS3101:1995 [45] following seismic design criteria. The column and joint were designed though the beam moment capacity which was the same as beam moment capacity of Group I. It is seen that compared to the units with non-seismic detailing reinforcement (units of Group I), the units designed by seismic code have adequate longitudinal and transverse reinforcement for shear strength and restraining the compression reinforcement against premature buckling. For the purpose of researching the shear resistance provided by steel fibres and stirrups in the joint region, the units of Group II were modified in the joint region. Some of the transverse reinforcement both in the joint region and potential plastic hinge region were replaced by using SFRC in order to find the shear resistance of a SFRC reinforced joint combined with/without stirrups. Furthermore, the behaviour of SFRC in the plastic hinge region was also investigated.

The overall dimensions and reinforcement detail of units in Group II and Group III are shown in **Figure 4-4**, **Figure 4-5**, **Figure 4-6** and **Figure 4-7.** The beams and columns of these four test units had a rectangular cross section (330 mm deep by 250 mm wide) and a square cross section (250 mm deep by 250 mm wide), respectively. The longitudinal reinforcement of the

beam was 8-12 mm diameter deformed bars of Grade 300 steel, with four corner bars and four intermediate bars. The longitudinal reinforcement of the column was 10-12 mm diameter deformed bars of Grade 300 steel, with four corner bars and four intermediate bars at the mid-depth and two middle bars at the mid-width of column in the plane of loading. The intermediate column bars were considered both as vertical shear reinforcement in the joint and as flexural reinforcement in the column.

For research purposes, in Group II the beam's plastic hinge length was reduced from 630 mm, depending on NZS3101:1995, to 350 mm (depending on either 1/10 of the overall beam length or the depth of the beam). The column plastic hinge length was the region adjacent to the joint over a length equal to twice of that column width (2×250=500 mm). Over the length of beams and columns in all units in Group II and Group III, the transverse reinforcement was of 10 mm diameter plain round bars of Grade 300 steel.

In Unit RC-6, the transverse reinforcement was spaced at 60 mm and 70 mm within the plastic hinge regions adjacent to the beam face and column face respectively. Over the length of the non-critical part of the beam and column, the transverse reinforcement was at 150 mm spacing for the beam and 75 mm spacing for the column. Only one stirrup was used in the joint region in order to evaluate the shear resistance force provided by the stirrup. The axial load during the test was maintained at 100 KN.

In Unit SF-4, the arrangement of the transverse reinforcement was similar to that in Unit RC-6. However in order to evaluate the shear resistance of the stirrups, concrete and steel fibre，1% steel fibre was used in the joint and beam plastic hinge region. Through analysing the seismic behaviour of tested unit, the relationship of shear resistance capacity of the stirrups, concrete and steel fibre was obtained.

In Unit SF-5, the transverse reinforcement was reduced to 50% in the beam and the column plastic hinge regions and 1% steel fibre by volume was added in the concrete used in these regions. The detail of transverse reinforcement in the other part of the unit was same as Unit RC-6.

Unit NZ-7 was designed by New Zealand concrete design code NZS3101:1995 [45]. The full amount of transverse reinforcement as recommended by the code was used in the potential plastic hinge and joint regions. No fibre was used in this specimen. Design detail is shown in **APPENDIX II**.

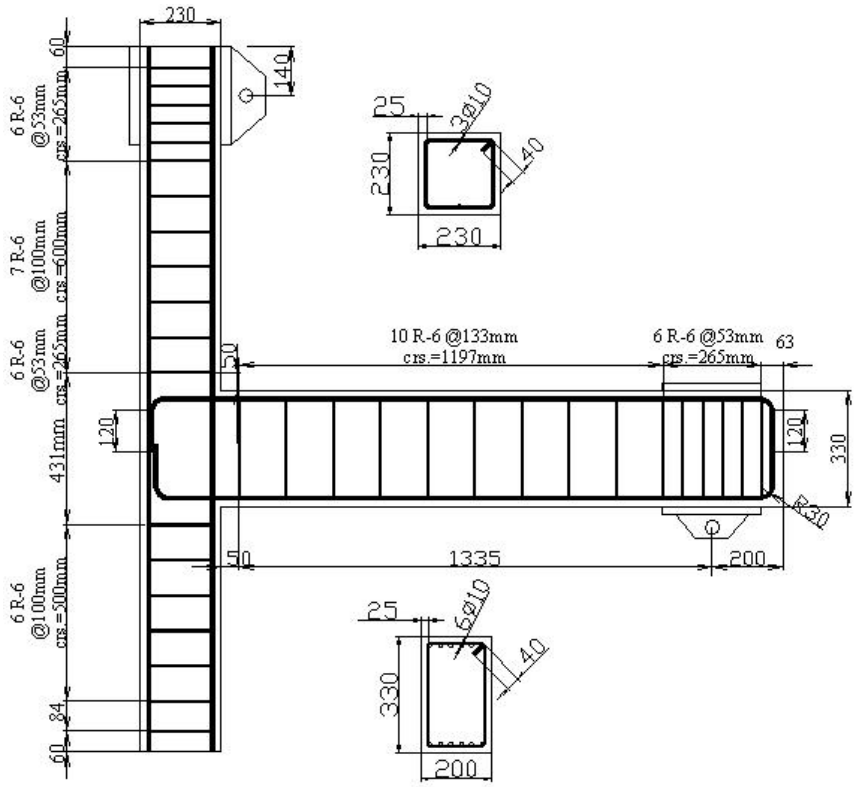

Figure 4 - 1: Unit RC-1

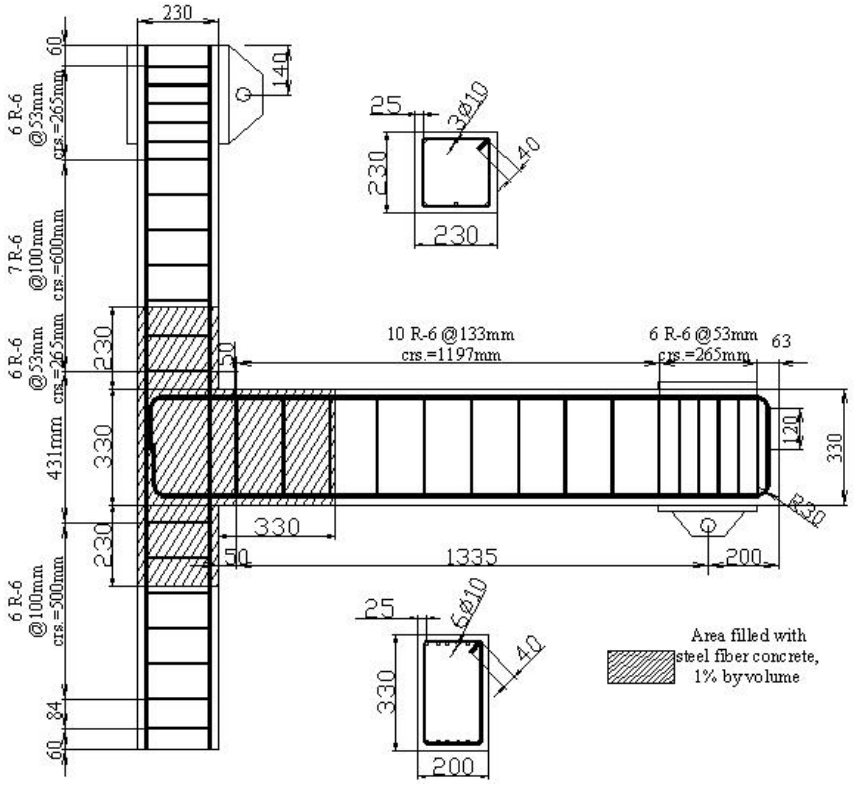

Figure 4 - 2: Unit SF-2

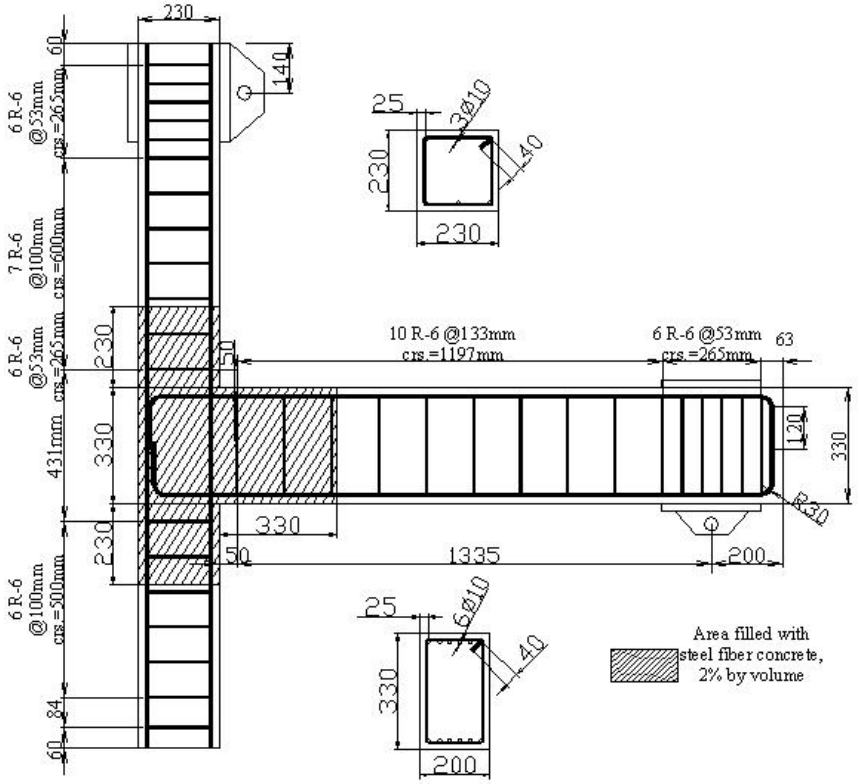

Figure 4 - 3: Unit SF-3

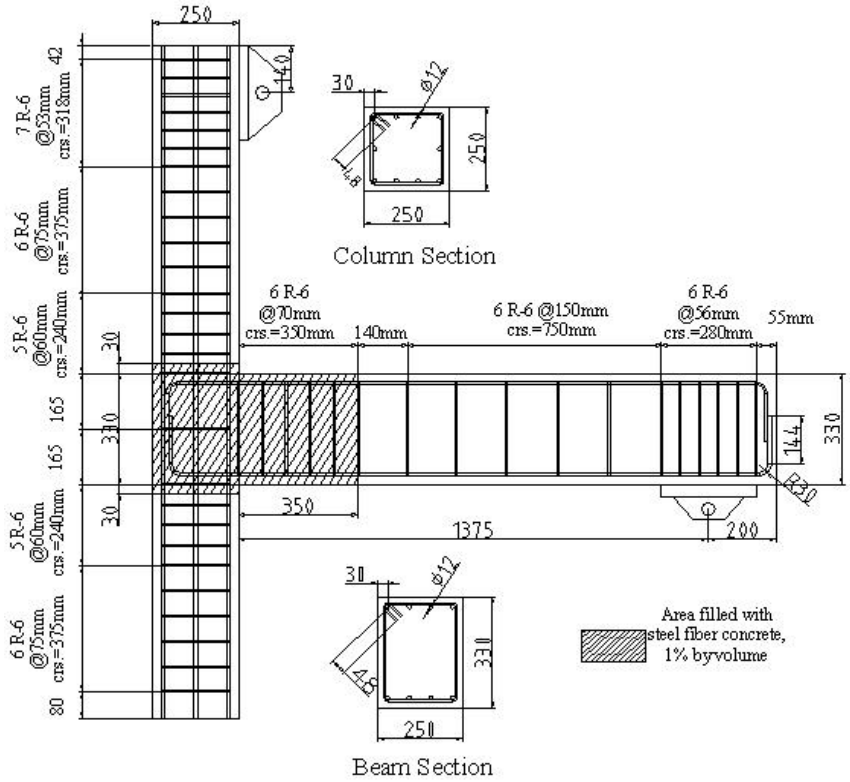

Figure 4 - 4: Unit SF-4

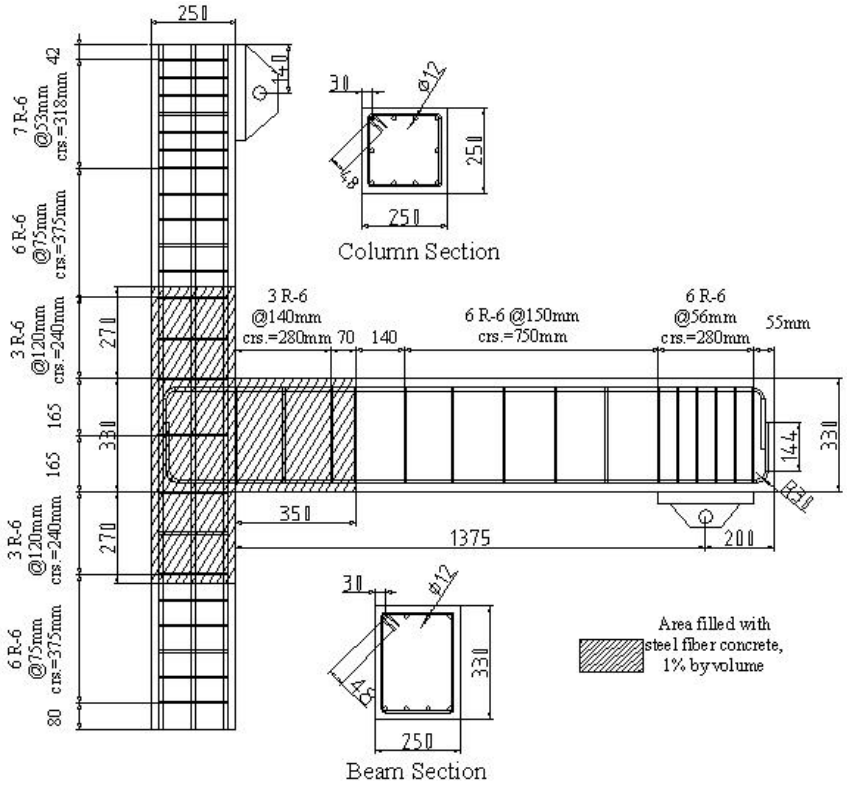

Figure 4 - 5: Unit SF-5

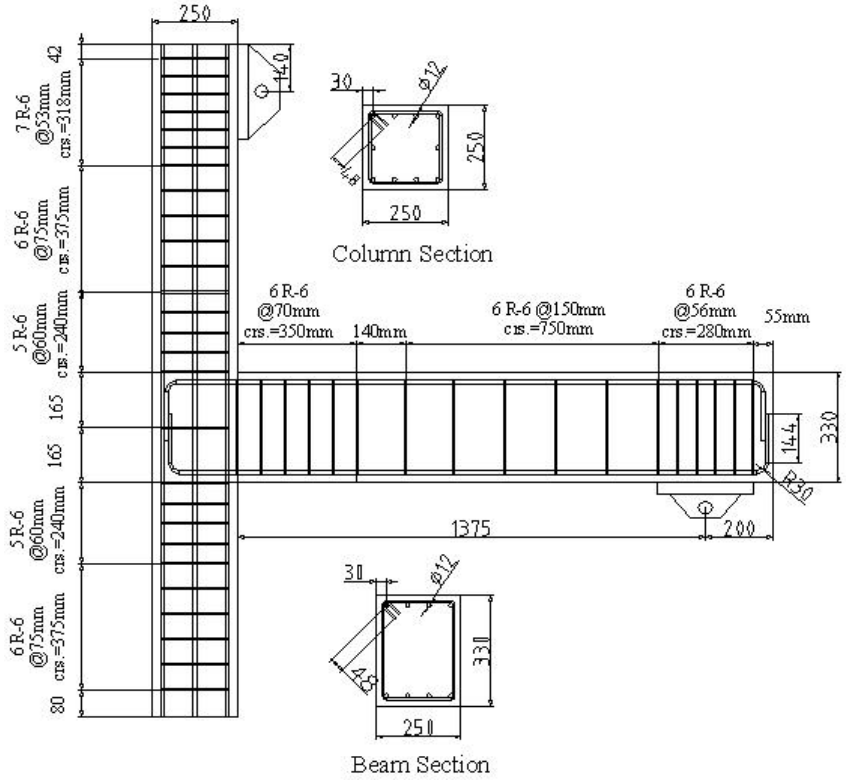

Figure 4 - 6: Unit RC-6

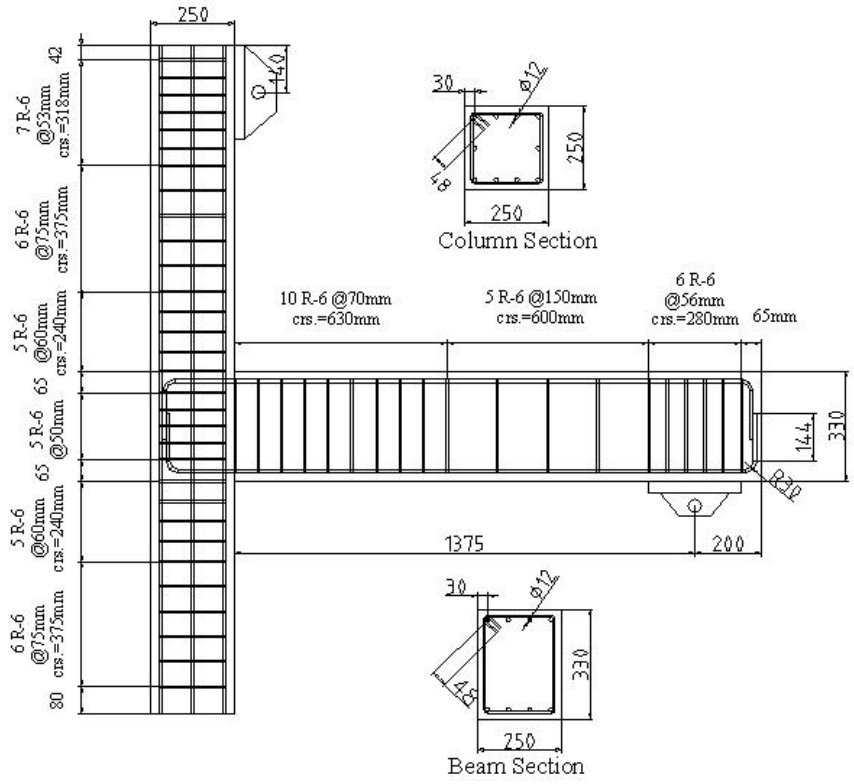

Figure 4 - 7: Unit NZ-7

4.3. Material properties

4.3.1. Concrete Plain mix

Seven units were separated into three groups. Units RC-1, SF-2 and SF-3 formed Group I and were cast together. Units SF-4, SF-5 and RC-6 were Group II. Unit NZ-7 was Group III. The plain concrete used in Group I and Group II was a commercially prepared mix supplied by Firth Industries Ltd., Christchurch with the slump values being 150 mm and 170 mm respectively. A cylinder compression test showed that target crushing strengths at 28 days were 18 MPa and 25 MPa for Groups I and II, respectively. A graded aggregate with a maximum size of 19 mm was specified.

4.3.2. Steel fibre reinforced mix

The steel fibre used in this research was Dramix hooked end type steel fibre as shown in **Figure 4-8**. The basic dimensions of this fibre were 35×0.55 mm with 45^{o} hooked ends which are generally considered to slowly deform during pull-out from concrete ensuring a controlled

ductile failure. However, it must be noted that adding a large amount of relatively long and stiff steel fibres into concrete may cause workability problems (see **Figure 4-9**).

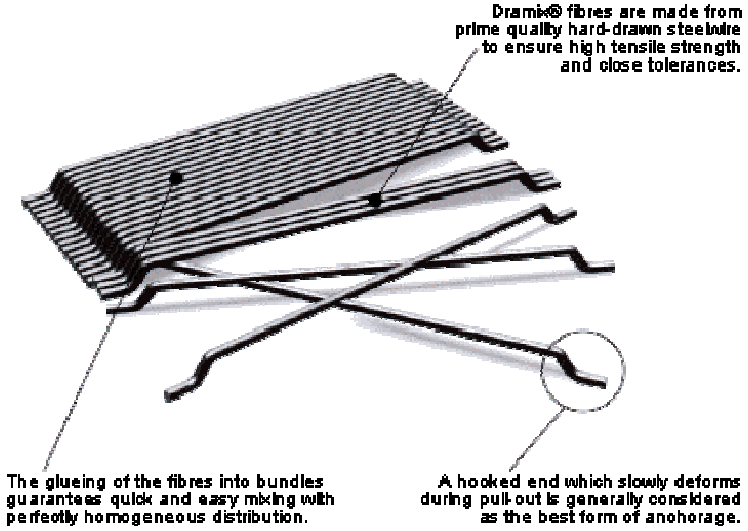

Figure 4 - 8: Dramix fibres (filaments of wire, deformed and cut into lengths) [50]

The fibre content of 79 kg/m^3 and 158 kg/m^3 adopted corresponded to 1.0% and 2.0% by volume of the concrete matrix, respectively. Firstly, the aggregates, cement, and water were mixed with a concrete track. Then fibres were mixed with concrete in a pan-type mixer (see **Figure 4-10**). For Groups I and II, three 100×200 mm cylinders of volume content each of SFRC were cast in standard steel moulds for testing the compression strength at 28 days and the test day respectively. The average results from these tests are shown in **Table 4-2**. The required volumes of SFRC in Unit SF-2, Unit SF-3, Unit SF-4 and Unit SF-5 were 0.064 m^3, 0.064 m^3, 0.053 m^3 and 0.083 m^3 respectively. A few pieces of wooden board were used to separate SFRC and conventional concrete as shown in **Figure 4-11**.

Figure 4 - 9: Steel fibres balling together (2.0% by volume)

The used steel fibre was Dramix steel fibre, and its detail is shown below.

Table 4 - 1: Detail of used steel fibre

Name	Aspect ratio	Tensile strength (MPa)	Geometry	Illustrations from manufacturer's website
Dramix 65/35 (low carbon, cold drawn wire fibre)	65	1150	Hooked end	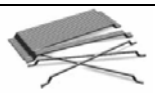

Table 4 - 2: Results of concrete cylinder test

Group I				
Type of cylinder	Testing day	NO.	value(MPa)	Average (MPa)
Normal concrete	28	1	17.7225	17.935
		2	17.85	
		3	18.2325	
1% SFRC	28	1	21.675	19.9325
		2	19.125	
		3	18.9975	
2% SFRC	28	1	28.9425	28.9425
		2	29.1975	
		3	28.6875	
Unit RC-1				
Normal concrete	35	1	20.145	19.38
		2	18.36	
		3	19.635	
Unit SF-2				
TEST NORMAL	50	1	18.105	18.615
		2	18.7425	
		3	18.9975	
1% SFRC	50	1	21.675	23.205
		2	24.8625	
		3	23.0775	
Unit SF-3				
Normal concrete	59	1	16.83	18.1475
		2	18.9975	
		3	18.615	
2% SFRC	59	1	24.735	28.05
		2	29.7075	
		3	29.7075	

Group II				
Type of cylinder	Testing day	NO.	value(MPa)	Average (MPa)
Normal concrete	28	1	23.3325	24.905
		2	25.8825	
		3	25.5	
1% SFRC	28	1	25.81875	25.18125
		2	24.225	
		3	25.5	
Unit SF-4				
TEST NORMAL	41	1	22.95	25.245
		2	24.6075	
		3	28.1775	
1% SFRC	41	1	28.6875	27.4975
		2	26.6475	
		3	27.1575	
Unit SF-5				
Normal concrete	48	1	24.99	24.99
		2	23.3325	
		3	26.6475	
1% SFRC	48	1	28.9425	28.05
		2	27.285	
		3	27.9225	
Unit RC-6				
Normal concrete	67	1	29.58	25.88
		2	22.3125	
		3	25.755	

Figure 4 - 10: Mixing steel fibres and concrete in a pan-type mixer

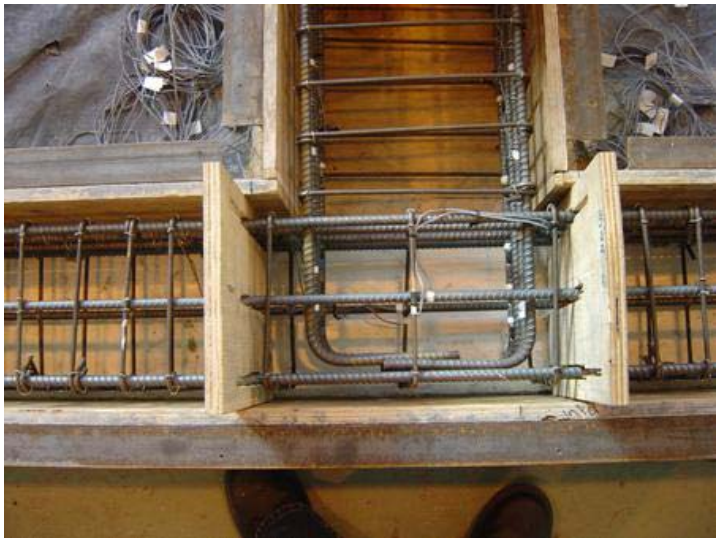

Figure 4 - 11: Wooden boards used to separate SFRC from conventional concrete

4.3.3. Longitudinal reinforcement

The longitudinal steel used in the beams and columns of test units consisted of deformed bars of size 10 mm and 12 mm diameter for Group I and Group II respectively. The steel of a particular size was taken from the same batch. All the deformed bars used in this research were manufactured from Grade 300 steel which has nominal higher yield strength of 300 MPa. Before caging specimens, three 40 mm length sample bars were randomly selected and tested in tension by using a 1000 KN Avery Universal Testing Machine to determine the yield and ultimate strengths. The average yield strength and ultimate tensile strength of tested bars are shown in **Table 4-3**. Typical monotonic stress-strain curves for each testing bar are shown in **Figure 4-13** and **Figure 4-14**.

4.3.4. Transverse reinforcement

Transverse reinforcement used in the beam, column and joint of the specimens was 10 mm diameter plain round grade 300 steel bars for all test units. Four sample testing bars were cut and tested by a 1000 KN Avery Universal Testing Marching (see **Figure 4-12**). The average yield strength and ultimate tensile strength of each bar size are shown in **Table 4-3**. Typical monotonic stress-strain curves for each testing bar are shown in **Figure 4-15**.

Table 4 - 3: Summary of the tensile properties of the reinforcing steel

300 MPA 10mm bar = 78.5 mm²					
	Yield		Work harden		Young's modulus
No.	stress (MPa)	strain	stress (MPa)	strain	(GPa)
1	325.05	1.28	322.73	24	235.55
2	324.28	1.48	321.95	25.78	224.26
3	321.95	1.36	326.6	26.63	267.99
Average	323.76	1.37333333	323.76	25.47	242.6
300 MPa 12mm bar = 113 mm²					
	Yield		Work harden		Young's modulus
No.	stress (MPa)	strain	stress (MPa)	strain	(GPa)
1	304.88	1.56	315.49	25.33	156.5
2	307	1.85	307	24.5	180.03
3	308.06	1.11	312.31	27.21	193.14
Average	306.6466667	1.50666667	311.6	25.68	176.5566667
300 MPA 6mm bar = 28.3 mm²					
	Yield		Work harden		Young's modulus
No.	stress (MPa)	strain	stress (MPa)	strain	(GPa)
1	386.42	2.43	401.44	22.22	195.34
2	373.54	1.85	390.71	21.66	234.62
3	395	2.51	401.44	20.34	205.36
4	379.98	2	399.3	24.94	207.58
Average	383.735	2.1975	398.2225	22.29	210.725

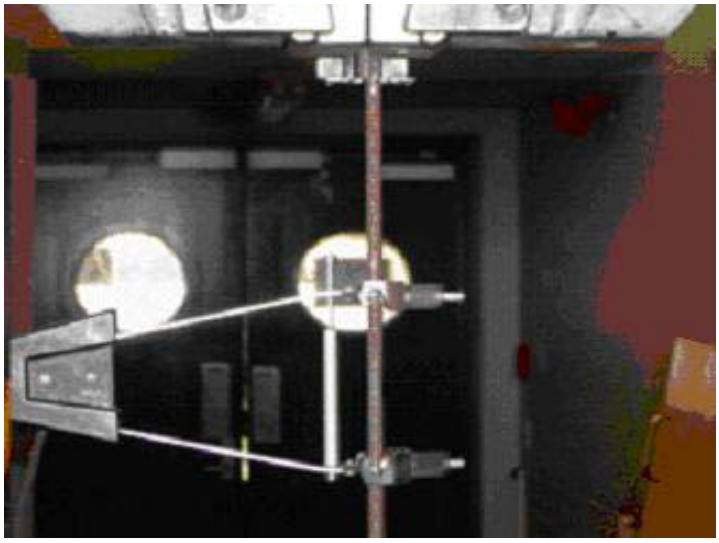

Figure 4 - 12: Test sample of the stirrups ready for testing

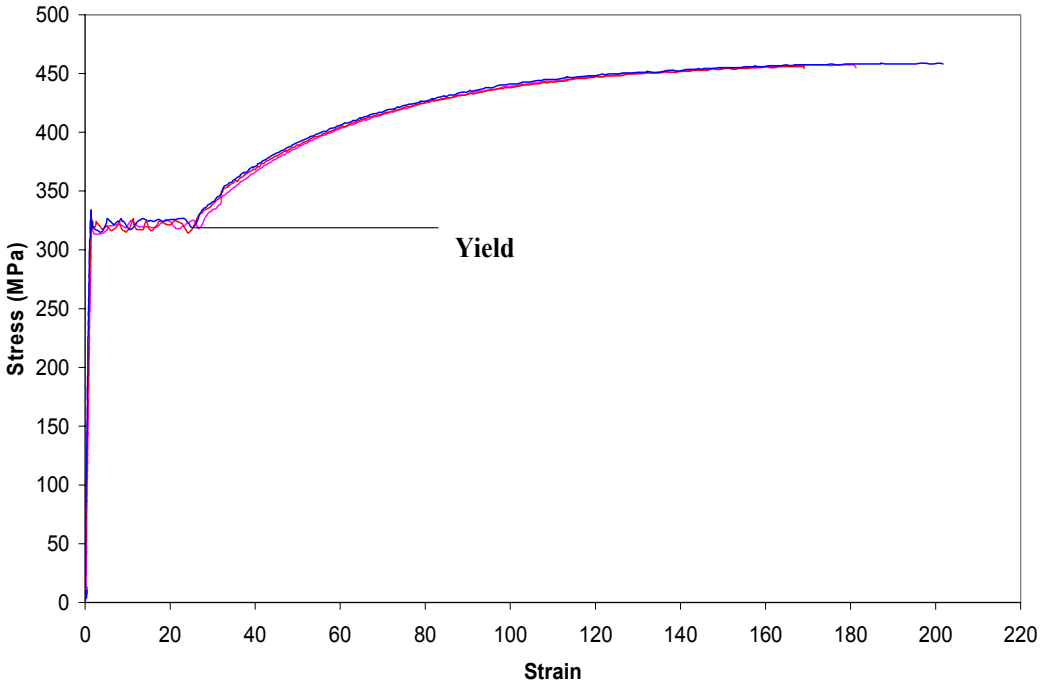

Figure 4 - 13: Typical stress strain diagram for Grade 300 steel sample (10 mm diameter)

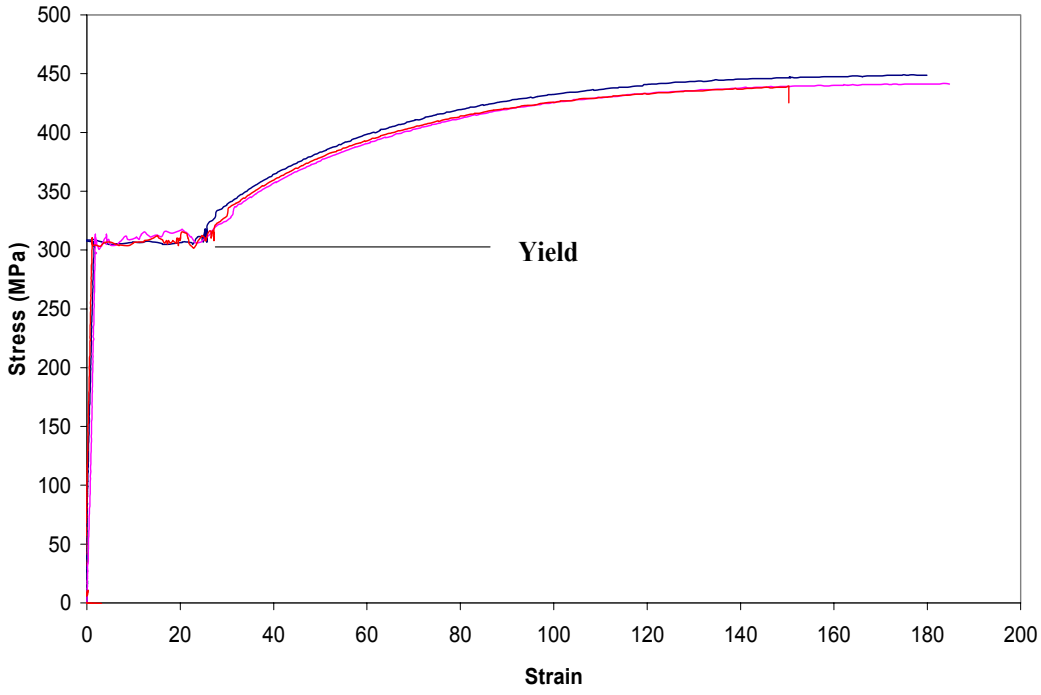

Figure 4 - 14: Typical stress strain diagram for Grade 300 steel sample (12 mm diameter)

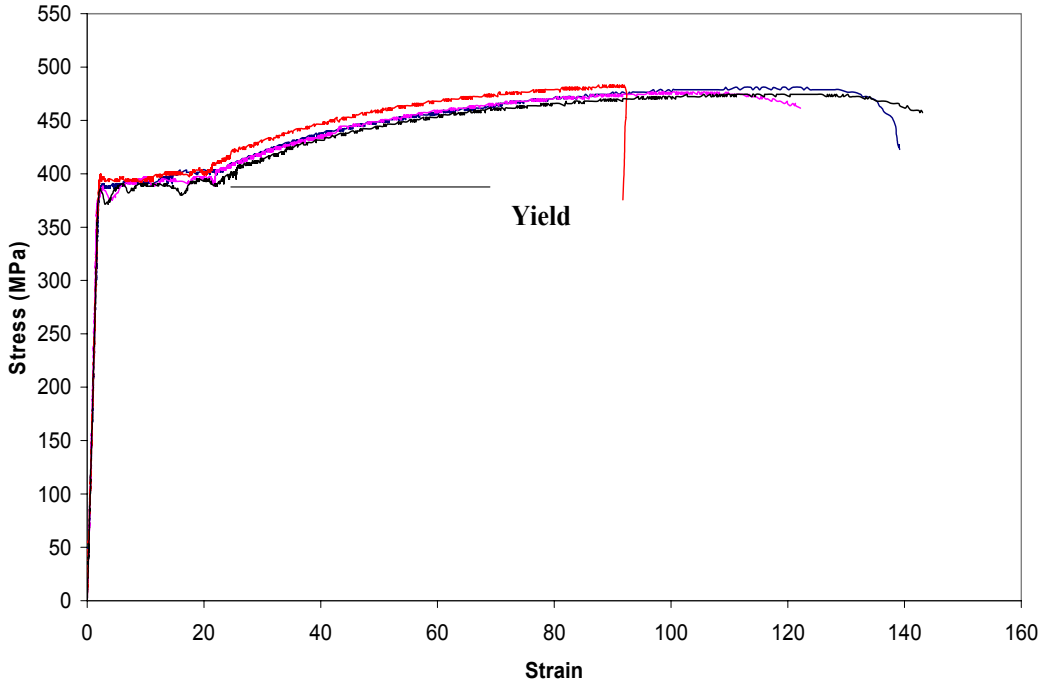

Figure 4 - 15: Typical stress strain diagram for Grade 300 steel sample (6 mm diameter)

4.4. Fabrication of specimens, test equipment and procedure

4.4.1. The test frames and load application

4.4.1.1 Seismic loading protocol

For all the tests on the exterior beam-column joint units of Group I and Group II, the same loading history was used. Gradually increasing reversed cyclic displacement was applied laterally of the top of the column, with the displacement increment in each step being 0.5 mm. The preset load–history shown in **Figure 4-16** demonstrates the displacement and drift for each cycle. For each drift two cycles were applied at the top of the column and one low-level cycle (0.1% drift) was applied after each second cycle. During each loading cycle run, the displacements at the top of the column were recorded on a personal computer until the target displacement level was reached.

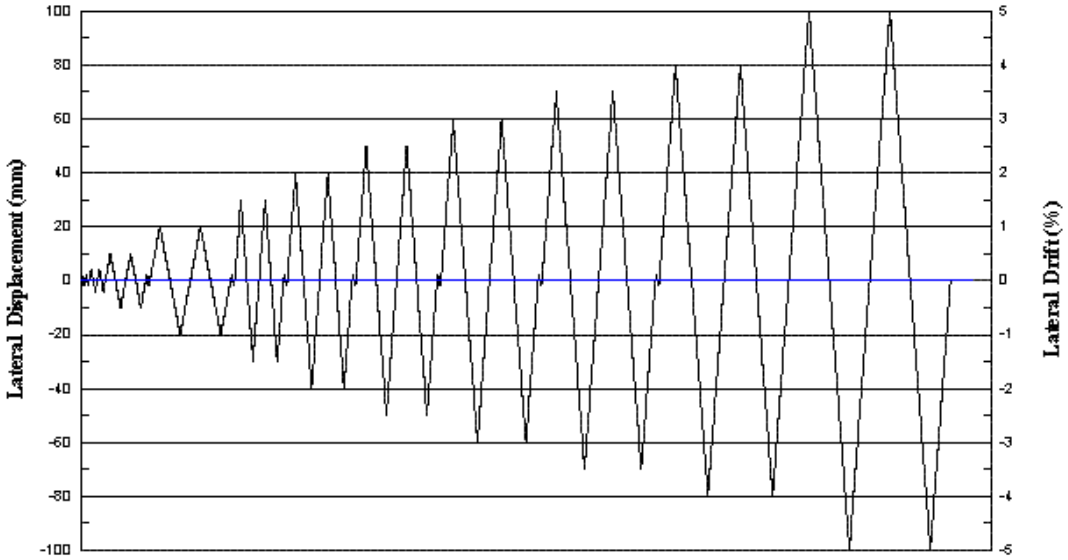

Figure 4 - 16: Typical load history

4.4.1.2 Measurement to determine the hysteresis loops

An important figure that must be generated to evaluate the structural seismic performance is the force-displacement hysteresis response. The force-displacement hysteresis response indicates the energy dissipation capacity of the structure by considering the area encompassed by the hysteresis loops. In this study, the lateral load and displacement of the column were measured for drawing the hysteresis loops.

4.4.1.3 Force and displacement measurement

Testing was carried out in the Structures Laboratory at the University of Canterbury. For Group I, units were tested under simulated seismic loading with a constant axial load of 75KN applied to the column. For Group II and III, units were tested under the same simulated seismic loading but with a constant 100 KN axial load. Independent loading reaction frames were designed to carry the reaction load of the simulated lateral seismic loading. The displacement controlled seismic load was simulated by applying horizontal forces at the top of the column while the beam was supported by a vertical hinging strut to hold the end of the beam in order to ensure the beam was free to rotate.

For each beam-column joint unit, three load cells were used to measure loads. Lateral load cell L1 was used to measure the lateral load applied by the hydraulic actuator, and beam load

cell L2 and column axial load cell L3 were used to measure beam end reaction and column axial compressive load as sketched in **Figure 4-17**.

For measuring the global displacement of the tested beam-column joint, three linear potentiometers were used as shown in **Figure 4-17**. Two linear potentiometers of 80 mm travel (P1) were used to measure the horizontal displacement of the beam end. Another 80 mm potentiometer (P2) was set on the reaction frame opposite to the position of the hydraulic actuator to measure the deformation of the rigid reaction frame. At the top of the column, a rotational potentiometer of 300 mm travel was used to measure the global displacement of the testing unit. A displacement controller was connected with this potentiometer through a computer which applied reversed cyclic loading (see **Figure 4-16**).

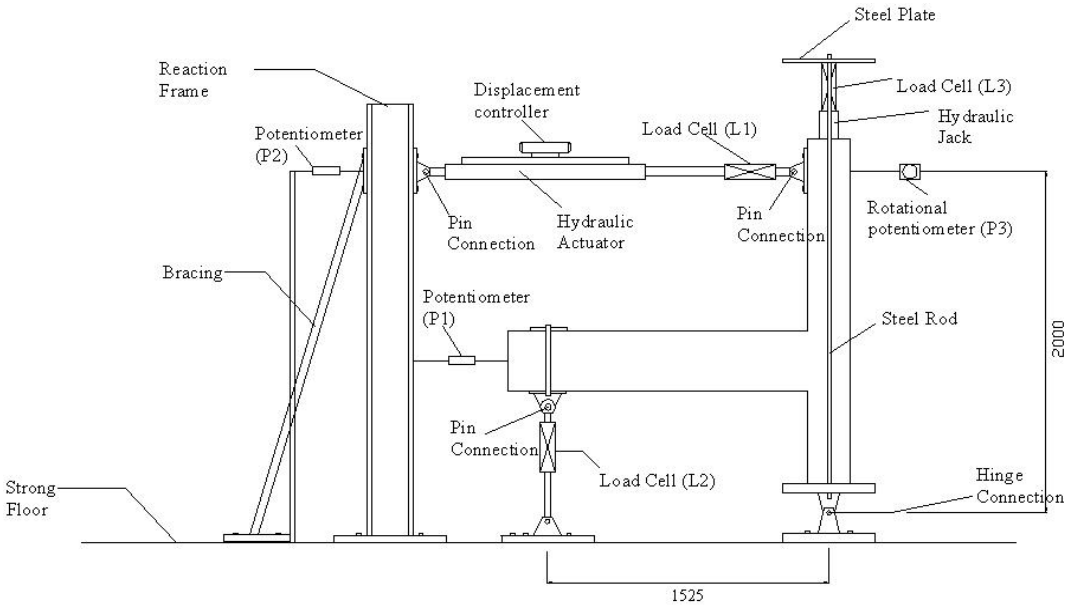

Figure 4 - 17: Experimental set up

4.4.2. Measurement of beam, column and joint

The arrangement of potentiometers measured the rotation of elements at the beam end, column end and joint region is shown in **Figure 4-18**. The linear potentiometers were placed at 14 different points on each unit to measure the deformations and displacements of the beam-column joint.

4.4.2.1 Joint shear distortion component

The shear distortion of the joint core was measured by six linear potentiometers set on the surface of the joint panel (see **Figure 4-18**). The relevant procedure used for determination of the joint distortion component is presented below (see **Figure 4-19**).

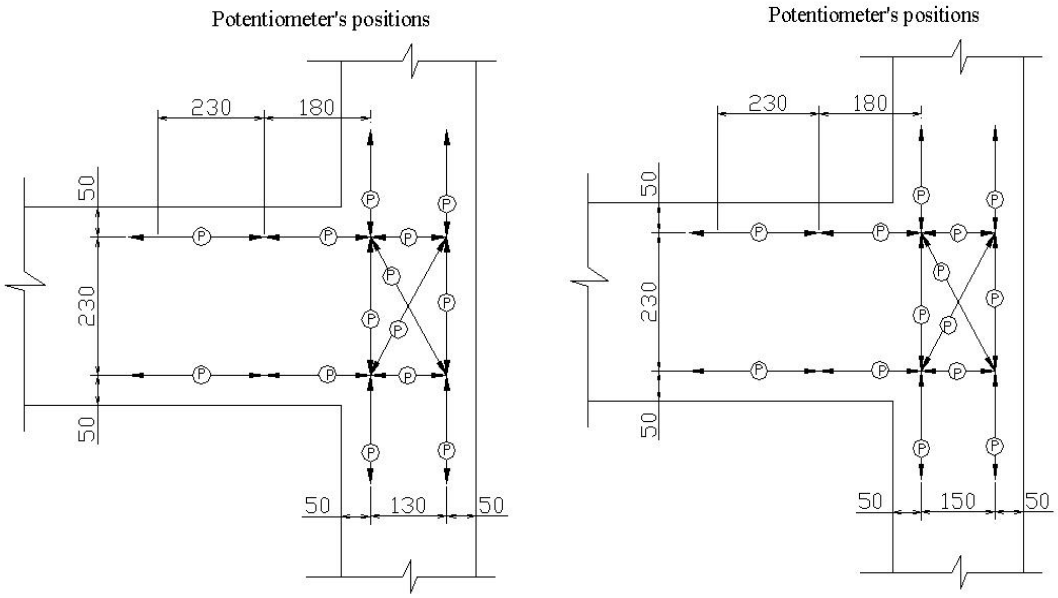

(a) Group I (b) Group II

Figure 4 - 18: Arrangement of potentiometers

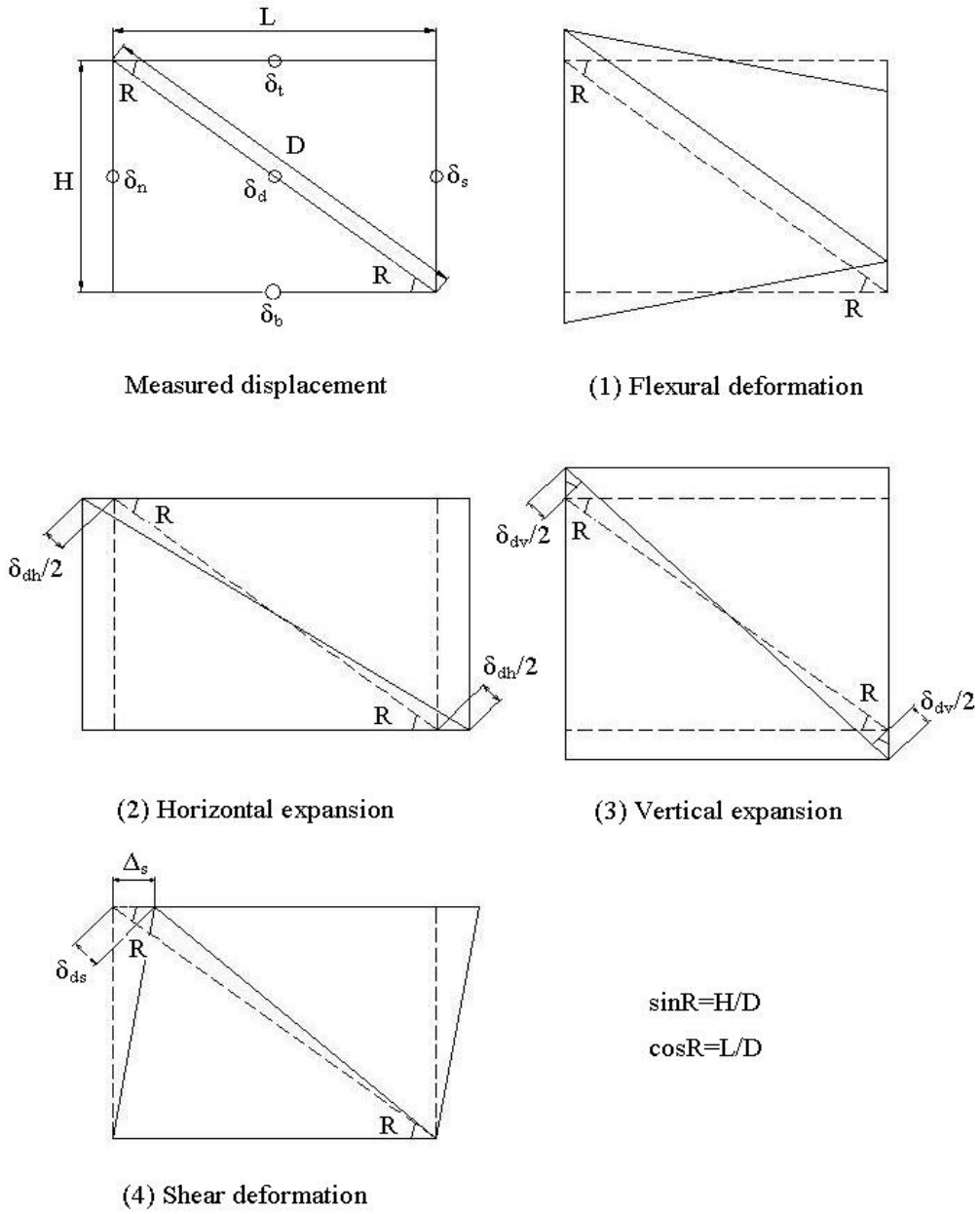

Figure 4 - 19: Procedure for evaluating the joint distortion component

Where:

$$\delta_{ds} = \delta_d - \delta_{dh} - \delta_{dv} \tag{4. 1}$$

$$\delta_{dh} = \frac{\delta_t + \delta_b}{2} \cos R \tag{4. 2}$$

$$\delta_{dv} = \frac{\delta_n + \delta_s}{2} \sin R \tag{4. 3}$$

Shear deformation:

$$\Delta_s = \frac{|\delta_{ds}|}{\cos R} \tag{4. 4}$$

4.4.3. Energy dissipation

4.4.3.1 Calculation of accumulated hysteretic energy and damping

The amount of accumulated hysteretic energy of a beam-column joint subassembly subjected to reversed cyclic loading was calculated as the integral of the area under the force versus displacement curve as given in Equation 4.5.

$$W_i = \int_{-\delta_i}^{\delta_i} P(x)dx + \int_{-\delta_i}^{\delta_j} P(x)dx \tag{4. 5}$$

$$W = \sum_{i=1}^{n} W_i \tag{4. 6}$$

Where W, is the total energy absorbed by each specimen, W_i is the accumulated hysteretic energy of i^{th} cycle, P(x) is the peak load and δ_i is the displacement at the i^{th} cycle.

Using the accumulated energy determined as shown above, the equivalent viscous damping of the units is able to be worked out. This equivalent viscous damping coefficient (ξ) is calculated as given in Equation 4.7.

$$\xi = \frac{A_{Total}}{4\pi A_{elastic}} \qquad (4.\ 7)$$

Where A_{Total} = summation of area of every cycle of load; $A_{elastic}$ = the area determined by the yield load and displacement as shown in **Figure 4-20**.

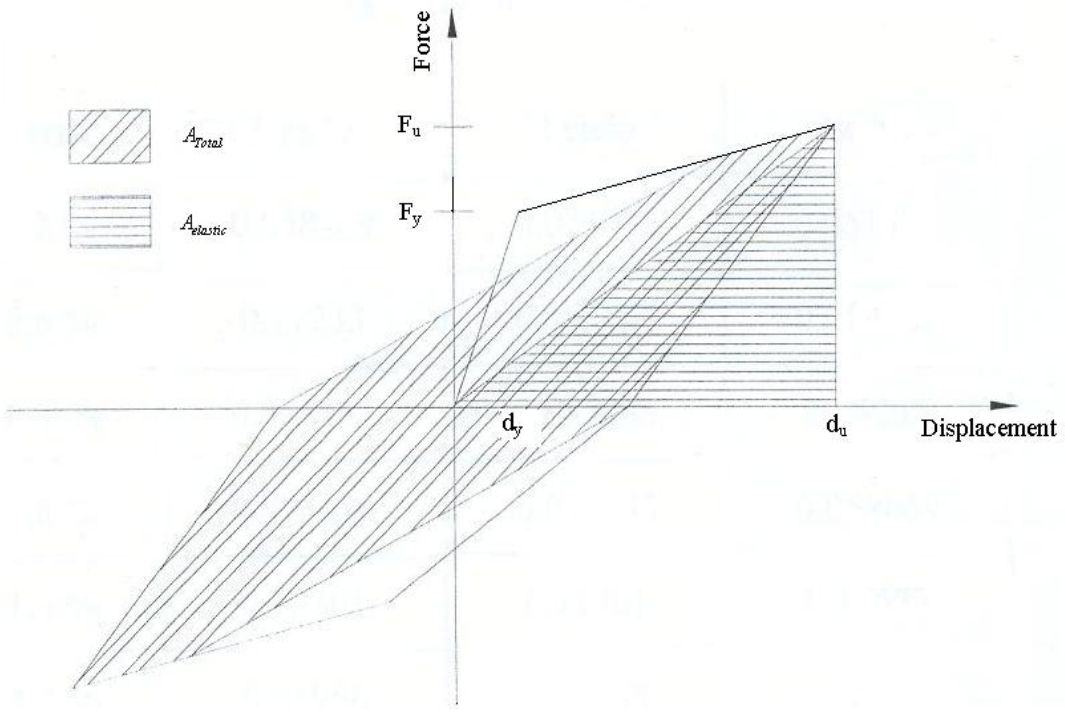

Figure 4 - 20: Evaluation of equivalent viscous damping

To study the energy dissipation capacity and damping of the beam-column joint units reinforced with different amounts of steel fibres or joint stirrups, the summation of the energy described by each cycle throughout the test was calculated. Moreover, for illustrating the plastic behaviour of the beam-column joint units subjected to reversed cyclic loading, the amount of total damping due to each cycle and the accumulated damping by all cycles were also calculated and compared amongst the units.

4.4.4. Crack detection

During the first five loading cycles corresponding to 0.1% to 1.5% drift, the widths of cracks were measured by using 'Eveready Microscope' hand crack detectors (a high magnification

hand microscope) for the further comparison of cracking patterns between conventional concrete joint and SFRC joint. All cracks were marked on the white painted surface.

4.4.5. Measurement of reinforcement strains

The strain variations along the longitudinal beam bars of the units of Group I were measured using twenty-four TML 120-ohm electrical strain gauges (Type FLA-3-11-3L). The arrangement of the strain gauges is shown in **Figure 4-21 (a)**.

The arrangement of the strain gauges of the units of Group II is shown in **Figure 4-21 (b)**. To determine the shear stress taken by hoops in a joint, not only the longitudinal beam bars' strains but also the strains of the transverse reinforcement in joints were measured by the same type of strain gauges as the units of Group II. In total, twenty-four electrical strain gauges were used in each unit of Group II (see **Table 4-4**).

At the same location, the strain gauges were set at two opposite faces, and the average values were taken as the real steel strains for further calculation.

All the electrical transmission lines of strain gauges cast into tested units were protected by plastic tubes (see **Figure 4-22**).

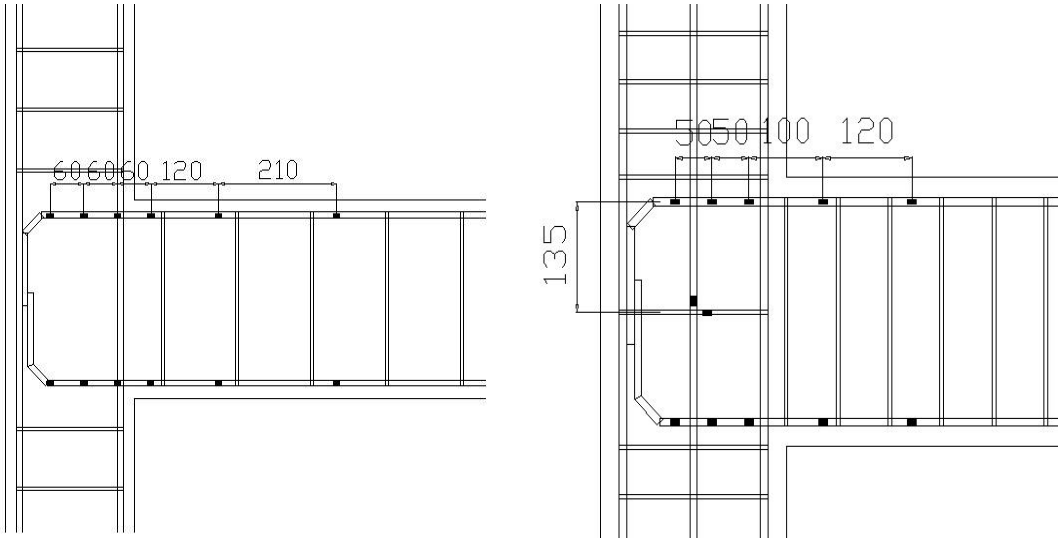

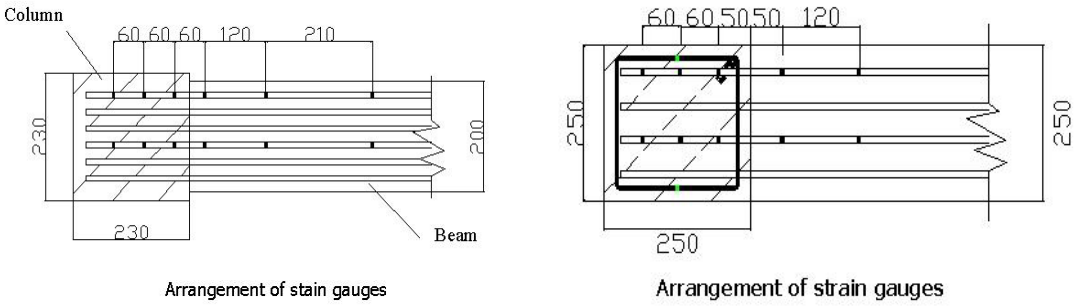

(a) Group I **(b) Group II**

Figure 4 - 21: Arrangement of strain gauges for tested units

Figure 4 - 22: Strain gauges in test unit

Table 4 - 4: Distribution of electrical resistance strain gauges

Test units	Components	No. of strain gauges
Beam-column joint units RC-1,SF-2 and SF-3	Beam longitudinal bars(R-10)	24
Beam-column joint units SF-4, F-5 and RC-6	Beam longitudinal bars(R-12)	20
	Column intermediate bars (R12)	2
	Joint hoops (R-6)	2

4.5. Testing procedure

Before the testing of each unit, a more complete set of readings of electrical resistance strain gauges, line potentiometers and beam end load cell was taken. For each test unit of Group I, a 75 KN axial load was applied. For each test unit of Group II, a 100 KN axial load was applied. The beam was supported in such a way that no beam moment was present at the column face

before testing. After the column axial load was applied, a displacement controlled cyclic loading (see **Figure 4-16**: Typical load history) was applied to the column top by using a hydraulic jack. In each cycle, a series of small force increments were taken until the target displacement was achieved, therefore force-displacement curve could be plotted in the connected data collecting computer. The procedure for each loading cycle is shown as follows:

1. Check all the connections of the instrumentations and load cell, and make sure that they are connected to the data collecting computer.
2. Set proper channels for each instrumentation and load cell. One channel should match one instrumentation or load cell
3. Set all channels to zero before testing.
4. Run the specified displacement loading cycle on the computer.
5. In each cycle run, check and mark the occurring cracking on the white painted surface. Then take photographs.

CHAPTER FIVE

5. TEST RESULTS AND THEORY VALIDATION

5.1. Introduction of Group Specimen I

The purpose of this section is to present the experimental results of units of Group I, Unit RC-1, Unit SF-2 and Unit SF-3, and investigate the joint seismic behaviour after adding steel fibre into the joint region. The contribution of the shear resistance of steel fibre in the joints was obtained by analysing the experimental results. Based on the experimental results exhibited in this chapter, the improvement in joint shear stress can be clearly seen through the method of the postulated hierarchy strength diagram method. The reinforcement detail of units of Group I were designed as non-seismic detailed beam-column joints. Different amounts of steel fibres, 1% and 2% by volume, were employed in the joint region of Unit SF-2 and Unit SF-3 respectively. The units were tested under the simulated seismic loading with a constant 75 KN axial load in order to investigate the seismic behaviour of joints with and without steel fibre.

5.1.1. Unit RC-1

5.1.1.1 Hysteretic response

Figure 5-1 shows the lateral force versus top displacement hysteretic response measured for Unit RC-1. Ductility and top drift are also shown in this graph. The first diagonal tension crack in the joint region occurred at a storey drift of 0.65% and reached the maximum strength of 20.66 KN. The interest is that after the first crack occurred in the joint panel, the strength was never recovered until the end of the test. Furthermore the strength degradation is clearly shown in **Figure 5-1**. Significant pinching of the loops caused by the degradation of shear strength resistance of the joint is shown in **Figure 5-1** indicating the energy dissipating capacity of Unit RC-1 was very poor. The pinching started at the early inelastic loading cycle (1.0% drift) and became worse and worse with accumulated displacement levels. During the testing process, the beam and column remained at the elastic stage and no critical cracks were found. A significant reduction in the strength of Unit RC-1 did not occurred with the increase in the imposed displacements after the maximum strength was attained, because the use of deformed beam bars well avoided the problem of bond slip. However buckling of the

longitudinal column bars and 90^{o} beam bars end in the joint region was found at the end of test.

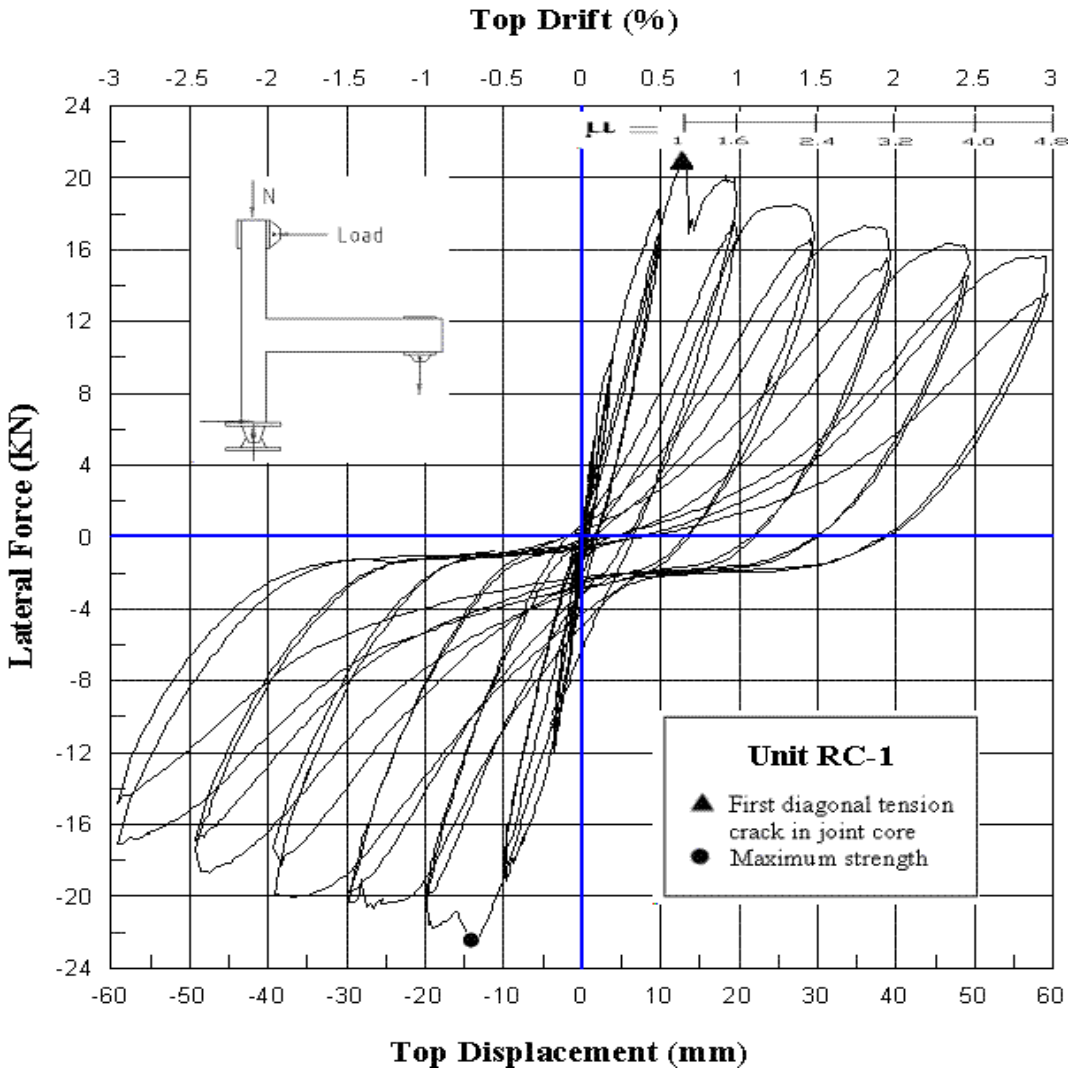

Figure 5 - 1: Lateral force vs. top displacement hysteretic response for Unit RC-1

5.1.1.2 Cracking and damage

The seismic performance of Unit RC-1 was extremely poor. Shear failure mode (shear hinge) occurred in the joint panel with significant crushing and spalling of the concrete cover during the last cycle run of 3.0% drift. The crack patterns at different cycle stages are presented in **Figure 5-2 (a)** to **(h)**. The inherent weakness of lack of transverse reinforcement in the joint region caused diagonal cracks to accumulate and concentrate in the joint region leading to

stiffness degradation and pinching of the hysteresis loops. As a subsequent result, the joint suffered from particularly brittle behaviour (spalling of the concrete wedge).

In elastic load cycles, 0.1% ~ 0.5% drift, fine flexural cracks spread along the top and bottom surface of the beam. The first flexural cracks at the positive side of the beam face adjacent to the joint started to open at the first positive loading cycle of 0.2% drift. A couple of additional fine cracks developed on each top and bottom columns adjacent to the joint panel along the beam faces when the unit was taken to a top drift of 0.5%.

The first positive and negative diagonal cracks which developed from corner to corner in the joint panel occurred during the first loading cycle of 1.0 % drift with widths of 0.16 mm and 0.2 mm. Besides, a few short diagonal cracks parallel with the first positive and negative diagonal cracks also developed on both diagonal directions of the joint panel.

After a 1% drift cycle run, the diagonal cracks were accumulating and concentrating in the joint region with the increasing intensity of the cycle load. During the last cycle loading, the peculiar degrading mechanism (named “concrete wedge”) occurred in the joint panel. After spalling of the concrete cover, the joint completely lost its capacity.

In the beam plastic hinge region, only a few fine cracks spread at the early elastic stage. No critical cracks were observed during the whole testing.

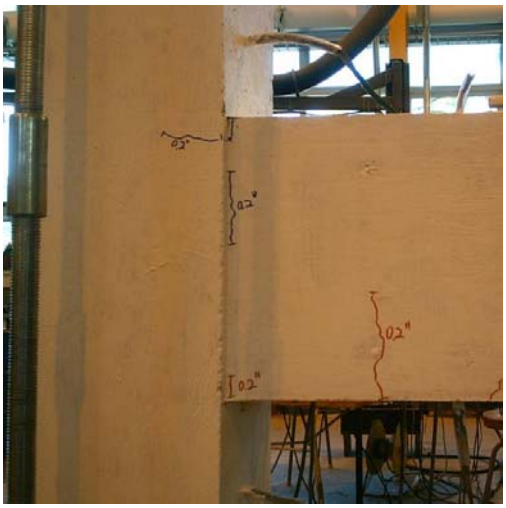

(a) 0.2% drift

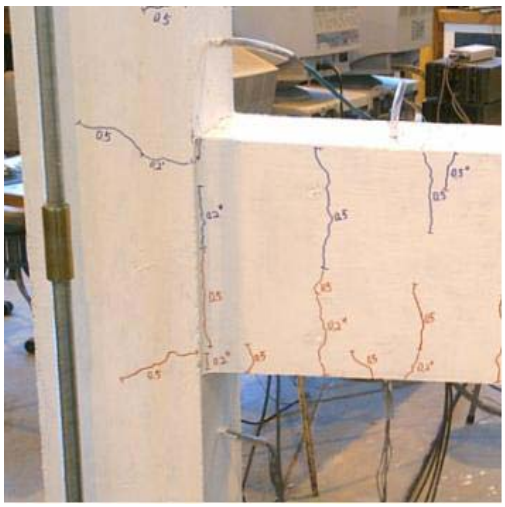

(b) 0.5% drift

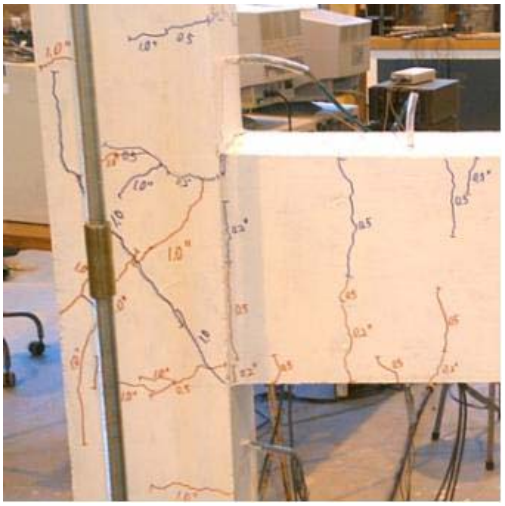

(c) 1% drift

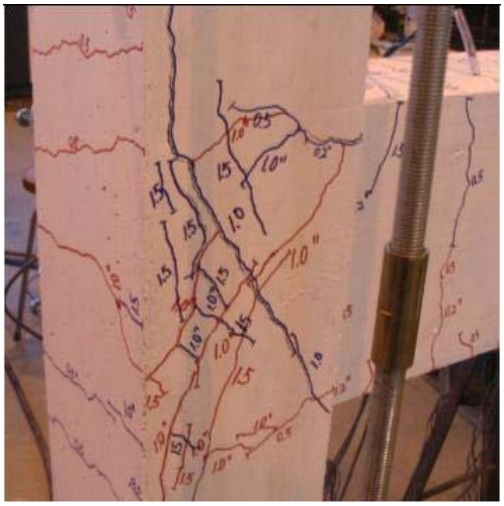

(d) 1.5% drift

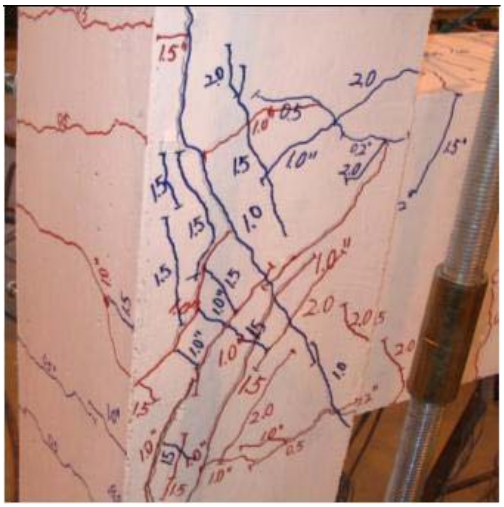

(e) 2% drift

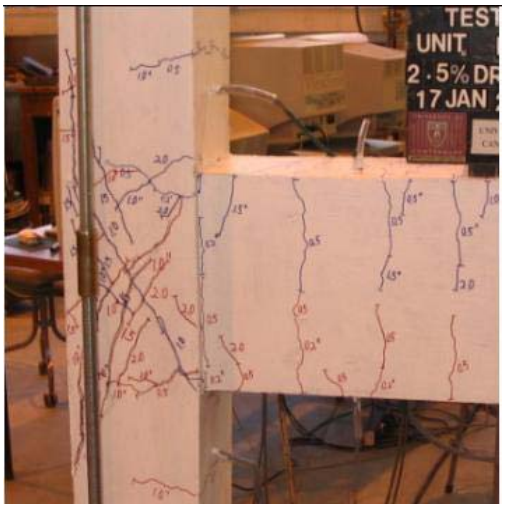

(f) 2.5% drift

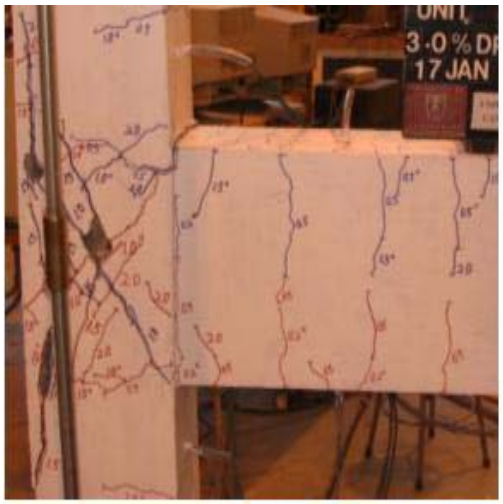

(g) 3% drift (First cycle)

(h) 3% drift (End)

Figure 5 - 2: Observed damage of Unit RC-1

5.1.1.3 Joint behaviour

Figure 5-3 shows a group graph analysing the behaviour of the joint for Unit RC-1. **Figures 5-3 (a)** and **(b)** illustrate the variations of the joint shear deformation and the measured joint shear stress respectively for Unit RC-1. The result of this unit showed that the joint region is the critical area for Unit RC-1, as the cracking damage accumulated. The joint shear deformation at the points of the first diagonal cracking and extensive damage were 0.000769 and 0.00136 in rad with the principal tensile stress (P_t) of 1.796 N/m^2 ($P_t / \sqrt{f'_c}$ = 0.4246) and 1.98 N/m^2 ($P_t / \sqrt{f'_c}$ = 0.4691) respectively, both were bigger than those ($P_t / \sqrt{f'_c}$ =0.29 for first cracking and 0.42 for extensive damage) presented by Pampanin's paper [11]. Other details of the critical points are shown in **Table 5-1**. Significant pinching of the loops, v_j versus γ and v_j versus displacement, caused by the degradation of shear strength resistance of the joint is shown in **Figure 5-3 (e)** and **(f)**, indicating the energy dissipating capacity of Unit RC-1 being very poor.

Table 5 - 1: Sequence of events of Unit RC-1

	Sequence of events	Force(KN)	v_j (MPa)	P_t(MPa)	$K=P_t/\sqrt{f'_c}$	γ (rad)	Drift
Unit RC-1	First cracking	20.66	2.425	1.796	0.4246	0.0007694	0.65
	Extensive cracking	22.6522	2.6409	1.9847	0.4691	0.00136	0.71
	End test	13.29	1.569106	0.906496	0.214259	0.0042256	2.96

5.1.1.4 Longitudinal beam bar strains

For Unit RC-1, the joint was expected to develop a shear hinge.

Figure 5-4 and **Figure 5-5** show the measured strain profiles from the strain gauges along the longitudinal beam bars. Before the first loading cycle of 1.0% drift, the tensile strain along the beam bars was gradually increased. In the loading cycle of 1.0% drift, in which the joint diagonal tension cracks were initiated, the top beam bars reached the yield strain in the joint region adjacent to the column's inner face indicating yield penetration into the joint core. Then, with a joint shear hinge ("concrete wage" mechanism) formed by the extensive joint diagonal tensile cracks, the subsequent loading cycle resulted in significant large tensile strain along the area of beam bar hooks indicating the bond forces were mainly provided by the beam bars around the inner column face and 90^o bend hooks.

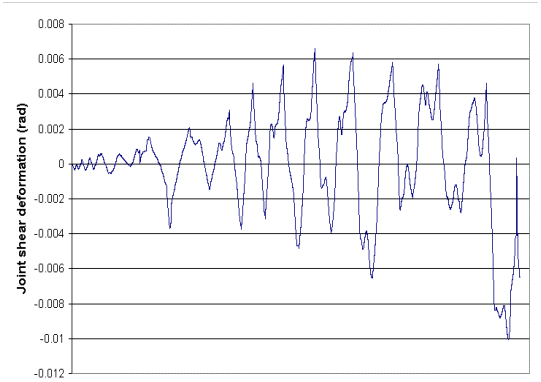

(a) Measured joint shear deformation history

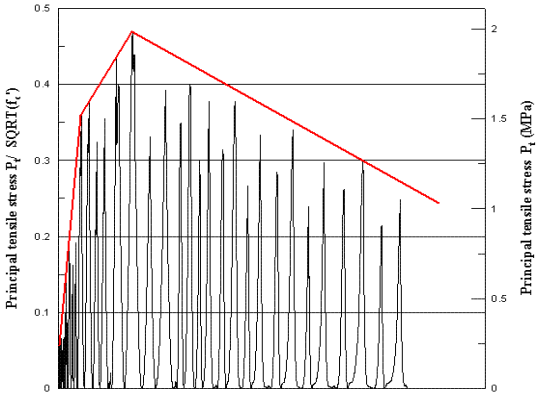

(b) Principal tensile stress history

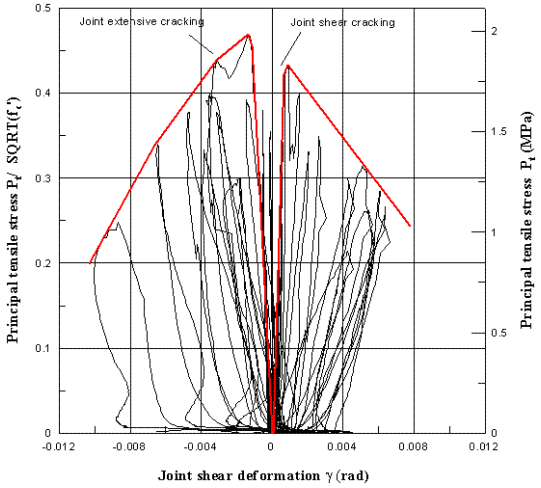

(c) Principal tensile stress vs. Joint deformation

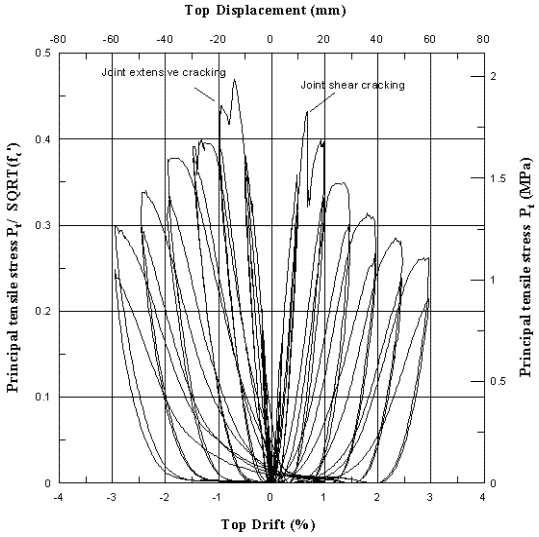

(d) Principal tensile stress vs. Top drift

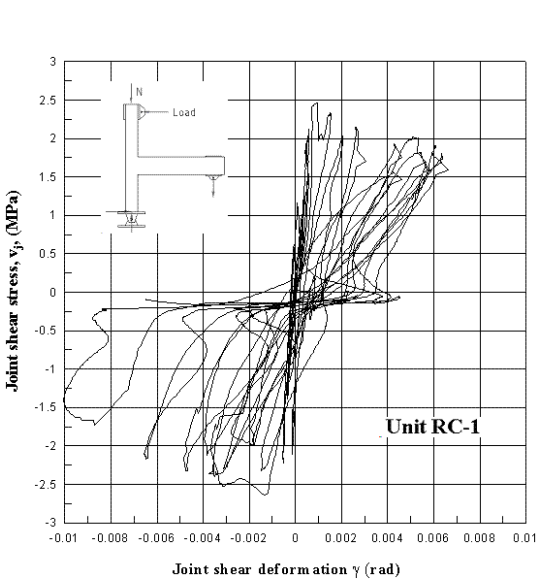

(e) Joint shear stress vs. Joint deformation

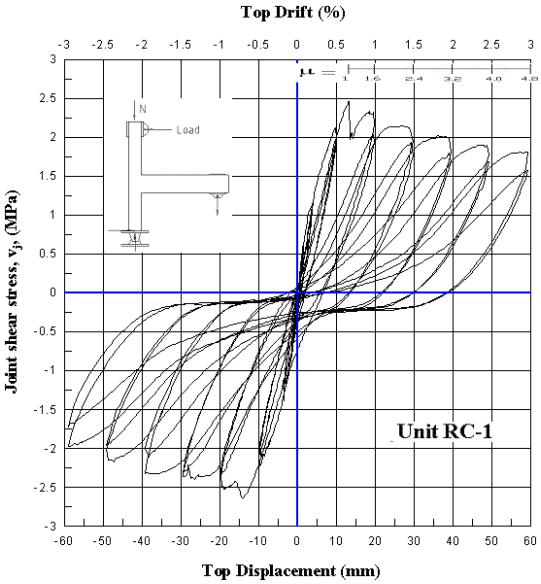

(f) Joint shear stress vs. Top displacement

Figure 5 - 3：Experimental joint behaviour for Unit RC-1

Compared with the top beam bars, the strains measured in the joint approached the yield strain in the loading cycle of 2.0% drift at both positive and negative loading direction. After that stage, the strain in this area became larger and larger indicating that the shear stress in the joint was mainly resisted by the beam bars adjacent to the column's inner face.

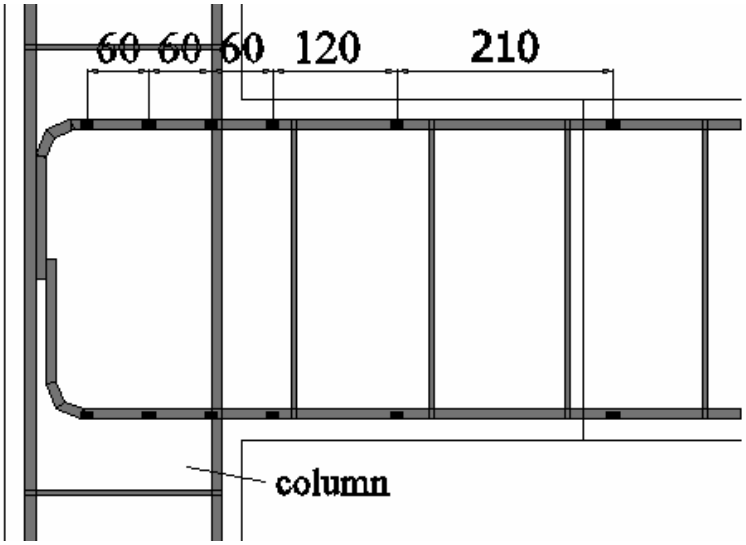

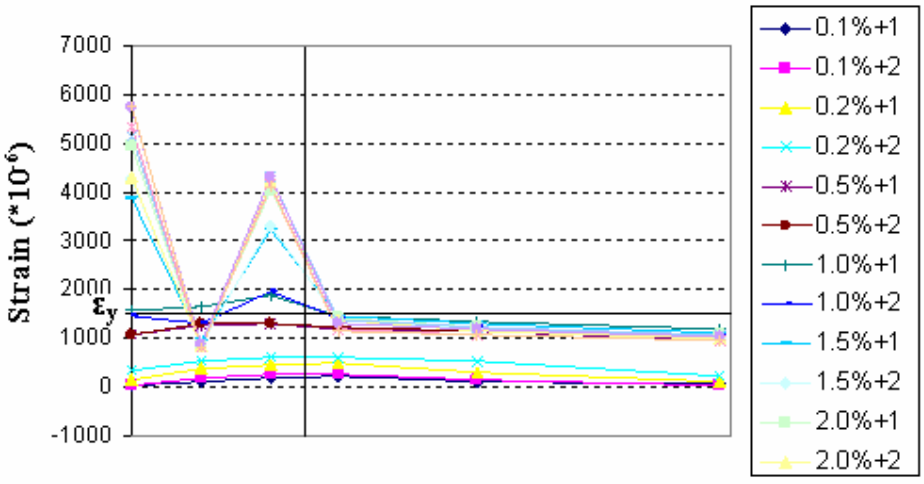

Top beam bar (positive loading cycle)

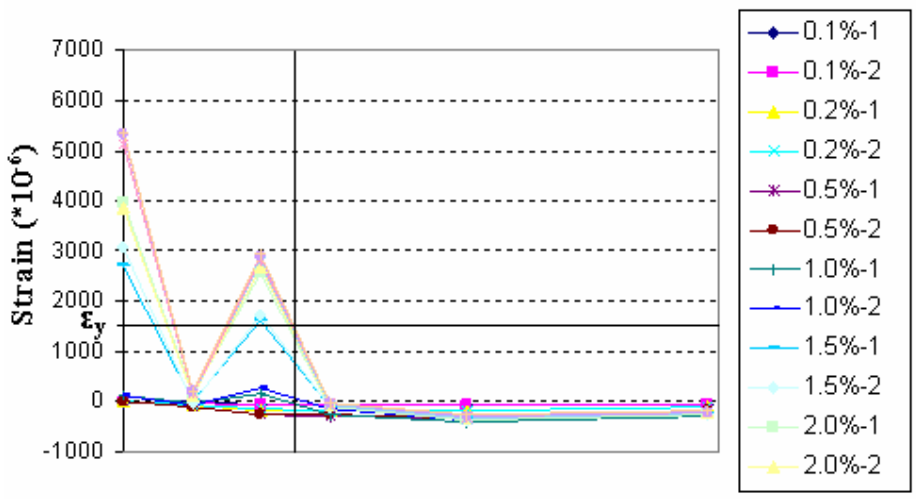

Top beam bar (negative loading cycle)

Figure 5 - 4: Strain profiles of beam bars measured by the strain gauges of Unit RC-1: top bar

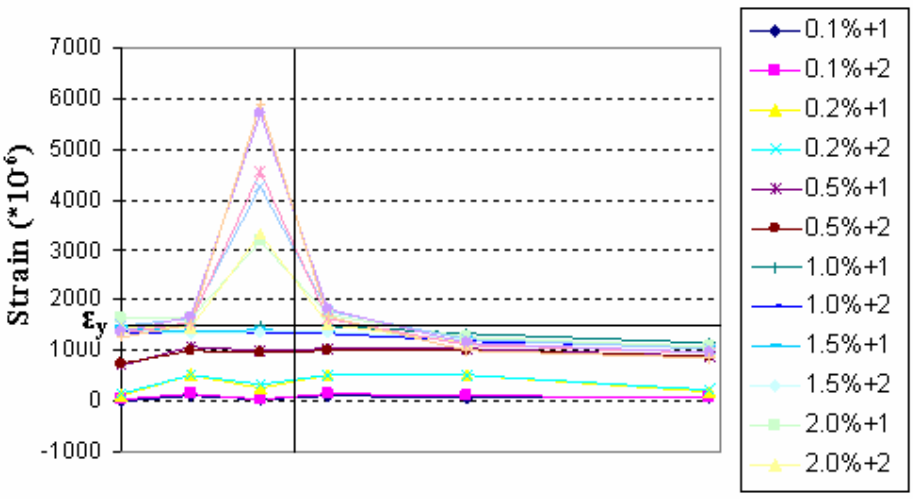

Bottom beam bar (positive loading cycle)

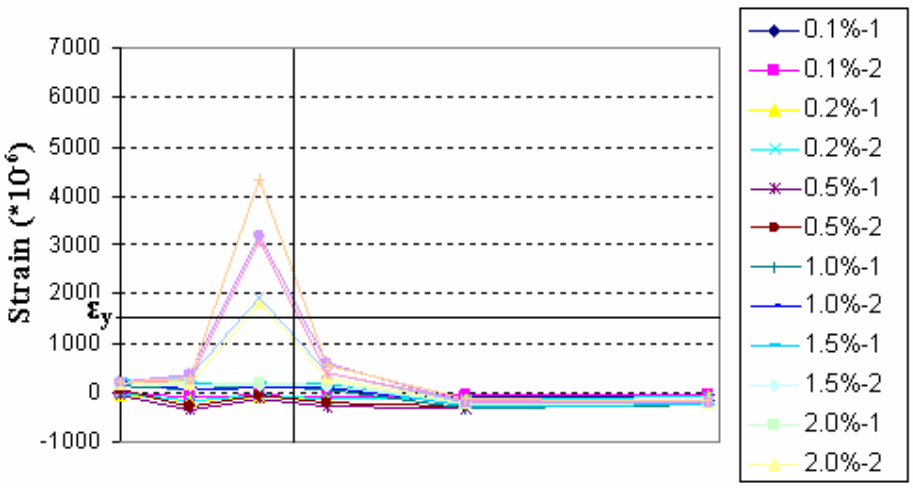

Bottom beam bar (negative loading cycle)

Figure 5 - 5: Strain profiles of beam bars measured by the strain gauges of Unit RC-1: bottom bar

5.1.2. Unit SF-2

5.1.2.1 Hysteretic response

The hysteresis loop of measured lateral force versus displacement for Unit SF-2 is shown as **Figure 5-6**. Compared with Unit RC-1, shear resistance capacity of Unit SF-2 was increased by adding 1.0% steel fibre in the joint region, then the simulating seismic load was run until 4.0% drift. The ductility of Unit SF-2 was less than that of Unit RC-1, as Unit SF-2 presented a high value of yield displacement.

The first diagonal micro tension crack in the joint was observed at a drift of 0.7% with the strength of 23 KN. The maximum strength was 25.4 KN with a drift of 0.9%. It should be noted that after the critical diagonal corner to corner crack occurred in the joint region, the strength did not drop down significantly. The amount of lost strength was only 0.5 KN, from 25.4 KN to 24.9 KN, which was much less than that of Unit RC-1 (5.56 KN, from 22.65 KN to 17 KN). These phenomena explained that steel fibres can carry the shear strength after the concrete matrix opens and reduce the damage to the joint.

The strength degradation of Unit SF-2 was flatter, from 25.4 KN to 21.3KN (16.8% reduction), compared with that of Unit RC-1 from 22.56 KN to 15.6 KN (26.4% reduction). However, pinching of the loops was present in **Figure 5-6**, indicating that the energy dissipation capacity was still unsatisfied.

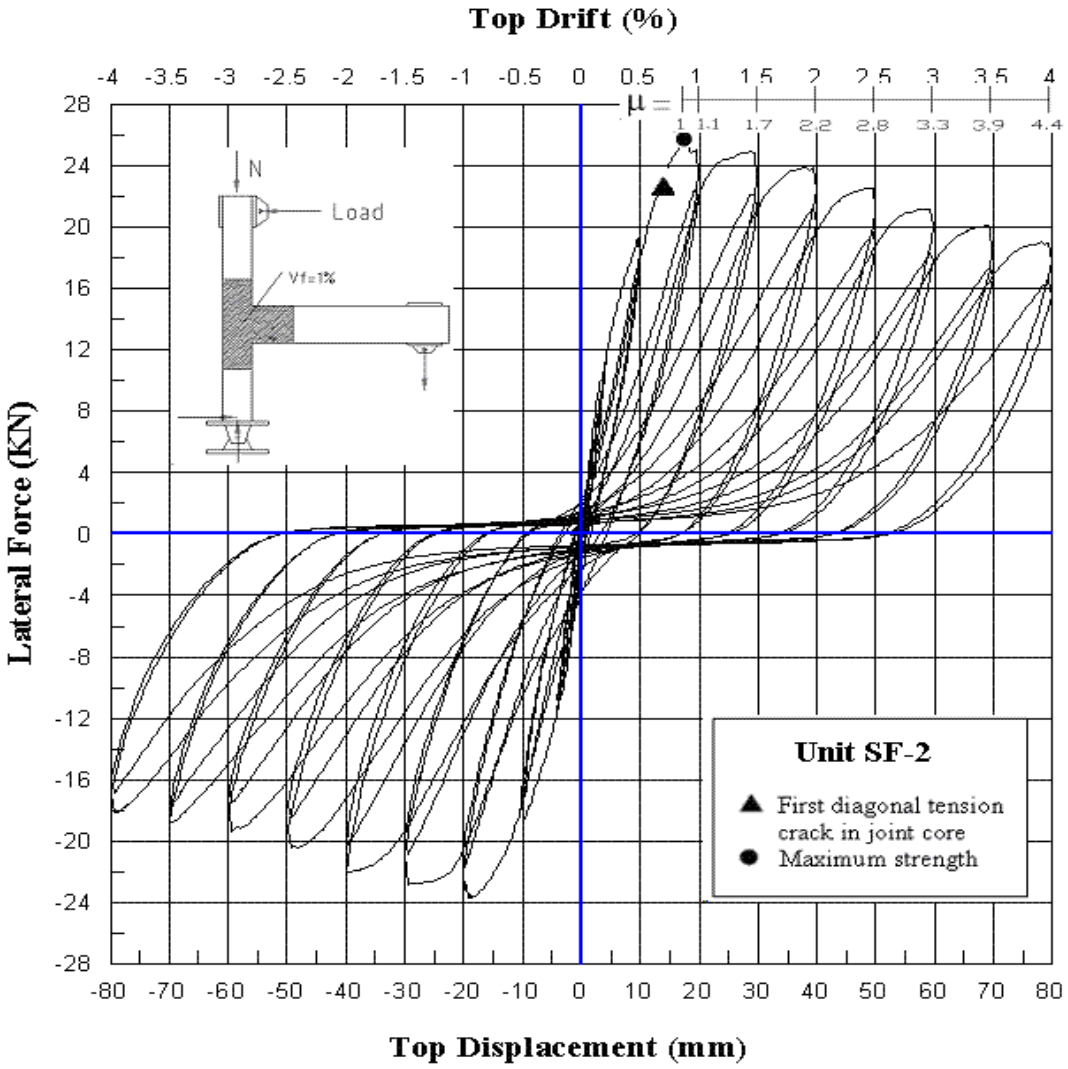

Figure 5 - 6: Lateral force vs. top displacement hysteretic response for Unit SF-2

5.1.2.2 Cracking and damage

The seismic performance of Unit SF-2 was much better than that of Unit RC-1. Although shear cracks were still found in the joint region, the flexural opening at the column end adjacent to the joint was the main failure mode. It must be noted that during the test cracks were formed with many fine non-continuous cracks, however, these cracks never connected to form serious cracks with the use of steel fibres. **Figure 5-6 (a) ~ (f)** shows the cracks mode at different stages under the seismic load.

Some fine micro cracks started to appear on the surface of the beam in early elastic loading cycles (before 0.2% drift) and increased and spread during the loading cycle of 0.5% drift.

The diagonal cracks occurred during the 1.0% drift cycle run with widths of 0.3 mm. With the increasing intensity of the load, many fine and non-continuous short diagonal cracks developed in the joint panel. From the photo (**Figure 5-7 (j)**) it can be seen that although a "concrete wedge" was formed by diagonal share cracks, the joint still retained its integrity (the "concrete wedge" did not spall out from the joint).

The flexure cracks on each top and bottom columns adjacent to the joint panel along the beam faces occurred at a drift of 0.2% and developed to become critical cracks when the unit was taken to a top drift of 2.0%. The test was finally stopped at a drift of 4.0% due to the possibility of column flexure opening leading to a serious safety problem (see **Figure 5-7 (i)**).

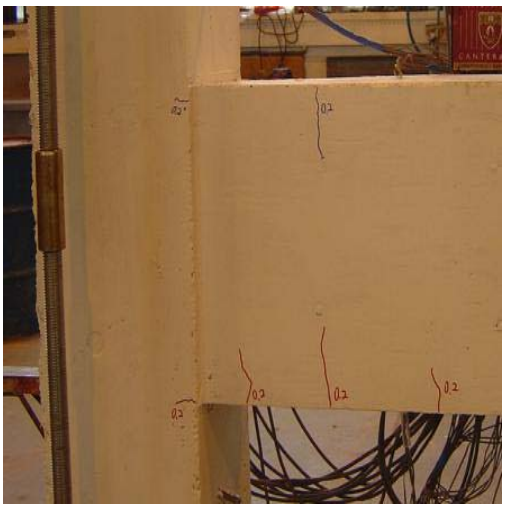

(a) 0.2% drift

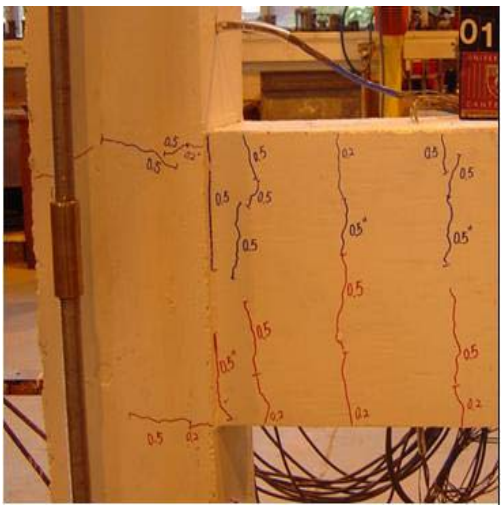

(b) 0.5% drift

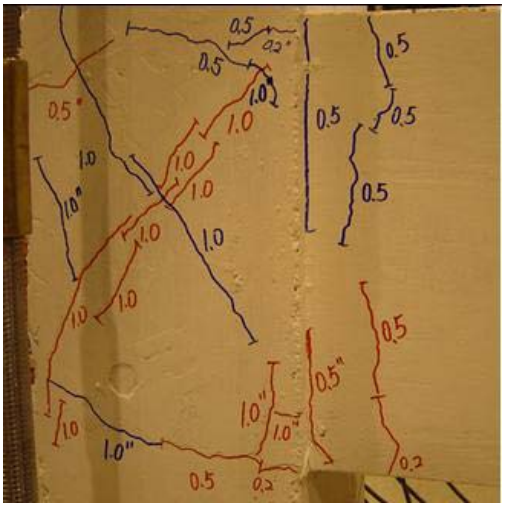

(c) 1% drift

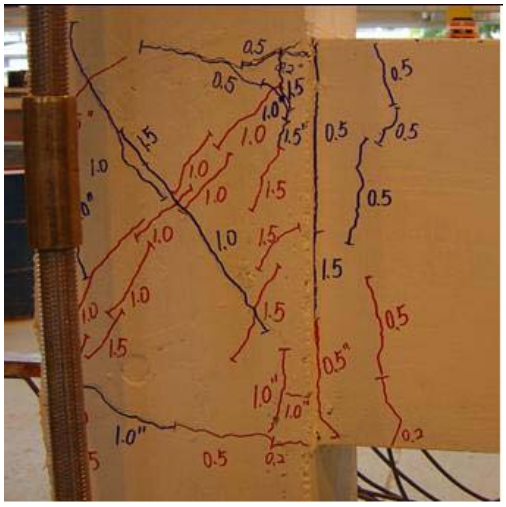

(d) 1.5% drift

(e) 2% drift

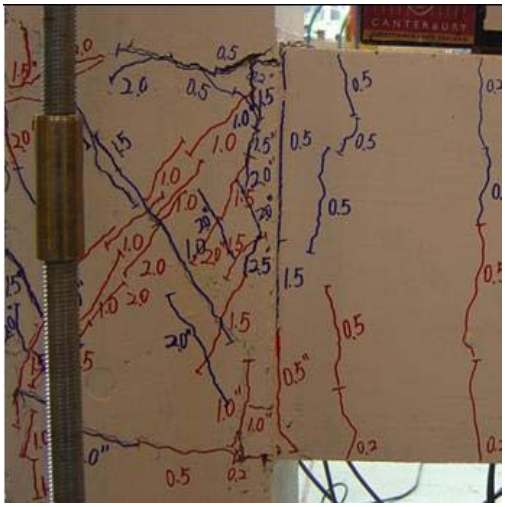

(f) 2.5% drift

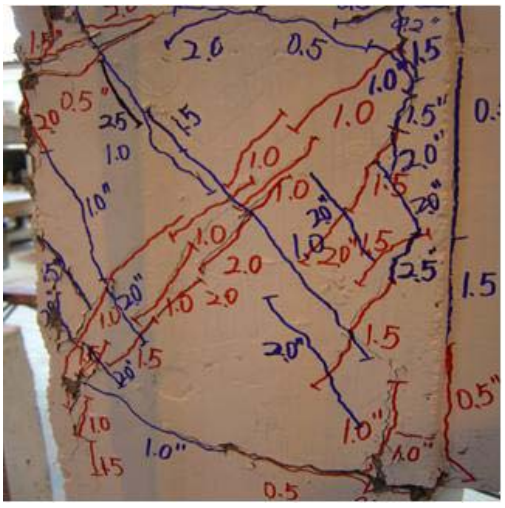

(g) 3% drift

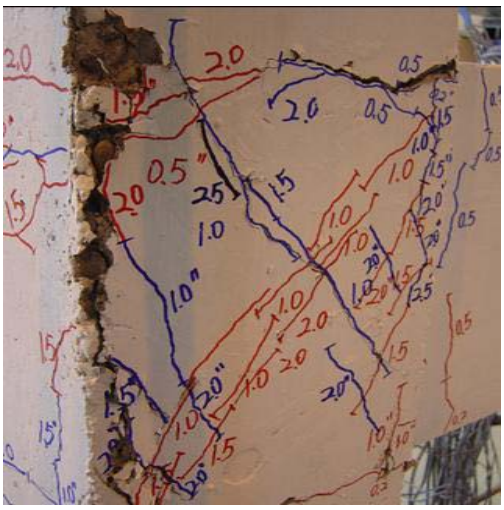

(h) 3.5% drift

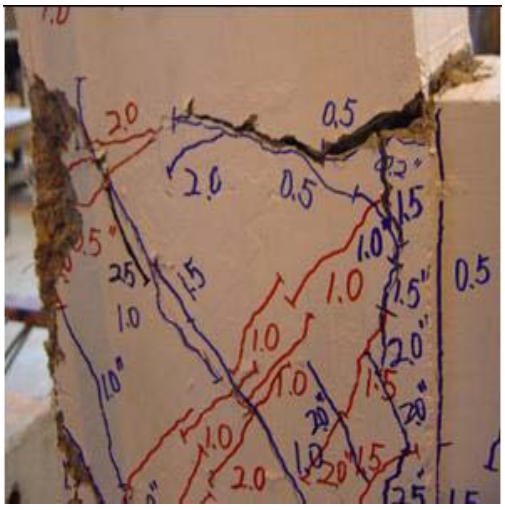

(i) 4.0% drift (Front side)

(j) 4.0% (back side)

Figure 5 - 7: Observed damage of Unit SF-2

5.1.2.3 Joint behaviour

Although the joint shear failure was still one of the failure modes, the joint seismic performance of Unit SF-2 was much better than Unit RC-1. **Figure 5-8 (a)** shows the joint shear deformation of Unit SF-2 measured until 4.0% drift testing. Compared with Unit RC-1, Unit SF-2 presented better integrity as it had only 0.005 rad of the joint shear deformation at the drift of 3.0%, which was approximately 50% of that of Unit RC-1 (0.01 rad at the drift of 3.0%). Throughout the whole loading histories, there was no severe bond degradation along the beam bars and strength degradation resulting from the brittle concrete cracks, because of the use of steel fibres. **Figure 5-8 (b)** shows the variations in the joint principal tensile stress (P_t) with the loading history for Unit RC-1. After reaching the maximum value (2.3 MPa), P_t gradually reduced with the increasing displacement. The percentage of the strength reduction of P_t of Unit SF-2 was only 43% (from 2.3 to 1.31 MPa), slightly less than that of Unit RC-1, 54% (from 1.98 to 0.9 MPa). However, pinching of the loops was still found, indicating an unsatisfied energy dissipation capacity

Figure 5-8 (c) ~ (d) shows the graphs of the joint principal tensile stress versus the joint shear deformation and top displacement of Unit SF-2. Significant joint shear cracks within the joint region were still found in this unit. The first diagonal crack occurred at 0.49 ($P_t / \sqrt{f'_c}$) with 0.000162 rad, after that the tested unit reached the extensive damage of 0.54 with 0.00042 rad. The measured hysteresis loops of the joints shear stress versus joint shear deformation (v_j versus γ) and the joint shear stress versus displacement (v_j versus displacement) for Unit SF-2 are shown as **Figure 5-8 (e) ~ (f)**. Compared with Unit RC-1, Unit SF-2 showed a better shear resistance response, as it reached a higher value of joint shear stresses with lower joint deformation. The first cracking and the extensive damage occurred at the joint shear stress point of 2.72 MPa with 0.000162 rad of joint deformation and 2.976 MPa with 0.00042 rad of joint deformation respectively.

Table 5 - 2: Sequence of events of Unit SF-2

	Sequence of events	Force(KN)	v_j (MPa)	P_t(MPa)	$K=P_t/\sqrt{f'_c}$	γ (rad)	Drift
Unit SF-2	First cracking	23.0633	2.725256	2.078318	0.491231	0.000162	0.71
	Extensive cracking	25.4422	2.976771	2.306277	0.545111	0.0004231	0.90
	End test	16.11	1.925668	1.316205	0.311098	0.0099162	3.95

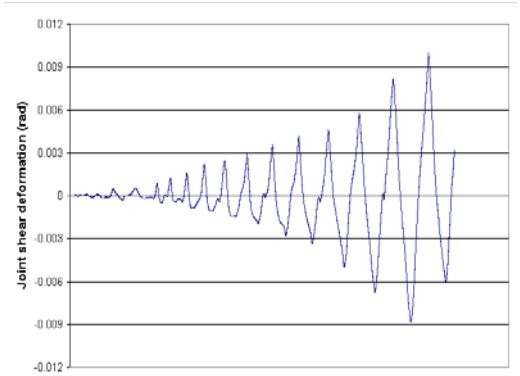

(a) Measured joint shear deformation history

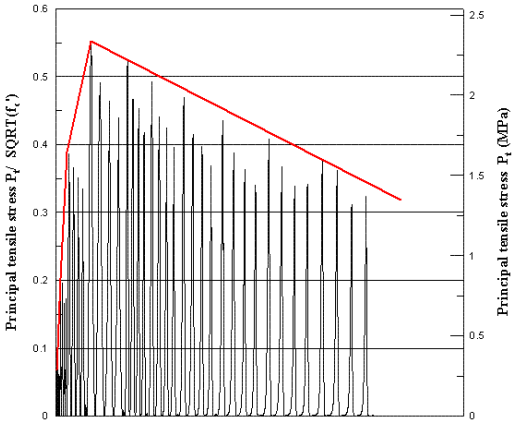

(b) The principal tensile stress history

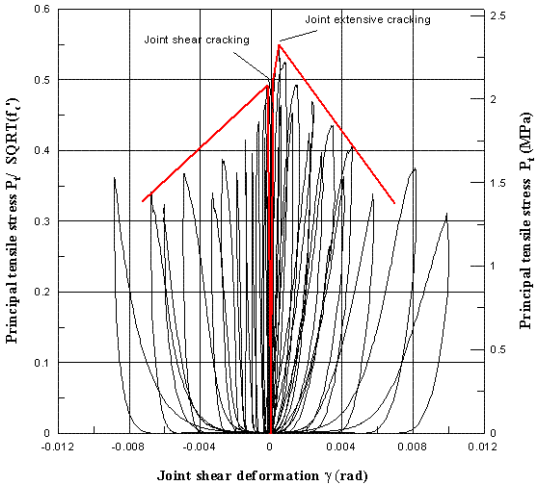

(c) Principal tensile stress vs. Joint deformation

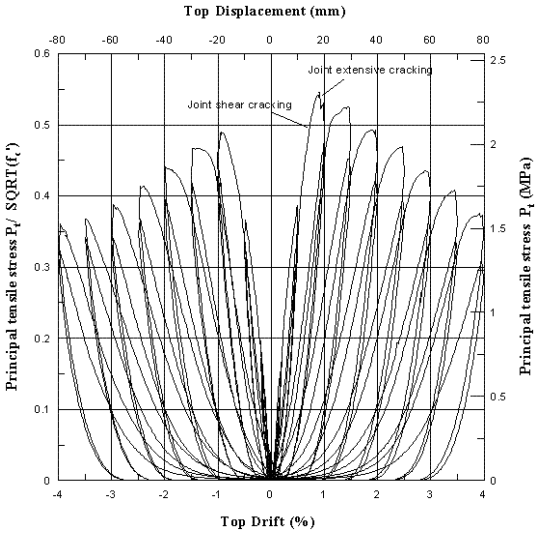

(d) Principal tensile stress vs. Top drift

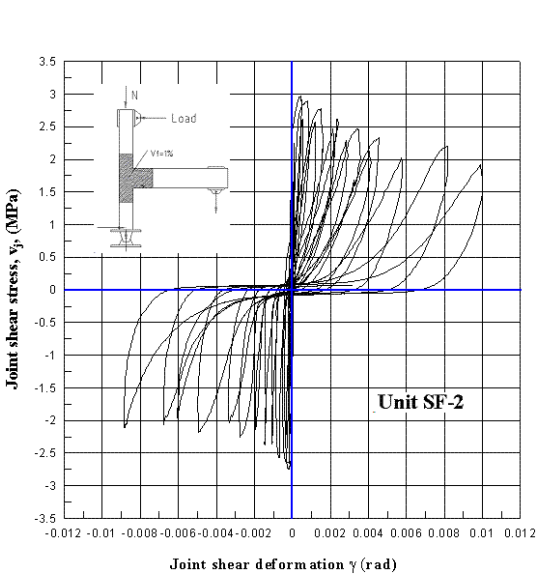

(e) Joint shear stress vs. Joint deformation

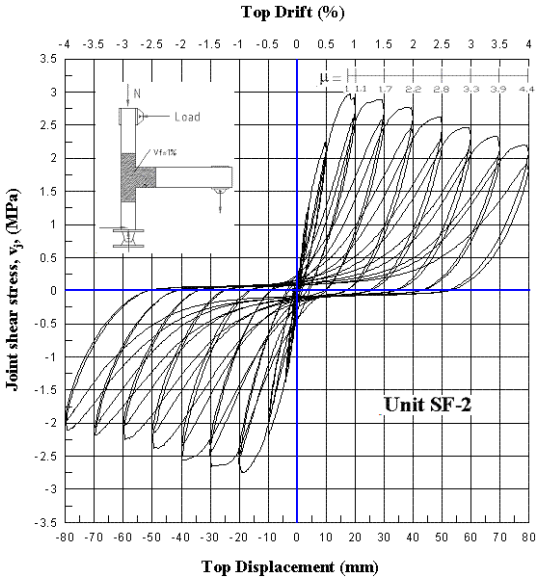

(f) Joint shear stress vs. Top displacement

Figure 5 - 8： Experimental joint behaviour for Unit SF-2

5.1.2.4 Longitudinal beam bar strains

Strains measured along the longitudinal beam bars are shown in **Figure 5-10** and **Figure 5-11**. It was seen that the beam bars still remained in the elastic strain stage in the inelastic loading cycle (1.0% drift) because of the bridging action of steel fibre (see **Figure 5-9**). After the concrete cracked in the joint region, pullout resistance (dowel action) and the bridging action of steel fibres significantly improved the post-cracking tensile strength of concrete and resisted the joint shear stress. Hence such effects delayed the yield strains stage of longitudinal beam bars of Unit SF-2 to the loading cycle of 1.5%. Furthermore, by comparison, the beam bars strains of Unit SF-2 were more than 50% greater than for the non-fibre specimen of Unit RC-1 indicating the better bond and anchorage capacity of the SFRC joint.

The bottom longitudinal beam bars showed a similar behaviour to the top beam bars, but the yield stage was delayed to a loading cycle of 2% drift. The yield positions of beam bars, for both top bars and bottom bars, occurred in the area adjacent to the column's inner face indicating the joint still was the critical area of Unit SF-2.

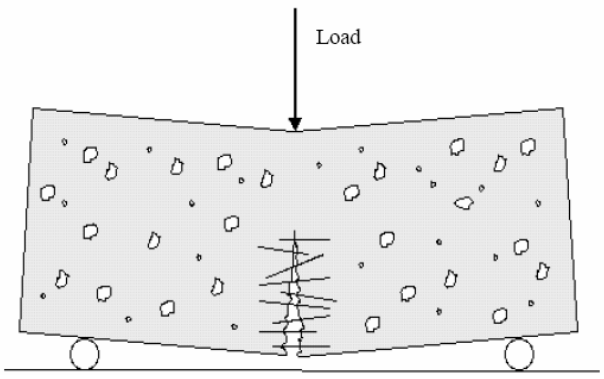

Figure 5 - 9: Bridging action of steel fibre

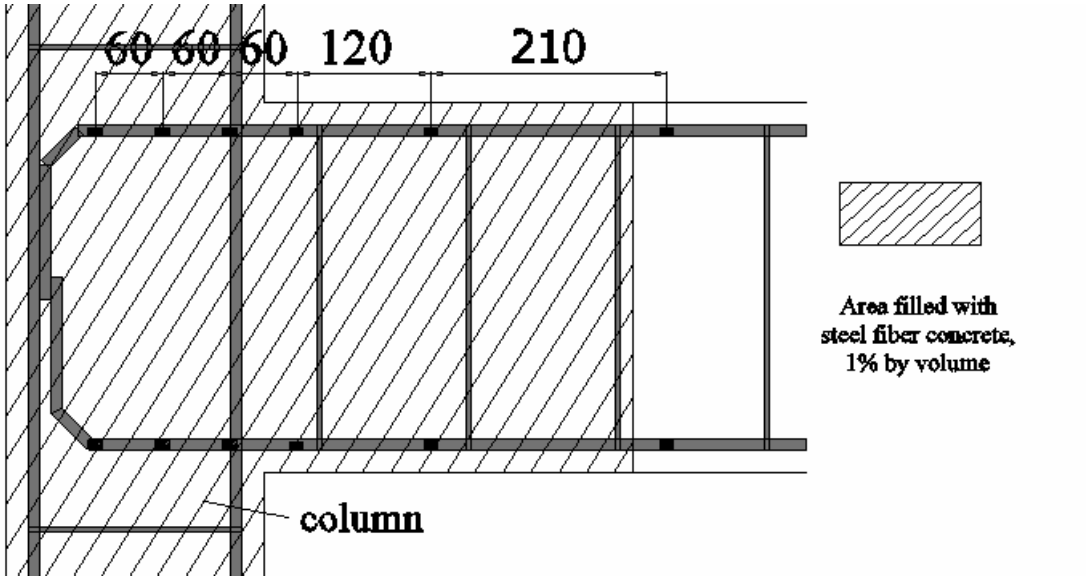

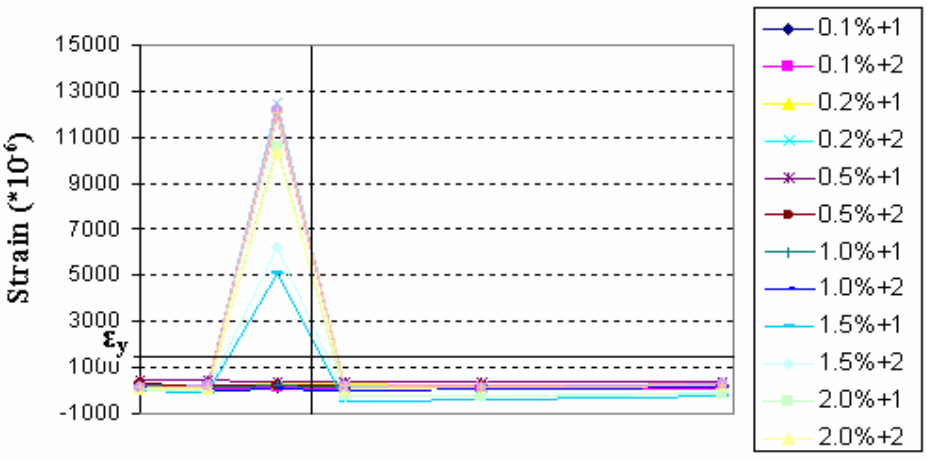

Top beam bar (positive loading cycle)

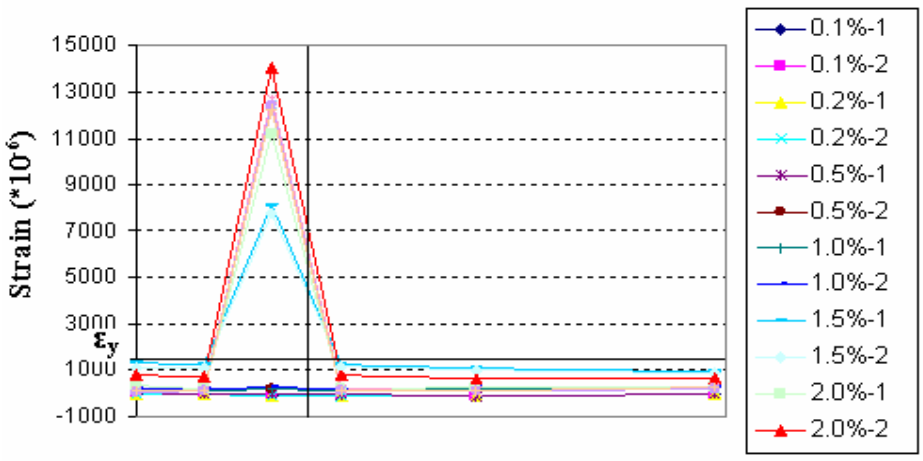

Top beam bar (negative loading cycle)

Figure 5 - 10: Strain profiles of beam bars measured by the strain gauges of Unit SF-2: top bar

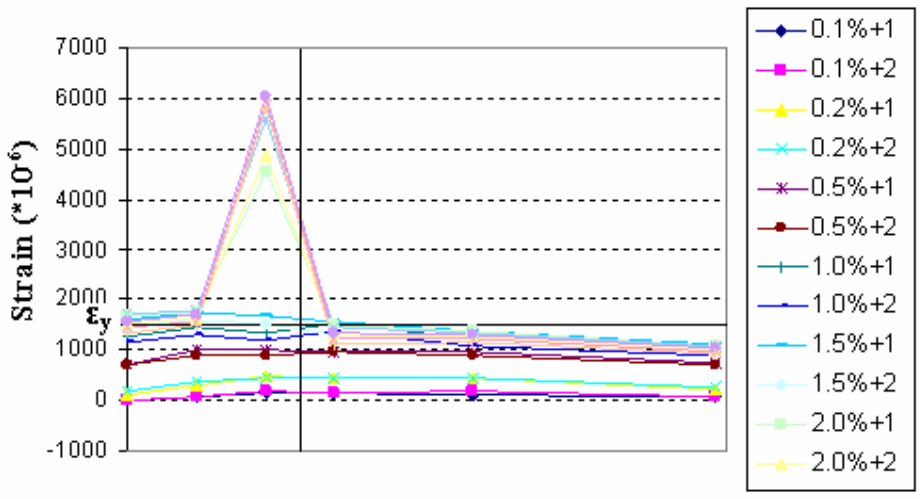

Bottom beam bar (positive loading cycle)

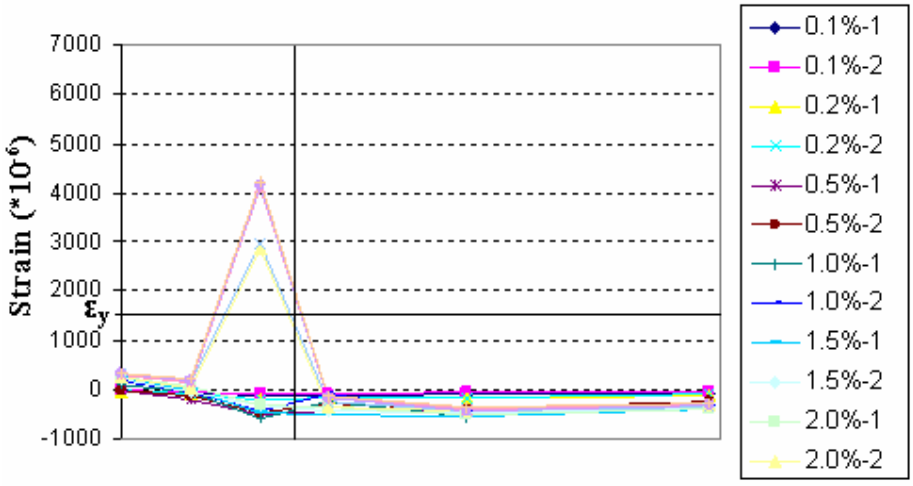

Bottom beam bar (negative loading cycle)

Figure 5 - 11: Strain profiles of beam bars measured by the strain of Unit SF-2: bottom bar

5.1.3. Unit SF-3

5.1.3.1 Hysteretic response

Figure 5-12 shows the lateral force versus top displacement hysteretic response measured for Unit SF-3. A crack circled in **Figure 5-13 (a)** was caused by a mechanical problem when the unit was being set to the reaction frame. This crack led to significant strength degradation on the positive loading direction. However, the seismic performance of Unit SF-3 can be presented by the loop on the negative loading direction.

No corner to corner diagonal cracking occurred in the joint during the test. The maximum strength was 25.1 MPa at a drift of 1.0%. Furthermore, Unit SF-3 also showed the highest yield displacement in Group I.

The interest for Unit SF-3 is the crack which was mainly concentrated along the beam bars' 90^o hook and finally formed a rotational surface in the joint region (see **Figure 5-13 (j)**). The pinching of the loops was slightly less than that of the other two units in Group I. The phenomenon of pinching was mainly caused by the rotational surface along the beam bars' hook indicating the energy dissipating capacity of Unit RC-1 being still poor.

The strength degradation of Unit SF-3 was from 24.9 KN to 19.6KN (21% reduction) which was slightly higher than that of Unit SF-2 (16.8% reduction), but better than that of Unit RC-1 (26.4% reduction).

5.1.3.2 Cracking and damage

The crack development and the final appearance of Unit SF-3 are shown in **Figure 5-13** from **(a)** to **(j)**. Throughout the whole test, it can be found that due to use of 2.0% steel fibres in Unit SF-3, the number of cracks was significantly reduced not only in the beam, but also in the joint compared with first two units. It was also found that no continuous corner to corner diagonal crack occurred in the joint region.

The beam flexural cracking was characterised by being sparely spaced and never developed to critical cracks. The joint diagonal cracking started to occur at 1.5% drift and developed with the increase of the drift. The main cracks occurred along the beam bars' 90^o hook and finally formed a rotational machine.

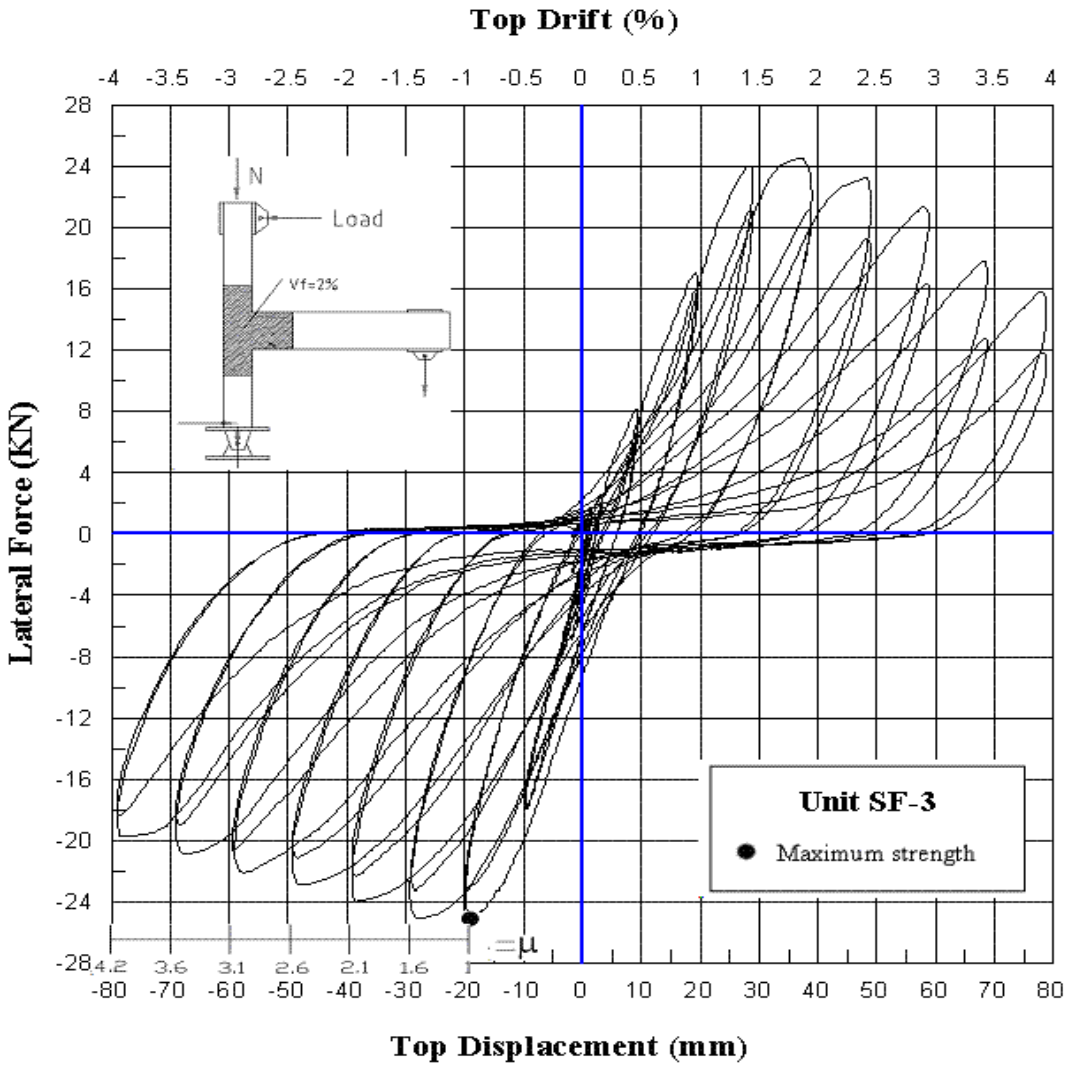

Figure 5 - 12: Lateral force vs. Top displacement hysteretic response for Unit SF-3

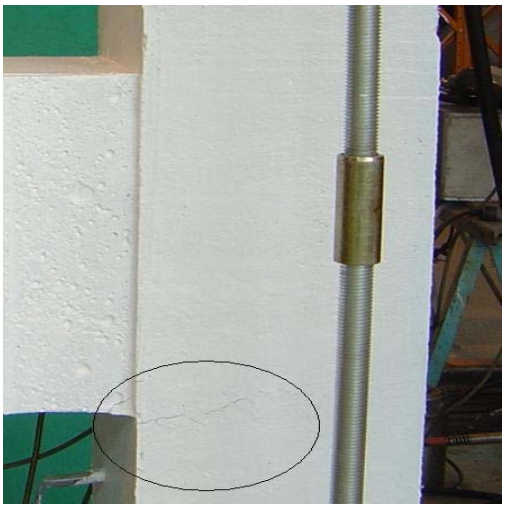

(a) Before test

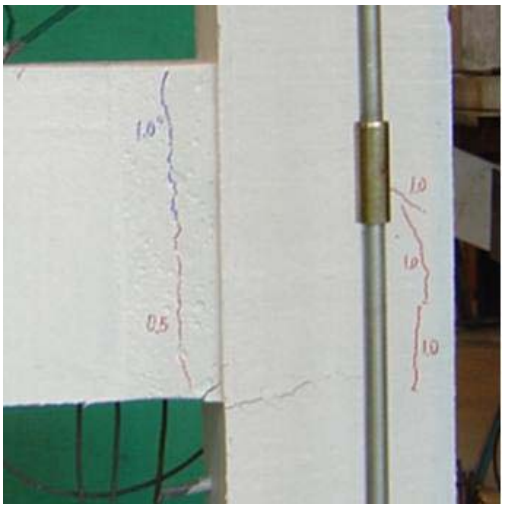

(b) 0.5% drift

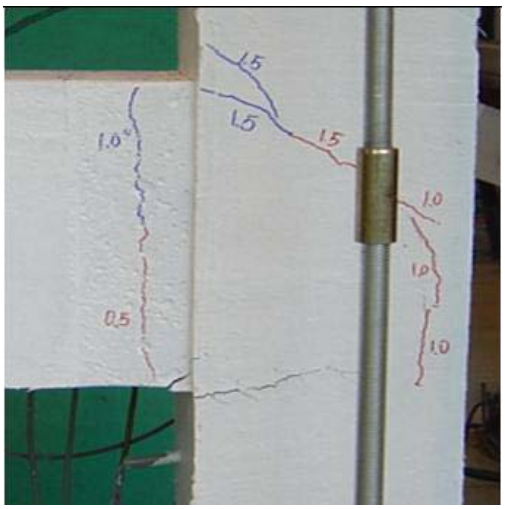

(c) 1% drift

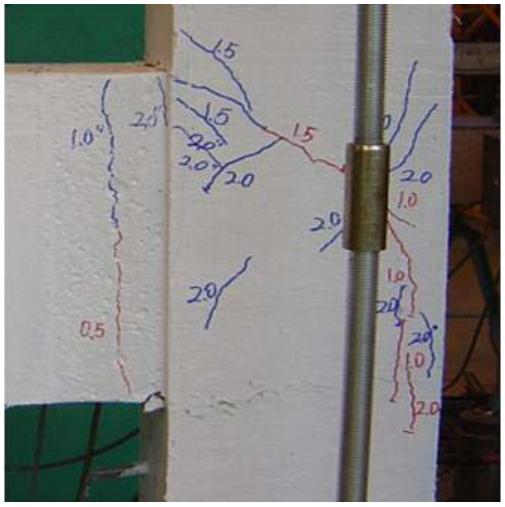

(d)1.5% drift

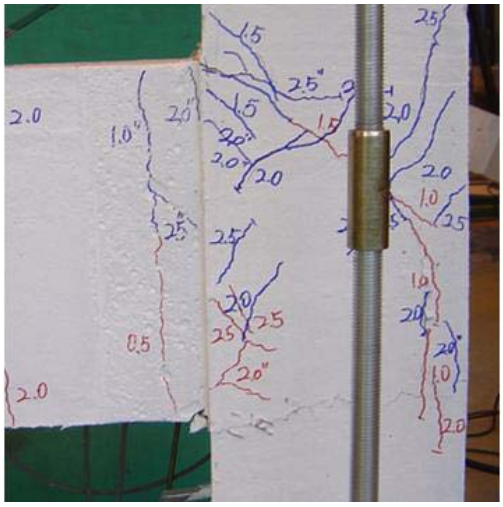

(e)2% drift

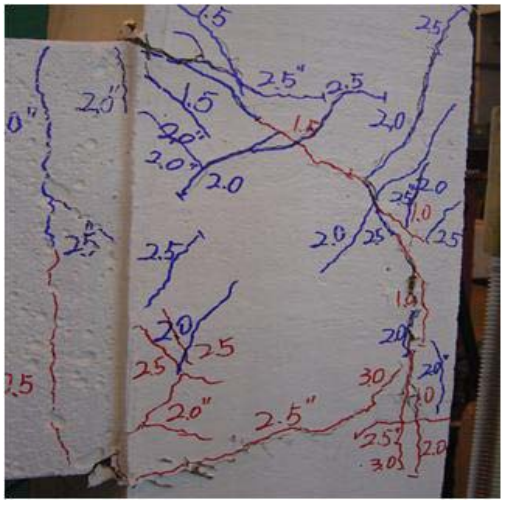

(f) 2.5% drift

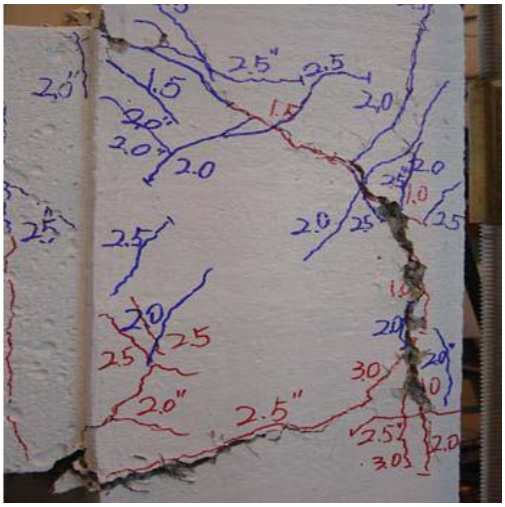

(g) 3% drift

(h) 3.5% drift

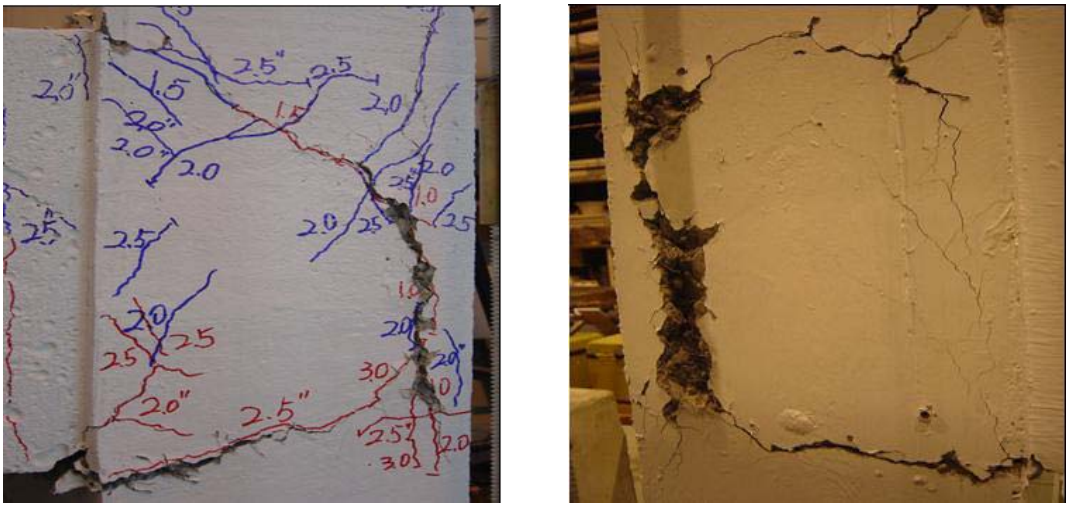

(i) 4.0% drift (Front side) **(j) 4.0% (back side)**

Figure 5 - 13: Observed damage of Unit SF-3

5.1.3.3 Joint behaviour

The joint shear deformation for Unit SF-3 is shown in **Figure 5-14 (a)**. It can be seen that the magnitude of joint shear deformation was bigger than that of Unit SF-2, because most of the flexural cracks of the column were concentrated along the beam bars and beam bars' 90^o hook. **Figure 5-14 (b)** shows the joint principal tensile strength with the loading history. After reaching maximum value, and forming flexural damage to columns at the point of 2.27 MPa ($0.54\sqrt{f'_c}$), the joint principal tensile strength gently decreased until 1.69 MPa ($0.4\sqrt{f'_c}$).

Figure 5-14 (c) ~ (f) show a group of graphs created from calculated principal tensile stress (P_t) and joint shear stress (v_j) versus joint shear deformation and top displacement for Unit SF-3. Because of the volume of steel fibres used in the joint region (2%), the behaviour of the joint of Unit SF-3 was very different from those of units RC-1 and SF-2. As the damage mainly occurred in the area of the joint adjacent to the column plastic hinge and no diagonal corner to corner shear cracks occurred in the joint area, the joint strength degradation curve was difficult to work out. In this test, the maximum strength of the joint occurred at the point of the first cracking with a horizontal shear force of 25.1 KN. When the first crack occurred in the joint area with a drift of 0.96%, the principal tensile stress reached the maximum value, 2.27 MPa ($0.54\sqrt{f'_c}$), with the joint shear rotation of 0.0002 rad which was slightly higher than that of Unit SF-2, but much smaller than that of Unit RC-1. After the phase of the first

crack, the strength of the overall unit gently decreased, even in the phase of the extensive damage to the joint.

Table 5 - 3: Sequence of events of Unit SF-3

Unit SF-3	Sequence of events	Force(KN)	v_j (MPa)	P_t(MPa)	$K=P_t/\sqrt{f'_c}$	γ (rad)	Drift
	First cracking	25.11111	2.92296	2.272774	0.537192	0.000234	0.96
	End test	19.74557	2.2963	1.68813	0.399006	0.0118285	3.91

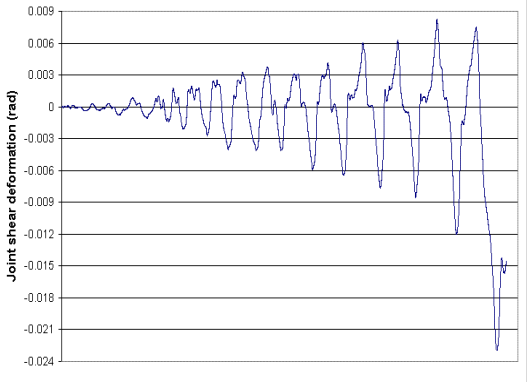

(a) Measured joint shear deformation history

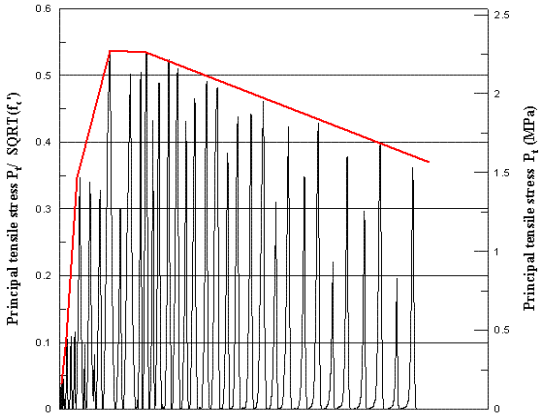

(b) The principal tensile stress history

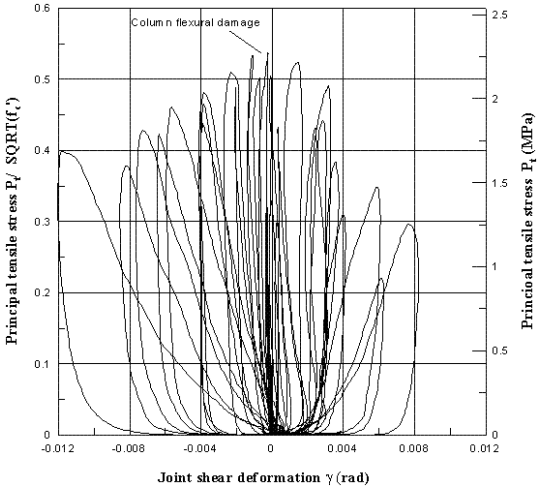

(c) Principal tensile stress vs. Joint deformation

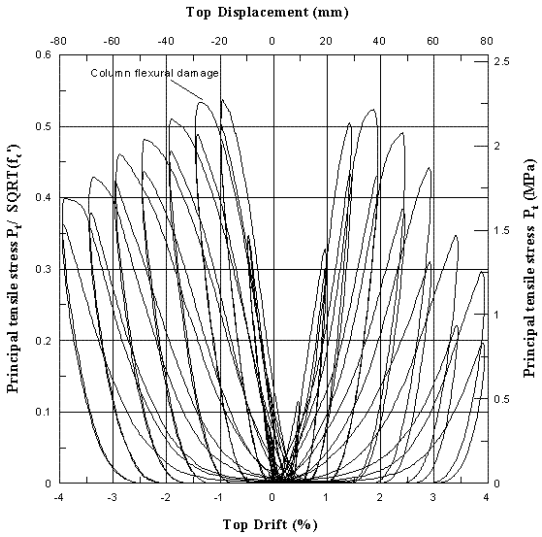

(d) Principal tensile stress vs. Top drift

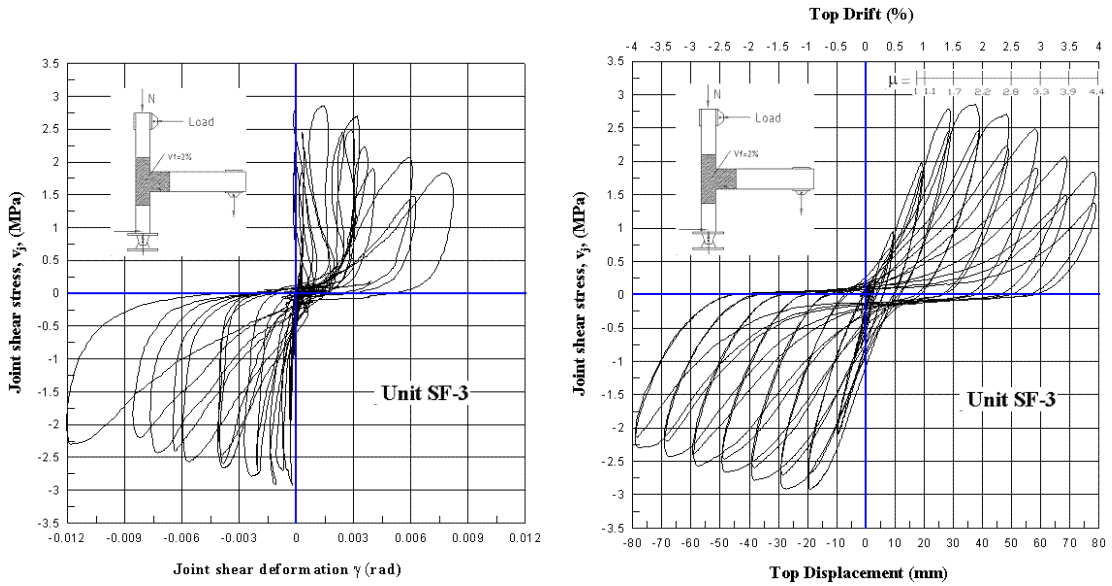

(e) Joint shear stress vs. Joint deformation **(f) Joint shear stress vs. Top displacement**

Figure 5 - 14：Experimental joint behaviour for Unit SF-3

5.1.3.4 Longitudinal beam bar strains

For Unit SF-3, the column flexural failure was the final failure mode. Therefore the profiles of measured strain, shown in **Figure 5-15** and **Figure 5-16**, are slightly different from first two units.

From Figures, it can be seen that the top beam bars around the column's inner face showed a lower value during the elastic stages (before 1.5% drift). However after the critical opening along the beam bars, the beam bars in the beam plastic hinge region showed the maximum yield value. Compared with first two tested units, this phenomenon indicates that a joint reinforced with the proper content of steel fibre can resist the shear stresses and change the critical area from the joint core region to another part of the beam-column joint.

Furthermore, compared with the observed strain profile of the beam bottom bars of the first two units, it was also found that Unit SF-3 had an approximately similar bond condition along the beam longitudinal bars, even in the joint region. The yield stress penetrated into the joint core in the loading cycle of 1.5% drift.

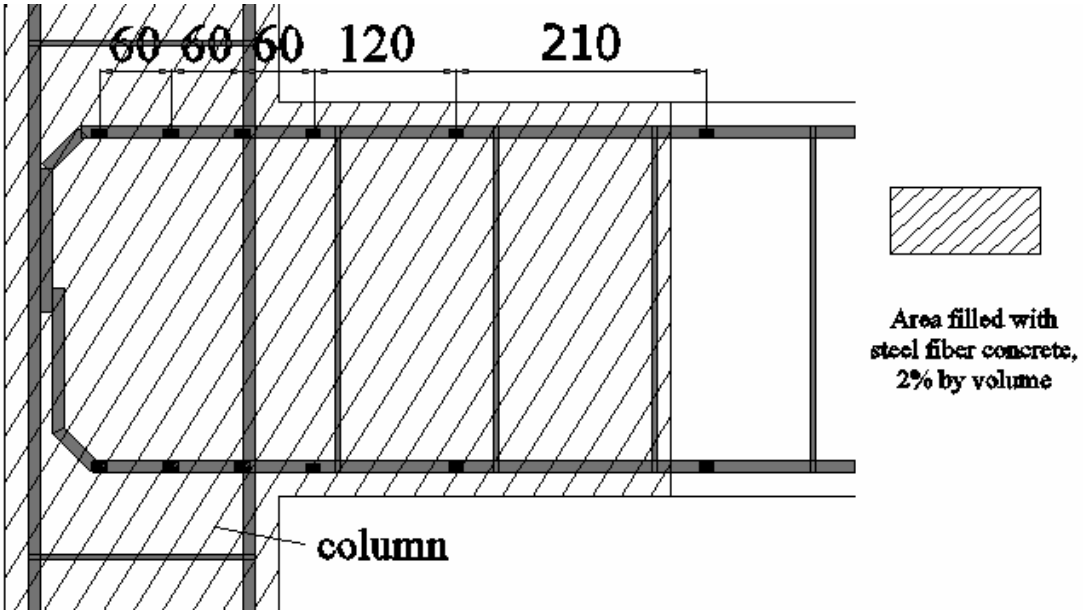

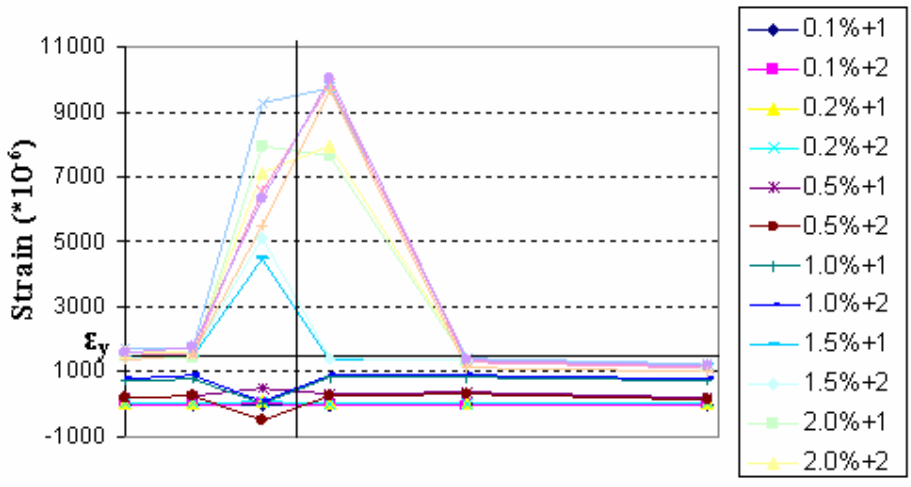

Top beam bar (positive loading cycle)

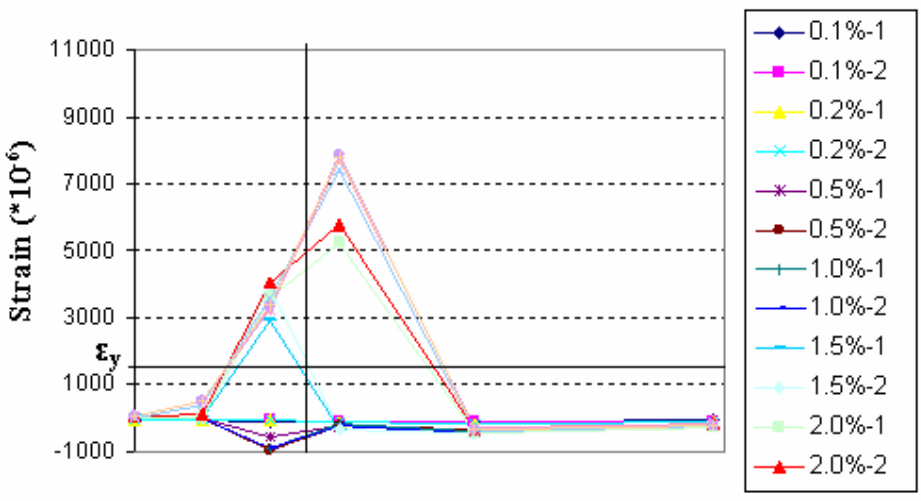

Top beam bar (negative loading cycle)

Figure 5 - 15: Strain profiles of beam bars measured by the strain gauges of Unit SF-3: top bar

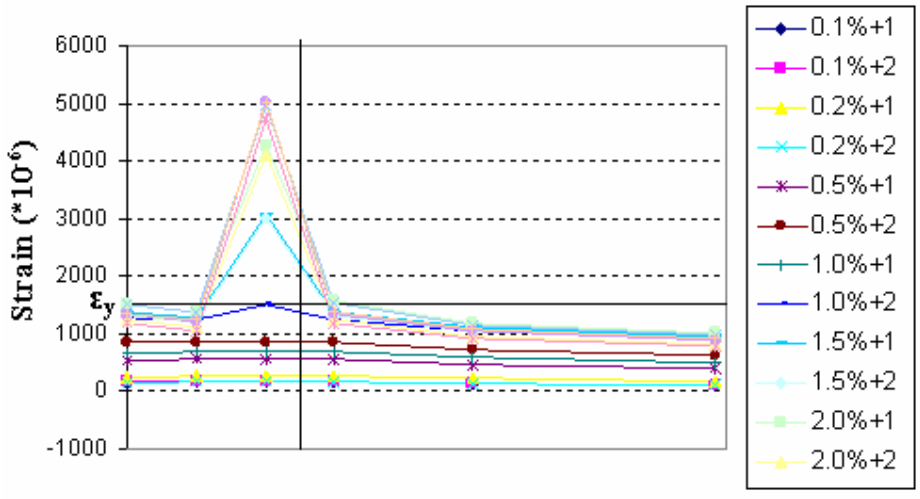

Bottom beam bar (positive loading cycle)

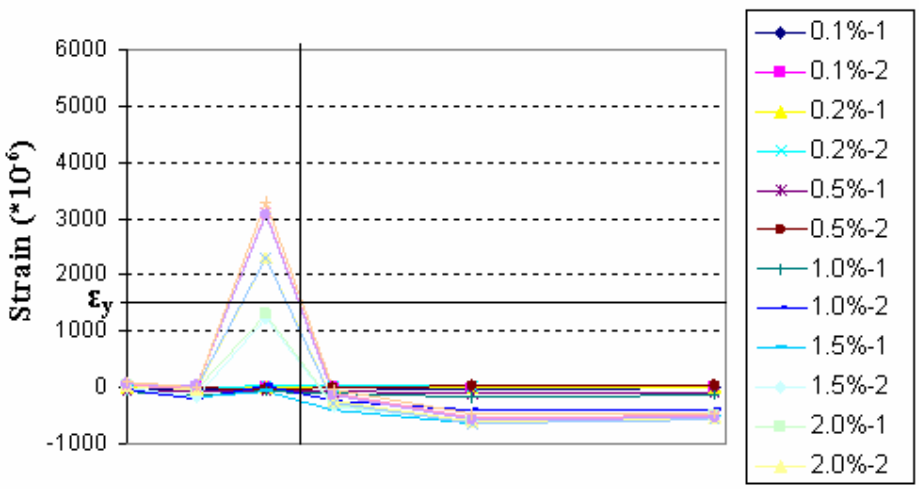

Bottom beam bar (negative loading cycle)

Figure 5 - 16: Strain profiles of beam bars measured by the strain of Unit SF-3: bottom bar

5.2. Introduction of Group Specimen II

The results of the shear resistance of the joints reinforced with steel fibres only were presented as shown above. Based on that result, three units designed by seismic code NZS 3101: 1995 [45] were constructed and tested by the same seismically simulated load as Group I. The units of Group II were modified in the joint region, reducing the transverse reinforcement in the joint region and the potential plastic hinge region by using steel fibres, in order to find the relationship of shear resistance of SFRC reinforced joints combined with stirrups and steel fibres. The purpose of this section is to investigate the shear resistance of joints when stirrups and steel fibres were both used in the joint region. In addition, to investigate the behaviour of SFRC in the plastic hinge region, a unit (Unit SF-5) was constructed by (1) using 1% steel fibres to replace the stirrups in the potential plastic hinges of the beam and columns (50% reduction) (2) using 1% steel fibres to replace the joint stirrups (80% reduction). The behaviour of the joints is presented and discussed in this section.

5.2.1. Unit SF-4

5.2.1.1 Hysteretic response

Figure 5-17 shows the lateral force versus top displacement hysteresis loops measured for Unit SF-4. The first cracking strength and maximum strength are also shown in **Figure 5-17**. The displacement at first cracking and maximum strength point were 13.4 mm (0.7% drift)

with 26.8 KN of strength and 19.3 mm (0.9% drift) with 27.75 KN respectively. As 1.0% steel fibre was used in the joint region, there was no drop in strength after the first cracking occurred. The pinchings were slightly represented in the loops, because there some diagonal cracks occurred in the joint region during the test. However, the fatter hysteresis loops indicate a good energy dissipation capacity of Unit SF-4.

The strength degradation of Unit SF-4 was really small, from 27.75 KN at maximum strength point to 22.8 KN at the first cycle of 5.0% drift, 19% reduction.

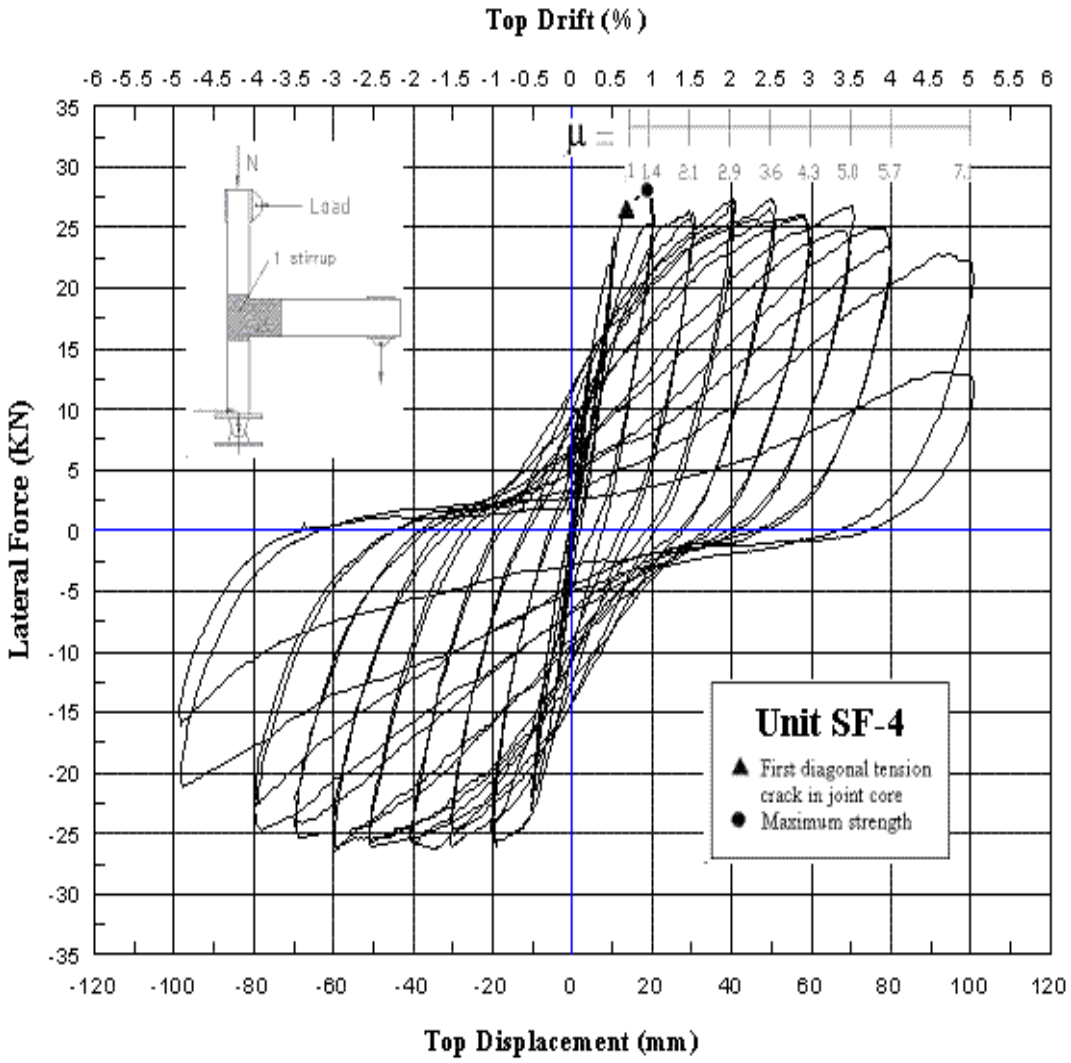

Figure 5 - 17: Lateral force vs. top displacement hysteretic response for Unit SF-4

5.2.1.2 Cracking and damage

Observed cracking after testing is presented in **Figure 5-18 (a)** to **(j)**. Although many short shear diagonal cracks were found in the joint region, the flexure cracks in the beam plastic hinge region adjacent to the joint caused the main failure mode.

The first diagonal crack opening in the joint was at the drift of 0.67% with a width of 0.06 mm. During the drift of 1.0% cycle running, a few short diagonal cracks parallel with the first one were found in the joint panel region. The first diagonal crack in the opposite direction started during the test of 1.5% drift. The number of this kind of crack increased with the increasing imposed displacements. The average width of these diagonal joint cracks was 0.1 mm at the end of the test.

The flexure cracks started to open at 0.5% drift with a width of 0.06 ~ 0.07 mm at the beam plastic hinge region and tended to become wider and wider with the increasing drift. At the end of the test, a huge crack with a width of 17 mm was present. It must be noted that cracks in the joint adjacent to the column's outer face caused by the buckling of the beam bars started at 3.5% drift and accumulated to form another critical crack. At the end of the test, these cracks had increased to a width of 4 mm.

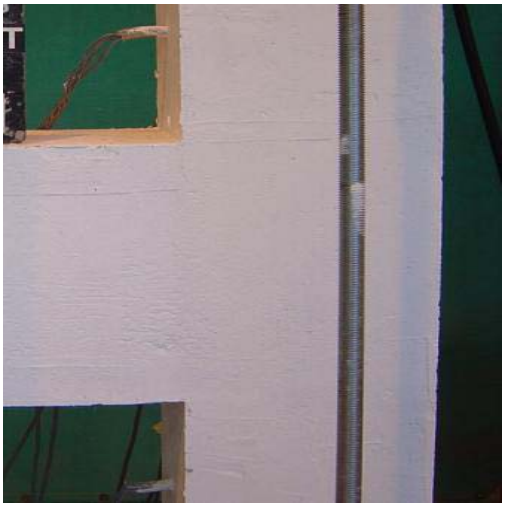

(a) 0.2% drift

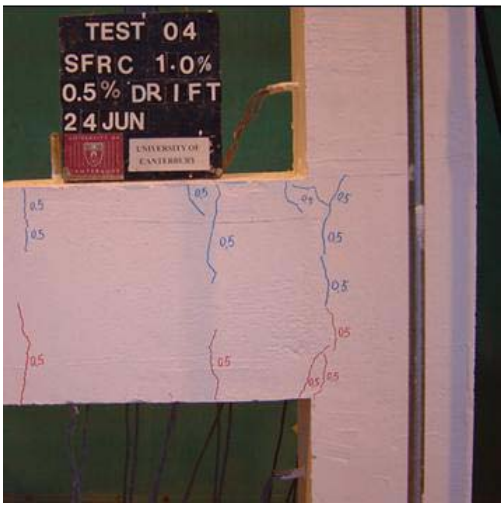

(b) 0.5% drift

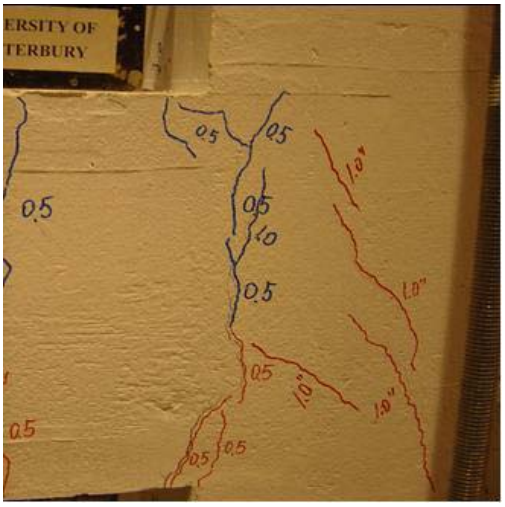

(c) 1% drift

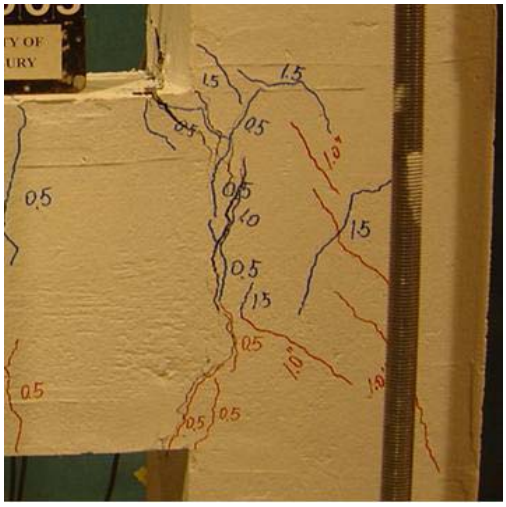

(d)1.5% drift

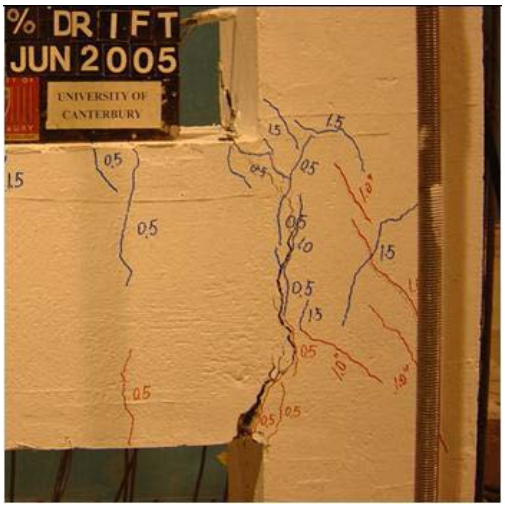

(e) 2% drift

(f) 2.5% drift

(g) 3% drift

(h) 3.5% drift

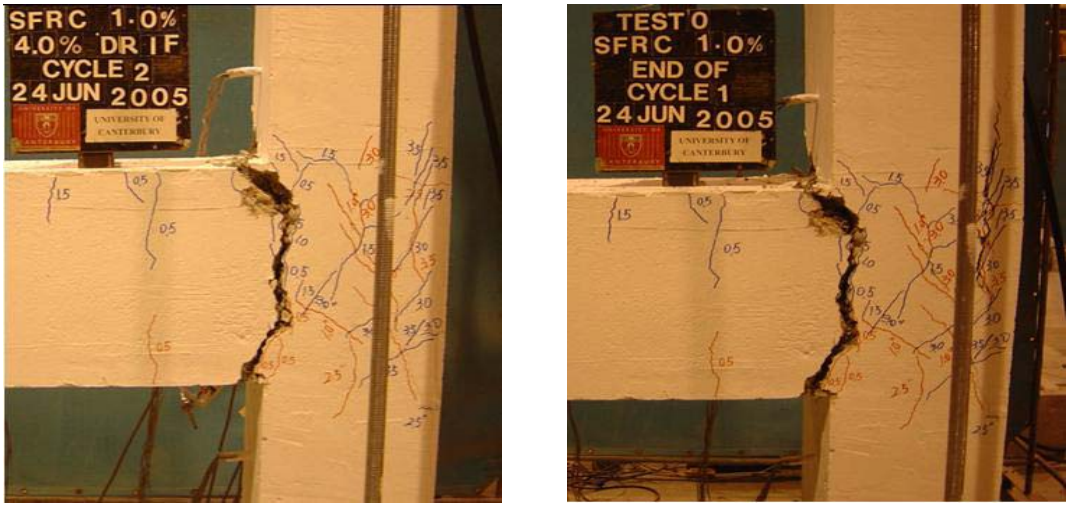

(i) 4.0% drift **(j) 5.0% (end)**

Figure 5 - 18: Observed damage of Unit SF-4

5.2.1.3 Joint behaviour

A group of figures, **Figure 5-20 (a)** ~ **(f)**, presents the joint behaviour under the simulated seismic cycle load for Unit SF-4. The joint first diagonal crack occurred at the drift of 0.7% with 2.45 MPa ($0.48\sqrt{f'_c}$) of joint principal tensile stress and 0.0002 rad of joint shear deformation. After the joint first diagonal crack, a beam plastic hinge formed at the drift of 0.9% with the maximum horizontal shear force (27.75KN). Although the damage was mainly concentrated on the beam's plastic hinge area in the following test, more diagonal joint cracks still occurred at the joint panel. The reason leading to this phenomenon is that the horizontal joint shear resistance capacity decreased with the increasing drift and the curvature ductility factor. Such degradation models of the horizontal joint shear strength based on the experimental tests of exterior joints, when expressed in terms of k ($v_j = k\sqrt{f'_c}$), were proposed by Priestley (shown in **Figure 5-19 (a)**) and Park (shown in **Figure 5-19 (b)**). Both models assumed that the joint failure in exterior beam-column joints is a result of large principal tensile stress. From **Table 5-4** and **Figure 5-20 (d)**, it can be seen that the joint extensive damage occurred with the maximum principal tensile stress, 2.59 ($0.517\sqrt{f'_c}$), with a drift of 1.9%. However the joint shear deformation was still in a small range, ≤ 0.004 rad, indicating that the joint still retained its integrity and still could carry more shear stress.

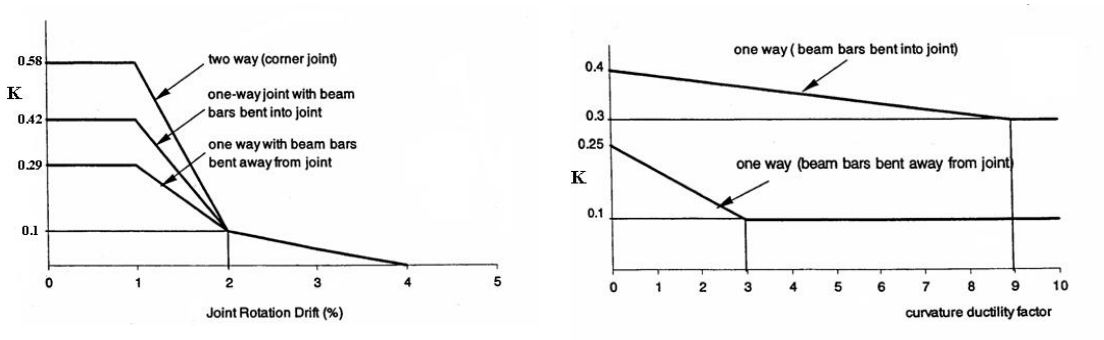

(a) **(b)**

Figure 5 - 19: Degradation of joint shear force resisted by concrete mechanism for exterior beam-column joints (a) proposed by Priestley [51] (b) proposed by Park [52]

5.2.1.4 Longitudinal beam bar strains

Figure 5-21 and **Figure 5-22** illustrates the measured strains along the longitudinal beam bars. Before the loading cycle of 1.5% drift, the tensile strains gently increased along the beam bars. After that stage, the beam bars in the joint region reached the yield strain in the first loading cycle of 1.5% drift. The second loading cycles of 1.5% drift resulted in the significantly large tensile strain in both the middle joint and the beam plastic hinge region. In the subsequent loading cycles, the profiles showed a clear strain distribution, in which the strains distributing along the longitudinal beam bars can be observed. The maximum strain was in the joint region because the major flexure cracks at the beam end developed into the joint adjacent to the column's inner face.

Table 5 - 4: Sequence of events of Unit SF-4

	Sequence of events	Force(KN)	v_j (MPa)	P_t(MPa)	$K=P_t/\sqrt{f'_c}$	γ (rad)	Drift
Unit SF-4	First cracking	26.892	3.15298	2.450219	0.48766	0.0002	0.7095
	Extensive cracking	26.6	3.295125	2.599283	0.517328	0.0015	1.918
	Beam hinging	27.756	2.525805	3.233782	0.502704	0.0004	0.9
	End test	15.65	1.839969	1.1981	0.238454	0.0037	4.90596

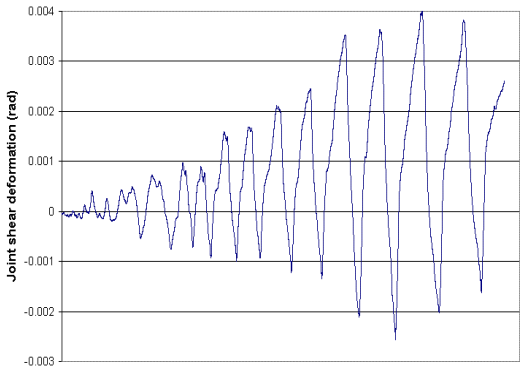

(a) Measured joint shear deformation history

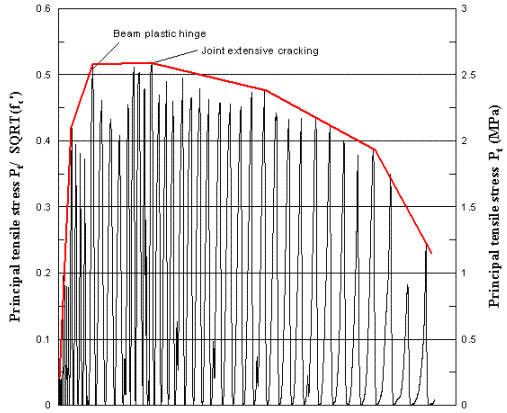

(b) The principal tensile stress history

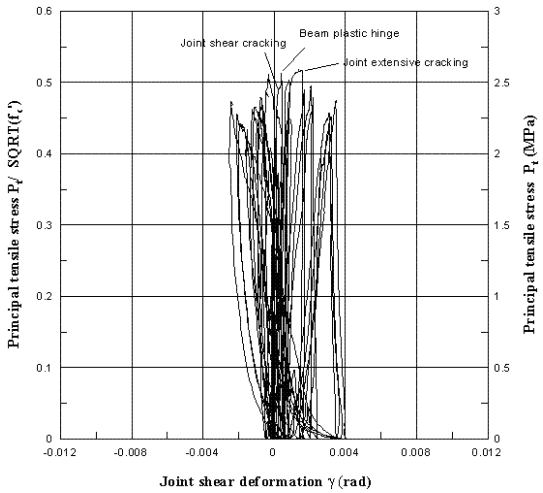

(c) Principal tensile stress vs. Joint deformation

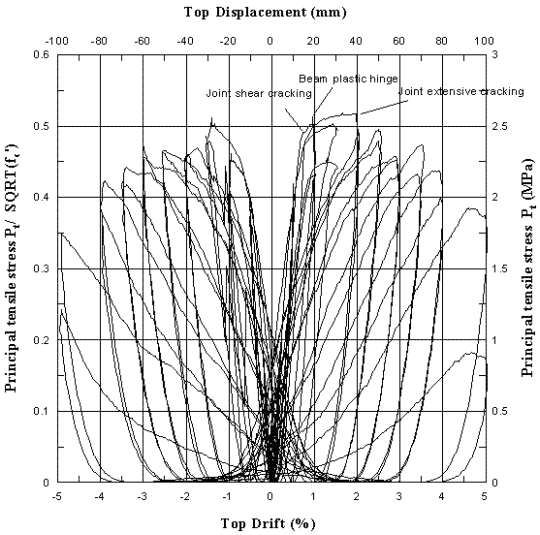

(d) Principal tensile stress vs. Top drift

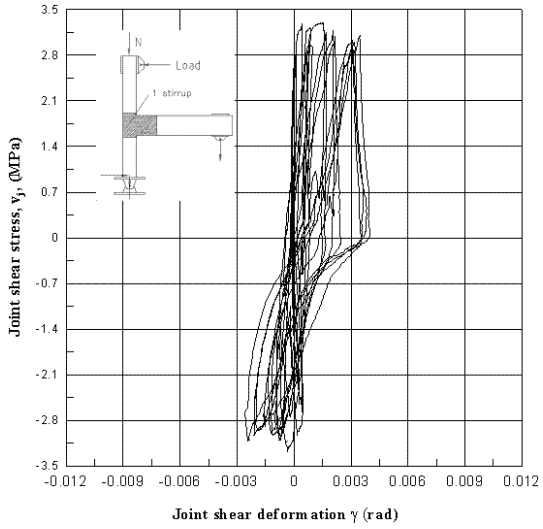

(e) Joint shear stress vs. Joint deformation

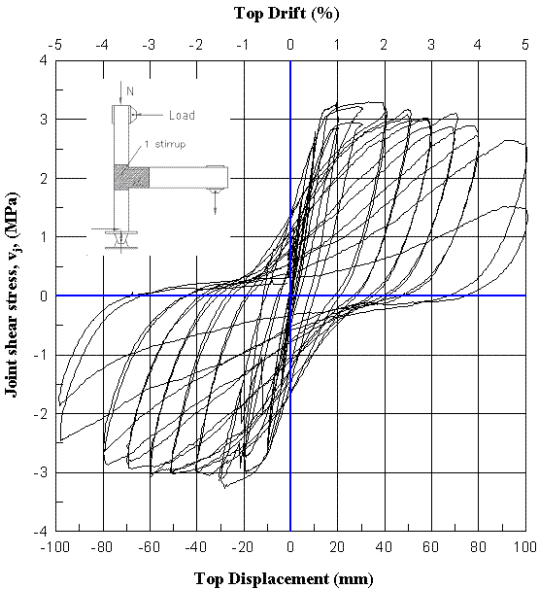

(f) Joint shear stress vs. Top displacement

Figure 5 - 20: Experimental joint behaviour for Unit SF-4

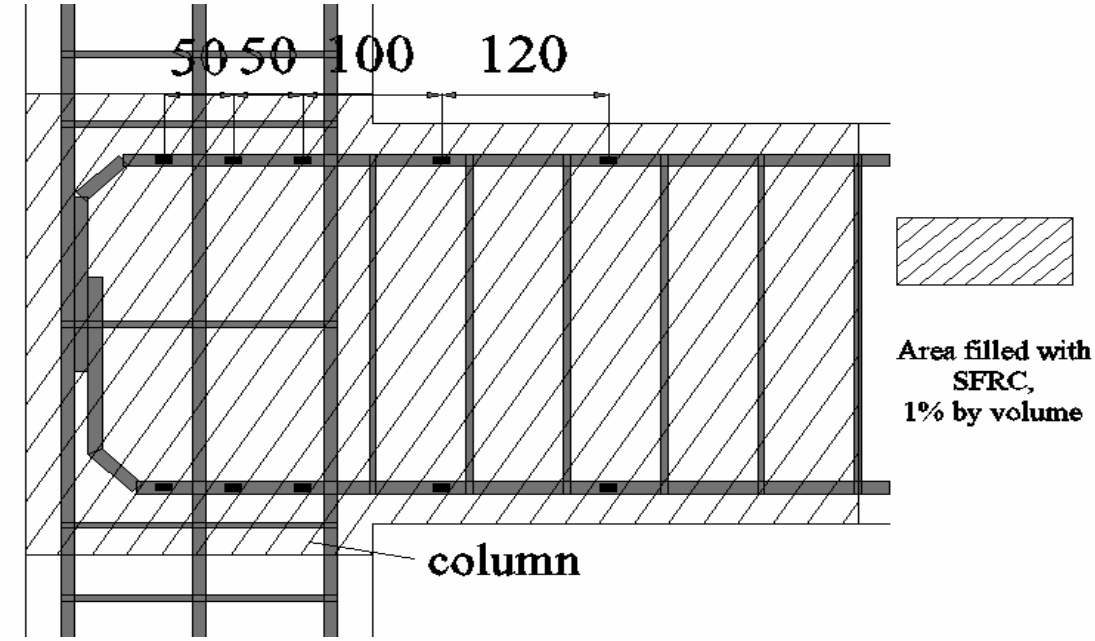

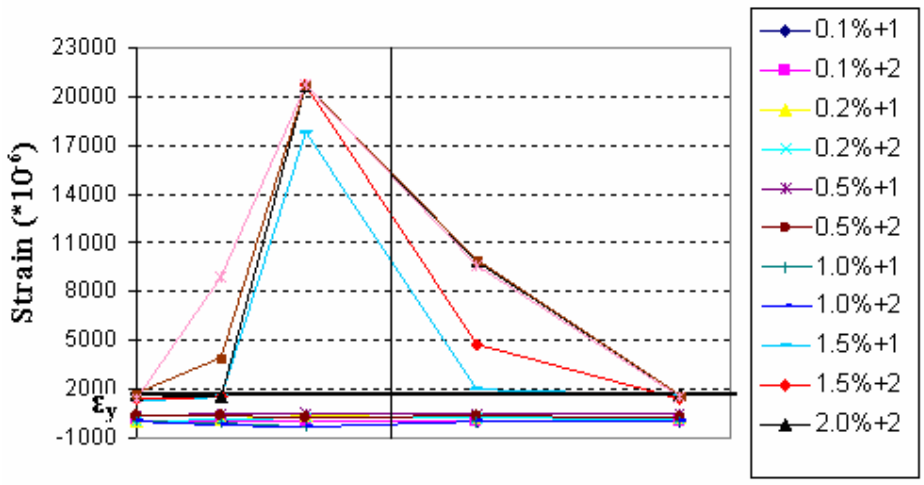

Top beam bar (positive loading cycle)

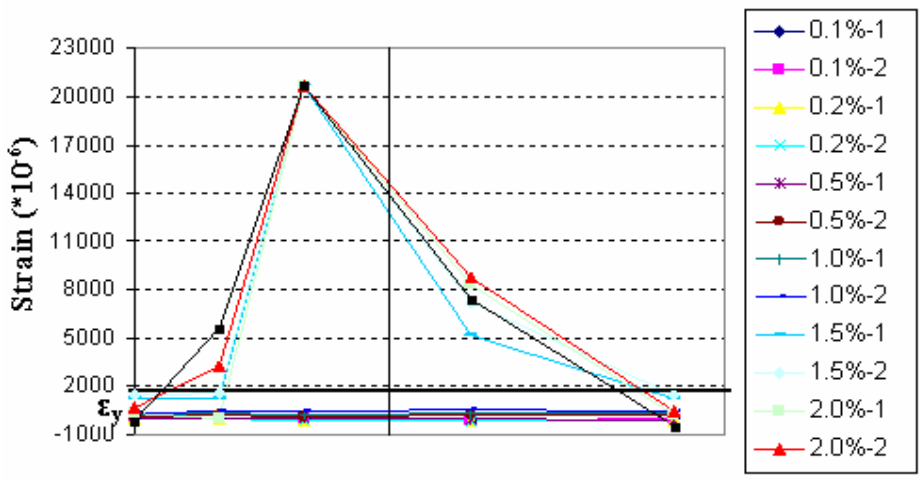

Top beam bar (negative loading cycle)

Figure 5 - 21: Strain profiles of beam bars measured by the strain gauges of Unit SF-4: top bar

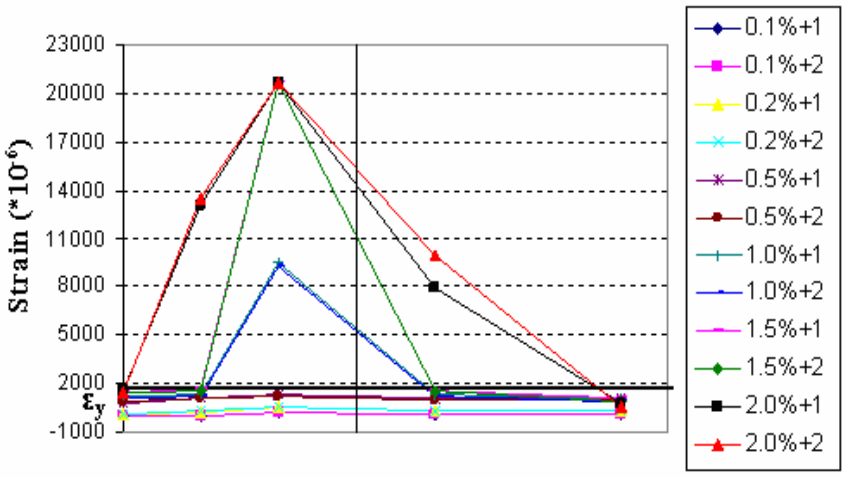

Bottom beam bar (positive loading cycle)

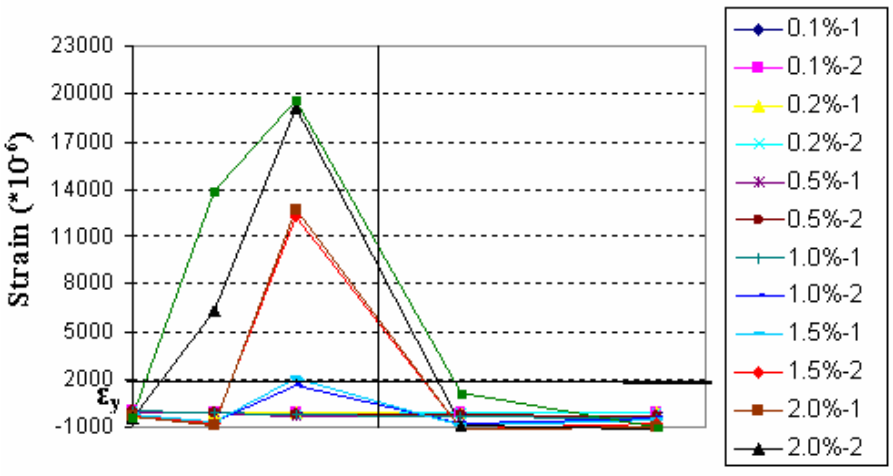

Bottom beam bar (negative loading cycle)

Figure 5 - 22: Strain profiles of beam bars measured by the strain of Unit SF-4: bottom bar

5.2.2. Unit SF-5

5.2.2.1 Hysteretic response

The lateral force versus top displacement and top drift hysteresis loop measured for Unit SF-5 is presented in **Figure 5-23**. The maximum strength and the first cracking strength are also shown in **Figure 5-23**. Compared with Unit SF-4, 1% steel fibres were used to replace the 50% lateral reinforcement in the beam and columns plastic hinge regions. As a consequence of this change, the overall behaviour and final failure of the tested Unit SF-5 were very different from Unit SF-4.

The first diagonal tension crack in the joint panel was observed at a drift of 0.7% with strength of 25.3 KN and 2.5 um of width. After the strength slightly dropped down to 24.5 KN, then the strength achieved the peak value of 27 KN at the drift of 1.0%. Many diagonal cracks occurred during the test. Those cracks caused significant pinching of the loops and indicated that the joint shear resistance capacity and energy dissipation capacity of Unit SF-5 were still not satisfied.

The problem of strength degradation of Unit SF-5 was worse than that of unit SF-4, from 27 KN to 17.7 KN (34.4 % reduction), because of the insufficient lateral reinforcement in the beam and columns plastic hinge region.

5.2.2.2 Cracking and damage

The beam-column joint of this unit performed unsatisfactorily overall as a result of the low amount of lateral reinforcement provided, which was only 50% of that required by NZS 3101 [45]. A “concrete wedge” was found at the end of the test formed by the significant diagonal shear cracks in the joint region. **Figure 5-24 (a) ~ (j)** shows the cracks at different stages of seismic load.

The first diagonal crack which occurred in the joint region was at a drift of 0.7% with a width of 0.06 mm. With the increase in the intensity of the simulating seismic load, the diagonal cracks developed and connected to form a “concrete wedge” at a drift of 4.0%, which was the main factor of the strength degradation in the overall behaviour of the hysteresis loops.

The beam cracks started to appear at the first cycle run of 0.2% drift with a width of 0.05 mm at the beam end adjacent to the joint and increased and spread during the cycle run from 0.2% drift to 1.0% drift. Finally this flexural crack developed to be the main failure mode.

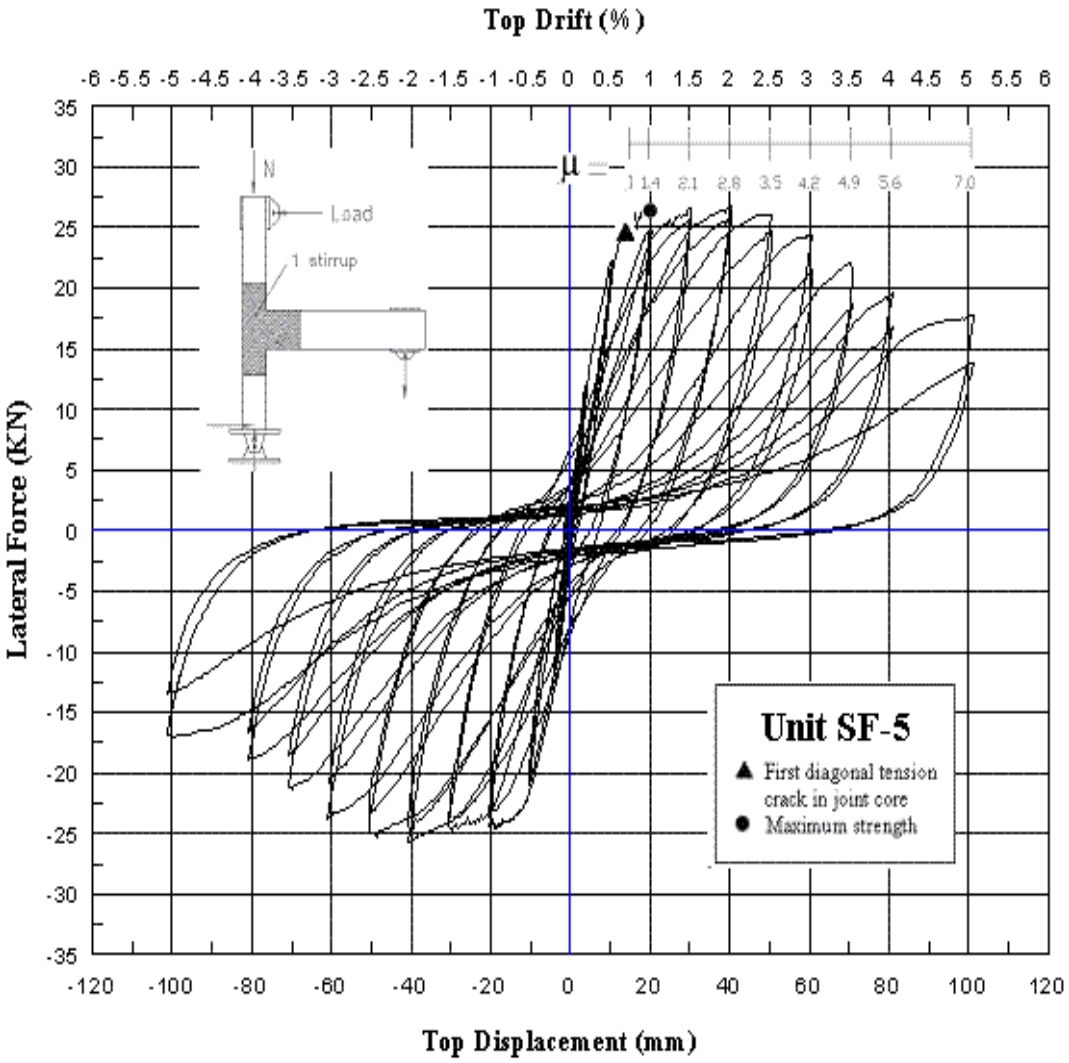

Figure 5 - 23: Lateral force vs. top displacement hysteretic response for Unit SF-5

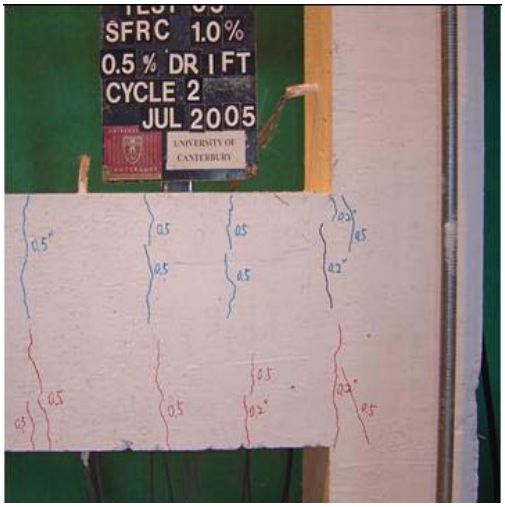

(a) 0.5% drift

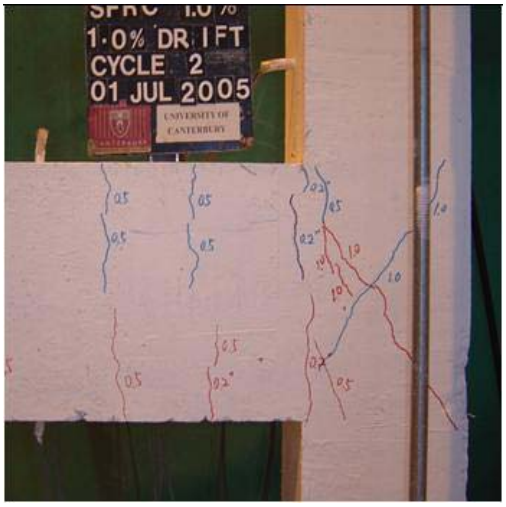

(b) 1.0% drift

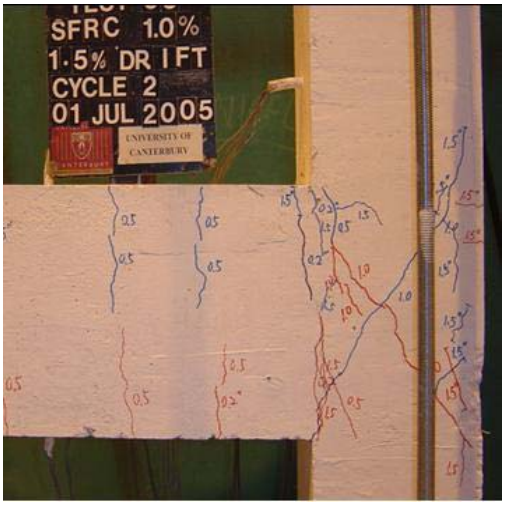

(c) 1.5% drift

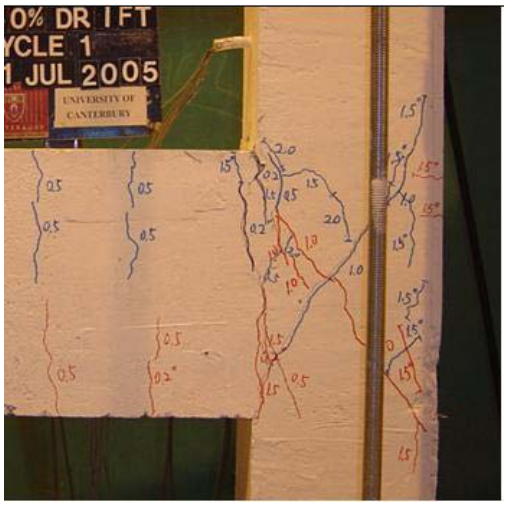

(d) 2.0% drift

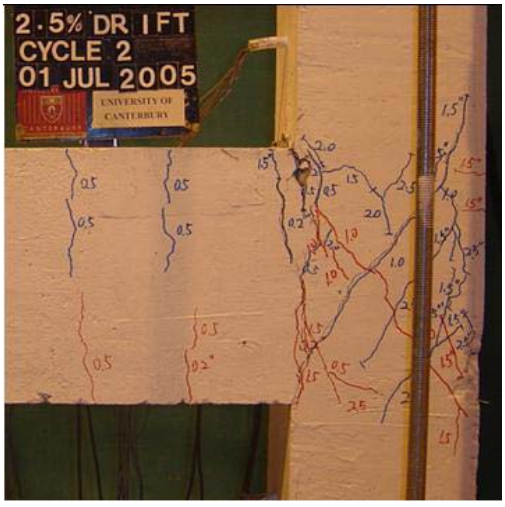

(e)2.5 % drift

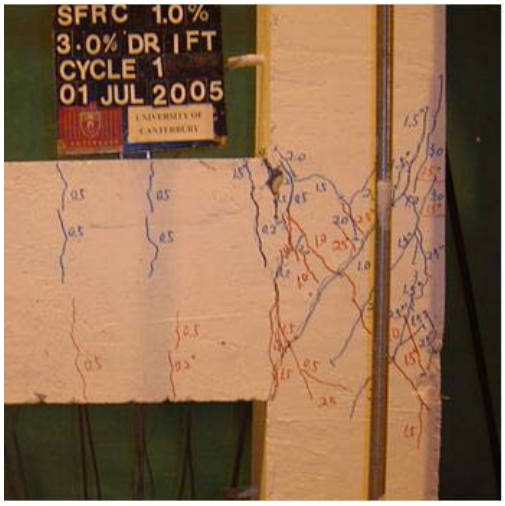

(f) 3.0 % drift

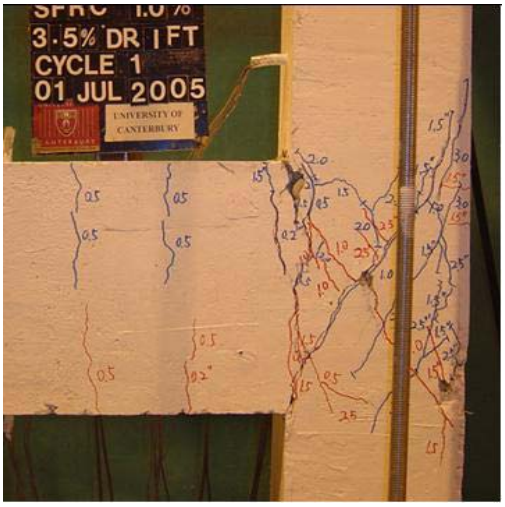

(g) 3.5% drift

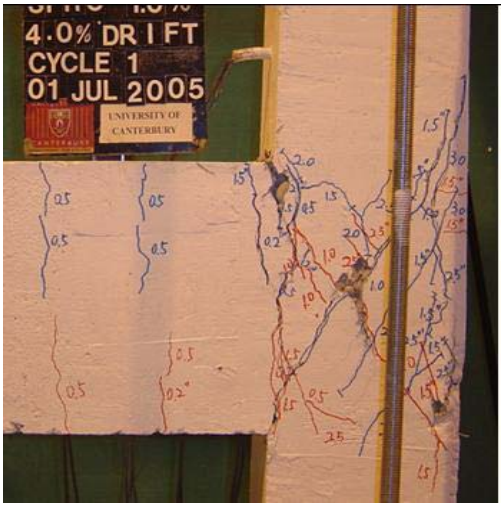

(h) 4.0% drift

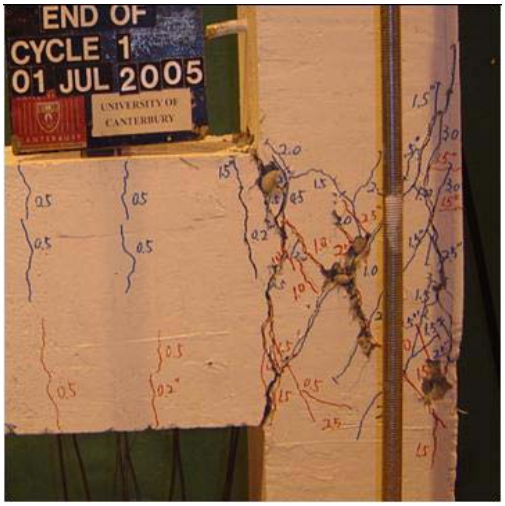

(i) 5.0% drift (front side)

(j) 5.0% (back side)

Figure 5 - 24: Observed damage of Unit SF-5

5.2.2.3 Joint behaviour

The joint behaviour of Unit SF-5 is presented in **Figure 5-25 (a)** ~ **(f)**. Compared with Unit SF-4, lateral reinforcement in the beam and columns plastic hinge regions was reduced by 50% in order to investigate the effect of using steel fibre in the potential plastic hinge region to replace the lateral reinforcement. The joint of Unit SF-5 showed unsatisfactory characteristics in both joint principal tensile stress and joint shear deformation. The joint first diagonal crack started to open at the drift of 0.69% with 2.22 MPa ($0.44\sqrt{f'_c}$) of joint principal tensile stress and 0.0007 rad of joint shear deformation. After the joint first diagonal crack, a beam plastic hinge formed at the drift of 1.0% with the maximum overall horizontal shear force (26.65KN). However, as in the case of Unit SF-4, the extensive joint shear

damage occurred after forming hinging at the beam plastic hinge region with the maximum joint tensile stress, 2.37 MPa ($0.47\sqrt{f'_c}$) and 0.0024 rad of joint shear deformation. From **Figure 5-25 (b)**, it can be seen that the strength degradation of joint principal tensile stress reduced much more rapidly after the joint shear stress reached the maximum value compared with that of Unit SF-4, indicating that 1.0% steel fibre is not adequate to reduce a large amount of lateral reinforcement in the critical area of a beam-column joint.

5.2.2.4 Longitudinal beam bar strains

For Unit SF-5, the combination of joint shear failure and column flexural failure was observed. **Figure 5-26** and **Figure 5-27** illustrate the profiles of measured strain during the different loading cycles.

After the gradual increase in tensile strains along the beam bars during the elastic loading cycles (from 0.1% to 0.5% drift cycles), the top beam bars reached the yield strain in the joint region adjacent to the column's inner face in the loading cycle of 1.0% drift while the joint shear diagonal tensile cracks were observed. The strain distribution profiles also showed that after the cycles of 2.0% drift the overall yield stage occurred along the beam bar. The similar strain profiles were observed for the bottom beam bars, however only a position in the joint adjacent to the column showed a yield strain in the negative loading cycle.

Table 5 - 5: Sequence of events of Unit SF-5

	Sequence of events	Force(KN)	v_j (MPa)	P_t(MPa)	$K=P_t/\sqrt{f'_c}$	γ (rad)	Drift
Unit SF-5	First cracking	25. 3	2.938444	2.228959	0.443623	0.0007366	0.691
	Extensive cracking	24. 28112	2.826817	2.102638	0.418482	0.0031054	3.0
	Beam hinging	26. 65	3.110337	2.37783	0.473253	0.0024974	1.0
	End test	13.351094	1.565621	0.957236	0.190516	-0.012258	5.0

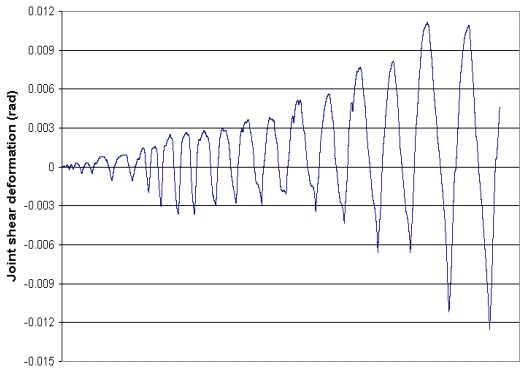

(a) Measured joint shear deformation history

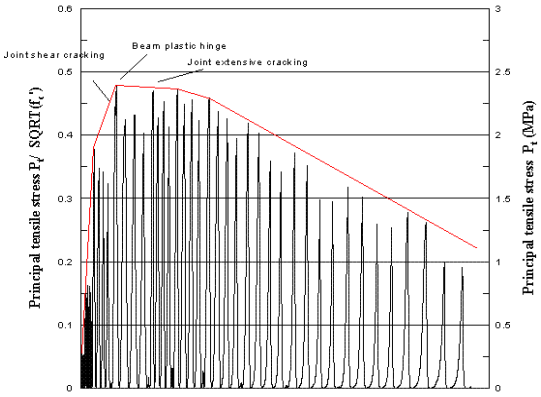

(b) The principal tensile stress history

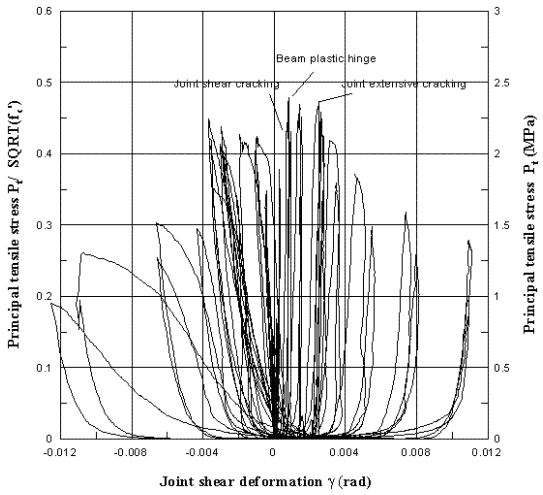

(c) Principal tensile stress vs. Joint deformation

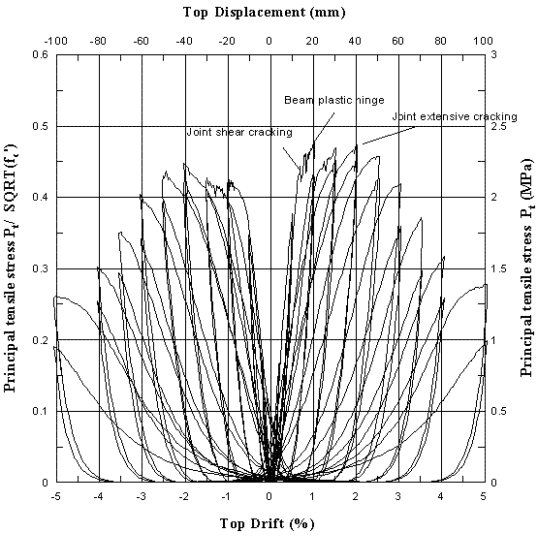

(d) Principal tensile stress vs. Top drift

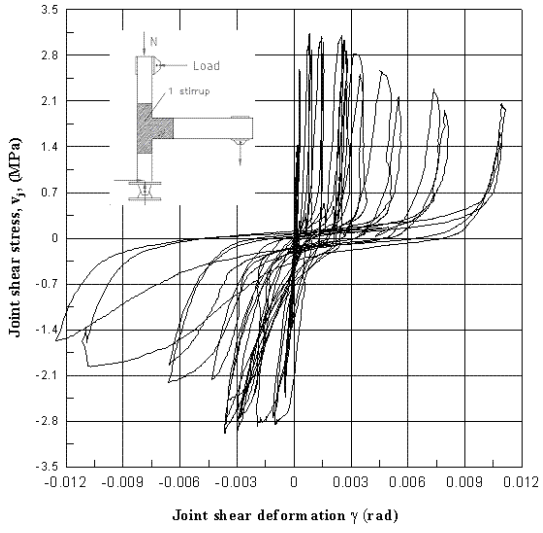

(e) Joint shear stress vs. Joint deformation

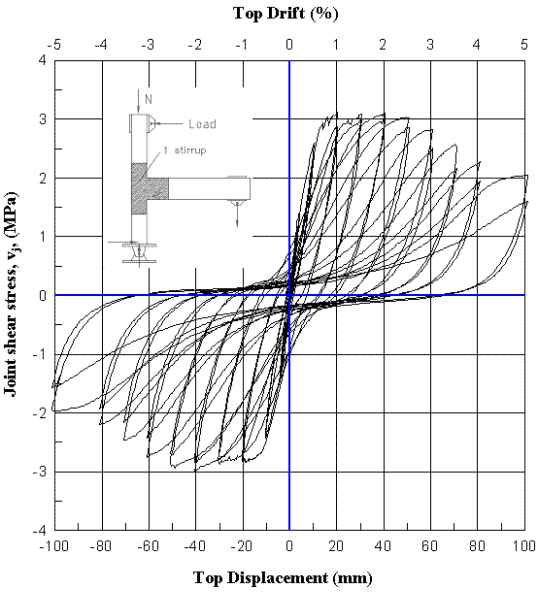

(f) Joint shear stress vs. Top displacement

Figure 5 - 25: Experimental joint behaviour for Unit SF-5

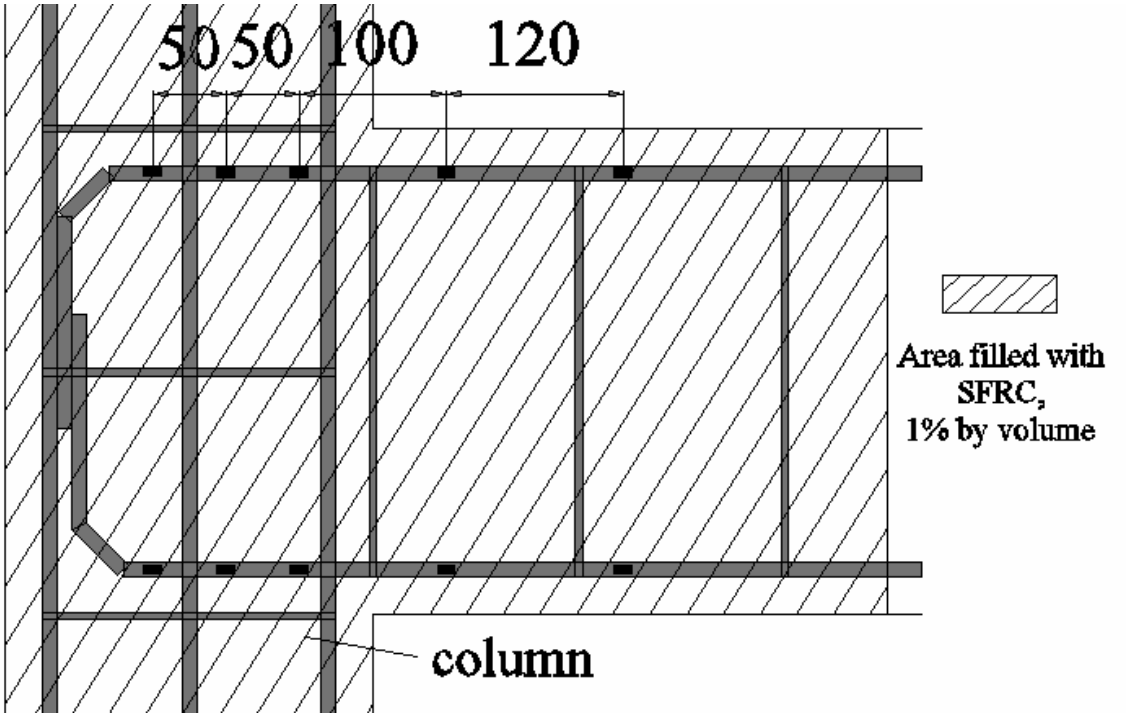

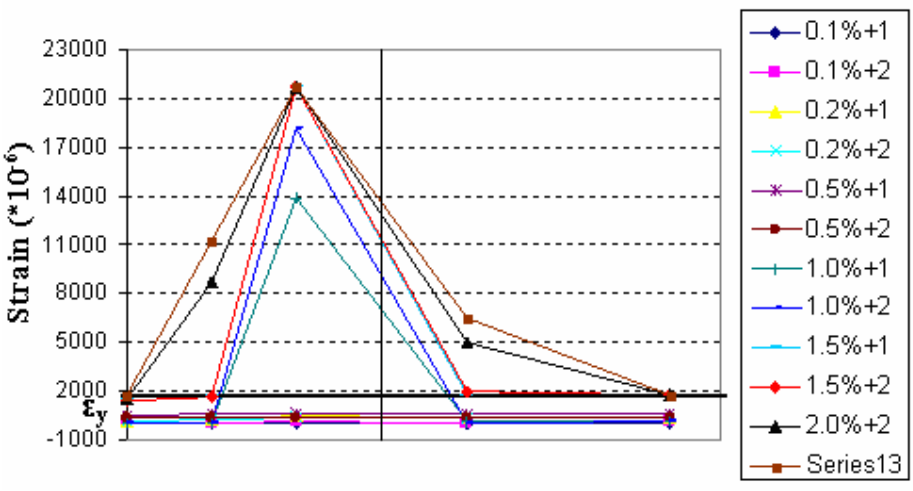

Top beam bar (positive loading cycle)

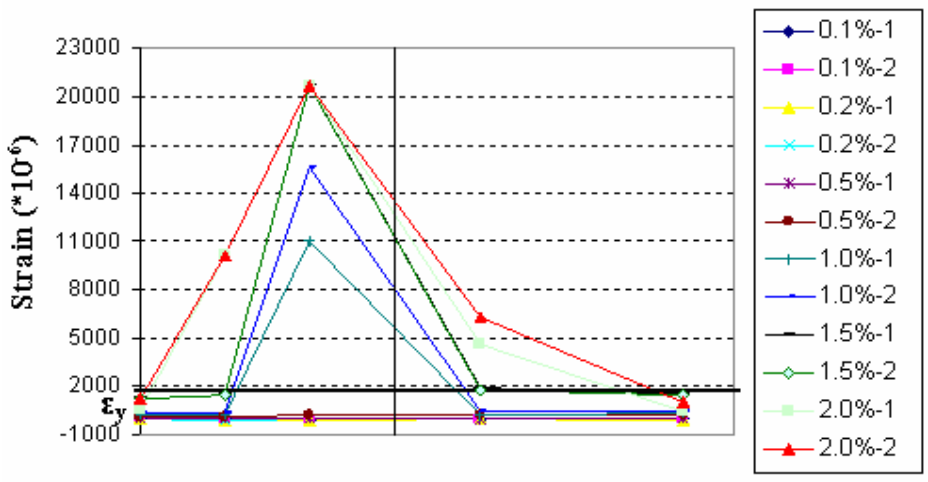

Top beam bar (negative loading cycle)

Figure 5 - 26: Strain profiles of beam bars measured by the strain gauges of Unit SF-5: top bar

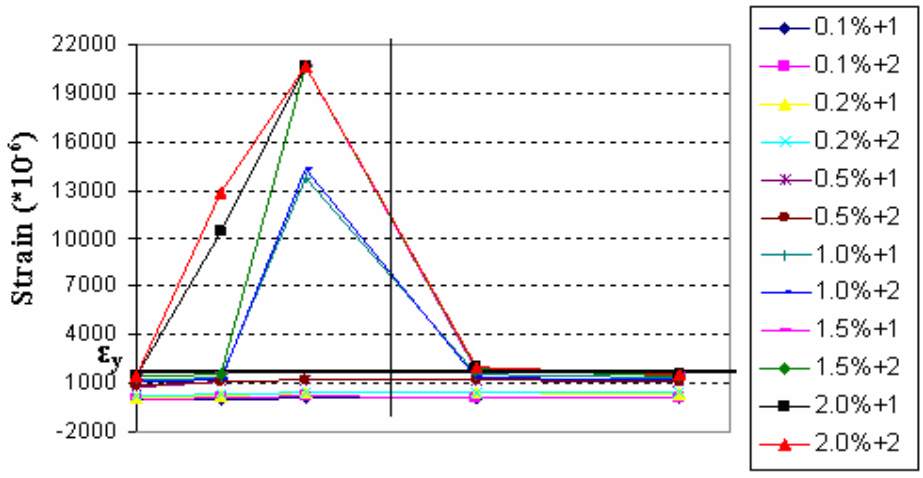

Bottom beam bar (positive loading cycle)

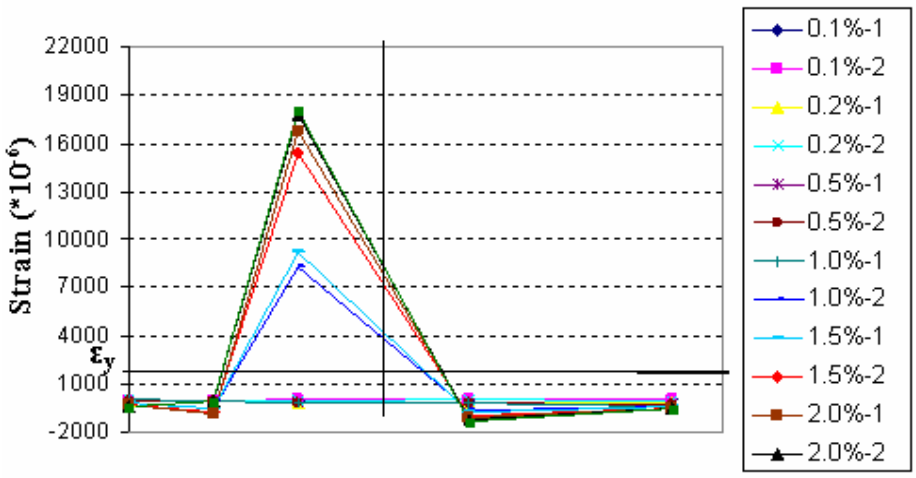

Bottom beam bar (negative loading cycle)

Figure 5 - 27: Strain profiles of beam bars measured by the strain of Unit SF-5: bottom bar

5.2.3. Unit RC-6

5.2.3.1 Hysteretic response

Figure 5-28 shows the lateral force versus top displacement and top drift hysteresis loops measured for Unit RC-6. The maximum strength was 24.4 KN with a drift of 2.4%. Compared with Unit SF-4 and SF-5, sufficient confinement was not used in the joint region of this unit, hence the buckling at the beam bars 90^o hook and flexural cracks at the beam plastic hinge were observed at the end of the test. There was no corner to corner diagonal crack occurring in the joint during the test. Unit RC-6 also showed the lowest strength in Group II.

The pinching can be seen in **Figure 5-28** indicating that the energy dissipating capacity of Unit RC-6 was still poor.

The significant strength degradation of Unit RC-6 was found to be from 24.4 KN at a drift of 2.4% to 13.3 KN at a drift 5.0% (45.5% reduction).

5.2.3.2 Cracking and damage

The cracks occurring during the whole test are presented in **Figure 5-29 (a) ~ (j)**. The beam showed critical flexural cracks with noticeable negative effects on the lack of confinement in the joint region (no steel fibres and only one stirrup), which was only 20% of that required by the seismic code of NZS 3101 [45]. Therefore the bucking along the beam bars 90^o hook adjacent to the outer face of the column was presented at the end of the test.

The beam cracks started to appear at the first cycle run of 0.2% drift with a width of 0.095 mm at the beam end adjacent to the joint. This crack finally developed into a critical crack with a width of 18 mm at the end of the test. The buckling started to appear at the 1.0% drift and became a critical crack at a drift of 3.5%. At the end of the test this splitting crack had developed into a 12mm width cracking.

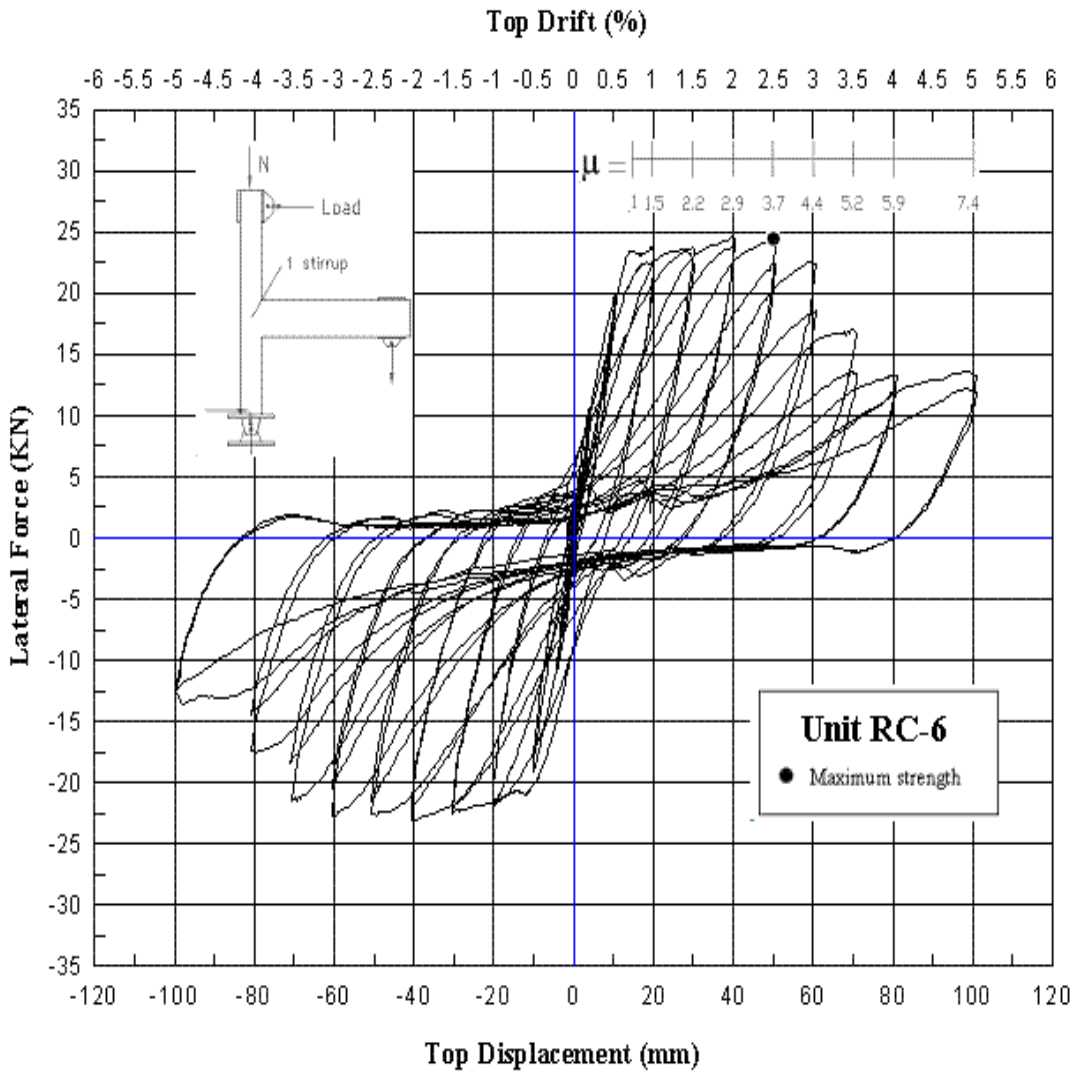

Figure 5 - 28: Lateral force vs. top displacement hysteretic response for Unit RC-6

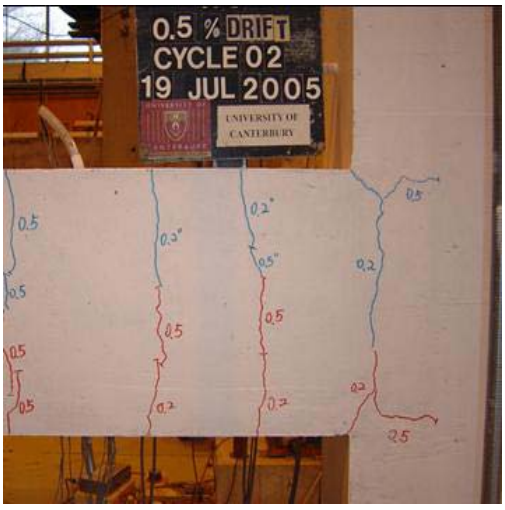

(a) 0.5% drift

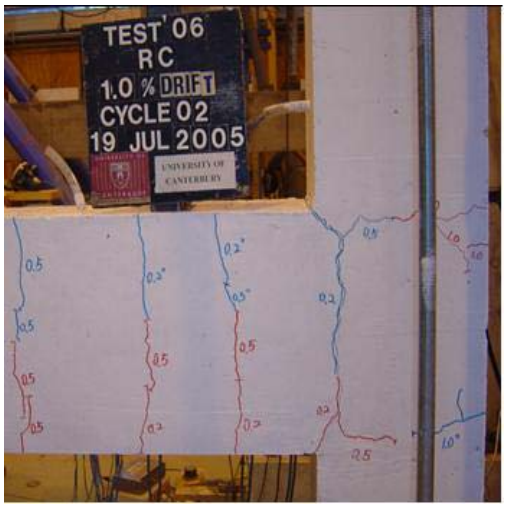

(b) 1.0% drift

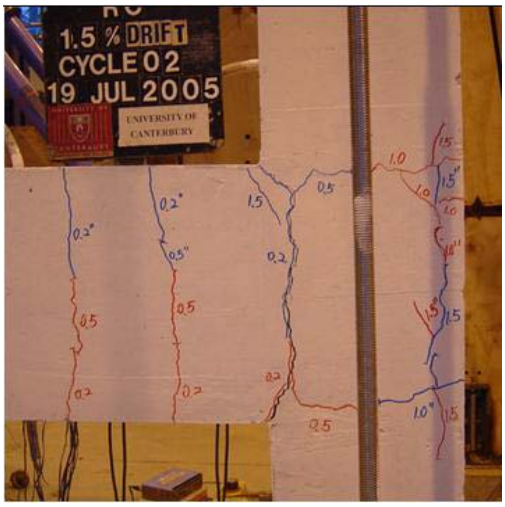

(c) 1.5% drift

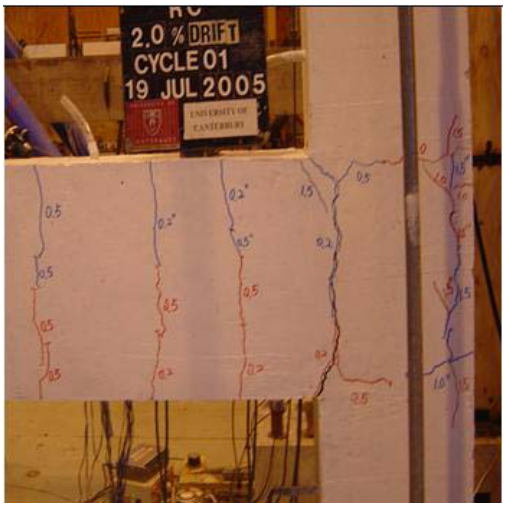

(d) 2.0% drift

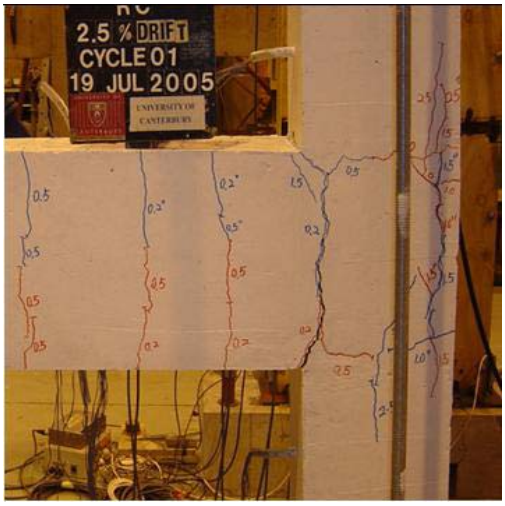

(e) 2.5 % drift

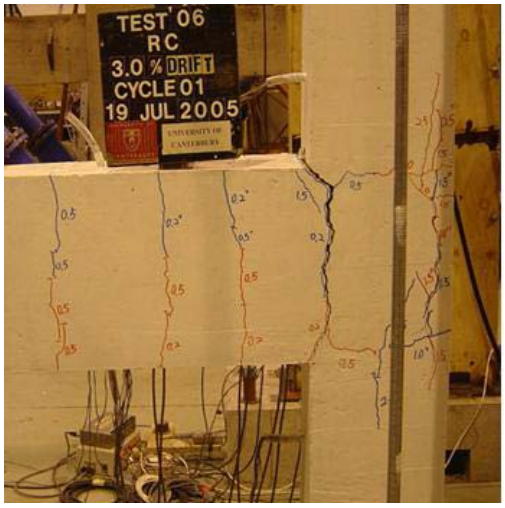

(f) 3.0 % drift

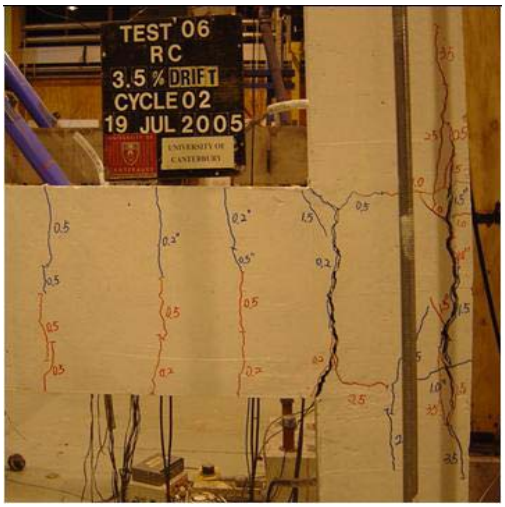

(g) 3.5% drift

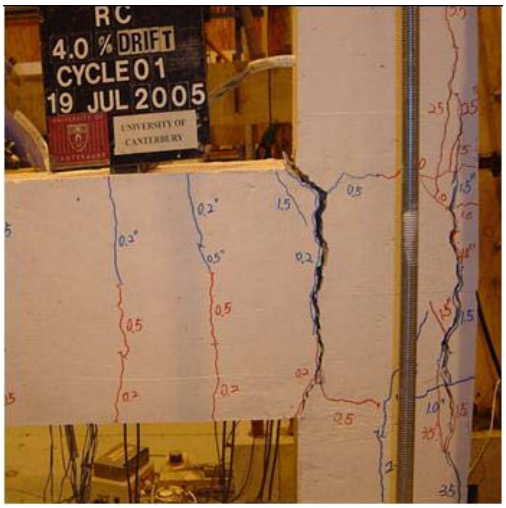

(h) 4.0% drift

(i) 5.0% drift (front side)

(j) 5.0% (back side)

Figure 5 - 29: Observed damage of Unit RC-6

5.2.3.3 Joint behaviour

The flowing group **Figure 5-30 (a) ~ (f)** present the joint behaviour of Unit RC-6. The cracks and damage mainly accumulated in the beam flexural failure and the joint buckling along the beam bars 90^{o} hook adjacent to the outer face of the column. Therefore there was no diagonal shear damage in the joint core. The principal tensile stress was 2.0 MPa ($0.4\sqrt{f'_c}$) with 0.7% drift when the cracks in the beam just started to open. The recorded maximum shear strengths of the joint occurred at the phase of the start of the combination failure, combining the beam plastic hinge and the joint bucking, with the joint principal tensile stress of 2.1 ($0.42\sqrt{f'_c}$) MPa. As the joint buckling cracks occurred at the position of the instrumentations of the joint, the measured joint shear deformation was slightly bigger than its real value, being at 0.0031 rad at the point of the extensive combination damage.

Table 5 - 6: Sequence of events of Unit RC-6

	Sequence of events	Force(KN)	v_j (MPa)	P_t(MPa)	$K=P_t/\sqrt{f'_c}$	γ (rad)	Drift
Unit RC-6	Beam hinging	23.103	2.710	2.023	0.403	0.0001671	0.7
	Extensive damage	24.22	2.834	2.112	0.420	0.0031872	2.5
	End test	13.559	1.544	0.924	0.184	0.0051368	5.0

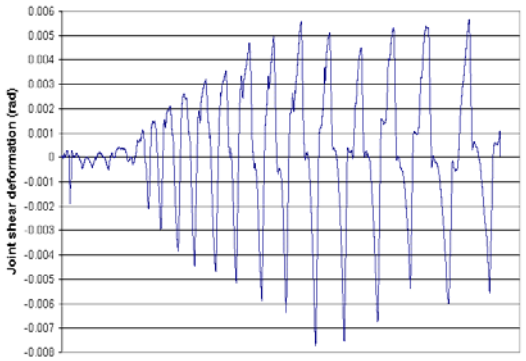

(a) Measured joint shear deformation history

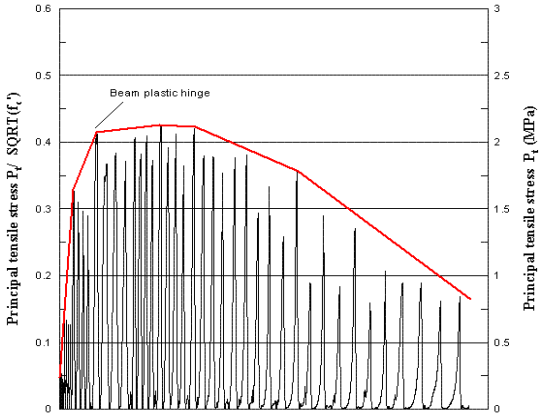

(b) The principal tensile stress history

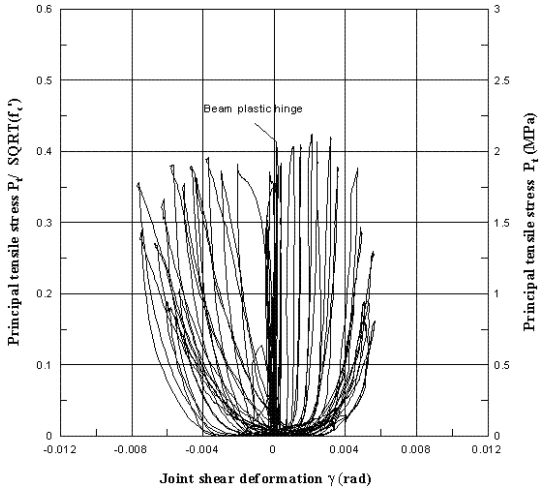

(c) Principal tensile stress vs. Joint deformation

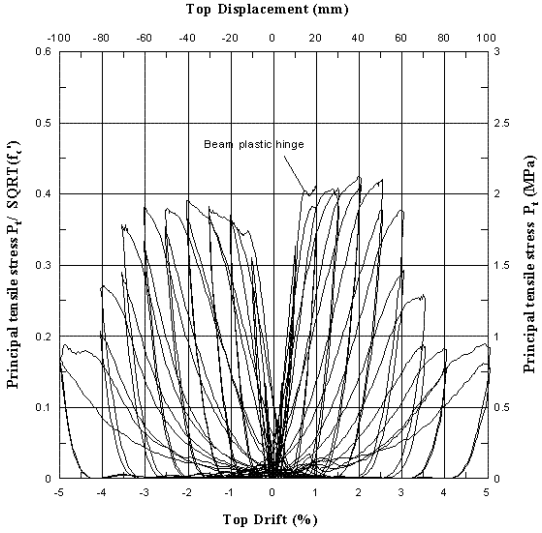

(d) Principal tensile stress vs. Top drift

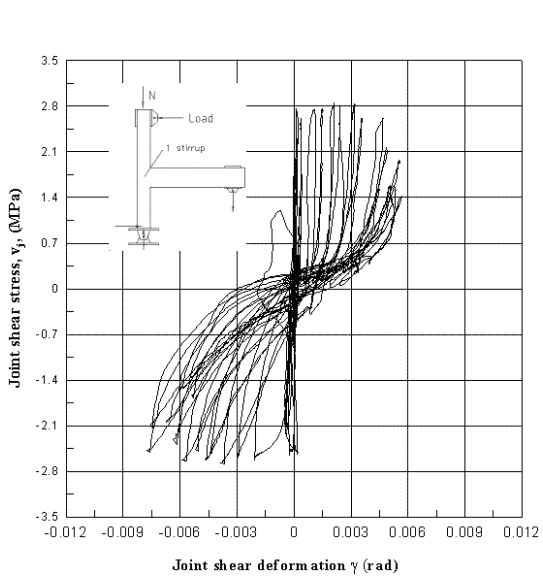

(e) Joint shear stress vs. Joint deformation

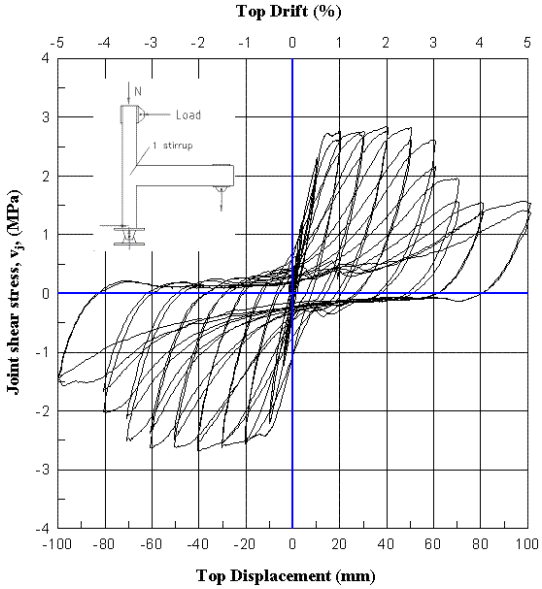

(f) Joint shear stress vs. Top displacement

Figure 5 - 30: Experimental joint behaviour for Unit RC-6

5.2.3.4 Longitudinal beam bar strains

Figure 5-31 and **Figure 5-32** show the measured strain profiles from the strain gauges along the longitudinal beam bars. Compared with the first two units of Group II, the final failure mode of Unit RC-6 was the combination of beam flexure failure and beam bars buckling failure. Therefore the strain profiles of Unit RC-6 are different from those of the first two units.

In the loading cycle of 1.0%, in which beam flexure cracks developed in the joint, the top beam bars reached the yield strain in the joint region adjacent to the column's inner face. Then, as buckling occurred around the beam bars hook, the beam bars yielded at both in the beam plastic hinge region and in the middle joint region in the subsequent loading cycles.

From these Figures, the lower value of the strains indicate that the bond and anchorage capacity of Unit RC-6 are not as good as those of the first two units.

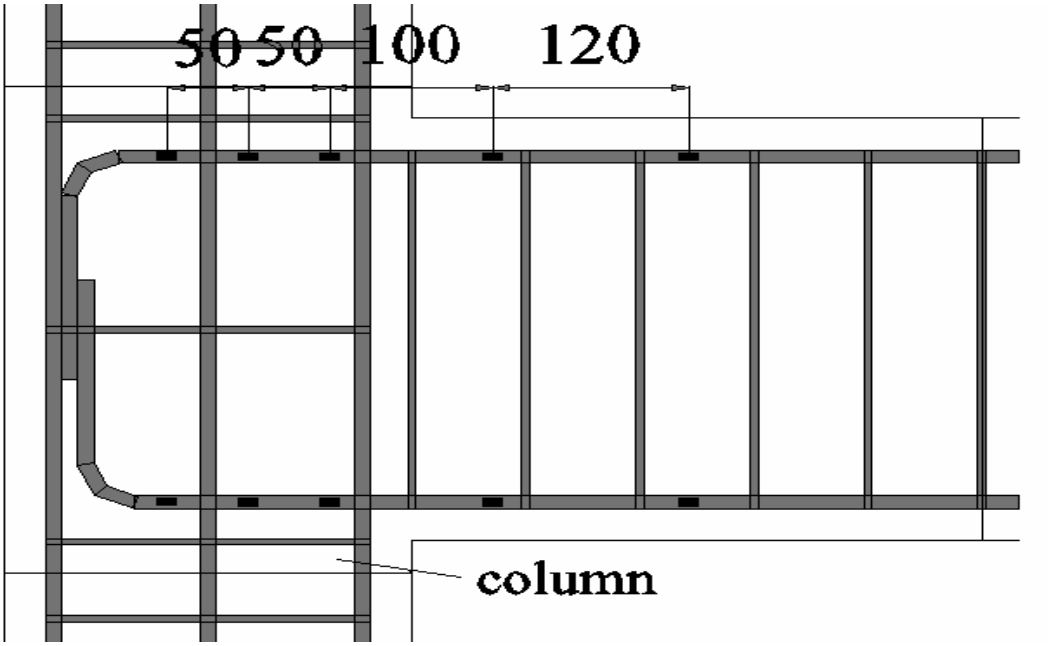

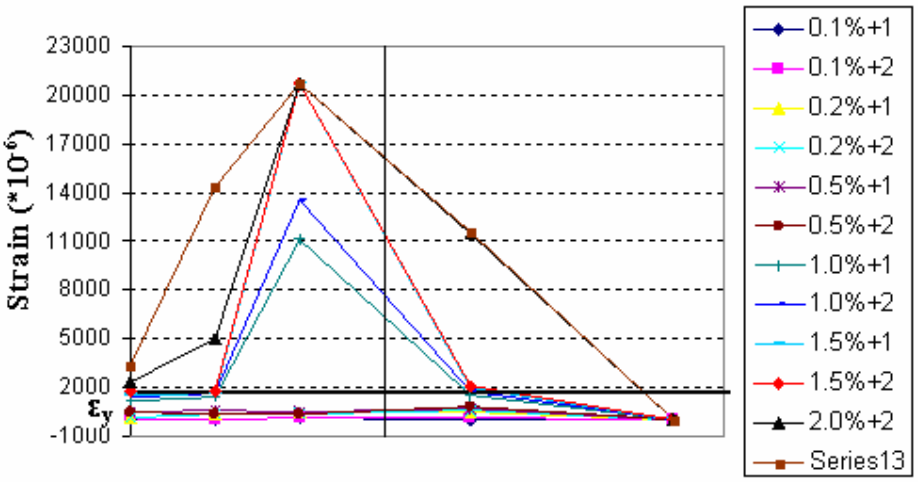

Top beam bar (positive loading cycle)

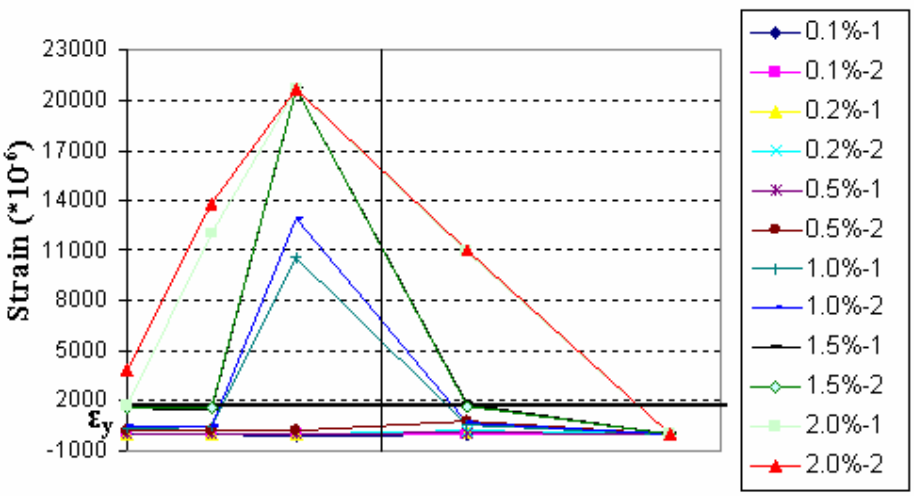

Top beam bar (negative loading cycle)

Figure 5 - 31: Strain profiles of beam bars measured by the strain gauges of Unit RC-6: top bar

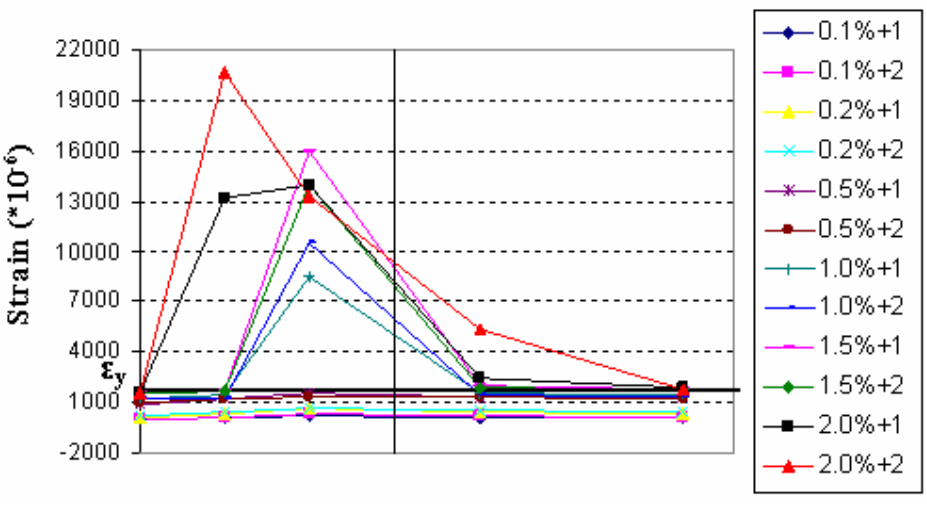

Bottom beam bar (positive loading cycle)

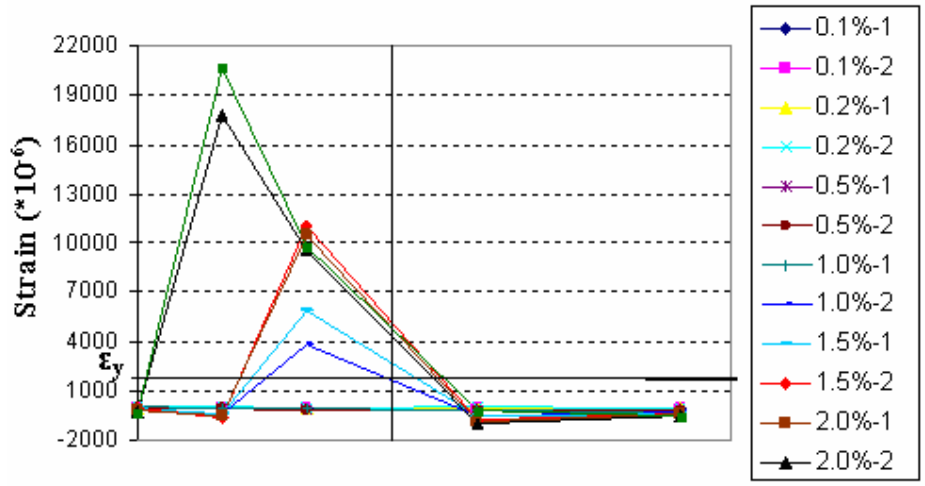

Bottom beam bar (negative loading cycle)

Figure 5 - 32: Strain profiles of beam bars measured by the strain of Unit RC-6: bottom bar

5.3. Introduction of Group Specimen III

The purpose of this section is to present the experimental results of Unit NZ-7 and investigate the seismic behaviour of a full seismic code designed beam-column joint. According to NZS 3101:1995 [45], the joint was designed to ensure a certain hierarchy of strength in which the joint was the strongest link in the beam-column joint assembly and was also protected by the formation of a plastic hinge failure mechanism located in the beam. The lateral reinforcement throughout the beam ensured an adequate ductility which protected the beam-column joint from brittle failure and provided an adequate energy dissipation capacity through rotation of the beam. The unit was tested under the simulated seismic loading, and a constant 100 KN axial load was used to simulate the column in an actual frame under minimum compression during an earthquake.

5.3.1. Unit NZ-7

5.3.1.1 Hysteretic response

Figure 5-33 shows the lateral force versus top displacement hysteretic response measured for Unit NZ-7. The first yield displacement measured for the tested unit was 10 mm with strength of 22 KN. This was the equivalent of a storey drift of 0.5% and 0.6 time to those steel fibre reinforced units in Group II. After 0.5% drift, the plastic hinge formed in the beam and a slight strength reduction can be seen due to the initial flexural cracking in the beam. In the following cycles, the strength generally increased with the increasing drift until 4.0% drift in which the maximum strength was reached (26 KN). Through the whole test, the loops tended to became fatter and fatter with the increasing load. The enlarged hysteretic loops indicated an increase in energy dissipation. This continued up to 4.0% drift. After that the loops began to flatten out, showing that less force was required to make the same displacement in the beam-column joint. Furthermore, cracking consumed less energy, and the beam lost stiffness.

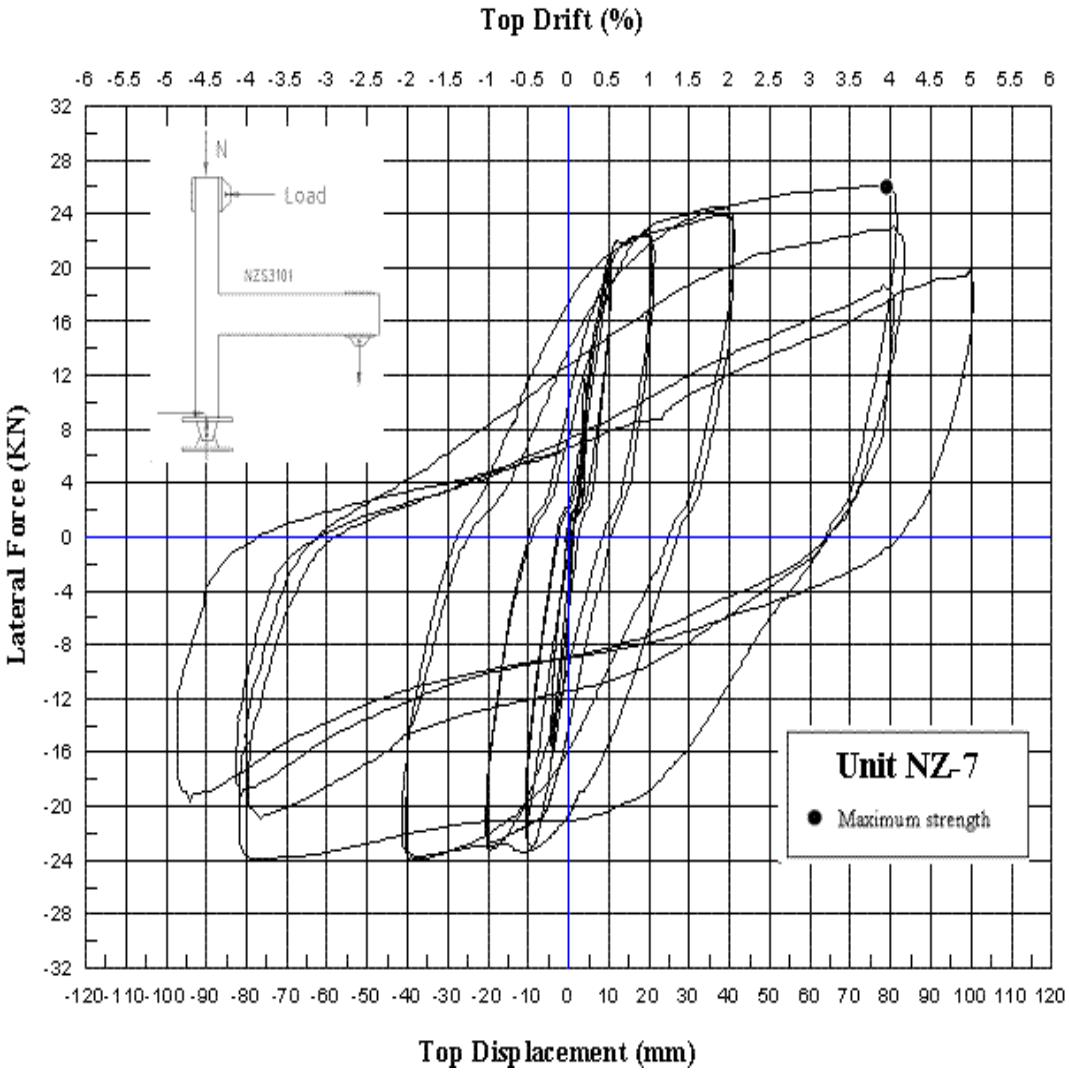

Figure 5 - 33: Lateral force vs. top displacement hysteretic response for Unit NZ-7

5.3.1.2 Cracking and damage

Figure 5-34 (a) ~ (f) shows the crack pattern of Unit NZ-7. The plastic hinge in the beam and fewer joint cracks can be clearly observed from this group figure proving that the full seismically designed joint can provide adequate seismic resistance.

In elastic load cycles of 0.2% ~ 0.5% drift, the first cracking of the beam occurred at the interface of the beam and joint at 0.2% drift. This crack started at the bottom of the beam and extended up through to the middle of the beam. When the drift increased to 0.5% drift, the beam was subjected to more cracking further from the interface. The original cracks increased in length and width.

In inelastic load cycles, 1.0% ~ end of test, the first cracking in the joint occurred during the cycle run of 1.0% drift with a strength of 21.5 KN. There was more cracking in the beam and the major crack at the interface increased in width and length. At 1.0% drift the resulting strength was the same as at 0.5% drift of 22 KN which shows there was no loss in stiffness. As the drift increased to 2.0%, there was a significant increase in the width of the cracks at the interface. The strength recorded in this drift was 24 KN. When the drift was at 4.0%, the measured strength of the tested unit achieved the maximum value, 26 KN. This led to yielding in the beam bars in the plastic hinge region causing the unconfined concrete to spall off under compression.

Throughout all the cycles the majority of damage was confined to the plastic hinge region. Minor cracking was the only evidence of damage to the column and joint area.

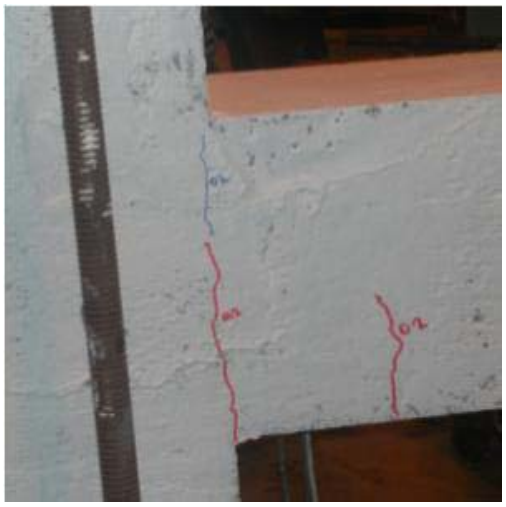

(a) 0.2% drift

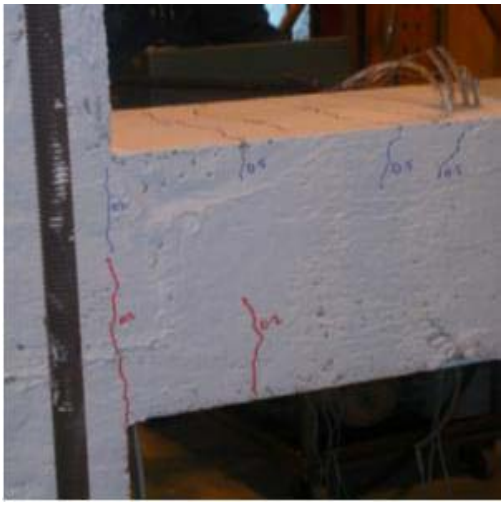

(b) 0.5% drift

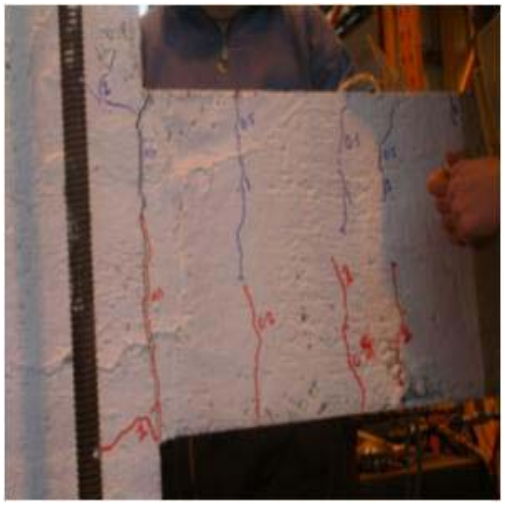

(c) 1.0% drift

(d) 2.0% drift

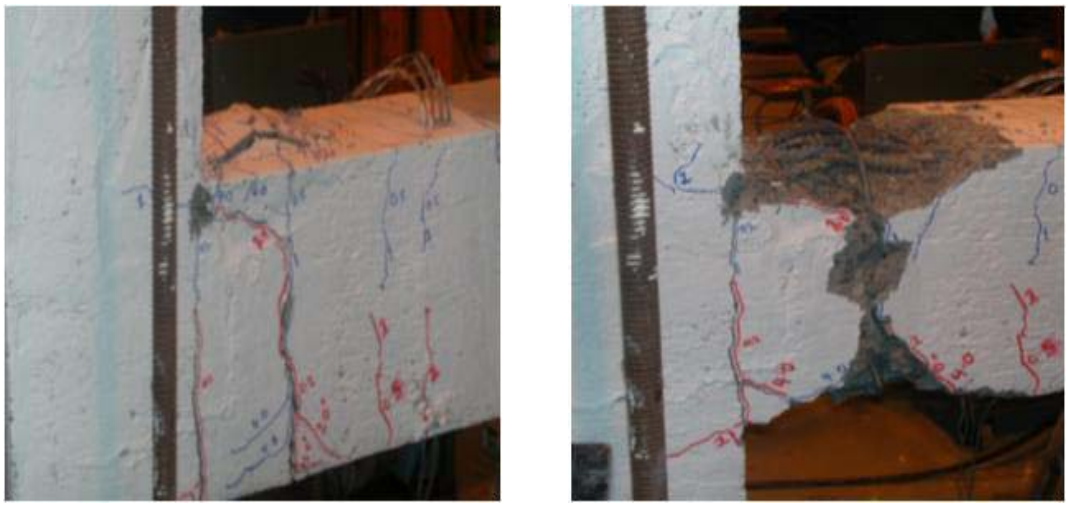

(e) 4.0 % drift **(f) Drift beyond 4.0%**

Figure 5 - 34: Observed damage of Unit NZ-7

5.4. The comparison of energy dissipation capacity

5.4.1. Introduction

From the experimental test of each unit, ductility factors μ_Δ, yield load P_y and yield displacement Δ_y could be obtained. As a measure of the dissipated energy of the units, the area under the full load–displacement envelope was computed and defined as the energy dissipated by the specimens. Two groups of graphs present the cumulative values of energy dissipation for each tested unit of Group I and II.

5.4.1.1 Dissipated energy of tested specimen units in Group I

Figure 5-35 (a) shows the comparison of the full energy dissipation capacity of three units in Group I. For the full response, a substantial increase in dissipating energy for SFRC units mainly occurred at the large inelastic-deformation stage compared to that of the RC joint unit (Unit RC-1). The reason is that when steel fibres are progressively pulled from the matrix during the period, the toughness and dissipated energy can be increased properly. Therefore, the SFRC joint could have greater inelastic deformation and fewer cracks. It is also clearly seen from **Figure 5-35 (a)** that the best energy dissipation was exhibited by the Unit SF-3 indicating the dissipated energy increased with the increase in fibre volume fraction.

5.4.1.2 Equivalent viscous damping of specimen units in Group I

According to the definition in Equation 4.7 as shown in **Chapter four**, the equivalent viscous damping of tested units taking into account the area of elastic deformation can be determined. So as an important index of the energy dissipation capacity, damping of the units in Group I was evaluated and compared. At the end of the tests, the damping coefficient was calculated as the summation of the amounts of accumulated damping for each cycle as given in **Figure 5-35 (c)**.

From **Figure 5-35 (c)**, it is shown that units had the approximately same value of equivalent viscous damping. On one hand, although the total area of the load–displacement of SFRC joints can be improved by adding steel fibres, the elastic area of each cycle defined by the yield load P_y and yield displacement Δ_y is also increased. On the other hand, the pinching of the load–displacement loops of SFRC joints caused by the critical flexure opening in the column plastic hinge regions reduced the energy dissipation capacity of the SFRC units significantly. Therefore, the RC joint shows a higher damping value than that of Units SF-2 (1% steel fibre used). Furthermore, Unit SF-3 still shows the best performance of damping compared with Unit SF-2 indicating the damping of the unit increased with the increasing fibre volume fraction.

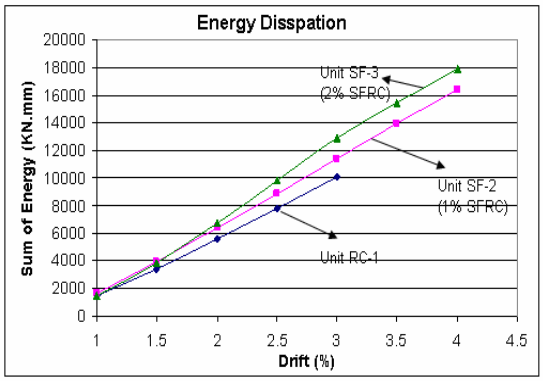

(a) Dissipated energy (per drift)

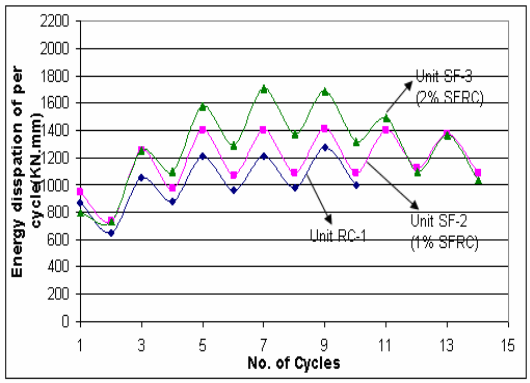

(b) Dissipated energy (per cycle)

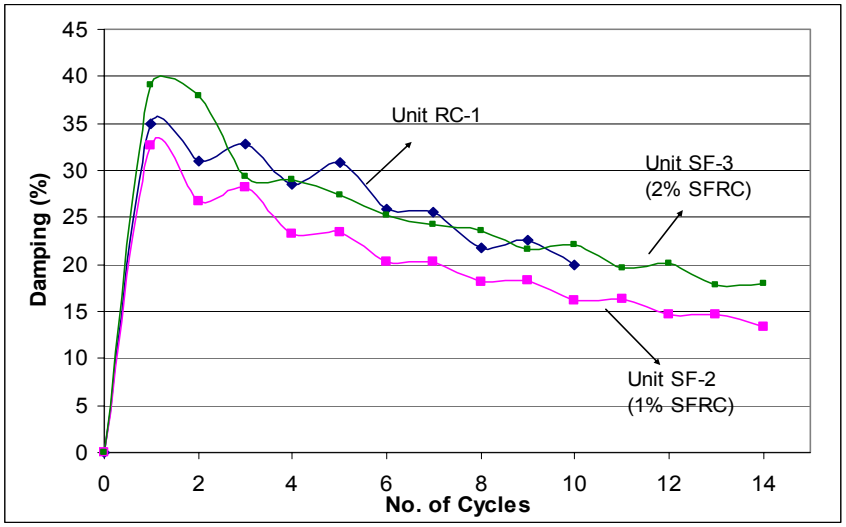

(c) Equivalent viscous damping ξ (per cycle)

Figure 5 - 35: Comparison of energy dissipation capacity of the tested units in Group I

5.4.1.3 Dissipated energy and equivalent viscous damping of units in Group II

The units in Group II were designed by seismic code NZS3101:1995. However, in order to research the shear resistance provided by steel fibres and stirrups in the joint region, the units in Group II were modified in the joint region, the stirrups replaced by steel fibres in both the joint region and the potential plastic hinge region.

Figure 5-36 (a) ~ (c) show the comparison of the energy dissipation capacity of the three units in Group II. The results indicate that: (1) as the drift increased, the unit reinforced with full stirrups and steel fibre in both joint region and potential plastic hinge region showed the best energy dissipation capacity. (2) Unit SF-5 reinforced with 1.0% steel fibres (50% stirrup reduction in the joint region and beam and column potential plastic hinge region) exhibited approximately similar energy dissipation capacity to those of RC-6 (without steel fibres reinforcement). This means the usage of SFRC can reduce the amount of lateral reinforcement in the plastic regions without losing joint seismic resistance capacity. Thus, SFRC can be seen as an appealing alternative to conventional confining reinforcement.

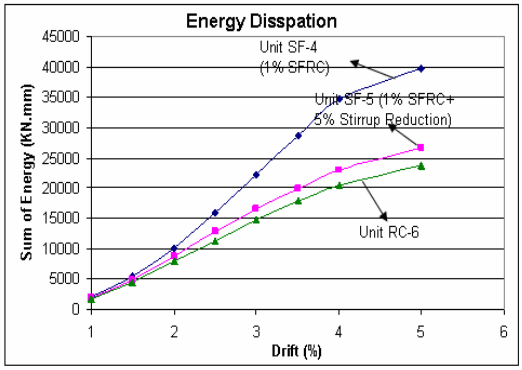

(a) Dissipated energy (per drift)

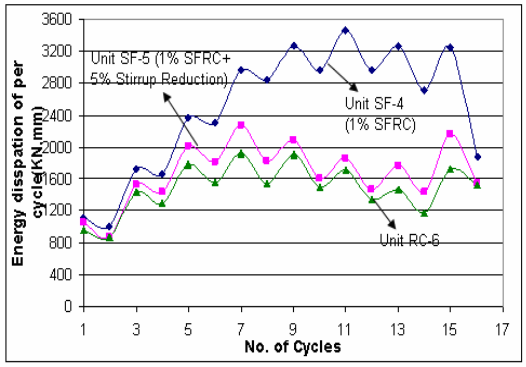

(b) Dissipated energy (per cycle)

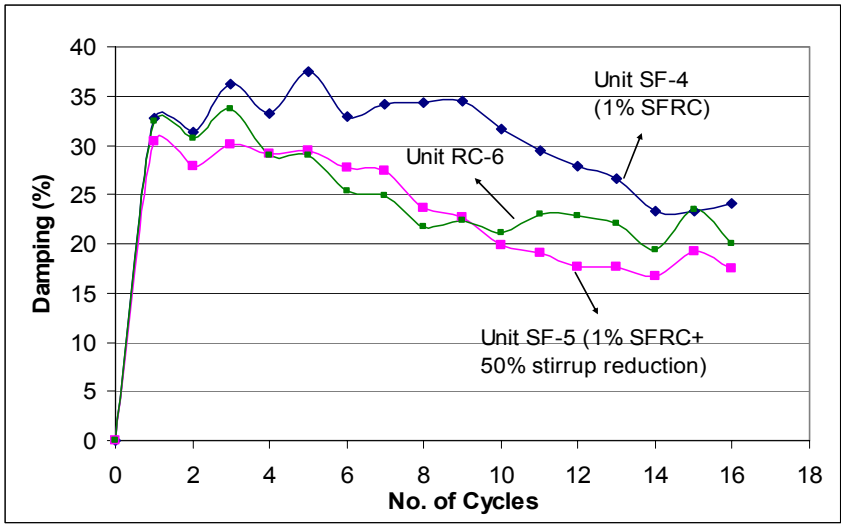

(c) Equivalent viscous damping ξ (per cycle)

Figure 5 - 36: Comparison of energy dissipation capacity of the tested units in Group I

5.5. Steel fibre contribution to joint shear capacity

5.5.1. Experimental comparison of joint strength degradation curve

The envelope curves of the relationships of joint shear stress vs. shear deformation and joint shear stress vs. top displacement for Group I and Group II are shown in **Figure 5-37**. Comparing **Figure 5-37 (a) ~ (d)**, the following interesting tendency can be noticed. For the units which are reinforced without steel fibre, Unit RC-1 and Unit RC-6, the shear stiffness of the RC joints were found to degrade much more rapidly after diagonal cracking in the joints. Moreover, the joint shear stress of the SFRC joint was higher that that of a normal RC joint indicating the improvement from using steel fibres.

As shown in **Figure 5-37 (a)** and **(b)**, all units show larger shear deformation of joints after cracking. However, the difference between joints with transverse reinforcement and without transverse reinforcement still can be seen. In Group I, with no transverse reinforcement used in joints, the RC joint showed approximately similar joint shear deformation behaviour to that of SFRC joints, Unit SF-2 and Unit SF-3 (see **Figure 5-37 (a)**). In Group II, the joint, Unit SF-4, reinforced with steel fibres and transverse reinforcement showed the least joint shear deformation, only 0.4% at the end. Furthermore, the units provided with more lateral reinforcement in the joint and plastic hinge region, such as Unit RC-6, show less joint shear deformation (0.8%) compared with that of Unit SF-5 (1.2%), in which 50% lateral reinforcement was replaced by using 1% steel fibre. This indicates that the lateral reinforcement in the joint and plastic hinge is still needed to reduce the joint stiffness degradation and deformation.

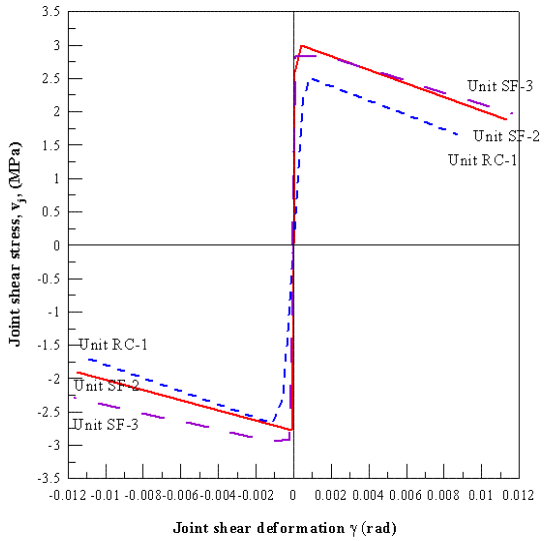

(a) Envelope curves in the relations of joint shear stress vs. Joint shear deformation (Group I)

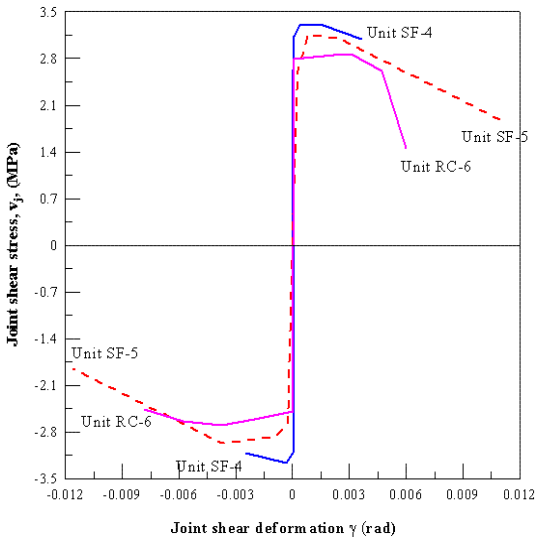

(b) Envelope curves in the relations of joint shear stress vs. Joint shear deformation (Group II)

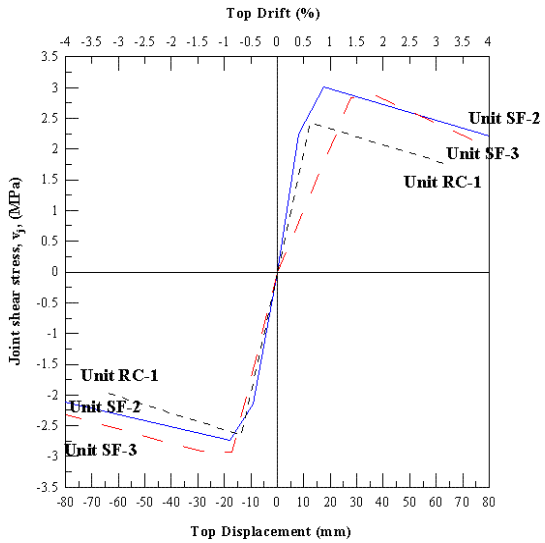

(c) Envelope curves in the relations of joint shear stress vs. Top displacement (Group I)

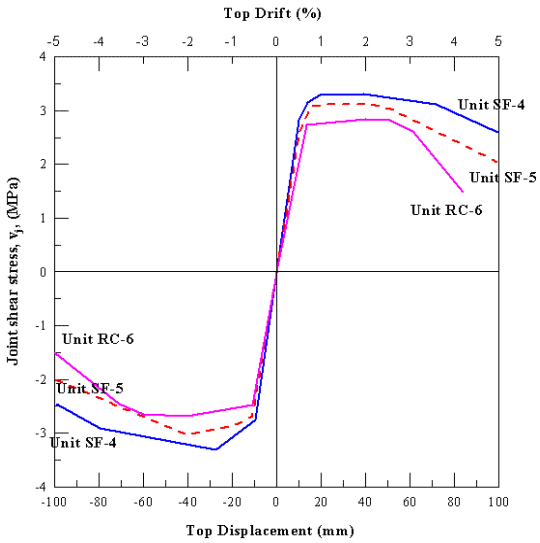

(d) Envelope curves in the relations of joint shear stress vs. Top displacement (Group II)

Figure 5 - 37: Comparison of joint shear deformation and joint shear stress

5.5.2. Strength degradation curve for exterior joints influenced by using steel fibres and stirrups

At a local level (joint panel zone), the elastic stiffness of SFRC joints can be predicted through a modified strength degradation model, while the limit states of first cracking and extensive damage are estimated in terms of principal tension stress. Deformation and drift limits value level for the SFRC joints can be obtained from experimental results. As a consequence of the comparison between the analytical results and experimental results, the joint strength limitation and shear resistance mechanism can be obtained. The limited number of specimens tested may not be sufficient to formulate a reliable degradation curve. However, an approximate qualitative trend of the degradation curve for exterior joints reinforced with steel fibres or steel fibres combined with stirrups can be proposed as illustrated in the procedure below.

The shear stress of a SFRC joint is simply classified into three contributions, provided by concrete (v_{jc}), steel fibres (v_{jf}), and stirrups (v_{js}) respectively. It should be noted that such estimation of the strength degradation curves of joints may be different when using different content of steel fibres because the material property of SFRC can be influenced by the physical property and type of steel fibres (see **CHAPTER two**). Therefore, three main

contributions of steel fibres, length, diameter, and amount of fibres (by volume), should be taken into account.

$$v_j = v_{jc} + v_{jf} + v_{js} \qquad (5.\ 1)$$

v_j = shear stress of the SFRC joint containing stirrups and steel fibres

v_{jc} = shear stress carried by concrete, based on principal tension strength

v_{jf} = shear stress carried by steel fibres.

v_{js} = shear stress carried by the joint stirrup.

The summary of the test results for joint shear stress, ultimate strength, and joint shear deformation is shown in **Table 5-7**, and their comparison with the calculated value of principal tensile stress, when expressed as a strength degradation model (see **Figure 3-12**), is shown in **Figure 5-38**. The value of the joint principal tensile strength (P_t) of joints, when expressed as a constant value K ($P_t = K\sqrt{f'_c}$), has been calculated from the lateral top column load. The first joint principal tensile strength is in the range between 0.4 and 0.5. For determining the joint shear stress provided by steel fibres and stirrups, the units whose failure modes are joint shear hinge are compared in **Figure 5-39**.

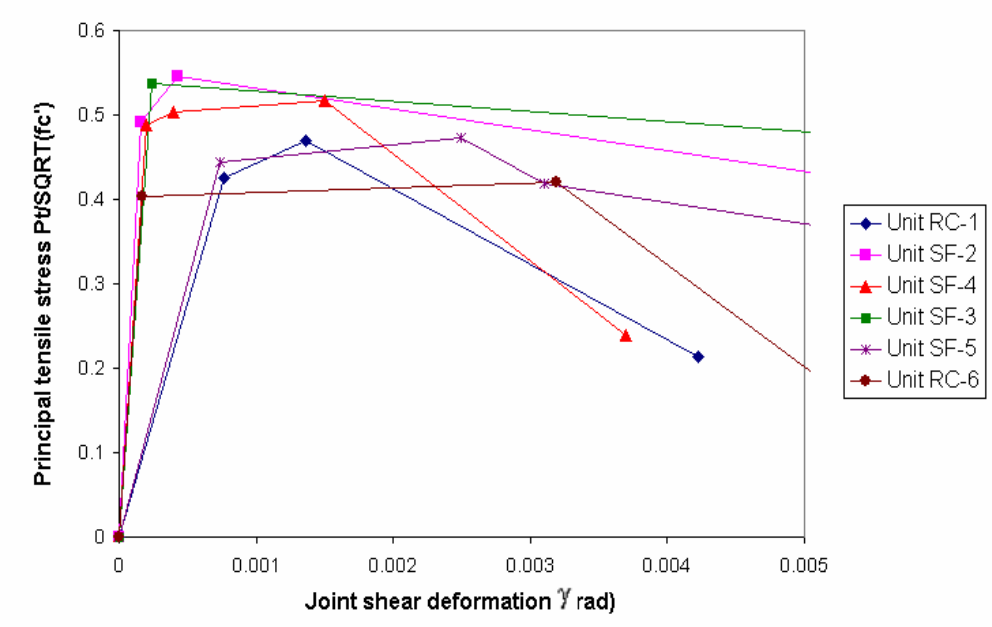

Figure 5 - 38: Strength degradation of all test units

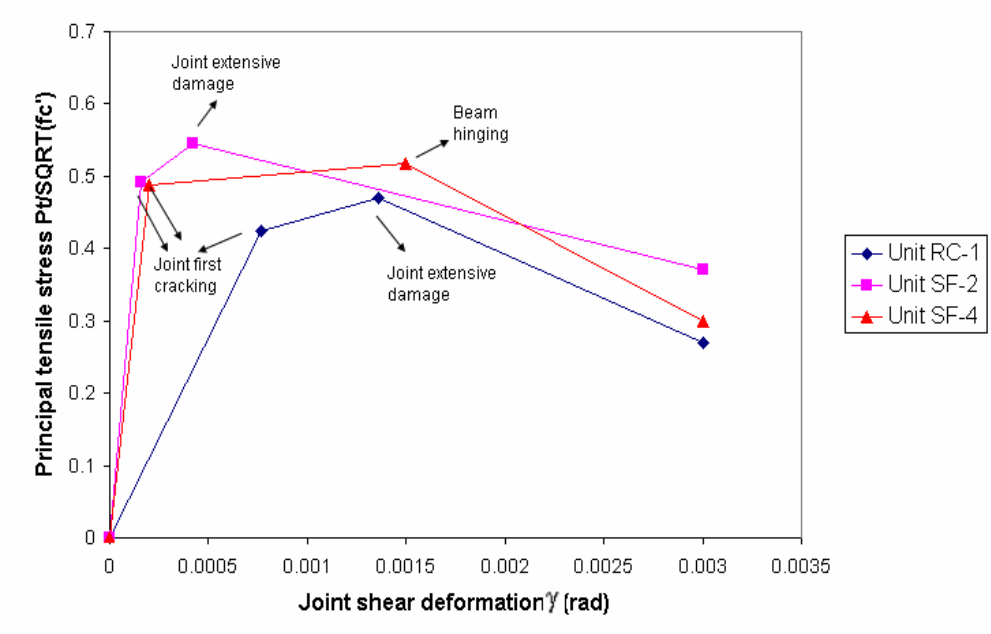

Figure 5 - 39: Joint shear strength degradation of Unit RC-1, Unit SF-2 and Unit SF-4

Table 5 - 7: Experimental test results

Units	Sequence of events	Force(KN)	v_j (MPa)	P_t(MPa)	$K=P_t/\sqrt{f'_c}$	γ (rad)	Drift
Unit RC-1	First cracking	20.66	2.425	1.796	0.4246	0.0007694	0.65
	Extensive cracking	22.65	2.640	1.984	0.4691	0.00136	0.71
	End test	13.29	1.569	0.906	0.214259	0.0042256	2.96
Unit SF-2	First cracking	23.06	2.725	2.078	0.491231	0.000162	0.71
	Extensive cracking	25.44	2.976	2.306	0.545111	0.0004231	0.90
	End test	16.11	1.925	1.316	0.311098	0.0099162	3.95
Unit SF-3	First cracking	25.11	2.922	2.272	0.537192	0.0002343	0.96
	End test	19.74	2.296	1.688	0.399006	0.0118285	3.90
Unit SF-4	First cracking	26.89	3.152	2.450	0.48766	0.0002	0.70
	Extensive cracking	26.6	3.295	2.599	0.517328	0.0015	1.91
	Beam hinging	27.75	2.525	3.233	0.502704	0.0004	0.90
	End test	15.65	1.839	1.198	0.238454	0.0037	4.90
Unit SF-5	First cracking	25.3	2.938	2.228	0.443623	0.0007366	0.69
	Extensive cracking	24.28	2.826	2.102	0.418482	0.0031054	3.0
	Beam hinging	26.65	3.110	2.377	0.473253	0.0024974	1.0
	End test	13.35	1.565	0.957	0.190516	0.0122577	5.0
Unit RC-6	Beam hinging	23.10	2.710	2.022	0.402586	0.0001671	0.7
	Extensive	24.22	2.833	2.111	0.420251	0.0031872	2.5
	End test	13.55	1.543	0.924	0.183908	0.0051368	5.0

The joint shear force contributed by steel fibre can be calculated by the comparison of Unit RC-1 and Unit SF-2. In these two units, there is no extra shear reinforcement used in the joint region, therefore the improvement of joint shear stress can be determined as the contribution of steel fibres. From **Figure 5-39** and **Table 5-7**, it can be seen that after adding 1% steel fibres in the joint, the joint first cracking strength, when expressed as a constant value K, was significantly improved from 0.42 for Unit RC-1 to 0.49 for Unit SF-2, 17% improvement. The extensive cracking strength was from 0.45 to 0.55, 22.2% improvement. For the purpose of designing a SFRC joint, a formula of joint shear stress carried by steel fibres is defined as $v_{jf} = K_f \frac{l_f}{d_f} V_F$, where V_F is the volume content of steel fibres (by volume) and $\frac{l_f}{d_f}$ is the aspect ratio of steel fibres. In some previous research, the value of K_f was defined as 2 by Tang [12]. The test results and the comparison between their calculation and experimental results are shown in **Figure 5-40** and **Table 5-8**. In this research, based on the test results discussed above, the proper value of K_f is defined to be 0.5 for Dramix steel fibre with 38 mm length and an aspect ratio of 65. However, the limited number of tested units in this research may not to be adequate to give a proper value of K_f. A comprehensive comparison of calculated K_f, based on previous research results (see Chapter Two), is listed in **Table 5-9** and shown in **Figure 5-41**. From this comparison, it can be seen that the values of K_f in most previous researches are in the range between 0.3 and 1.5. Therefore, 1.0 may be recommended for calculating joint shear stress carried by steel fibre in designing a SFRC joint.

Table 5 - 8: Calculation of ultimate strength in literature [12]

Specimen (1)	Cube strength of concrete f_{cu} (MPa) (2)	Axial compressive strength of concrete, f_c (MPa) (3)	Aspect ratio, l_f/d_f (4)	Fiber volume fraction, v_f (%) (5)	Shape of fiber (6)	Joint stirrups (7)	Yield strength of stirrup, f_y (N/mm²) (8)	$N/f_c b_c h_c$ (9)	Measured shear strength, V_f^t (KN) (10)	Calculated shear strength, V_f^c (KN) (11)	V_f^t/V_f^c (12)	Note (13)
(*a*) Exterior Joint												
SF-1	21.3	10.65	66.8	1.2	round	—	—	0.315	325.24	262.74	1.238	Yang (1988)
SF-2	32.1	16.05	52	1.5	rectan.	3Φ 8	290.0	0.210	383.13	393.95	0.973	
J1-0.8	33.8	16.89	75	0.8	round	—	—	0.223	293.22	244.91	1.197	Zhang (1989)
J1-1.0	28.1	14.04	75	1.0	round	—	—	0.423	302.52	262.31	1.153	
J1-1.2	35.0	17.5	75	1.2	round	—	—	0.278	347.17	302.78	1.147	
J1-1.5	30.4	15.8	75	1.5	round	—	—	0.216	321.10	307.18	1.045	
J1-2.0	37.5	18.5	75	2.0	round	—	—	0.215	395.77	393.64	1.005	
J3-1	31.6	15.8	75	0.8	round	4Φ 6	256.0	0.308	332.24	302.99	1.097	
(*b*) Interior Joint												
SF-6	18.2	9.1	54.2	1.5	rectan-	—	—	0.251	340.90	241.90	1.409	Hu Chao-bin
SF-7	18.2	9.1	54.2	1.5	gular	3Φ 6	496.8	0.251	398.64	317.43	1.256	(1990)
SF-8	37.9	18.66	65	1.5	round	3Φ 6	496.8	0.123	456.55	410.83	1.111	
SF-9	18.2	9.1	54.2	1.5	rectan-	—	—	0.251	339.53	241.90	1.404	
SFL-10	31.4	15.7	54.2	1.5	gular	—	—	0.146	303.29	244.57	1.240	
RC-11	21.9	10.76	—	—	—	5Φ 10	356.3	0.209	381.56	395.5	0.965	
Average ratio	—	—	—	—	—	—	—	—	—	—	1.160	
Mean square error	—	—	—	—	—	—	—	—	—	—	0.137	
Coefficient of variation	—	—	—	—	—	—	—	—	—	—	0.118	

Note: N = axial compression load of column; and V_f^c = calculated shear strength based on (6).

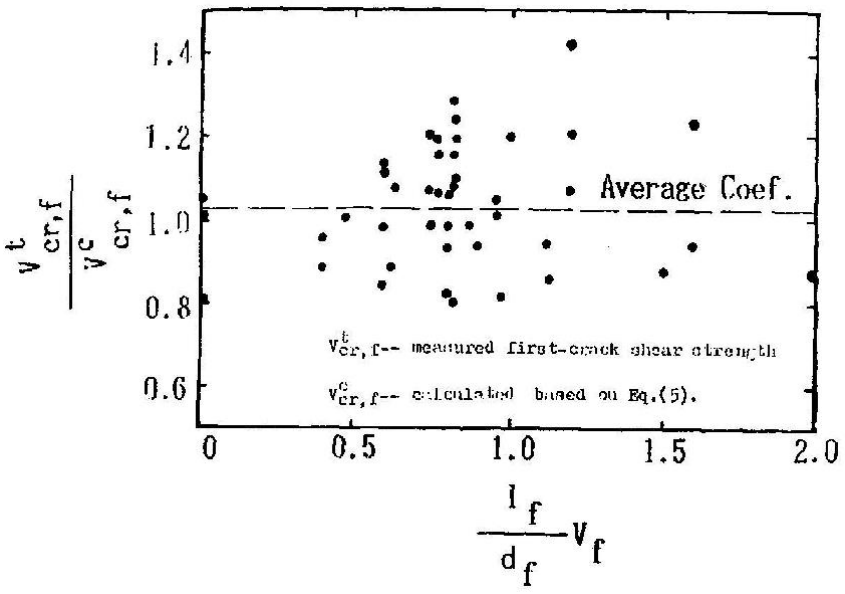

Figure 5 - 40: Calculation of shear strength for SFRC joints compared with experimental results [12]

Table 5 - 9: Evaluated K_f from previous tests in available literature

Ref. No Specimen	Failure mode	Concrete's strength (MPa)	Axial load (KN)	Fibre type	Aspect Ratio (l_f/d_f)	Fibre volume fraction V_f (%)	Joint shear stress v_j	Shear stress carried by concrete v_{jc} (MPa)	Shear stress carried by stirrup v_{js} (MPa)	Shear stress carried by steel fibre v_{jf} (MPa)	K_f	$\frac{l}{d} V_f$	Scale Factor
(a) Exterior Joint													
Henager (1977) [41]	JS(F)+FL	34.45	0	smooth, round, cold-drawn, brass-plated	74.5098	1.67	5.92	2.4652	None	3.455	2.78	1.24	Full scale
Gefken and Ramey (1989) [34]	JS	38	44	straight steel brass-coated fibres	60.9756	2	4.5878	2.5894	None	1.998	1.64	1.22	N/A
	JS	38	44	straight steel brass-coated fibres	60.9756	2	4.9917	2.5894	0.404	1.998	1.54	1.22	N/A
	JS	20	44	straight steel brass-coated fibres	60.9756	2	4.9917	1.8787	0.6059	2.507	2.06	1.22	N/A
	JS	20	44	straight steel brass-coated fibres	60.9756	2	3.9241	1.8787	0.8079	1.238	1.01	1.22	N/A
Katzensteiner and Mindess (1992) [40]	JS	34.5	160	Dramix hooked end	60	0.76	3.844	2.4692	None	1.375	3.02	0.46	N/A
Filiatrault et al. (1994)	JS	34	350	N/A	60	1	5.0379	2.4504	None	2.587	4.31	0.6	Full scale
	JS	38	350	N/A	100	1.6	5.8776	2.5905	None	3.287	2.05	1.6	Full scale
Gebman (2001) [39]	JS	23	0	Dramix hooked end	62	2	1.7161	1.3908	N/C	0.325	0.26	1.24	1/2
	JS	23	0	Dramix hooked end	62	2	1.6343	1.3908	N/C	0.244	0.2	1.24	1/2
	JS	23	0	Dramix hooked end	62	2	1.6513	1.3908	N/C	0.261	0.21	1.24	1/2
	JS	23	0	Dramix hooked end	62	2	1.4227	1.3908	N/C	0.032	0.03	1.24	1/2
Gencoglu and Eren (2002) [42]	JS(F)+FL	22	0	hooked-end steel fibres	75	1	1.5	1.3602	0.6542	0.14	0.19	0.75	Full scale
	JS(F)+FL	22	0	hooked-end steel fibres	75	1	1.4063	1.3602	None	0.046	0.06	0.75	Full scale
This research (2005)	JS(F)+FL	17.9	75	Dramix hooked end	65	1	2.98	2.64	None	0.34	0.52	0.65	2/3
	FL(C)	17.9	75	Dramix hooked end	65	2	2.92	2.64	None	0.28	0.22	1.3	2/3
	JS(F)+FL	25.2	100	Dramix hooked end	65	1	3.15	2.71	N/C	0.44	0.68	0.65	2/3

	FL(B)	25.2	100	Dramix hooked end	65	1	3.11	2.83	N/C	0.28	0.43	0.65	2/3
(b) Interior Joint													
Stevenson (1980) [13]	JS	30	996	N/A	30	2.3	2.3797	2.3045	None	0.075	0.11	0.69	Full scale
Filiatrault (1995) [36]	JS	46	670	hook-end steel fibre	100	1.6	8.0014	2.8507	1.884	3.27	2.04	1.6	Full scale
Shannag (2005) [37]	JS	28	0	brass-coated	60	2	2.4657	2.2224	None	0.24	0.2	1.2	1/3
	JS	28	0	brass-coated	60	4	2.7938	2.2224	None	0.57	0.24	2.4	1/3
	JS	28	0	hooked-steel fibres	60	2	3.3381	2.2224	None	1.12	0.93	1.2	1/3
	JS	28	0	hooked-steel fibres	60	4	3.4335	2.2224	None	1.21	0.5	2.4	1/3

Note: N/A = not available; N/C = Not considered (for joint first cracking, stresses carried by joint stirrups are not considered); JS = Joint shear failure; JS (F) + FL = Joint first shear cracking observed, and the final failure mode is the combination failure (joint shear combining flexural failure); FL (B) = Flexural failure in the beam; FL (C) = Flexural failure in the column

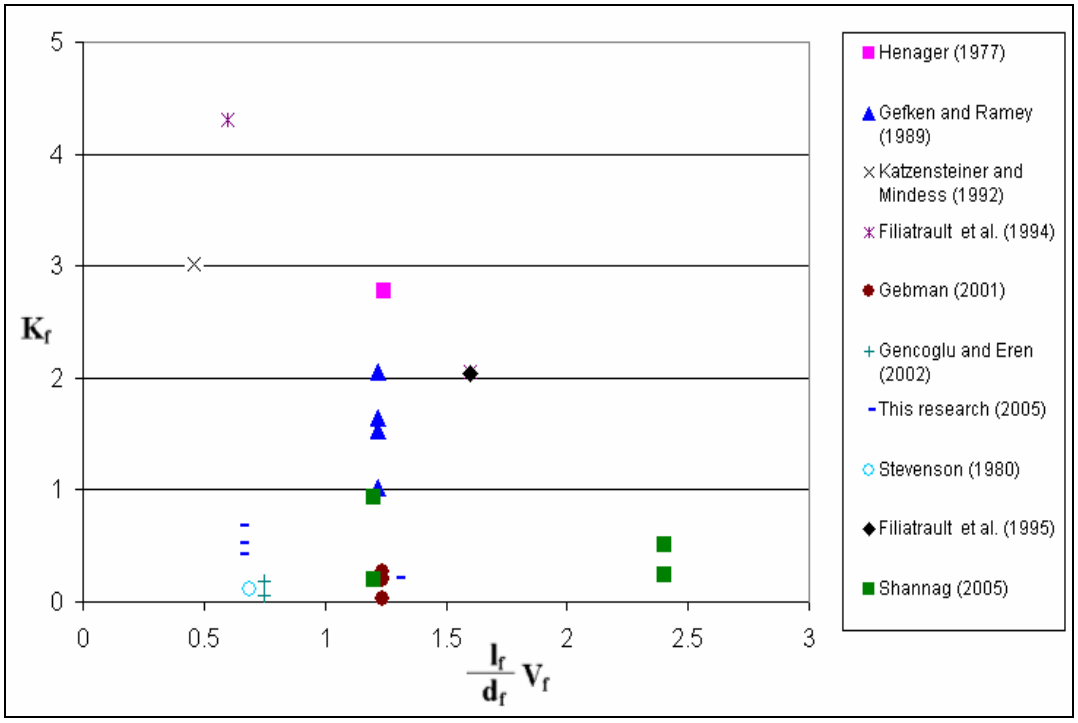

Figure 5 - 41: Comparison of fibre shear resistance coefficient K_f values from experimental tests available in literature (based on Table 5-9)

The joint shear force influenced by adding joint stirrups can be partially obtained by comparing Unit SF-4 with Unit RC-1 and Unit SF-2. Because the final failure mode of Unit SF-4 is beam flexural failure, therefore only first joints shear cracking strength has been obtained from the testing. The result obtained from testing shows the joint reinforced with 1% steel fibres and stirrups had an approximately the same first shear cracking strength when comparing the joint shear strength of Unit SF-4 and Unit SF-2. For the purpose of designing SFRC joints combined with normal shear reinforcement, a formula of joint shear force carried by stirrups is defined as $V_{js} = f_{yv} \frac{A_{sh}}{b\,s}$, where, f_{yv} is the strength of stirrups; A_{sh} is the area of stirrups, s is the spacing of transverse reinforcement; and b is the width of the beam.

Based on the discussion above and Equation 3.7, the strength degradation model of a joint, such as Unit SF-4, reinforced with stirrups or steel fibres or stirrups combined with steel fibres can be analysed properly (see **Table 5-10** and **Figure 5-42**). The calculation detail is shown in **APPENDIX I**. However, it must be noted that the values of the joint shear deformation in **Figure 5-42** are randomly chosen as those are difficult to calculate with

unknown material properties, such as the elastic modulus (E) and the shear modulus (G) of SFRC.

Table 5 - 10: Prediction of determined Coefficient K

Joint Type		Determined Coefficient K	
		First cracking	Extensive damage
v_c	Joint without any reinforcement	0.29	0.42
v_c+v_s	Joint reinforced with 1 stirrup	0.29	0.52
v_c+v_f	Joint reinforced with 1.0% steel fibre	0.35	0.48
$v_c+v_s+v_f$	Joint reinforced with 1 stirrup and 1.0%steel fibres	0.35	0.58

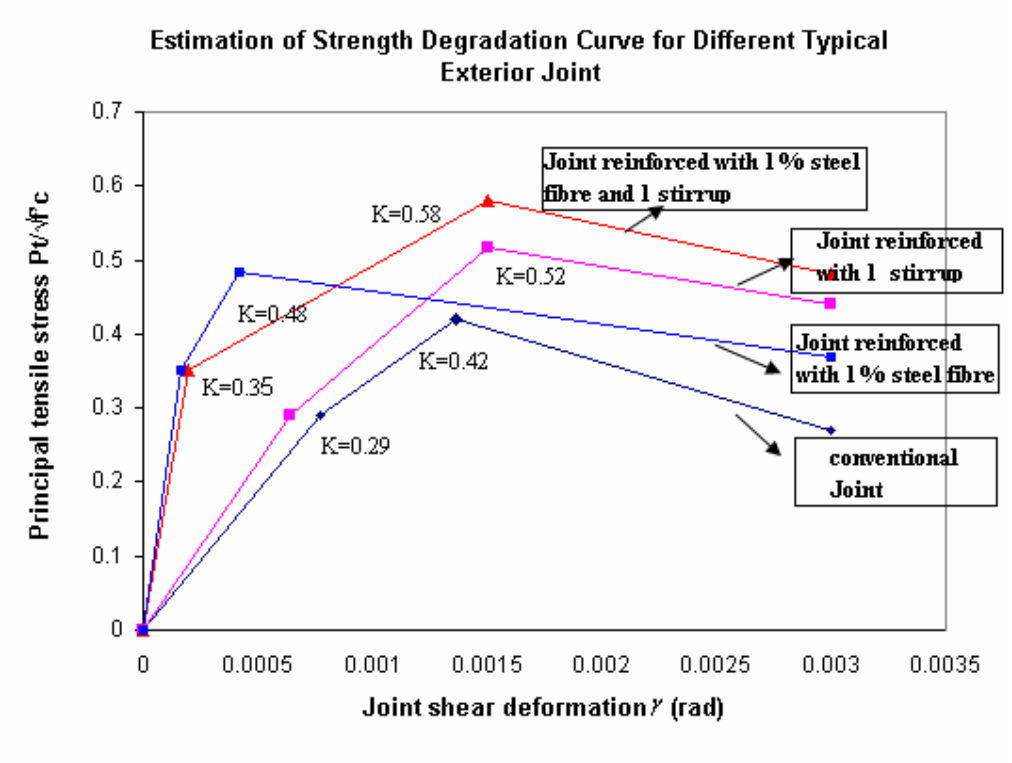

Figure 5 - 42: Predicted strength degradation curves for the exterior joints reinforced with different type of shear reinforcement

5.5.3. Global failure mechanisms

The peculiarities of the beam-column joint damage may be caused by hybrid failure mechanisms. Typical degradation curves of joints reinforced with different types of reinforcement (shown in **Figure 5-42**) are based on the ideal joint shear damage mechanism without considering the flexural behaviour of beam and column elements. For analysing and predicting the failure model of a joint, therefore, a simple analytical model describing a hybrid failure mechanism, which can demonstrate the failure mechanism due to combination of plastic hinges in beam and column elements and shear hinges in joint regions, should be introduced.

The effects of using different types of reinforcement such as stirrups, steel fibres, and hybrid reinforcement in the joint region can be validated by using the hierarchy of strength diagram. In the hierarchy of strength diagram, the moment-axial load interaction diagram of column, beam moment, the axial load demand line, and shear strength of the joint are clearly presented (**Figure 5-43**). For example, when the first diagonal shear cracking occurs in the region of an exterior joint, if no alternative shear resistant reinforcement is available, progressive brittle diagonal cracking develops and extends to heavy damage. After the first diagonal cracking (principal tensile stress $P_t = 0.29\sqrt{f'_c}$), higher strength (up to principal tensile stress $P_t = 0.42\sqrt{f'_c}$) can be achieved (see Figure 3-9) if column and beam reinforcement are sufficient; otherwise, column hinging or beam plastic hinging can occur. If additional shear reinforcement, such as stirrups and steel fibres, exist in the joint, the shear strength can be increased significantly and may change the failure mode from joint shear hinge to beam or column plastic hinge failure.

Figure 5-44 shows a graph of the hierarchy of the strength of joints reinforced with different types of confinement. As discussed above, a clear visualisation of the hierarchy of strength is shown among component elements, depending on the axial load demand line. This equivalent interaction diagram is also used to predict the failure mode for an exterior beam-column joint.

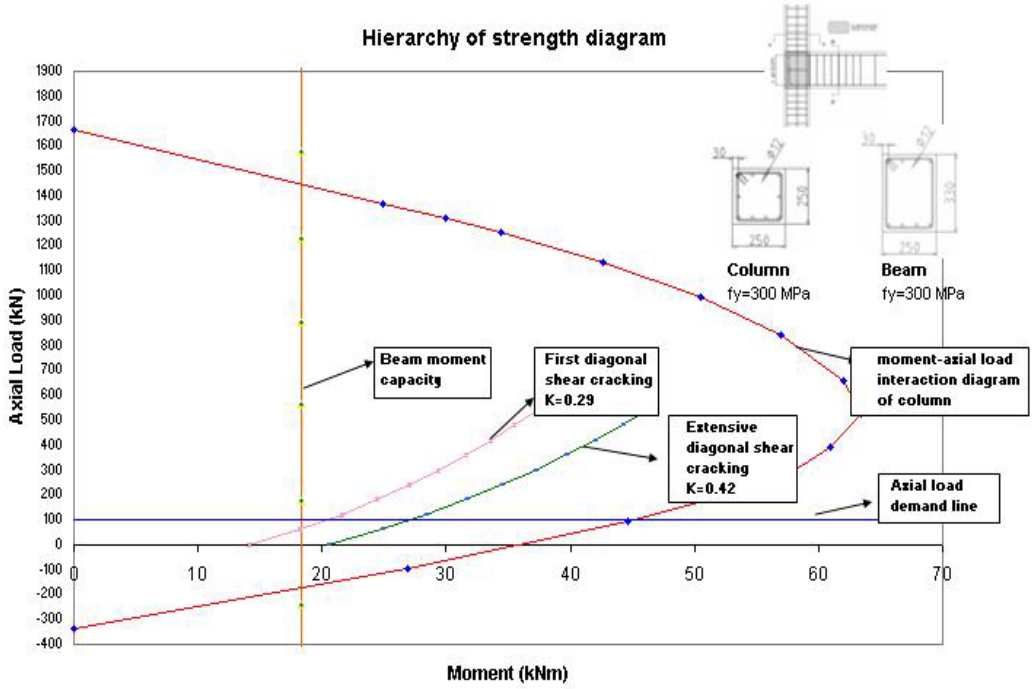

Figure 5 - 43: Hierarchy of strength diagram for a conventional beam-column joint

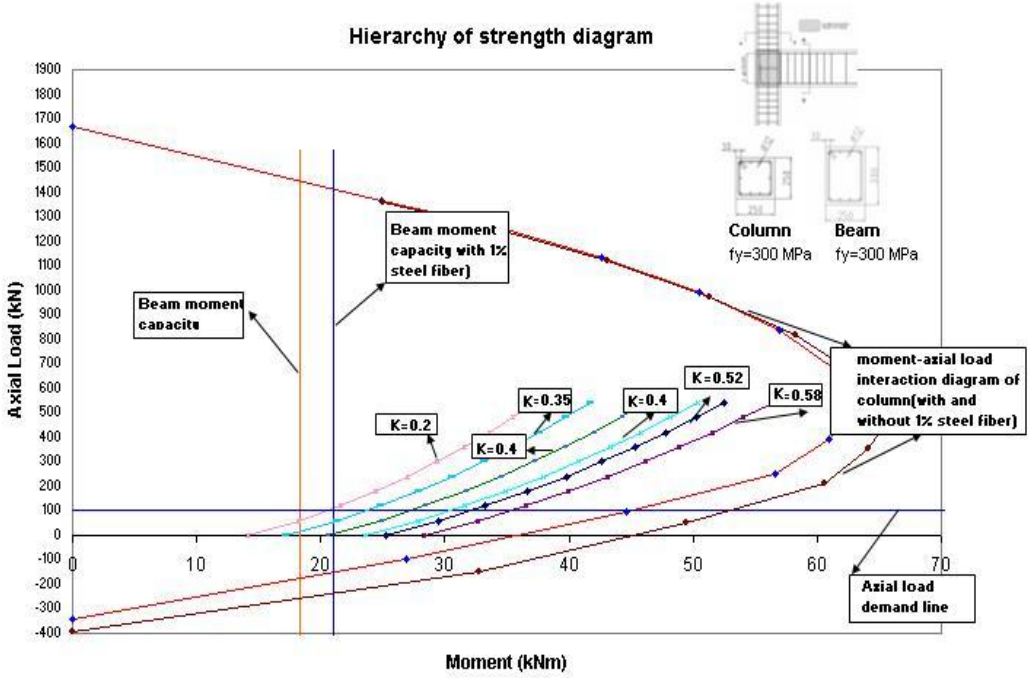

Figure 5 - 44: Hierarchy of strength diagram for a beam-column joint reinforced with different types of shear reinforcement

5.5.4. Factors of the material properties of steel fibre reinforced concrete in the behaviour of fibre reinforced exterior joints

As reviewed in **Chapter two**, the effect of using steel fibre reinforced concrete (SFRC) in seismic application can be influenced significantly by changing the toughness of SFRC which is influenced by many aspects such as the volume content of fibres, aspect ratio of the fibres, fibre type, and the strength of the concrete. However, there are two factors, the dosage and the aspect ratio of fibres, which mainly determine the capacity of toughness of SFRC. In terms of calculating the shear resistance of steel fibre in the joint region, the equation $v_{jf} = K_f \frac{l_f}{d_f} V_F$ is used. From this equation it can be seen that the two main factors are both to be considered. The following hierarchy of strength diagrams (**Figures 5-45** and **5-46**) demonstrate how much these two factors influence the final shear strength of SFRC joints.

Figure 5-45 shows the estimated shear strengths of joints reinforced with the same volume content (1.0%) but different aspect ratios (ranging from 45 to 95) of steel fibres. It can be seen that the shear resistance capacity of SFRC joints is slightly increased with the increase in the aspect ratio of steel fibres used. A similar comparison of SFRC joints reinforced with different volume contents (ranging from 0.3% to 2.1%) but containing the same aspect ratio of fibres is shown in **Figure 5-46**. This figure shows that the increase in the volume content can also increase the shear resistance capacity of SFRC joint.

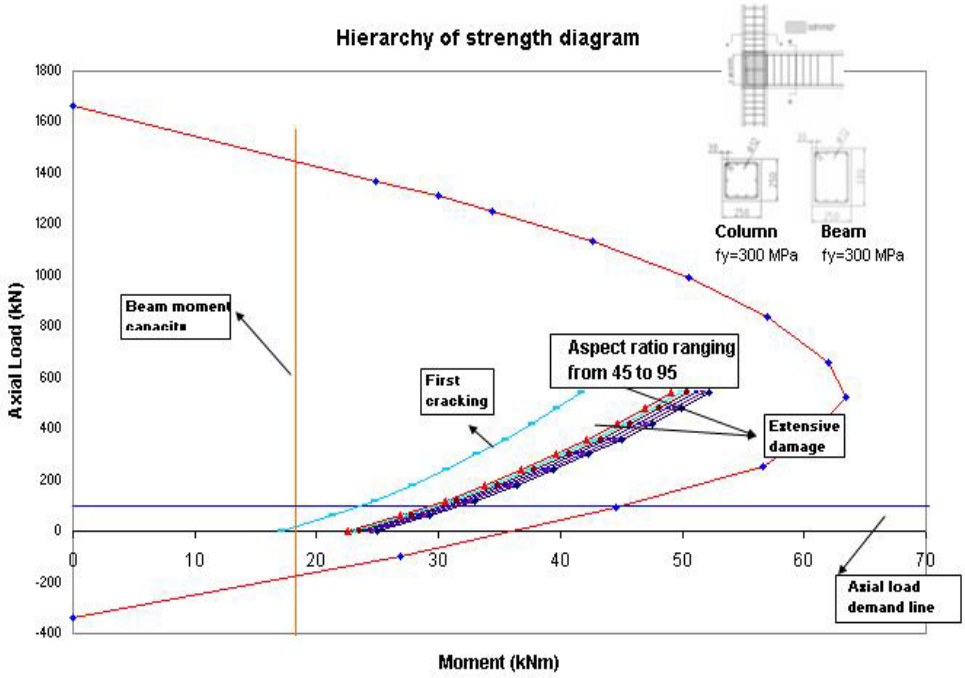

Figure 5 - 45: The shear-resistance capacity of SFRC joints influenced by different aspect ratio of fibres

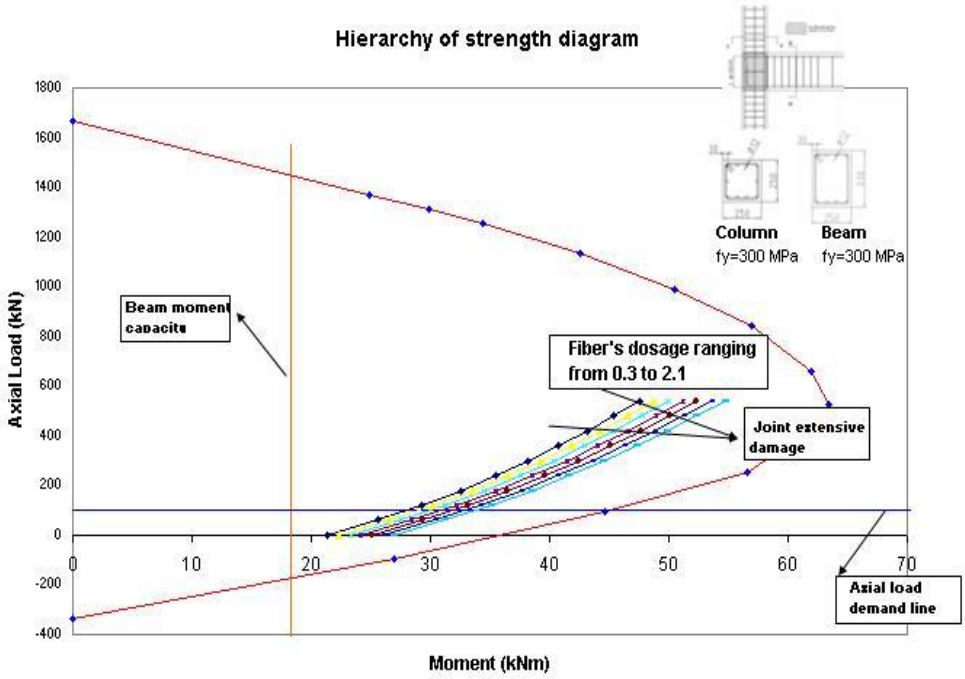

Figure 5 - 46: The shear-resistance capacity of SFRC joints influenced by different volume content of fibres

CHAPTER SIX

6. ANALYTICAL MODELS OF SFRC JOINTS AND COMPARISON WITH EXPERIMENTAL RESULTS

6.1. Introduction

Many models have been proposed for analysis of the behaviour of SFRC with different properties. These models include strain-stress relationship, shear resistance and moment capacity equations of SFRC, which have been also used to formulate design rules for SFRC structural members. In this chapter, the modelling of steel fibre reinforced concrete (SFRC) members is reviewed. The non-linear dynamic analysis of reinforced concrete beam-column joints using multi-spring and finite element methods are also discussed. Finally, a simple computer model is developed for analysing the seismic behaviour of tested SFRC beam-column joint units.

For the non-liner dynamic analysis modelling of beam-column joints, it is very important to use correct parameters to represent the behaviour of the regions where non-liner deformation occurs. A simple rotational spring modelling with calibrated parameters has been introduced as a feasible tool to analyse the seismic behaviour of the tested units. The rotational spring, based on the lumped plasticity approach, is used to model the joint behaviour in both linear and non-linear stage. Furthermore, a proper hysteresis rule which can effectively represent the pinching behaviour of shear hinging joints is proposed to govern the analysis. The proper parameters of the introduced hysteresis rule are obtained though calibration with experimental results.

6.2. Literature review: The modelling of SFRC element

6.2.1. Modelling of strain - stress relationship of SFRC

One of the advantages of adding steel fibre into a concrete matrix is the enhancement of the compressive strength. Some studies have been done to investigate the effect of the post-peak softening branch of the compressive stress-strain curve of SFRC. However, only a few

constitutive equations are published for SFRC, such as Hughes and Fattuhi [53], Fanella and Naaman [54], Ezeldin and Balaguru [55], Barros and Figueiras [56] and Dhakal [57]. It was found that the increasing steel fibre dosage may improve compressive strength ranging from 0 to 15 percent, but influence the slope of descending branch of the stress-strain curve significantly. Unfortunately, there are no studies to show constitutive equations which could be used for SFRC with the different fibre type and fibre dosage.

Sample of a proposed modelling of strain - stress relationship of SFRC

Barros and Figueiras [56] proposed a stress-strain model for steel fibre reinforced concrete in 1999. In this research, two types of hooked-end Dramix steel fibres (30 mm in length 0.5 in diameter, and 60 mm in length and 0.8 in diameter, respectively) were used. Based on the experimental results, a stress-strain relationship for steel fibre reinforced concrete in compression was derived for analysing SFRC structures, as shown in **Figure 6-1**. To evaluate the flexural resistance of SFRC members, a layer model was also proposed for the analysis of steel fibre reinforced concrete cross sections, shown in **Figure 6-2**.

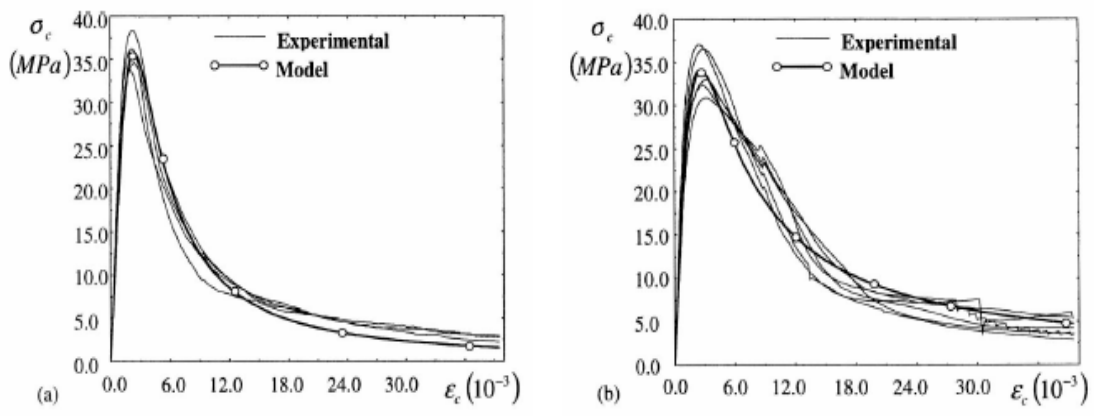

Figure 6 - 1: The numerical modelling of stress-strain relationship from [56]

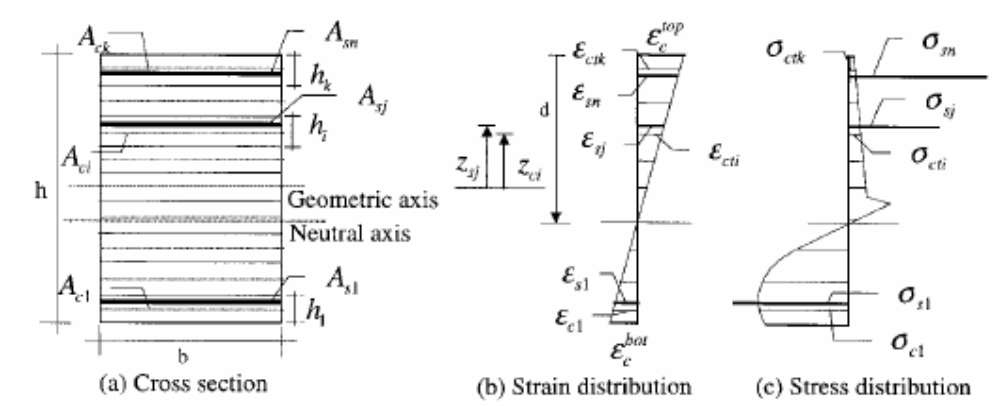

Figure 6 - 2: Assumed strain and stress diagrams from [56]

6.2.2. Shear modelling of SFRC beams

Many advantages of adding steel fibres into concrete have been reported by researchers, such as higher energy absorption, higher impact resistance and resistance against crack propagation. As one of these advantages, the enhanced shear capacity which may help to reduce the shear reinforcement is more attractive topic for researchers. SFRC beam under simulated loading are commonly used to obtain an effective modelling. There are many studies on the shear behaviour of SFRC beams as mentioned in section **2.3.1**. The result of these investigation showed that steel fibres are capable of resisting shear stresses and addition of fibres increases shear capacity of the cross-section. **Table 6-1** shows several numerical models for calculating the ultimate shear strength of SFRC beams.

Table 6 - 1: Models for Steel Fibre Reinforced Beam

Model proposed by	Steel fibre contribution	Notes
Mansur et al. [28], in 1986 Krstulovic [58], in 2000	$V_{fb} = \sigma_f \, b \, d$ $\sigma_f = 0.6 \cdot \sigma_{pc}$ $\sigma_{pc} = \lambda_1 \lambda_2 \lambda_3 \tau V_f \frac{l_f}{d_f}$	λ_1 length efficiency factor, taken as 0.25 λ_2 bond characteristic factor, taken as 1.2 λ_3 orientation factor, taken as 1 τ shear stress between fibre and concrete matrix, taken as 4.137 MPa
Banthia et al. [32], in 1999	$V_{fy} = F_t \cdot \sin\alpha = F_1 \, b(h-c)$ $\quad F_0 = \tau \pi d_f \frac{l_f}{4}$ $F_t = F_1 \{b(h-c)/\sin\alpha\}$ $\quad n = 0.5 \frac{V_f}{\pi r_f^2}$ $F_1 = \mathrm{n} \cdot F_0 = 0.5 \tau d_f \frac{l_f}{4} \frac{V_f}{r_f^2}$	τ shear stress between fibre and concrete matrix, taken as 4.15 MPa
Narayanan [31], (1986)	$V_b = 0.41 \cdot \frac{L}{D} \cdot \rho_f \cdot \tau$	V_b - fibre pullout forces along the inclined crack ρ_f - volume fraction of fibres τ -average fibre matrix interfacial bind stress, taken as 4.15 N/mm^2

Lim et al. [59], in (1987)	$V_{SF} = 0.6 \cdot \sigma_{tu} \cdot b_w \cdot d \qquad \sigma_{tu} = \frac{\eta_1 \eta_0^{'} V_f l_f \tau_u}{2 r^{'}}$ $\eta_0^{'} = \frac{\int_0^{\rho}\int_0^{\theta} \cos^4\theta \cos^4\rho \; d\theta \; d\rho}{\int_0^{\rho}\int_0^{\theta} d\theta \; d\rho}$	l_f - is the length of the fibre $r^{'}$ - is the ratio of the area of cross section to the perimeter of the fibres. V_f - is the volume fraction η_1 - is the length efficiency factor $\eta_0^{'}$ - is the orientation factor l_c - denotes a length twice that required to developed the ultimate fibre stress $\eta_1 =$ 0.5 for $l_f < l_c$ $1 - \frac{l_c}{l_f}$ for $l_f \geq l_c$
Swamy and Bahia [26], in 1985	$V_u = 0.517 + 0.283\sigma_{cu}$	

6.2.3. Flexure modelling of SFRC elements

Research by Dhakal

Cyclic path-dependent models for reinforced concrete incorporated in a finite element program were modified by Dhakal [57] to simulate the cyclic behaviour of SFRC columns. The compressive stress versus compressive strain relationship of SFRC could be obtained through the Elasto-plastic and fracture (EPF) model (**Figure 6-3 (a)**). The tensile stress-strain relationship of SFRC was developed from tension softening/stiffening model for conventional concrete. Furthermore, cover concrete spalling model and reinforcement buckling model developed from normal reinforced concrete were modified to extend their application to SFRC. Based on results of such analysis, monotonic stress-strain envelopes for SFRC and reinforcing bars were obtained, as shown in **Figure 6-3 (c)**. Finally, after combining the cyclic loops with the envelopes the path-dependent material models were encoded into a finite-element based analysis program which was used to simulate the performance of SFRC column under cyclic loading. The comparison between experimental and proposed modelling results (shown in **Figure 6-3 (d)**) represented that the proposed models could reasonably predict the flexural behaviour of SFRC columns. However, the author mentioned that the model was derived based on the test results of 1.0% (by volume) SFRC, and the behaviour of SFRC may be influenced by different amount of fibres.

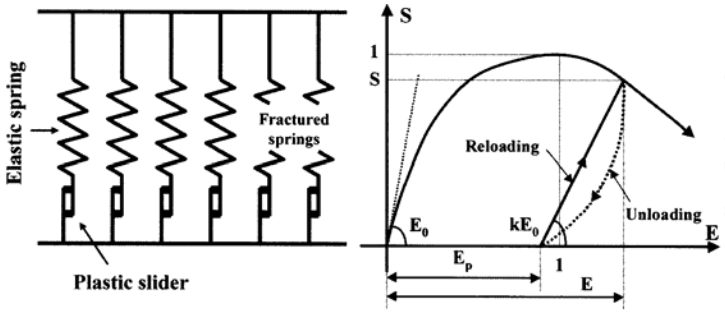

(a) Elasto-plastic and fracture EPF model

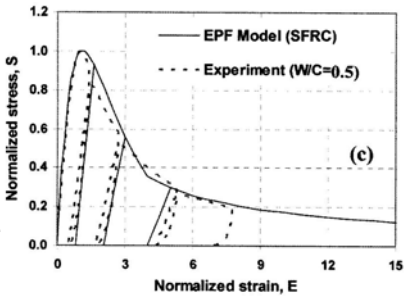

(b) Comparison with EPF model

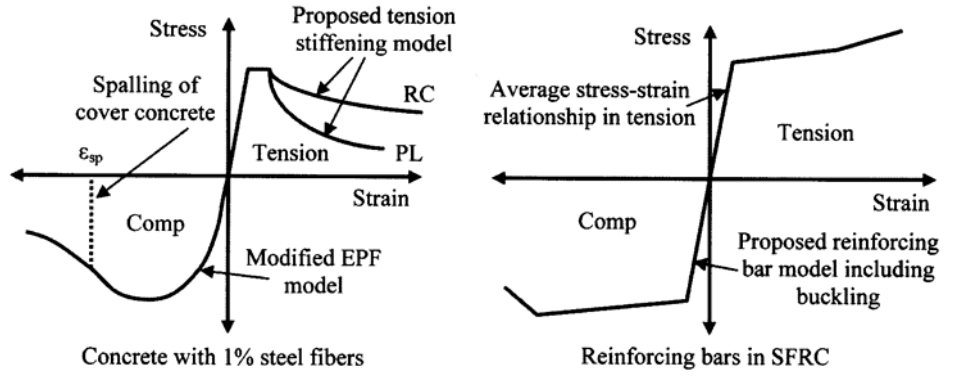

(c) Constitutive models for fibre analysis of SFRC members

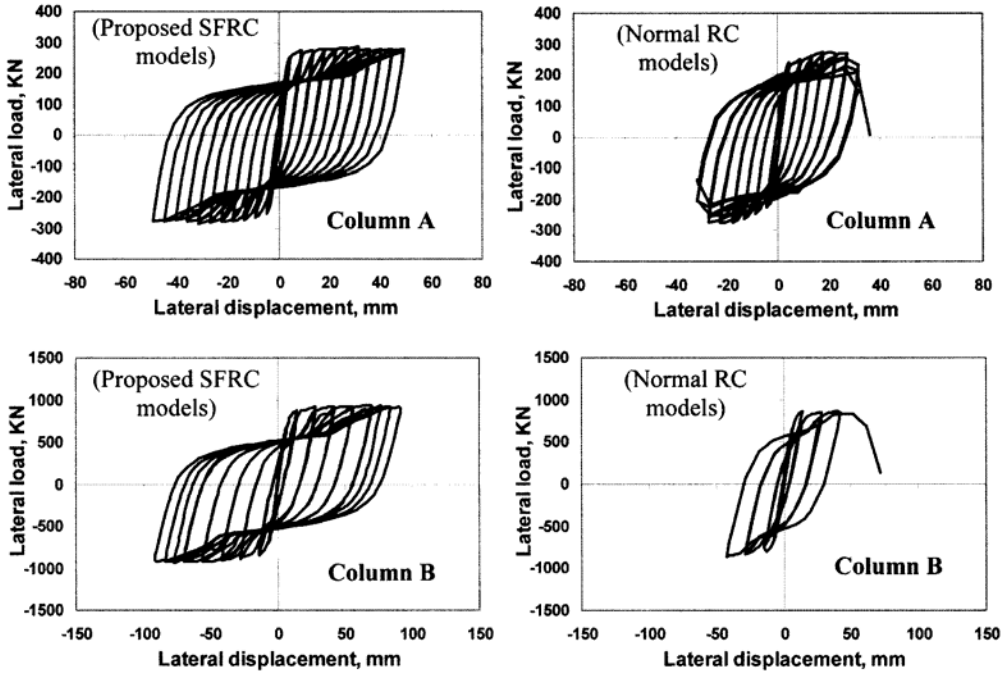

(d) Load-displacement relationships (analyses with normal RC & proposed SFRC models)

Figure 6 - 3: Analysis model of SFRC columns proposed by Dhakal from [57]

Research by Buyle-Bodin and Madhkhan

In 2002, to assess the efficiency of fibre reinforced concrete piles in seismically active regions, Buyle and Madhkhan made eight large scale specimens subjected to alternating cyclic flexure with or without axial load. The dimension of the tested specimens was 50 cm in diameter and 5m in length. Twin-cone fibres and new twin-crimped fibres in weight fraction varying between 40 and 50 kg/m^3 were used. An analytical model was also developed to compute load–deflection behaviour of SFRC piles. The discontinuous model of FRC flexural behaviour combined with crack opening was used, but it was adapted to a circular section for

this study. The comparison between analysis results and experimental results is shown in **Figure 6-4**.

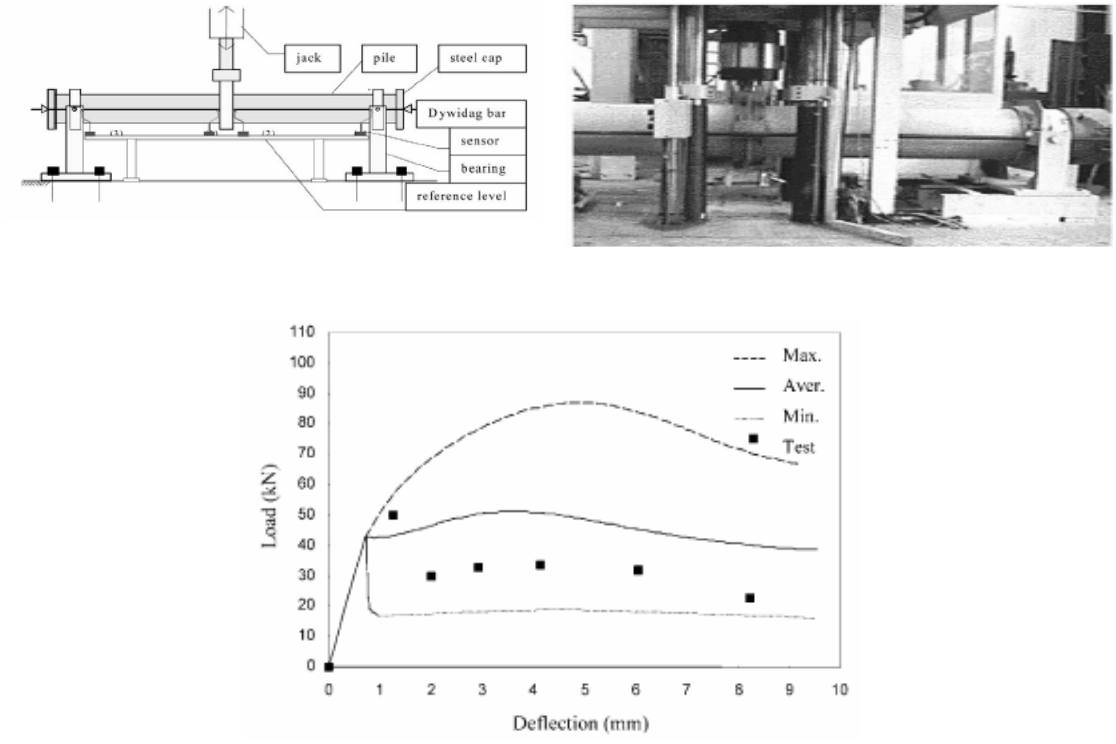

Figure 6 - 4: Experimental set-up and compassion of load-deflection curve between experimental and analytical results [60]

6.2.4. Analytical modelling for beam-column joints

Finite Element Analysis

With rapid decline in the cost of computers and the phenomenal increase in computing power, the finite element method has emerged as a powerful tool for evaluating structural performance. The method can simulate the behavior of the structure by breaking down the structure into finite-sized elements. The overall behavior of the structure can be obtained by formulating a system of constitutive relationship and algebraic equations that can be readily solved with computer processors. Many FEM studies have been made to analyse the joint behaviour under cyclic loading, ranging from predicting failure to analyzing the overall behaviour [61] [62] [63] [64]. The detail of the proposed models are illustrated in a group **Figure 6-5 (a) ~ (d)**.

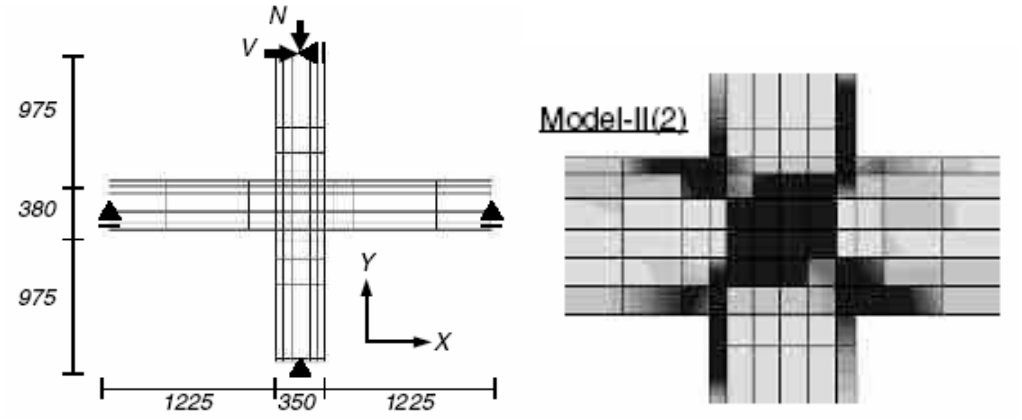

(a) FEM model proposed by Kazuki [61]

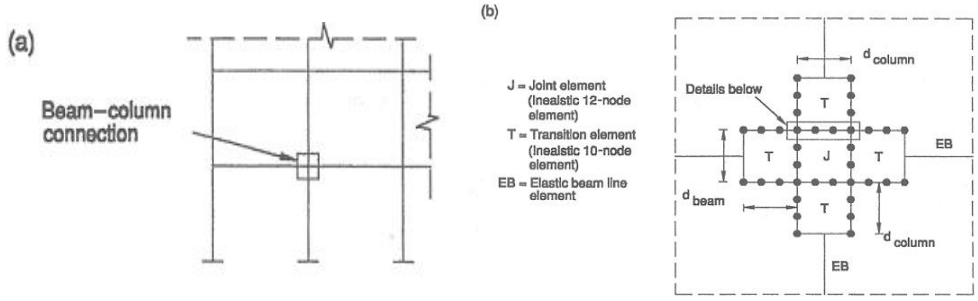

(b) FEM model proposed Elmorsi [62]

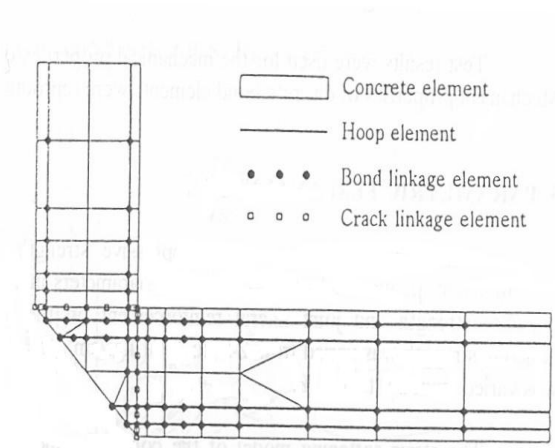

(c) FEM model proposed Kashiwazaki [63]

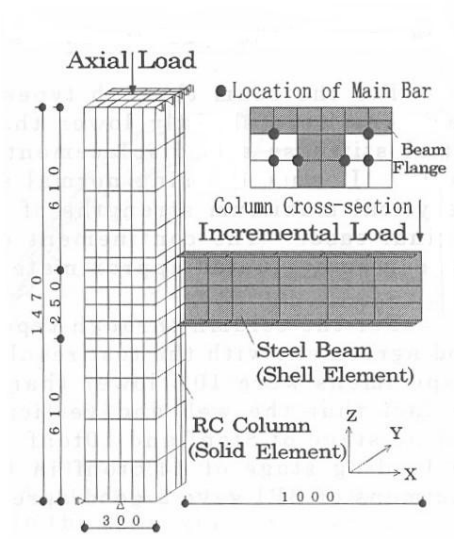

(d) FEM model proposed Kim [64]

Figure 6 - 5: Detail of the proposed models

Multi-spring models

A multi-spring model was proposed by Lowes and Altoontash [65] to represent the inelastic response of reinforced-concrete beam-column joints under reversed-cyclic loading. The proposed model, shown in **Figure 6-6**, provides a simple inelastic mechanism with two translation springs and one rotational spring. A four-node 12-degree-of-freedom element was used to determine inelastic beam-column joint behavior through the combined action of one-dimensional shear-panel, bar-slip, and interface-shear components. Failure of the joint core under shear loading and anchorage failure of beam and column longitudinal reinforcement embedded in the joint were investigated, and comparison of simulated and observed response for a series of beam-column joint subassemblies was also achieved in this research.

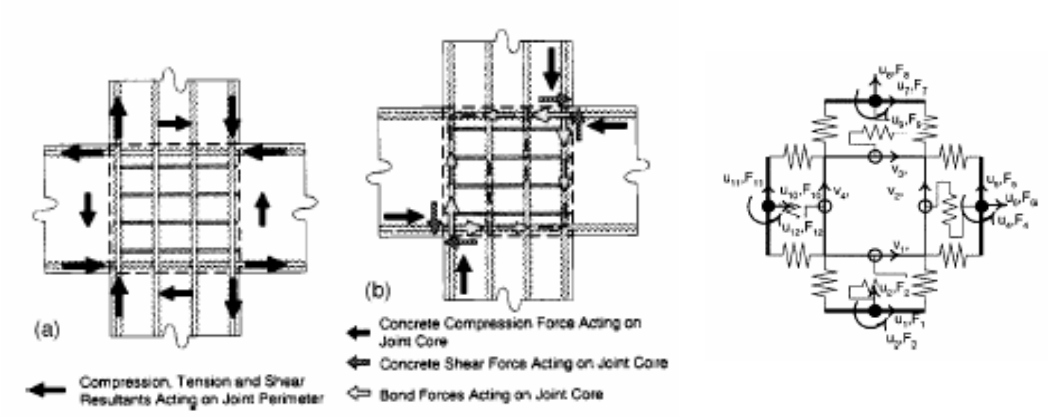

Figure 6 - 6: Detail of tested specimens and proposed model [65]

8.3 Analysis model in this research: Rotational Spring Model

Figure 6-7 shows the geometry and detail of a simplified analysis model for joint behaviour proposed by Pampanin et al [66], which may be a useful tool for studying the seismic response of SFRC joints. A computer approach was also developed by the Inelastic Dynamic Analysis Program RUAUMOKO [67]. In this model, a rotational spring with zero length is used to connect the beam and the column and represent the joint shear hinge both in the linear and the non-liner range. The rotational spring in the joint is split into two springs to connect the column and beam, and each of them has half properties of the joint. In this way, the effect of column axial load can be reacted. Rigid elements (mono dimensional-elastic element with plastic hinges at the edges) are employed between joint panel and the beam and column, and

the properties of all elements are obtained from the experimental result. The ideal model in this research has two areas of lumped plasticity, the shear hinge in the joint region (Unit RC-1, Unit SF-2, Unit SF-3 and Unit SF-5) and the plastic hinge forming at the end of beams (Unit SF-4, Unit RC-6 and Unit NZ-7) , to simulate the two main failure modes for the tested units. Other parts of the member are modelled as linear elastic elements presented as 'Giberson one component beam model' as shown in **Figure 6-8**.

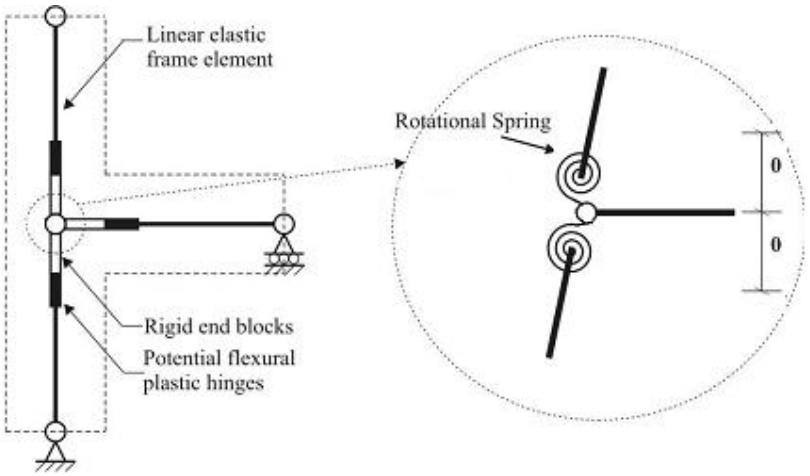

Figure 6 - 7: Analytical model for joints behaviour in this research

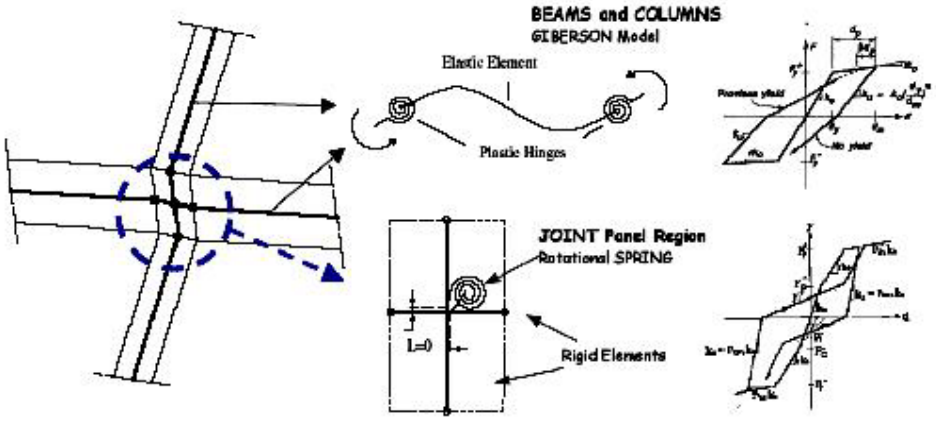

Figure 6 - 8: Modelling of Structural Elements: Beam, Columns and joint

The moment-rotation relationship of the spring is derived from the principal tensile stress versus shear deformation relationship. **Figure 6-9** shows the reinforced concrete beam-column joint model proposed by Pampanin et al [66]. The characteristic of moment-rotation of the joint spring is simply modelled by the empirical strength degradation curve, p_t-γ principle tensile stress versus shear deformation, discussed in **Chapter five**. The basic

procedure of strength degradation curve is shown in **Figure 6-9**. From this approach, the joint characteristic is defined with the critical cracking points derived from strength degradation curve, p_t-γ curve, (e.g. p_t=0.29 $\sqrt{f'_c}$ and p_t=0.42 $\sqrt{f'_c}$ for first cracking and extensive cracking respectively). In the model, appropriate stiffness-degradation of the hysteresis loop and axial load on the column were also considered.

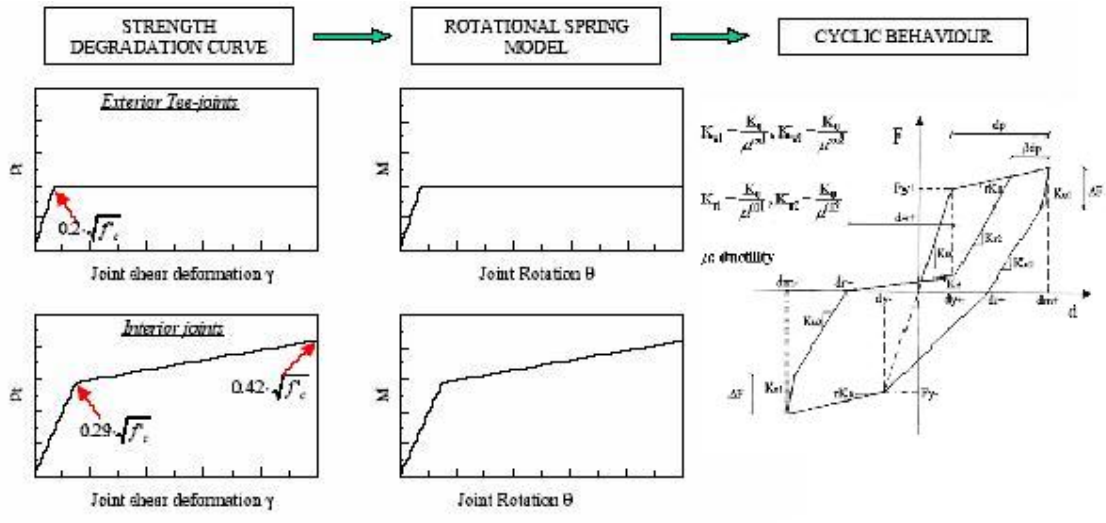

Figure 6 - 9: Basic concept and cyclic Behaviour of the Shear Hinge Model

6.2.5. Hysteresis modelling

In order to analyse the non-linear dynamic response of reinforced concrete structures, the hysteretic modelling is required. A number of hysteretic models have been developed in the past forty years from the simple elasto-plastic bilinear rules to more complicated rules.

There are many available hysteresis models for reinforced concrete elements. According to the application, hysteretic models of reinforced concrete can be simply classified into two categories, one for flexure-dominated hysteretic behaviour (such as bi-linear hysteretic model shown in **Figure 6-10**) and another for pinched hysteretic behaviour (stiffness degrading hysteretic models such as Wayne Stewart model shown in **Figure 6-11**). For a well-designed reinforced concrete member, the flexural moment capacity after the first yield can be well maintained due to the steel strain hardening. In the second cycle, nearly the same flexural moment capacity can be achieved when the deflection reversal is repeated. However, many factors can affect the load-deflection hysteresis loops of reinforced concrete element. As a

result of shear deformation or bond deterioration, the hysteretic behaviour of the reinforced concrete element can not achieve flexure-dominated shape. When the bond deterioration occurs along the longitudinal bars adjacent to the beam-column interfaces or shear deformations becomes significant in plastic hinge zones, the hysteretic behaviour of the structural element can exhibit a phenomenon of pinching. The typical behaviour of pinching hysteretic loops exhibits rapid strength degradation and lower stiffness during reloading. Therefore stiffness degrading hysteretic models have been well used.

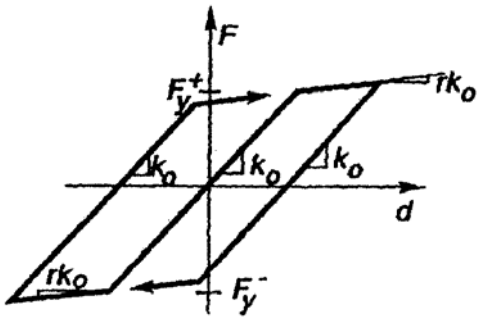

Figure 6 - 10: Bi-linear hysteresis model

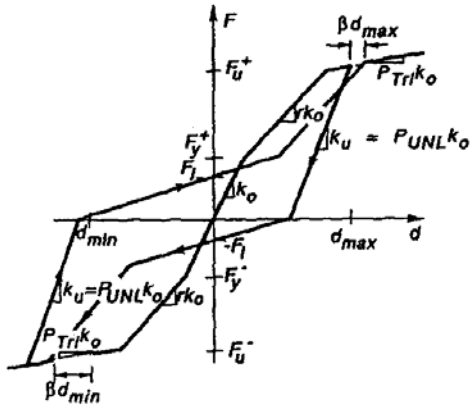

Figure 6 - 11: Wayne Stewart degrading model

6.2.6. Joint moment-rotation relationship

From test results in **Chapter five**, it can be seen that pinching and strength degradation occurred in most units. Therefore an advanced hysteresis, Pampanin hysteresis rule in Ruaumoko [67], was used to simulate the joint seismic behaviour. Using this hysteresis loop shown in **Figure 6-12**, the yielding, pinching behaviour, strength degradation and the moment-rotation relationship of the joint can be simulated properly. The reloading stiffness K_{r1}, K_{r2} and the unloading stiffness K_{u1}, K_{u2} can be estimated by the initial stiffness K_0 and the empirical coefficients α_{u1}, α_{u2}, α_{r1} and α_{r2}, which will be established through the calibration of the experimental results.

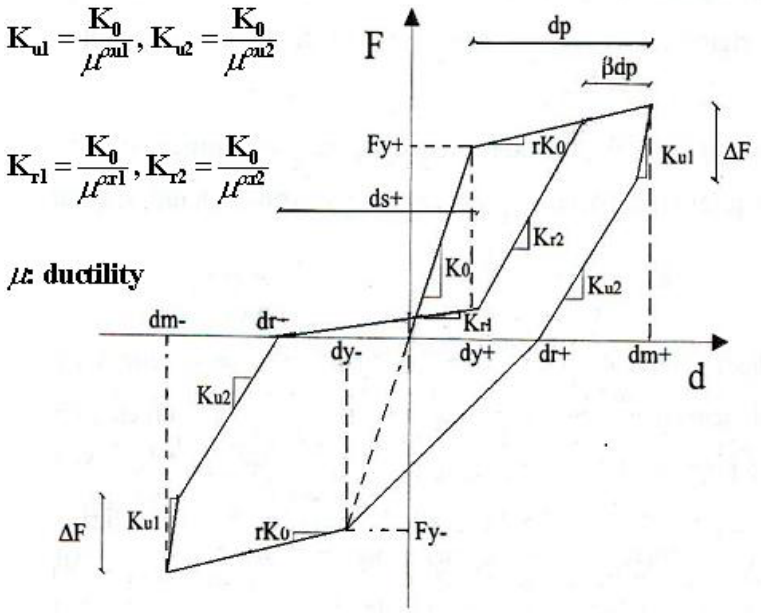

Figure 6 - 12: Pampanin Hysteresis loop from [67]

6.2.7. Determination of hysteretic parameters

The Pampanin hysteresis model selected in this analysis will be calibrated versus the experimental results. The numerical analysis will be first conducted by using Ruaumoko computer programme, which was developed at the University of Canterbury. The calibration was conducted for joint and beams, as the shear hinge and plastic hinges were expected to develop in joints and beams, respectively. For the modelling of Units RC-1, SF-2, SF-3 and SF-5 (shear hinges occurred in the joint region), the cracking points of concrete are determined using the method discussed in **Section 5.5.2**. For Units SF-4, RC-6 and NZ-7 (plastic hinges occurred in beams), the first yielding strength and the moment capacity was determined by the simple calculation and calibration with experimental results. The group **Figure 6-13 (a) ~ (h)** show the experimental and analytical force versus displacement hysteresis loops for tested units (from RC-1 to NZ-7 respectively). It can be seen that the analytical modelling results matched the observed hysteresis loops reasonably well.

As the shear hinge occurred in the joint region while the beam and column were still in elastic range, the experimental hysteresis loops show significant pinching response. Pampanin hysteresis loop was therefore used to model the joint behaviour with the proper parameters (see **Table 6-2**). The comparison between the experimental results and analytical modelling

results for the units (Unit RC-1, Unit SF-2 and Unit SF-3) are shown in **Figure 6-13 (a), (b) and (c)**. It is seen that Pampanin hysteresis rule can reflect the joint shear hinge behaviour satisfactorily.

The global behaviour of Unit SF-5 was governed by the combination of joint shear hinge and beam plastic hinge, because both joint shear hinge and beam plastic hinge occurred during the testing. As joint shear hinge formed before the beam plastic hinge, the early global behaviour was considered to be governed by joint shear hinge mechanism. Therefore Pampanin hysteresis was still used for modelling this unit behaviour,

For the verification of the Unit SF-4, RC-6 and NZ-7, Takeda hysteresis was used to model seismic behaviour of units, as the plastic hinge faiure mainly governed the global behaviour. Pampanin hysteresis was not chosen. The comparison between the experimental results and analytical modelling results for units are shown in **Figure 6-13 (e), (g) and (h)**.

Table 6 - 2: Coefficients Used for Pampanin Hysteresis Loop

Units	Steel dosage in joint	Option 1: Reloading Power Factor	α_1	α_2	ΔF (%)	β
RC-1	0 %	Reloading	2.0	0.7	30	-0.05
		Unloading	-0.5	0.5		
SF-2	1.0 %	Reloading	2.0	0.8	30	-0.05
		Unloading	-0.5	0.5		
SF-3	2.0 %	Reloading	1.7	0.7	30	-0.05
		Unloading	-0.5	0.5		
SF-5	1.0 %+ 1 stirrup	Reloading	1.7	1.0	30	-0.05
		Unloading	-1.0	0.65		

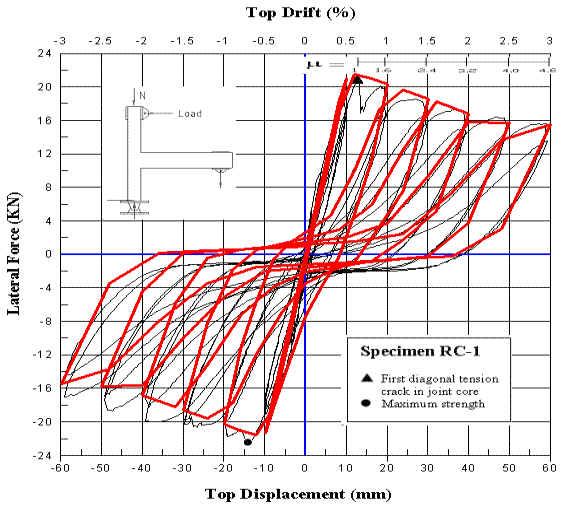

(a)

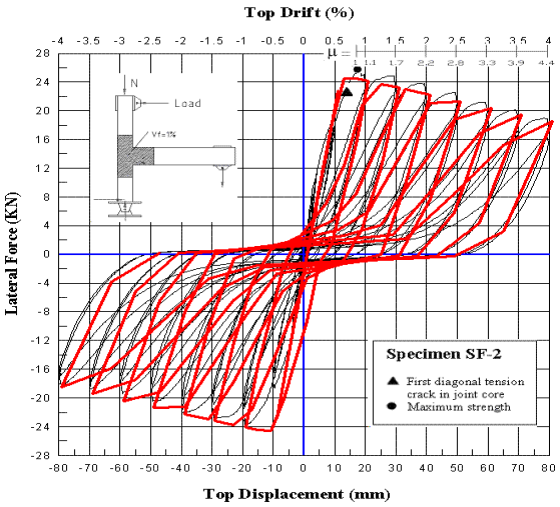

(b)

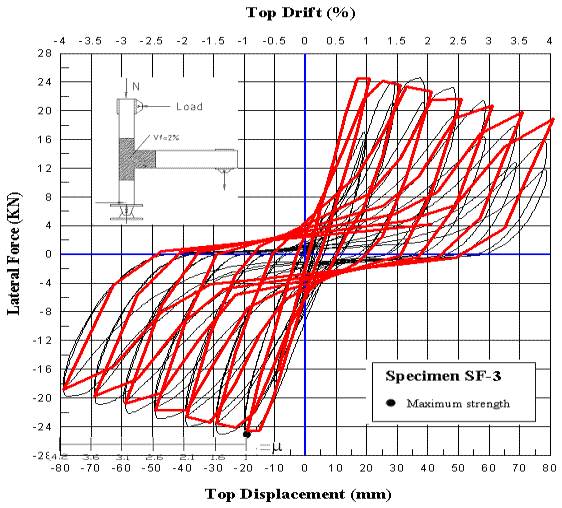

(c)

Group I (Unit RC-1, Unit FS-2 and Unit FS-3)

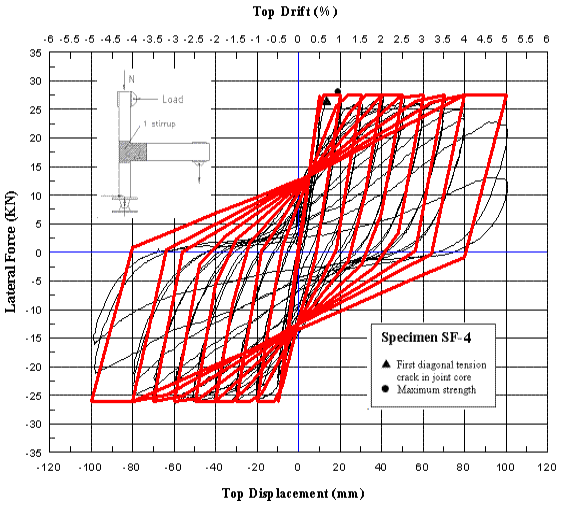

(e)

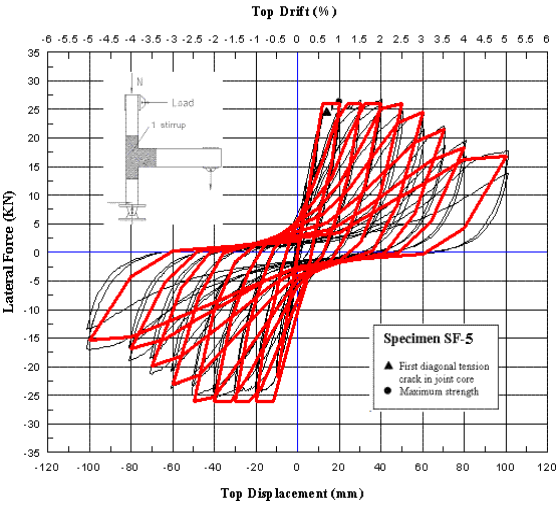

(f)

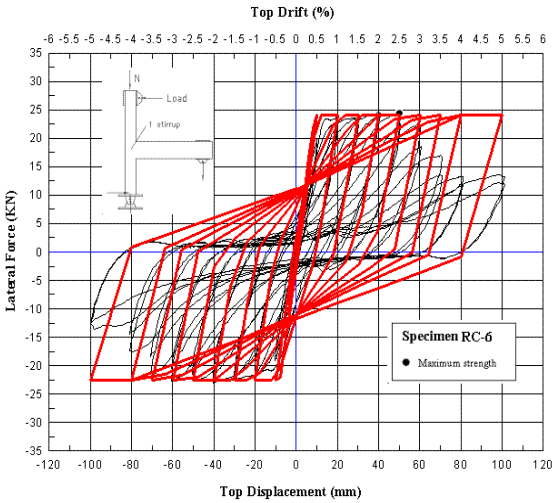

(g)

Groups II (Unit SF-4, Unit SF-5 and Unit RC-6)

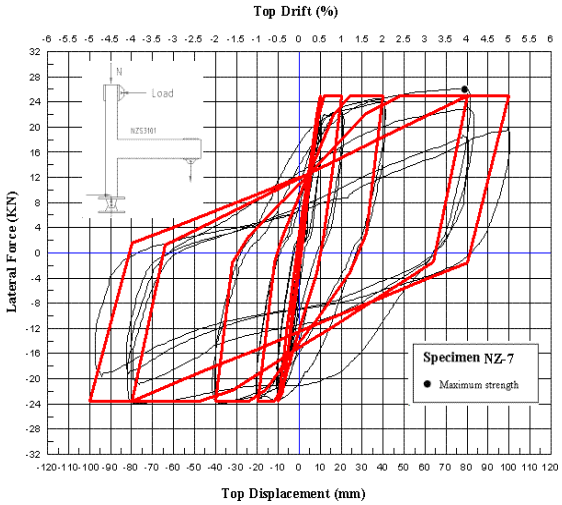

(h)

Groups III (Unit NZ-7)

Figure 6 - 13: Comparison between numerical and experimental results

CHAPTER SEVEN

7. CONCLUSIONS AND RECOMMENDATIONS FOR FUTURE RESEARCH

7.1. Results from seismic loading tests

Over the last ten years, there has been a dramatic increase in using steel fibre reinforced concrete (SFRC) in structural areas. Based on the literature review, it can be seen that much progress has been made not only towards understanding the properties of the material itself, but also investigating the feasibility of using SFRC in seismic structural member application. However, due to a critical lack of available information in the literature as well as of adequate seismic design code guidelines, the evaluation of the actual performance of seismic resisting systems adopting SFRC in their critical structural, members or regions still require a significant effort within more comprehensive investigations.

This study investigated the efficiency of using steel fibre reinforced concrete to replace the shear reinforcement in exterior beam-column joints. A simple analytical procedure, based on the hierarchy of strength considerations and on joint strength degradation models, was introduced into this study to provide a rational formulation of the shear strength contribution provided by the introduction of steel fibres in the joint region. A M-N performance domain was used to visualize the relative hierarchy of strength and thus to expect sequence of events in the beam-column joint subassembly. Furthermore, in this analytical procedure, critical parameters, such as the effects of the column axial load were considered and presented in a graph. The nominal shear stress v_j is typically used to develop proper joint strength degradation models of SFRC joints. Moreover, in order to analyse the shear stress (v_j), principle tensile and compression stresses, capable of better representing the effects of the column axial load onto the joint strength or damage level, are adopted.

In order to assess the contribution of steel fibres to the joint (panel zone) shear strength, both under-designed systems (with no transverse reinforcement in the joint, following older practice before the pre-1970s) and well designed systems (following the NZ concrete design standard NZS 3101:1995) were adopted as benchmark specimens. Six 2-D exterior beam-

column joint subassemblies were tested under simulated seismic tests (quasi-static cyclic regime). Based on the experimental results, a tentative relationship between the joint shear contributions provided by concrete, stirrups and steel fibres have been proposed as a viable tool for design of a SFRC joint, where a defined number of stirrups can be replaced by steel fibres. Furthermore, the use of SFRC in the plastic hinge regions of beam-column joints, instead of code-required stirrups, was also investigated in this study. A comparison of the energy dissipation capacity of three beam-column joint subassemblies (Units in Group II) subjected to seismic reversal loading was carried out. Given these promising results, SFRC is suggested to be used also in the flexural members of a beam-column subassembly, thus allowing for a more cost-effective implementation of the solution in the construction phase.

Furthermore, it is worth noting that the specimen units in Group I were designed as pre-1970s joints with the direct scope to enforce the formation of joint shear hinge mechanism in the panel zone, thus allowing for a direct evaluation of the fibre contribution to the overall joint shear resistance. The joints in Group II were designed according to the NZS 3101:1995 seismic code-provisions, except for an intentional reduction of the joint transverse reinforcement, in order to directly evaluate the synergistic effect of steel fibres and stirrups. The unit in Group III were designed and constructed according to the NZS3101:1995 seismic code-provisions as a traditionally "well-designed" reference specimen.

In Group I, all beam-column joint units exhibited a reduction in strength and stiffness during the seismic loading test owing to progressive shear hinge forming in the joint cores. In Group II, all beam-column joint units finally failed in the beam plastic hinge region. However, shear cracking still occurred in the joint region due to the degradation of shear resistance capacity with the units' ductility increasing. In Group III, the beam-column joint unit exhibited a very satisfactory flexural mode in the beam plastic hinge.

When comparing with the SFRC joint, the conventional reinforced joint illustrated the need for sufficient confinement in both the joint region and the plastic hinge region to provide high shear maximum and residual strength capacity. From the experimental performance of the SFRC joints of Group I, it is evident that steel fibre reinforcement can enhance the joint shear resistance. However, the test results also showed that the use of reinforcing bars confined only by steel fibre reinforced concrete was inadequate to inhibit buckling. The presence of SFRC joint units of Group II showed that using steel fibre reinforcement in the critical flexural regions of joints can provide adequate strength and ductility capacity. Lateral reinforcement

can be reduced by up to 50% without decreasing the seismic performance of the units. Furthermore, the Unit SF-4, reinforced with steel fibre and adequate beam lateral reinforcement, but with 80% reduction in joint shear reinforcement, shows approximately the same seismic performance of that shown by the full seismically designed unit (Unit NZ-7). The integrity of SFRC joint units, and hence the required flexural and shear resistance capacity of the beam-column joints, can provide a satisfactory seismic performance under high drift level.

This research demonstrated the feasibility of using steel fibre reinforced concrete in seismic beam-column joints, while confirming the strong need for the development of appropriate comprehensive design guidelines for the seismic design of fibre reinforced concrete structures according to performance-based design approach.

Main results of this study can be summarized as follows:

1. Using steel fibre reinforced concrete (SFRC) within beam-column joints can significantly enhance the shear resistance capacity of joints. The increased tensile strength and the bridging action of SFRC can confine tension cracking to the joint diagonals and thus reduce the requirements for closely spaced joint ties and preserving the integrity of the joint concrete core. Furthermore, the inclusion of a proper steel fibre reinforcement dosage within a beam–column joint may prevent shear failure occurring in the joint core, altering the failure mode from joint shear hinge to flexural failure of the beam or column. Moreover, using SFRC in the seismically designed joint region can improve the seismic performance due to the higher load levels, larger displacements and more damage tolerance.

2. Using 1% (by volume) steel fibre reinforcement can significantly reduce the lateral reinforcement in the beam plastic hinge region. The performance can be at least as satisfactory as that of a conventional seismically detailed unit with similar joint shear reinforcement and appropriate seismic details in the beam plastic hinge region. It can be anticipated that the construction difficulties associated with reinforcement congestion may be partially solved by employing SFRC in the critical regions of the construction (i.e. joint and plastic hinges).

3. The presence of steel reinforcement alone cannot prevent the buckling of the column longitudinal bars, even in the joint region. Therefore, a minimal quantity of additional confinement, in the form of stirrups, shall still be provided in the joints region.

4. Steel fibre reinforcement combined with full designed lateral reinforcement provides a very efficient seismic performance in flexural members. Owing the advantages of SFRC, such as the improved energy dissipation capacity and extended stress-strain characteristics, a high level of moment can still be retained after high intensity cycle loading.

5. A simplified analytical procedure based on the hierarchy of strength and joints strength degradation models has been proposed to evaluate the sequence of events and assess the required fibre shear contribution. For analysing and predicting the failure model of a joint, therefore, a simple hybrid failure mechanism, which can demonstrate the failure mechanism due to combination of plastic hinges in beam and column elements and shear hinges in joint regions, is also introduced. The nominal shear stress v_j is typically used by adopting principle stresses to develop proper joint strength degradation models of SFRC joints. The joint strength degradation curves (principal tensile stress vs. joint shear deformation) have been calibrated on the experimental data Based on the developed formula, the shear stress v_j contributed by steel fibres, concrete and stirrups can be clear known. Then, M_N performance based domain visualization has been used to evaluate the hierarchy of strength and sequence of events of beam-column joint subassemblies. Joint shear coefficient K_f contributed by steel fibres has been also compared with previous experimental test available in literature to obtain a reliable value for design purpose.

7.2. Recommendations for future research investigations

Further research into the application of fibre reinforcement in seismic design is required in the following areas:

(1) The combination of transverse reinforcement (steel fibre combined with stirrups) is recommended to use in the critical regions of joints.

(2) Strength degradation models, based on principal tensile stress, should be developed as being a simple and effective method for designing a SFRC joint. However, more similar

experimental tests are still recommended to confirm the exact shear failure level of SFRC joints.

(3) Additional experimental tests are needed to refine the proposed shear strength degradation model for SFRC joints. Furthermore, in order to predict the global failure mode of a SFRC joint (discussed in **Chapter five**), the moment capacity of flexure members of beam-column joints, such as the plastic hinge region, needs to be better evaluated by proper analysis. Based on that, a reliable hierarchy of strength diagram including joint, beams and columns within a beam-column subassembly, could be introduced and adopted for practical design applications.

(4) The use of steel fibres can also reduce the transverse reinforcement required in potential plastic hinge regions of both beam and column members. However, the amount of the allowed reduction needs to be evaluated by appropriate analytical methods and subsequently validated by experimental tests.

(5) It is well known that the properties and behaviour of SFRC are closely related to the aspect ratio of the fibres, the volume content, fibre type, as well as to the fibre dispersion in the concrete mix. The influence of these parameters on the joint behaviour should be independently investigated by numerical and experimental analyses. Ultimately, design guidelines are required to promote a wide and reliable use of this technology in earthquake-resistant design.

References

1. Zia, P. and National Science Foundation (U.S.), *International Workshop on High-Performance Concrete, November 21-22, 1994, Bangkok, Thailand*. 1996, Farmington Hills, Mich. (P.O. Box 9094, Farmington Hills 48333): American Concrete Institute. ix, 456.

2. Shah, S.P. and S.H. Ahmad, *High performance concrete: properties and applications*. 1994, New York: McGraw-Hill. xii, 403.

3. American Concrete Institute. Convention, *High-performance concrete: research to practice*. 1999, Farmington Hills, Mich.: American Concrete Institute. vii, 466.

4. Malhotra, V.M. and American Concrete Institute., *High-performance concrete: design and materials and recent advances in concrete technology: proceedings, Third CANMET/ACI International Conference, Kuala Lumpur, Malaysia, 1997*. 1997, Farmington Hills, Mich.: American Concrete Institute. ix, 1017.

5. Malhotra, V.M. and American Concrete Institute., *High-performance concrete: proceedings, ACI international conference, Singapore, 1994*. 1994, Detroit, Mich.: American Concrete Institute. vii, 844.

6. Malhotra, V.M., Canada Centre for Mineral and Energy Technology., and American Concrete Institute., *High-performance concrete and performance and quality of concrete structures: proceedings, second CANMET/ACI International Conference, Gramado, RS, Brazil, 1999*. 1999, Farmington Hills, Mich.: American Concrete Institute. viii, 793.

7. French, C., M.E. Kreger, and American Concrete Institute., *High-strength concrete (HSC) in seismic regions*. 1998, Farmington Hills, MI: American Concrete Institute. vii, 471.

8. Midrand, *Fibre reinforced concrete*. Cement & Concrete Institute, 1997.

9. Anon, *Design considerations for steel fiber reinforced concrete.* ACI Structural Journal (American Concrete Institute), 1988. 85(5): p. 563-580.

10. Soroushian, P., F. Mirza, and A. Alhozaimy, *Bonding of confined steel fiber reinforced concrete to deformed bars.* ACI Materials Journal (American Concrete Institute), 1994. 91(2): p. 141-149.

11. Pampanin, S., G.M. Calvi, and M. Moratti. *Seismic beahviour of R.C. beam-column joints designed for gravity loads*. in *12th European Conference on Earthquake Engineering*. 2002. London: Elsevier Science Ltd.

12. Tang, J., et al., *Seismic behavior and shear strength of framed joint using steel-fiber reinforced concrete.* Journal of Structural Engineering, 1992. 118(2): p. 341-358.

13. Stevenson, E.C., *Fibre reinforced concrete in seismic design*. 1980, Christchurch: Dept. of Civil Engineering University of Canterbury. viii,95,[11] leaves.

14. Zia, P., S.H. Ahmad, and M. Leming. *High-Performance Concretes:A State-of-Art Report (1989-1994).* 1989-1994 [cited; Available from: www.tfhrc.gov/structur/hpc/hpc2/contnt.htm.

15. Standards America., *American Society of Testing of Materials*. 1992: Standards America.

16. Goodier, C.I., *Development of self-compacting concrete.* Proceedings of the Institution of Civil Engineers: Structures and Buildings, 2003. 156(4): p. 405-414.

17. Luo, S.-R., J.-L. Zheng, and G.-J. Wang, *Mechanical property of self-compacting concrete and its engineering application.* Gongcheng Lixue/Engineering Mechanics, 2005. 22(1): p. 164-169.

18. Vengala, J., M.S. Sudarshan, and R.V. Ranganath, *Experimental study for obtaining self-compacting concrete.* Indian Concrete Journal, 2003. 77(8): p. 1261-1266.

19. Barragan, B., et al. *Development and application of fibre-reinforced self-compacting concrete*. 2005. Dundee, Scotland, United Kingdom: Thomas Telford Services Ltd, London, E14 4JD, United Kingdom.

20. Grunewald, S., et al., *Tunnel Segments of Self-Compacting Steel Fibre Reinforced Concrete, 3rd International Symposium on Self-Compacting Concrete, 17-20 August 2003, Reykjavik, Iceland* 2003, Reykjavik. 715.

21. Miao, B., J.-C. Chern, and C.-A. Yang, *Influences of fiber content on properties of self-compacting steel fiber reinforced concrete.* Journal of the Chinese Institute of Engineers, Transactions of the Chinese Institute of Engineers,Series A/Chung-kuo Kung Ch'eng Hsuch K'an, 2003. 26(4): p. 523-530.

22. Takayama, H., *Proceedings of the JCI International Workshop on Ductile Fiber Reinforced Cementitious Composites (DFRCC)-Application and Evaluation*. 2002, Tokyo: Japan Concrete Institute.

23. Parra-Montesinos, G.J. and J.K. Wight, *Seismic Behavior, Strength and Retrofit of RC Column-to-Steel Beam Connections*, in *Department of Civil and Environmental Engineering*, A. Arbor, Editor. 2000, University of Michigan: Michigan. p. 296.

24. Kim, K. and G.J. Parra-Montesinos. *Behavior of HPFRCC Low-Rise Walls Subjected to Displacement Reversals*. in *High Performance Fiber Reinforced Cement Composites (HPFRCC 4), Proceedings of the Fourth International RILEM Workshop*. 2003. France: RILEM Publications S.A.R.L.

25. Canbolat, B.A., G.J. Parra-Montesinos, and J.K. Wight, *Experimental study on seismic behavior of high-performance fiber-reinforced cement composite coupling beams.* ACI Structural Journal, 2005. 102(1): p. 159-166.

26. Swamy, R.N. and H.M. Bahia, *Effectiveness of steel fibers as shear reinforcement.* Concrete International: Design and Construction, 1985. **7**(3): p. 35-40.

27. Sharma, A.K., *Shear strength of steel fiber reinforced concrete beams.* Journal of The American Concrete Institute, 1986. 83(4): p. 624-628.

28. Mansur, M.A., K.C.G. Ong, and P. Paramasivam, *Shear strength of fibrous concrete beams without stirrups.* Journal of Structural Engineering, 1986. 112(9): p. 2066-2079.

29. Ashour, S.A., G.S. Hasanain, and F.F. Wafa, *Shear behavior of high-strength fiber reinforced concrete beams.* ACI Structural Journal (American Concrete Institute), 1992. 89(2): p. 176-184.

30. Tan, K.H., K. Murugappan, and P. Paramasivam, *Shear behavior of steel fiber reinforced concrete beams.* ACI Structural Journal (American Concrete Institute), 1993. 90(1): p. 3-11.

31. Narayanan, R. and I.Y.S. Darwish, *Use of steel fibers as shear reinforcement.* ACI Structural Journal (American Concrete Institute), 1987. 84(3): p. 216-227.

32. Banthia, N., et al., *Structural applications of fiber reinforced concrete*. Structural Behavior of Steel Fiber Reinforced Concrete Beams in Shear. 1999, Farmington Hills, Michigan: American Concrete Institute. vi, 257.

33. Falkner, H. and U. Gossla. *Design and safety of steel fibre reinforced concrete structural members*. in *Proceedings of the 1st fib Congress*. 2002. Osaka.

34. Gefken, P.R. and M.R. Ramey, *Increased joint hoop spacing in type 2 seismic joints using fiber reinforced concrete.* ACI Structural Journal (American Concrete Institute), 1989. 86(2): p. 168-172.

35. Filiatrault, A., K. Ladicani, and E. Massicotte, *Seismic performance of code-designed fiber reinforced concrete joints.* ACI Structural Journal (American Concrete Institute), 1994. 91(5): p. 564-571.

36. Filiatrault, A., S. Pineau, and J. Houde, *Seismic behavior of steel-fiber reinforced concrete interior beam-column joints.* ACI Structural Journal, 1995. 92(5): p. 543-552.

37. Shannag, M.J., N. Abu-Dyya, and G. Abu-Farsakh, *Lateral load response of high performance fiber reinforced concrete beam-column joints.* Construction and Building Materials, 2005. 19(7): p. 500-508.

38. Bayasi, Z. and M. Gebman, *Reduction of lateral reinforcement in seismic beam-column connection via application of steel fibers.* ACI Structural Journal, 2002. 99(6): p. 772-780.

39. Gebman, M., *"Application of Steel Fiber Reinforced Concrete in Seismic Beam-Column Joints"*, in *Department of Civil Engineering*. Spring 2001, San Diego State University: San Diego.

40. Swamy, R.N., *Fibre Reinfored Cement and Concrete*. 1992, E & FN Spon: London. p. 613-628.

41. Henager, C.H., *Steel fibrous, ductile concrete joint for seismic-resistant structures.* Publ SP Am Concr Inst SP-53, Symp on Reinf Concr Struct in Seism Zones, 1974, 1977: p. 371-386.

42. Gencoglu, M. and I. Eren, *An experimental study on the effect of steel fiber reinforced concrete on the behavior of the exterior beam-column joints subjected to reversal cyclic loading.* Turkish Journal of Engineering and Environmental Sciences, 2002. 26(6): p. 493-502.

43. Soubra, K.S., et al., *Fiber reinforced concrete joints for precast construction in seismic areas*. 1992, Ann Arbor, MI: Dept. of Civil and Environmental Engineering University of Michigan. xix, 306.

44. Tuleasca, L., J.M. Ingham, and A. Cuciureanu. *Seismic response of a cast-in-place steel fibre concrete joint connecting precast beams and columns*. in *Proceedings of Pacific Conference on Earthquake Engineering*. 2003. Christchurch.

45. Standards New Zealand., *Concrete structures standard*. 1995, Wellington [N.Z.]: Standards New Zealand. 2 v. (256, 264).

46. Cook, D.R.L., *The design and detailing of beam-column joints: a report submitted in partial fulfilment of the requirements for the degree of Master of Engineering in the University of Canterbury*. 1984. xxiv, 284 leaves.

47. Milburn, J.R., *Behaviour of reinforced concrete beam-column joints designed to NZS 3101 : a report submitted in partial fulfilment of the requirements for the degree of Master of Engineering in the University of Canterbury*. 1982. viii, 108 leaves, bound.

48. Scarpas, A., *The inelastic behaviour of earthquake resistant reinforced concrete exterior beam-column joints : a report submitted in partial fulfilment of the requirements for the degree of Master of Engineering [Civil Engineering] at the University of Canterbury, Christchurch, New Zealand*. 1981. x,114,[3] leaves, bound.

49. Paulay, T. and M.J.N. Priestley, *Seismic design of reinforced concrete and masonry buildings*. 1992, New York, N.Y.: Wiley. xxiii, 744.

50. Papworth, F. and R. Ratcliffe, *Steel Fibre Reinforced Concrete-A design and application guide*. February 1994: Scancem Materials Pty Ltd.

51. Priestley, M.J.N., *Displacement-based seismic assessment of existing reinforced concrete buildings.* Bulletin of the New Zealand National Society for Earthquake Engineering, 1996. 29(4): p. 256-272.

52. Park, R., *Static force-based procedure for the seismic assessment of existing reinforced concrete moment resisting frames.* Bulletin of the New Zealand National Society for Earthquake Engineering, 1997. 30(3): p. 213-226.

53. Hughes, B.P. and N.I. Fattuhi, *Stress-strain curves for fibre reinforced concrete in compression.* Cement and Concrete Research, 1977. 7(2): p. 173-183.

54. Fanella, D.A. and A.E. Naaman, *Stress-strain properties of fiber reinforced mortar in compression.* Journal of The American Concrete Institute, 1985. 82(4): p. 475-483.

55. Ezeldin, A.S. and P.N. Balaguru, *Normal- and high-strength fiber-reinforced concrete under compression.* Journal of Materials in Civil Engineering, 1992. 4(4): p. 415-429.

56. Barros, J.A.O. and J.A. Figueiras, *Flexural behavior of SFRC: Testing and modeling.* Journal of Materials in Civil Engineering, 1999. 11(4): p. 331-338.

57. Dhakal, R.P., *Post-peak response analysis of SFRC columns including spalling and buckling.* Structural Engineering and Mechanics, 2006. 22(3): p. 311-330.

58. Krstulovic-Opara, N. and Z. Bayasi, *High-performance fiber-reinforced concrete in infrastructural repair and retrofit*. 2000, Farmington, Mich.: American Concrete Institute. vii, 251.

59. Lim, T.Y., P. Paramasivam, and S.L. Lee, *Bending behavior of steel-fiber concrete beams.* ACI Structural Journal (American Concrete Institute), 1987. 84(6): p. 524-536.

60. Buyle-Bodin, F. and M. Madhkhan, *Performance and modelling of steel fibre reinforced piles under seismic loading.* Engineering Structures, 2002. 24(8): p. 1049-1056.

61. Kazuki, T., M. Takamichi, and S. Nobuaki, *3-D Finite Element Cyclic Analysis of RC Beam/Column Joint Using Special Bond Model: Proceedings, 13th World Conference on Earthquake Engineering, Vancouver, B.C, Canada, 2004*. 2004, Vancouver. 446.

62. Elmorsi, M., M.R. Kianoush, and W.K. Tso, *Modeling bond-slip deformations in reinforced concrete beam-column joints.* Canadian Journal of Civil Engineering, 2000. 27(3): p. 490-505.

63. Kashiwazaki, T. and H. Noguchi, *FEM analysis on the effects of joint lateral reinforcement on the shear strength of RC interior beam-column joints.* Transactions of the Japan Concrete Institute, 1997. 19: p. 287-294.

64. Kim, K. and H. Noguchi, *Effect of connection-type on shear performance of RCS structures.* Transactions of the Japan Concrete Institute, 1996. 18: p. 251-258.

65. Lowes, L.N. and A. Altoontash, *Modeling reinforced-concrete beam-column joints subjected to cyclic loading.* Journal of Structural Engineering, 2003. 129(12): p. 1686-1697.

66. Pampanin, S., G. Magenes, and A. Carr. *Modeling of The Shear Hinge Mechanism in Poorly Detailed RC Beam Column Joints*. in *FIB Symposium "Concrete Structures in Seismic Regions"*. 2003. Athens 2003.

67. Carr, A., *Ruaumoko-Inelastic Dynamic Analysis*. 2004, Christchurch, N.Z.: Dept. of Civil Engineering the University of Canterbury.

Appendix I

The example of shear strength of a beam-column joint containing stirrups and fibres

An example of an exterior joint is shown in **Figure 3-10**. The column axial force is 100 KN. The specified compression strength of concrete is f_c' =25 MPa. The strength of steel bars and stirrups is f_y =300 MPa. Dramix steel fibre, 1% by volume with aspect ratio 65, is used in the joint region. The procedure estimating the joint strength at the two specified points, the first cracking point and the extensive damage point, is shown in the following paragraph.

To determine the crack shear strength of a hybrid reinforced joint, based on Equation 3.11, the principal tensile stress P_t resulting from the simultaneous action of an axial compressive stress and a shear stress can be can be expressed as:

$$P_t = \sqrt{(\frac{f_v}{2})^2 + v_{jc}{}^2} - \frac{f_v}{2}$$ (Where, f_v is an axial compressive stress)

$$P_{t\,(Fir)} = \sqrt{(\frac{f_v}{2})^2 + v_{jc}{}^2} - \frac{f_v}{2} = 0.29\sqrt{f_c'} = 0.29\sqrt{25} = 1.45 \text{ MPa}$$ (At the first cracking point)

$$P_{t\,(Ext)} = \sqrt{(\frac{f_v}{2})^2 + v_{jc}{}^2} - \frac{f_v}{2} = 0.42\sqrt{f_c'} = 0.42\sqrt{25} = 2.1 \text{ MPa}$$ (At the extensive damage point)

Therefore, the joint shear stress contributed by concrete can be expressed as follows:

$$v_{jc} = \sqrt{P_{t\,(Fir)}{}^2 + f_v \cdot P_{t\,(Fir)}} = \sqrt{1.45^2 + 1.6 \times 1.45} = 2.1 \text{ MPa}$$

$$v_{jc} = \sqrt{P_{t\,(Ext)}{}^2 + f_v \cdot P_{t\,(Ext)}} = \sqrt{2.1^2 + 1.6 \times 2.1} = 2.78 \text{ MPa}$$

The crack shear strength of a joint reinforced with stirrups is expressed as: (Note the first cracking cannot be modified because a stirrup cannot change the material property of concrete)

$$v_{jc} = \sqrt{P_{t\,(Fir)}{}^2 + f_v \cdot P_{t\,(Fir)}} \quad = 2.1 \text{ MPa}$$

$$v_{jc} + v_{js} = \sqrt{P_{t\,(Ext)}{}^2 + f_v \cdot P_{t\,(Ext)}} + f_{yv}\frac{A_{sh}}{b\,s} = 2.78 + 300 \times \frac{56.52}{135 \times 250} \quad = 3.29 \text{ MPa}$$

Therefore, a new constant value of k can be estimated as

$$P_{t\,(Fir)}{}^{(v_{jc}+v_{js})} = \sqrt{(\frac{f_v}{2})^2 + (v_{jc})^2} - \frac{f_v}{2} = \sqrt{(\frac{1.6}{2})^2 + (2.1)^2} - \frac{1.6}{2} = 1.45 = 0.29\sqrt{f_c'}$$

$$P_{t\,(Ext)}{}^{(v_{jc}+v_{js})} = \sqrt{(\frac{f_v}{2})^2 + (v_{jc} + v_{js})^2} - \frac{f_v}{2} = \sqrt{(\frac{1.6}{2})^2 + (3.29)^2} - \frac{1.6}{2} = 2.57 = 0.52\sqrt{f_c'}$$

The following procedure is used to determine the crack shear strength of a joint reinforced with 1.0% Dramix steel fibre only (38 mm and aspect ratio ($\frac{l_f}{d_f}$) of 65).

$$v_{jc} + v_{jf} = \sqrt{P_{t\,(Fir)}{}^2 + f_v \cdot P_{t\,(Fir)}} + 0.5\frac{l_f}{d_f}V_F \quad = 2.1 + 0.32 = 2.42 \text{ MPa}$$

$$v_{jc} + v_{jf} = \sqrt{P_{t\,(Ext)}{}^2 + f_v \cdot P_{t\,(Ext)}} + 0.5\frac{l_f}{d_f}V_F \quad = 2.78 + 0.32 = 3.1 \text{ MPa}$$

Therefore

$$P_{t\,(Fir)}{}^{(v_{jc}+v_{jf})} = \sqrt{(\frac{f_v}{2})^2 + (v_{jc} + v_{jf})^2} - \frac{f_v}{2} = \sqrt{(\frac{1.6}{2})^2 + (2.42)^2} - \frac{1.6}{2} = 0.35\sqrt{f_c'}$$

$$P_{t\,(Ext)}{}^{(v_{jc}+v_{jf})} = \sqrt{(\frac{f_v}{2})^2 + (v_{jc} + v_{jf})^2} - \frac{f_v}{2} = \sqrt{(\frac{1.6}{2})^2 + (3.1)^2} - \frac{1.6}{2} = 0.48\sqrt{f_c'}$$

With the same procedure the estimated constant value of k for a joint containing both stirrups and steel fibres can be calculated as

$$v_{jc} + v_{jf} = \sqrt{P_{t\,(Fir)}{}^2 + f_v \cdot P_{t\,(Fir)}} + 0.5\,\frac{l_f}{d_f} V_F = 2.1 + 0.32 = 2.42 \text{ MPa}$$

$$v_{jc} + v_{js} + v_{jf} = \sqrt{P_{t\,(Ext)}{}^2 + f_v \cdot P_{t\,(Ext)}} + f_{yv}\frac{A_{sh}}{bs} + 0.5\,\frac{l_f}{d_f} V_F = 2.78 + 0.51 + 0.32 = 3.61 \text{ MPa}$$

Therefore

$$P_{t\,(Fir)}{}^{(v_{jc}+v_{js}+v_{jf})} = \sqrt{(\frac{f_v}{2})^2 + (v_{jc} + + v_{jf})^2} - \frac{f_v}{2} = \sqrt{(\frac{1.6}{2})^2 + (2.42)^2} - \frac{1.6}{2} = 0.35\sqrt{f_c'}$$

$$P_{t\,(Ext)}{}^{(v_{jc}+v_{js}+v_{jf})} = \sqrt{(\frac{f_v}{2})^2 + (v_{jc} + v_{js} + v_{jf})^2} - \frac{f_v}{2} = \sqrt{(\frac{1.6}{2})^2 + (3.61)^2} - \frac{1.6}{2} = 0.58\sqrt{f_c'}$$

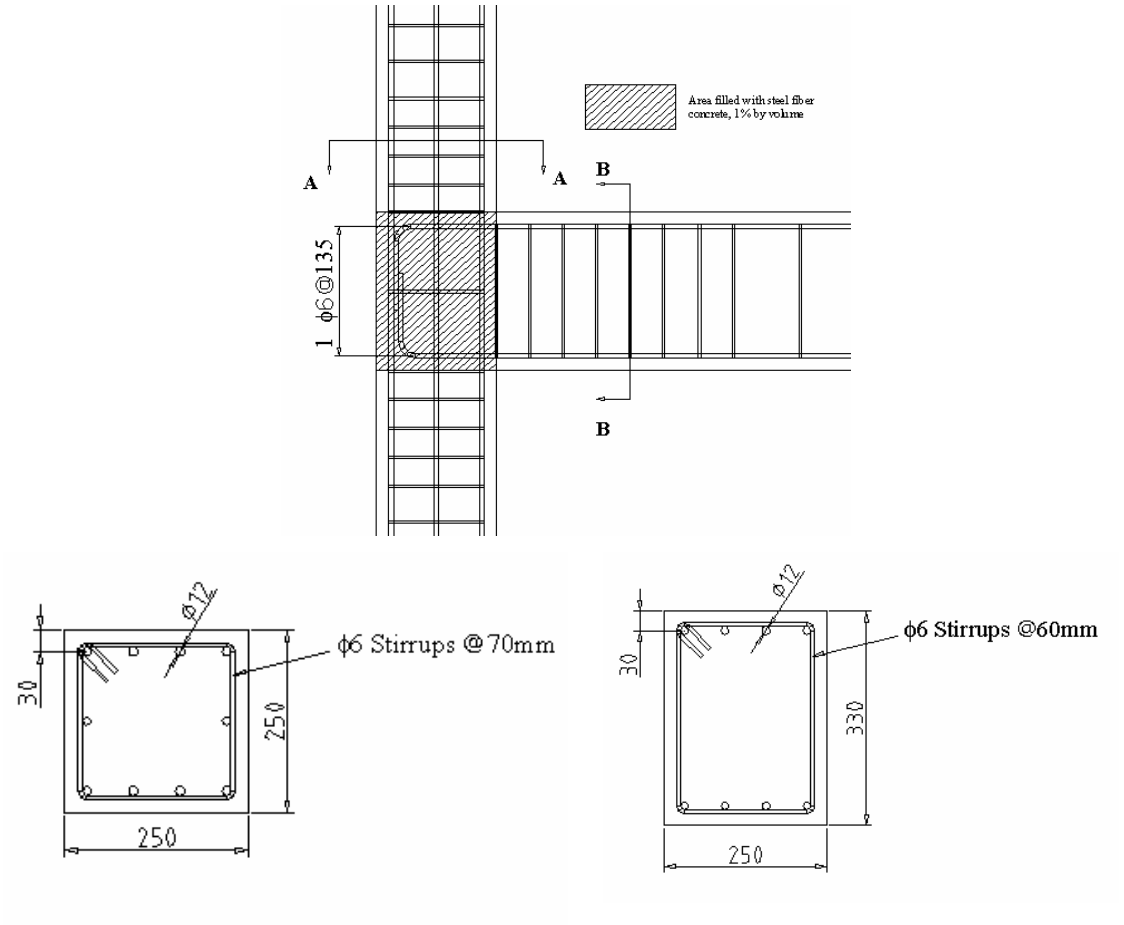

Section A-A

Section B-B

Figure 1: Details of an example of a beam-column joint

Table 1: Prediction of determined Coefficient K

Joint Type		Determined Coefficient K	
		First cracking	Extensive damage
v_c	Joint without any reinforcement	0.29	0.42
v_c+v_s	Joint reinforced with 1 stirrup	0.29	0.52
v_c+v_f	Joint reinforced with 1.0% steel fibre	0.35	0.48
$v_c+v_s+v_f$	Joint reinforced with 1 stirrups and 1.0%steel fibre	0.35	0.58

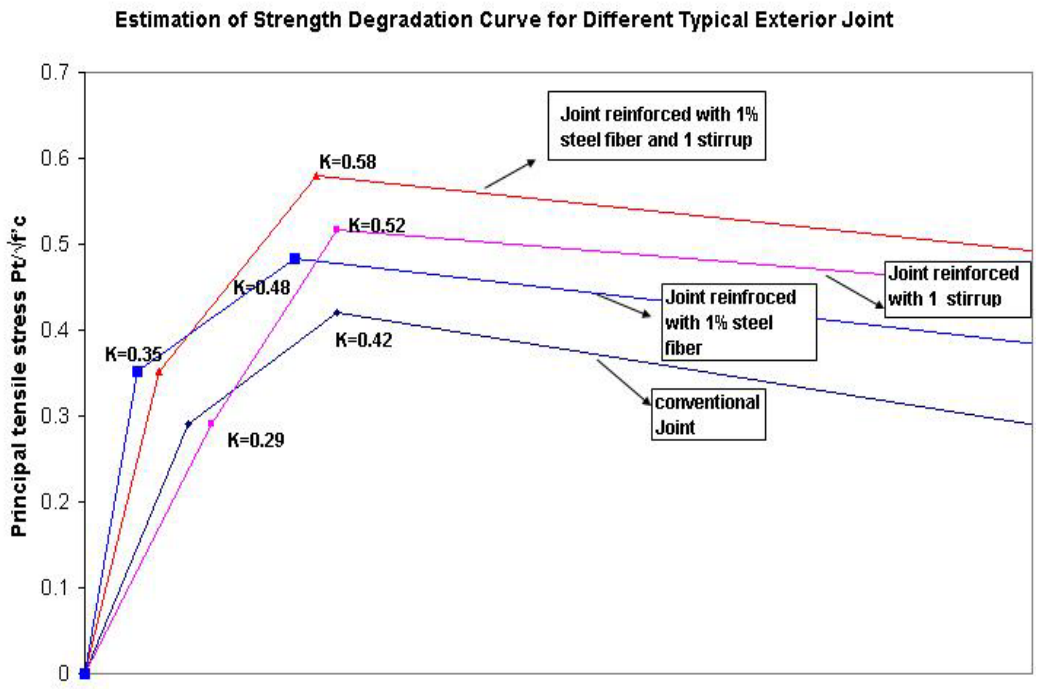

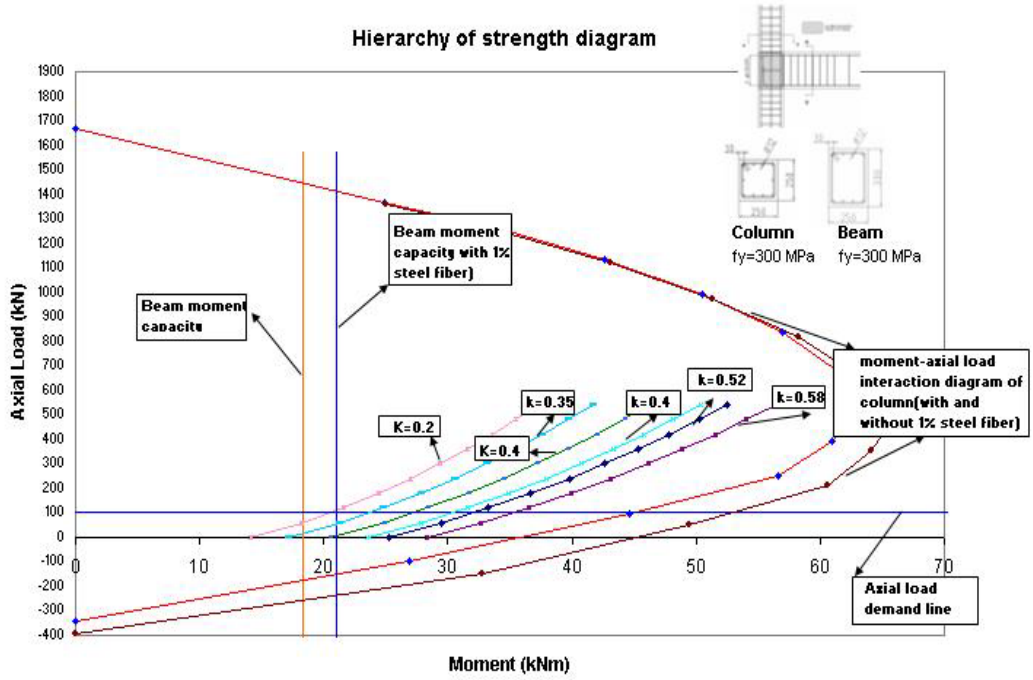

Figure 2: Hierarchy of strength diagram of a beam-column joint reinforced with different types of confinement

Appendix II

Flexure Design for Beam and Column

The geometric dimensions of the beam and column to be joined were determined and the concrete cover was also estimated. The approximate layout of the reinforcing steel in the beam and column sections was determined. The beam and column have to be designed for moment reversals so the area of tension steel and compression steel has to be equal. Material properties of the steel and the concrete are specified. The properties needed to specify are the compressive strength (f'_c) of the concrete and the yielding stress (f_y) of the steel. For the design Grade 300 steel and 30MPa concrete were used.

Using strain compatibility the strains in the steel and concrete can be related using a strain diagram. The concrete is assumed to crush at a strain of 0.003 and the steel's ultimate assumed strain at 5% strain. The yield strain of the grade 300 steel is 0.0015 after which point the stress is assumed to be the yield stress. Using the strain diagram the neutral axis position can be found by finding where the strain is zero. The distance from the top of the concrete to the neutral axis is the neutral axis depth (c).

Using constitutive relations the stress profile was determined. The steel stresses were determined from Hookes' Law with a modulus of elasticity of the steel being 200GPa. The concrete stress was approximated using Whitney's idealised stress block. The stress block approximated the stress in the concrete as a rectangle.

With the stresses in the steel and concrete known the neutral axis position can be found by equilibrium of forces. The force from the concrete stress (C_c) added to the force created by the compression steel (C_s) must equal the force created by the tension steel (T_s). The respective equations for the forces are shown below.

$$C_c = \alpha f'_c \beta c \qquad (1)$$

$$C_s = A_s' f'_s \qquad (2)$$

$$T_s = A_s f_s \qquad (3)$$

Both α and β are the same value 0.85. This is standard for α, and Whitney recommends this value for 30MPa concrete. With the three forces known, the equilibrium equation is used to find the neutral axis position. It is assumed initially that the steel is yielding and therefore f_s and f'_s are the yield stress f_y = 300MPa. The equation of equilibrium is

$$C_c + C_s - T_s = N \qquad (4)$$

N is equal to zero for a beam as there is no axial load.

After the neutral axis position is found, if the compression steel is not yielding the equilibrium equation can be used to find the real neutral axis position and the real stress in the compression steel.

With the forces in the equilibrium equation known the moment capacity of the beam or column can be found by summing the moments of the forces about the centroid of the section.

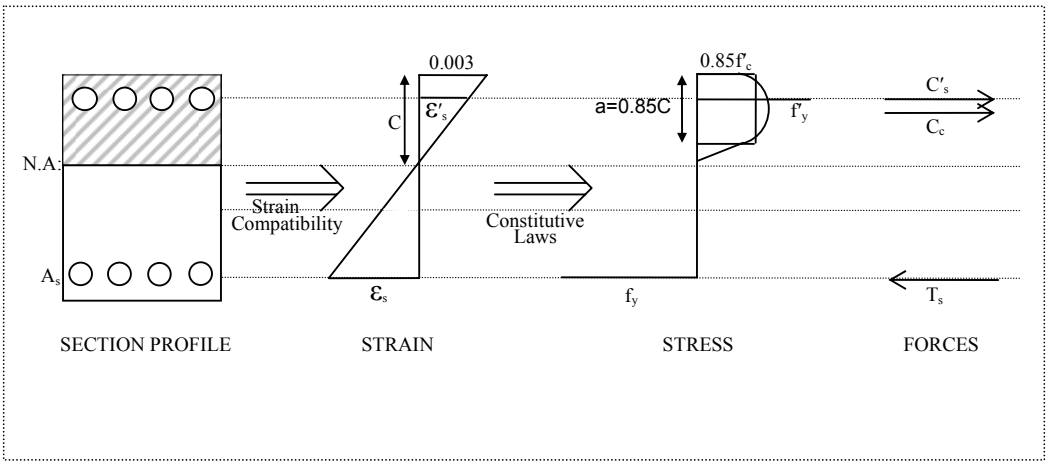

Figure 3: Strain and Stress profile showing the internal forces in the section

Shear Design for Beam and Column

The maximum value of shear in the beam can be calculated using equation (5), where M^* is the moment capacity of the section and l is the distance from the beam-column interface.

$$V_{\max} = \frac{M^*}{l} \qquad (5)$$

The maximum value of shear in the column is simply the lateral force applied to the top of the column at the point of yielding.

These values of shear must be divided by a safety factor to allow for any imperfections in the materials or any other unexpected variables that might influence the testing.

The shear that can be carried by the concrete alone is calculated with equation (6), where b_w is the width and d is the depth of the beam or column, and v_c is calculated from equation (7). Equation (8) can be used to calculate $\rho_{w,}$ where A_s is the area of longitudinal reinforcing steel on one side of the section. f'_c is the compressive strength of the concrete.

$$V_c = v_c b_w d \qquad (6)$$

$$v_c = 0.07(1 + 10\rho_w)\sqrt{f'_c} \qquad (7)$$

$$\rho_w = \frac{A_s}{b_w d} \qquad (8)$$

The spacing of the stirrups can be calculated using equation (9), where A_{str} is the area of one steel stirrup and f_y is the yield strength of the stirrup steel. Maximum spacing is limited to half the depth of the section.

$$S \geq \frac{A_{str} f_y d}{V_s} \qquad (9)$$

The spacing of the stirrups was calculated to be longer than the beam or column, however due to confinement requirements the spacing must actually be much smaller than calculated.

Shear Design for Joint

The horizontal shear stress across the joint is given by equation (10), where b_j is the width of the joint and h_c is the depth of the column. V_{jh} is obtained from equation (11), where f_y is the yield strength of the longitudinal reinforcing steel and A_s is the area of reinforcing in the

section. V_{col} is obtained from equation (12), where L and L_n are the lengths of the beam to the support from centre of the joint and the beam-column interface respectively, M_o is the moment capacity of the section and L_c is the length of the column.

$$v_{jh} = \frac{V_{jh}}{b_j h_c} \tag{10}$$

$$V_{jh} = 1.25 f_y A_s - V_{col} \tag{11}$$

$$V_{col} = \frac{2\left(\frac{L}{L_n} M_o\right)}{L_c} \tag{12}$$

The minimum area of horizontal shear reinforcement required in the joint is given by equation (13), where f'_c is the compressive strength of the concrete, β is the reinforcement ratio of the section, C_j is the axial load proportionality constant, N^* is the axial load, A_g is the area of the column section, f_{yh} is the yield strength of the shear reinforcement and A_{st} is the tension longitudinal reinforcement.

$$A_{jh} = \frac{6 v_{jh}}{f'_c} \beta \left(0.7 - \frac{C_j N^*}{f'_c A_g}\right) \frac{f_y}{f_{yh}} A_{st} \tag{13}$$

The minimum area of vertical shear reinforcing required in the joint is given by equation (14), where h_b is the depth of the beam, h_c is the depth of the column and f_{yv} is the yield strength of the shear reinforcement.

$$A_{jv} = \left[\frac{0.7}{\left(1 + \frac{N^*}{f'_c A_g}\right)}\right] \frac{h_b}{h_c} A_{jh} \frac{f_y}{f_{yv}} \tag{14}$$

The column longitudinal reinforcement was found to provide sufficient resistance to vertical shear, however stirrups were required to provide resistance to horizontal shear, as well as to cater to the confinement needs of the concrete.

Appendix III

Table 2: Detail of tested specimens [12]

		Joint Core			Beam				Column		
Specimen (1)		Cube strength of concrete (150 mm × 150 mm × 150 mm), f_{cu} (MPa) (2)	Percent fibers by volume, v_f (%) (3)	Volume ratio of stirrup in joint core, ρ_{sh} (%) (4)	Cube strength of concrete, f_{cu} (MPa) (5)	Percent fibers by volume, v_f (%) (6)	Area ratio of longitudinal tensile bar, ρ_s (%) (7)	Area ratio of stirrup, ρ_{sv} (%) (8)	Area ratio of longitudinal tensile bar, ρ_s (%) (9)	Area ratio of stirrup, ρ_{sv} (%) (10)	Notes (11)
(a) Exterior Joint											
1	SF1	21.3	1.2	0	31.9	0	Top or bottom, 3Φ 22(1.81%)	Φ 8@100(0.5%)	Every side, 2Φ 22 + 2Φ 12(1.25%)	Φ 8@ 100 (0.63%)	Cut-wire fibers
2	SF2	32.1	1.5	3Φ 8(0.87%)	31.9	0	Top or bottom, 3Φ 22(1.81%)	Φ 8@100(0.5%)			Sheared fibers
3	SF3	32.1	1.5	3Φ 8(0.87%)	32.1	1.5	3Φ 16(0.96%)	Φ 8@100(0.5%)			Sheared fibers
4	RC4	31.9	0	3Φ 8(0.87%)	21.3	0	3Φ 16(0.96%)	Φ 8@100(0.5%)			Conventional concrete
5	SF5	21.3	1.5	0	31.9	1.5	3Φ 16(0.96%)	Φ 8@100(0.5%)			Sheared fibers
(b) Interior Joint											
6	SF6	18.2	1.5	0	21.9	0	3Φ 22(1.81%)	Φ 8@100(0.5%)	4Φ 20(1.63%)	Φ 8@100 (0.63%)	Sheared fibers
7	SF7	18.2	1.5	3Φ 6(0.5%)	21.9	0	3Φ 22(1.81%)	Φ 8@100(0.5%)			Sheared fibers
8	SF8	37.9	1.5	3Φ 6(0.5%)	21.9	0	3Φ 22(1.81%)	Φ 8@100(0.5%)			Cut-wire fibers
9	SF9	18.2	1.5	0	21.9	0	3Φ 16(0.96%)	Φ 8@100(0.5%)			Sheared fibers
10	SFL10	31.4	1.5	0	31.4	1.5	3Φ 16(0.96%)	Φ 8@100(0.5%)			Lightweight concrete adding fibers
11	RC11	21.9	0	5Φ 10(2.29%)	21.9	0	3Φ 22(1.81%)	Φ 8@100(0.5%)			Conventional concrete
12	LC12	25.3	0	5Φ 10(2.29%)	25.3	0	3Φ 22(1.81%)	Φ 8@100(0.5%)			Lightweight aggregate concrete